University of Padova

Department of Physics and Astronomy "Galileo Galilei"

Master Thesis in Astrophysics and Cosmology

Probing Fundamental Physics With Galaxy Biasing

Supervisor
Prof. Sabino Matarrese
University of Padova

Co-supervisor
Prof. Nicola Bartolo
University of Padova

External co-supervisor
Prof. Licia Verde
University of Barcelona

Master Candidate
CHANASORN KONGPRACHAYA

Student ID
2071420

Academic Year
2023/2024

"Eppur si muove"

— Galileo Galilei

Abstract

In the presence of a new generation of large-scale structure surveys, this thesis aims to discuss the method to probe the fundamental physics of inflation from galaxy distribution. In particular, the thesis reviews the introduction of the inflation model. The state-of-the-art prediction of the initial condition from inflation is computed with the cosmological perturbation theory based on the theory of General Relativity (GR). The thesis focuses on two fundamental features. Firstly, Non-Gaussianity (NG) is discussed as an indicator of physics beyond the free-single-scalar field model. Observationally, NG is realized by the non-zero bispectrum of the primordial conserved curvature perturbation. The local, equilateral, enfolded and orthogonal types of bispectrum are introduced with the associated inflation models and their mode dependence. Secondly, the parity symmetry is recognized as a fundamental discrete symmetry of the standard GR, hence the property that one would expect from the observational consequence of inflation. Essentially, the reflection of space should not alter the mechanism generating perturbations during inflation. The thesis then discusses the theory of LSS distribution, particularly how the fluctuation from inflation evolves throughout different epochs. Standard Perturbation Theory (SPT) density perturbation is employed as a method to solve the nonlinear evolution of matter fluid. The theory of biased tracer is introduced as a description of the galaxy population. The tracer number density contrast is written as an expansion of bias parameters and their corresponding physical operators representing the quantity that affects the population. This thesis shows how the list of operators up to the third order is inferred from the gravitational evolution of the tracer. The relation between the statistics of tracers as discrete objects and the statistics of continuous density field are also discussed. With this complete connection from the essence of inflation to observable LSS, the prediction of the tracer's statistics and the bias parameter can be established. The thesis reviews how the NG from inflation introduce some scale dependence to the dark matter (DM) halo bias parameter. In particular, the Matarrese-Lucchin-Bonometto (MLB) approach is reviewed. The thesis discusses the formation theory of DM halo as a virialized object enclosing smaller structure clusters of galaxies. As its position can be inferred from the clustering of galaxies, the statistics can be probed from which the bias parameters can be inferred. Therefore, such measurement can be used to constrain the level of NG in the initial condition. The dependence on the sample's halo mass and the window function based on the MLB approach is also illustrated. Lastly, the parity violation (PV) of the galaxy's four-point correlation (4PCF) function is considered. In the presence of two independent analyses [1, 2] findings, this thesis assesses whether the redshift space distortion (RSD) effect can mimic the PV in the observed 4PCF. While the parity-odd mode of trispectrum (the Fourier-counterpart of 4PCF) has been studied in the literature [3], this thesis extends the result by considering the wide-angle effect and properly correcting the local

line-of-sight (LOS) for each galaxy with Taylor's expansion. It is shown in this thesis that the averaging over survey volume completely removes the PV introduced by RSD, suggesting that the isotropic 4PCF estimator used in [1, 2] are free of such contamination. Some fundamental sources of PV and caveats are commented on.

Contents

Listing of figures

Listing of acronyms

GR . . . . . General Relativity

PV . . . . . Parity Violation

FLRW . . . . . Friedmann-Lemaître-Robertson-Walker

RD . . . . . Radiation-Dominated

MD . . . . . Matter-Dominated

ΛD . . . . . Dark Energy-Dominated

EdS . . . . . Einstein-de Sitter

DM . . . . . Dark Matter

CDM . . . . . Cold Dark Matter

CMB . . . . . Cosmic Microwave Background

LSS . . . . . Large-scale Structure

BBN . . . . . Big Bang Nucleosynthesis

SSB . . . . . Spontaneous Symmetry Breaking

GUT . . . . . Grand Unified Theory

BAO . . . . . Baryon Acoustic Oscillation

TT . . . . . Transverse-Traceless

SVT . . . . . Scalar-Vector-Tensor

d.o.f. . . . . . Degree of Freedom

ADM . . . . . Arnowitt–Deser–Misner

PDF . . . . . Probability Density Function

NG . . . . . Non-Gaussianity

PNG . . . . . Primordial Non-Gaussianity

NL . . . . . Non-Linearity

NPCF . . . . . N-point Correlation Function

2PCF . . . . . Two-point Correlation Function

3PCF . . . . . Three-point Correlation Function

4PCF . . . . . Four-point Correlation Function

DBI . . . . . Dirac-Bold-Infeld

SPT . . . . . Standard Perturbation Theory

MLB . . . . . Matarrese-Lucchin-Bonometto

PBS . . . . . Peak-Background Split

RSD . . . . . Redshift Space Distortion

FOG . . . . . Finger-of-God

LOS . . . . . Line-of-sight

BOSS . . . . . Baryon Oscillation Spectroscopic Survey

SDSS . . . . . Sloan Digital Sky Survey

DESI . . . . . Dark Energy Spectroscopic Instrument

SKA . . . . . Square Kilometer Array

1 Introduction

The pursuit of understanding the dynamics of the universe is one of the main goals of Cosmology. Throughout decades of research, many discoveries have been brought to the eye of the community. Each one demonstrates how nature regulates itself in different scenarios and leaves us with the next open question invoking further exploration. For example, measuring the redshift factor of distant astrophysical objects unveils that the universe is expanding [4, 5, 6]. The surveys found that the electromagnetic waves from an object are subjected to a redshift factor proportional to the distance from us. Such a large-scale phenomenon is explained by the stretching of space causing the wavelength of the light to extend, regarded as the cosmological redshift. Moreover, Dark energy was popularized as one of the few physical objects that can accelerate the expansion. Such a radical concept has always been around in the scientific community, waiting to be unmasked and understood more about. Crucially, the detection of Cosmic Microwave Background Radiation (CMB) is the lighthouse that exposes the universe's climate at an early stage, providing a window to probe the physics of the early universe. These primordial electromagnetic waves were emitted around 13.7 billion years ago as electrons and protons were cooled down enough to first combine into Hydrogen atoms, the *recombination* [7]. The process is exothermic and the ionization energy is discarded into space as the first light, free-streaming across the cosmos, redshifted by the expansion, curved by some structure, and eventually reaches us as an observer. Along with the redshift observations, CMB helps us understand the universe's expansion and predict the energy contribution of each component, including ordinary matter, dark matter, radiation, and dark energy. In particular, the

universe's content nowadays consists of 70% of dark energy, 25% of dark matter, only 5% of ordinary matter and $< 1\%$ radiation [8, 9]; the ΛCDM model being the best model of the universe up until now, supporting the existence of dark matter, a hypothetical matter that interacts gravitationally only. Up until now, it has yet to be detected directly and remains an unknown object of the cosmos. With the expansion of the universe being confirmed and the early time snapshot from CMB, the expansion history can be interpolated. It is natural to start considering the thermodynamics of such a system to reveal the universe's status at different periods. The study is interesting since the state of matter should change with evolving background. In particular, the study of thermal history describes how elementary particles evolve as the universe dilutes and cools down by the expansion. Also, this standard Hot Big Bang model describes how the elementary particles are produced. These studies forced the fundamental theory of particle physics like the standard model into a consistency test with the observation, as many processes rely on the standard model physics such as the production of CMB introduced above. The study of *Big Bang Nucleosynthesis* describing the production of primordial nuclei abundances such as Hydrogen, Deuterium, Helium and Lithium is also highly dependent on the standard model. The ratios between these nuclei's abundances are determined by the parameters related to the standard model, e.g. neutron lifetime, weak interaction coupling constant, etc. Not to mention the existence of dark matter and dark energy regarded as beyond standard model physics. Another recent example is the measurement of Baryon Acoustic Oscillation (BAO), the matter density bumps exist across the universe with a characteristic separation length called the sound horizon [10, 11]. This peculiar structure is a consequence of baryon and photon coupling in the early times which stopped and stained the density with permanent density wave. The sound horizon is completely determined by early-time physics, i.e. *baryogenesis*. The measurement of such a length scale is a direct constraint to the corresponding physics [9]. Moreover, the estimator of BAO signature at different redshifts tells us step by step how the expansion rate changes across the evolution of the universe. The recent data analysis of Dark Energy Spectroscopic Instrument (DESI) [12] show the potential of unveiling the time-dependent equation of the state of dark energy. These are just a few examples of things we have learned from cosmological probes in the past few decades.

One of the most unknown fields in cosmology is the theory of inflation, the accelerated expansion period at the beginning of the universe. Despite being the solution to the shortcomings of standard Hot Big Bang Theory, i.e. the horizon problem, the flatness problem, and the magnetic monopole problem, most of its details remain unidentified and many possibilities are yet to be eliminated. However, understanding the mechanism of such a period will unfold the

physics that was never achieved in any experiment. In particular, the energy level of inflation is extremely high (> 100 GeV while LHC can achieve ~ 10 TeV) since the space is compressed at the beginning of the expansion. On such an energy scale, new physics that has never been discovered may be active. For example, General relativity as an effective theory of gravity may receive some modifications only at high energy [13, 14]. Furthermore, the hypothetical dominating scalar field during inflation, the *inflaton*, is constrained by just a handful of properties, just enough to maintain the accelerated expansion and satisfy the cosmological principle, i.e. isotropy and homogeneity on a large scale. The details such as interaction structure, mass, or the speed of propagation are yet to be determined. However, the nature of GR allows those high-energy properties to imprint some perturbation on space-time which will be conserved on a large scale after inflation ends. These signatures later become the initial condition for the universe's structure formation, the physical objects we can observe nowadays. Therefore, the fundamental physics during inflation can be probed through those observable. In particular, the statistics of late time structure can be used to infer the statistics of the primordial fluctuation.

This thesis focuses on two features of inflation: the non-Gaussianity (NG) and the parity violation (PV). The prior is the attempt to understand the model of inflation beyond the free-field approximation of a single field. The quantum fluctuation of a free field is known to be Gaussian through the quantum field theory. Specifically, the action is quadratic and there is no interaction part to mix the perturbation modes. Hence, each mode is an independent Gaussian stochastic process. The Gaussianity of field fluctuation resonates quite well with the CMB observation where the temperature fluctuation is also very close to Gaussian [15]. However, even in the simplest single-field model, the self-interacting term is needed to end inflation. Therefore, a departure from Gaussianity, the NG, is expected to some degree in the observation, reflecting a slight modification from the free-field approximation. In the literature, several models of inflation are investigated to identify the NG signature they might have left behind in primordial statistics [16, 17, 18, 19, 20, 21, 22]. The latest CMB observation by Planck collaboration [23] succeed to put a tight constraints on each kind of NG. However, the existence of them in the primordial statistics is still inconclusive. Now, CMB is closing towards its physical limitation. In particular, smaller perturbation modes are suppressed by the so-called *silk-damping* effect and the signal is flooded by other physical emission. Therefore, it is complementary to reach for another source. In recent years, Large-scale Structure (LSS) has been one of the competing sources that could constrain NG to CMB [24, 25, 26]. One key advantage of LSS over CMB is the three-dimensional field of data rather than two-dimensional, allowing more sample to be

extracted. It has been confirmed in the literature that discrete astrophysical objects like galaxies are biased tracers of the underlying matter distribution [27] (see also a comprehensive review [28]). Hence, it is possible to extract the primordial statistics by understanding this bias relation. Recent works [29, 30, 31, 32, 33] demonstrated an approach to probing NG through the scale-dependent bias which will be reviewed in this thesis.

Another fundamental aspect one can learn about inflation is the governing symmetry of the theory. In particular, this thesis will discuss the consistency check of parity symmetry, essentially a spatial reflective symmetry of the theory. If the fundamental mechanism works the same under the flipping of spatial direction, we would expect the resulting structure to respect the symmetry as well. However, recent analyses of galaxy four-point correlation function (4PCF) [1, 2] have found a parity violation in the LSS distribution. In particular, they use the CMASS and LOWZ galaxy catalogues from the Baryon Oscillation Spectroscopic Survey (BOSS) as a part of the Sloan Digital Sky Survey (SDSS) twelfth data release (DR12). Essentially, the mirrored configuration of four galaxies is unique and cannot be achieved by three-dimensional rotation. Hence, the parity violation property is realised by the different numbers of the pair of reflected configurations. This is highly radical since the elementary theory of gravity like GR inherits parity symmetry. If this asymmetric property is confirmed to be of primordial origin, an expansive list of inflation models would be ruled out, leaving us with just parity-violating models. However, the complexity of LSS required us to properly investigate any potential physics process that may introduce PV to the sample. Also, the fact that the observed LSS is the projection on the two-dimensional sky inevitably introduces some observer-related effects. One of which is the Redshift Space Distortion (RSD) effect, deceiving the real radial position of the galaxy. Since the galaxy's position is estimated from the cosmological redshift factor as mentioned before, the peculiar movement of the emitter would introduce an additional redshift by the relativistic Doppler effect resulting in the distorted distribution of galaxies [34, 35, 36, 37]. Recently, [3] have pointed out that the GR correction in the RSD effect can mimic the parity-violating signature in the galaxy trispectrum (Fourier counterpart of the four-point correlation function) without being primordial. This thesis will extend the matter by including the line-of-sight (LOS) correction due to the wide-angle effect [38] (see also [39] and reference therein). Moreover, we will demonstrate the consequence of the light-of-sight averaging procedure performed in [1, 2] on the PV introduced by RSD.

The thesis is organized as follows. In chapter 2, the fundamental physics including GR, the theory of inflation, and their predictions are reviewed. The chapter aims to provide the role of NG and PV in building the model of inflation as the fundamental feature that can be

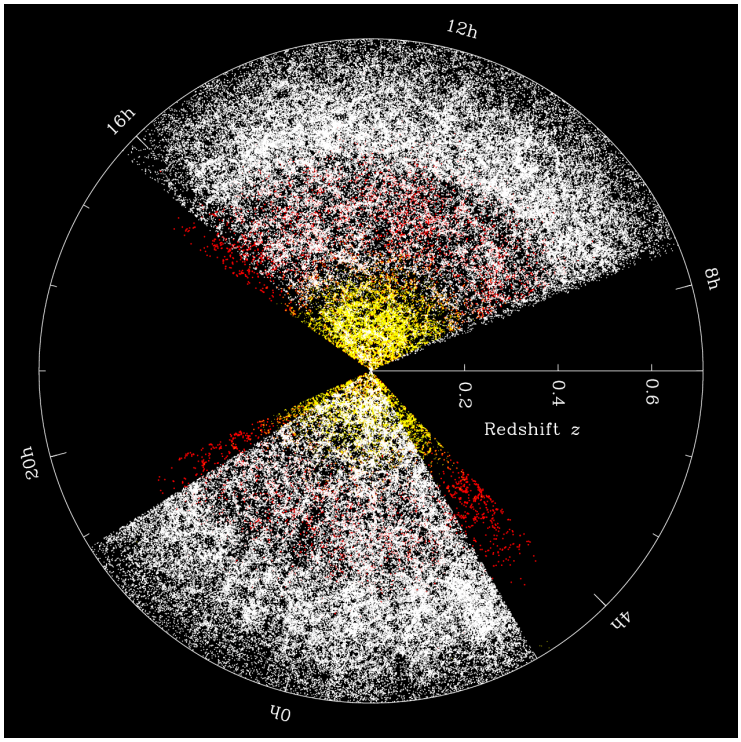

Figure 1.1: A Projection slice of the galaxies distribution observed in the SDSS in a range of redshift.

probed from the galaxy distribution. Chapter 3 will walk the reader through the development of LSS from the initial condition provided by inflation. The nonlinear evolution of matter fluid and the theory of biased tracer will be revised along with the basics of galaxy statistics. Then, the fundamentals from those two chapters are exploited in the discussion of the next chapters. The probing of NG with scale-dependent halo bias will be discussed in chapter 4. Lastly, the investigation of PV in 4PCF due to RSD effect is discussed in chapter 5.

2

Fundamental Physics

2.1 General Relativity and the Universe's Model

The current standard theory of gravity is the *General Relativity* (GR) proposed by Albert Einstein in the early 20th century [40]. The theory has been tested through a series of observations and experiments, such as the precession of mercury orbit and the existence of gravitation waves. Bounded by those validation results, the modification of such a theory becomes harder and harder, and GR stands firmly as a fundamental description of gravity. In the context of cosmology, GR is foundational for building the model of the universe. The interaction between matter and the geometry of the cosmos is described based on the so-called *Einstein Field Equation*. Hence, the behaviour and the entire history of the universe, as a prediction from the cosmological study, depends on the theory of GR. In this section, let us briefly introduce GR and its role in cosmology.

The master equation of GR is the Einstein Field Equation,

$$G_{\mu\nu} = 8\pi G T_{\mu\nu}, \tag{2.1}$$

where $G_{\mu\nu}$ is the Einstein tensor and $T_{\mu\nu}$ is the energy-momentum tensor. Here, we use the convention, $c \equiv 1$ for convenience. In GR, the effect of gravity is interpreted as the influence of the geometry of space and time on the trajectory of an object living on it. The equation describes the relation between the geometry, represented by the Einstein tensor, and the matter

living inside that geometry, represented by the energy-momentum tensor. Geometry dictates how the cosmic content moves through space and time, and the matter responds by curving the geometry in its vicinity. The interplay between these two members is the core function that creates the interaction between astrophysical objects, forming patterns of many-body systems from planetary orbits and galaxies' profiles, to cosmic structures like the cosmic web. In particular, the Einstein tensor is defined from the object trajectory, *the line element*, as

$$G_{\mu\nu} = R_{\mu\nu} - \frac{1}{2} g_{\mu\nu} R, \tag{2.2}$$

where

$$\begin{aligned} R_{\mu\nu} &= \partial_\sigma \Gamma^\sigma_{\mu\nu} - \partial_\nu \Gamma^\sigma_{\mu\sigma} + \Gamma^\sigma_{\mu\nu}\Gamma^\rho_{\sigma\rho} - \Gamma^\sigma_{\mu\rho}\Gamma^\rho_{\nu\sigma} \\ R &= g^{\mu\nu} R_{\mu\nu} \end{aligned} \tag{2.3}$$

are Ricci tensor and Ricci scalar. The Christoffel symbols are defined as

$$\Gamma^\sigma_{\mu\nu} = \frac{1}{2} g^{\sigma\rho} (\partial_\mu g_{\rho\nu} + \partial_\nu g_{\mu\rho} - \partial_\rho g_{\mu\nu}) \tag{2.4}$$

where the metric tensor, $g_{\mu\nu}$, defines the line element,

$$ds^2 = g_{\mu\nu} dx^\mu dx^\nu, \tag{2.5}$$

which is the infinitesimal space-time displacement of an object.

In the matter side of the equation, we have $T_{\mu\nu}$ that is a bit more challenging to define since it has to capture all of the characteristics of matter, such as interactions, creation, and annihilation. Typically, we can impose some assumption to the cosmic content we are dealing with to simplify the description.

2.1.1 Friedmann-Lemaître-Robertson-Walker (FLRW) Geometry

On a cosmological scale, the following simplifications are made. We assume that the universe is homogeneous and isotropic on the background level where the unperturbed tensors are position- and directional-independent. The standard choice of the metric tensor is the *Friedmann-Lemaître-Robertson-Walker metric* (FLRW metric) defined in Cartesian coordi-

nates as,

$$g_{\mu\nu} = \begin{pmatrix} 1 & 0 & 0 & 0 \\ 0 & -a^2(t) & 0 & 0 \\ 0 & 0 & -a^2(t) & 0 \\ 0 & 0 & 0 & -a^2(t) \end{pmatrix}, \tag{2.6}$$

which is motivated by the fact that we are confident that the universe is expanding. This is evident from the redshift observation of astrophysical objects, the first of which was the Nebula receding velocity observed by Edwin Hubble in 1929. In particular, the expansion of space is captured by the time-dependent scale factor, $a(t)$. This gives rise to the concept of the expanding physical coordinates compared to static coordinates (which we are going to refer it as *comoving coordinates*), $\boldsymbol{x}_{\text{phys}} = a(t)\boldsymbol{x}_{\text{com}}$. Let us also realize that we have the freedom to fix $a(t)$ at one specific time since we only care about the expansion ratio of space; the standard choice is unity at present, $a(t_0) \equiv 1$.

Since isotropy is assumed, spherical symmetry of 3D space is expected. Along with homogeneity, the universe can be imagined as a time ordering of 3D spatial hypersurface. Therefore, representing the line element in polar coordinates is useful where it is clear that the spherical symmetry constrains the geometry of the hypersurface to be of particular kinds. In cosmology, we can characterize space with 3 different geometrical (global) curvatures: Euclidean (flat universe), Spherical (closed universe), and Hyperbolic (opened universe). The line element of each case can be generalized as

$$\begin{aligned} ds^2 &= dt^2 - a^2(t)\gamma_{k,ij}(r)dx^i dx^j \\ &= dt^2 - a^2(t)\left[\frac{dr^2}{1-kr^2} + r^2 d\Omega^2\right] \;;\; k = \begin{cases} -1 & \text{Hyperbolic} \\ 0 & \text{Euclidean} \\ +1 & \text{Spherical} \end{cases}, \end{aligned} \tag{2.7}$$

where $\gamma_{k,ij}$ is the spatial part of the static metric and k is the curvature parameter. These three cases are still consistent with the observational data up until now. However, the standard assumption is a flat universe since, as we will see later, from observation, this global curvature gives a negligible contribution to the background dynamics of the universe. Hence, the relevance of the type of spatial geometry is suppressed in this scheme.

2.1.2 Perfect Fluid and Friedmann Equations

On the other hand, matter on a cosmic scale is assumed to be a perfect fluid. Namely, the objects and particles are collectively viewed as a homogenized fluid where heat conduction, viscosity, and other dissipative processes are negligible. In a general frame of reference, the tensor then takes the form of

$$T_{\mu\nu} = (\rho + P)u_\mu u_\nu - P g_{\mu\nu}, \tag{2.8}$$

where ρ and P are the energy density and pressure of the fluid. u_μ is the co-variant form of the observer's four-velocity. In cosmology, we define different cosmic content by the ratio $w = \rho/P$, the *equation of state*. Pressureless matter, radiation, and dark energy (cosmological constant) correspond to w equals 0, $1/3$, and -1, respectively. These numbers come from the fact that the energy density of each type dilutes with expansion differently. In particular,

$$\rho \propto a^{-3(1+w)}. \tag{2.9}$$

Intuitively, the matter dilutes with the 3D volume expansion while the radiation picks up another degree of $a(t)$ from the cosmological redshift effect. The cosmological constant stays the same by definition. With all of these ansatzes, we can find the solution to Einstein equations and obtain the *Friedmann equations*,

$$H^2 = \frac{1}{3M_{pl}^2}\rho - \frac{k}{a^2} \tag{2.10}$$

$$\dot{H} + H^2 = -\frac{1}{6M_{pl}^2}(\rho + 3P). \tag{2.11}$$

The constant $M_{pl} = (8\pi G)^{-1/2}$ is the Planck mass. The Hubble parameter H is introduced to represent the expanding rate of the scale factor compared to its magnitude defined as $H \equiv \frac{\dot{a}}{a}$. The dotted variable is the time derivative of that variable. These are basic ideas of the expanding universe model (FLRW universe) which explains the background evolution of the universe. It is useful to introduce a lowercase h as a parameter related to the present time Hubble parameter H_0 as

$$H_0 = 100h \text{ km/s/Mpc}. \tag{2.12}$$

The latest measurement by Planck CMB observation [9] point out that $h = 0.674 \pm 0.005$. There are also measurements from other sources like Cepheids [41] $h = 0.732 \pm 0.013$ which

are in tension with the CMB measurement. This is called the *Hubble tension* which we will not discuss in this thesis but rather lead the reader to nice reviews [42, 43].

Conformal Metric

Before continuing to the next topic, it is convenient to introduce the conformal metric. It is defined such that both space and time are expanding together. Therefore, the angle of a distance in space-time is preserved under the expansion. Thus, the metric is conformal and comoving with the expansion. This is a handy way of seeing things that evolve in the expanding universe since we do not have to worry about the disparity between the scale of time and space. This metric is written as

$$ds^2 = a^2(\tau)\left[d\tau^2 - \gamma_{k,ij}(r)dx^i dx^j\right]. \tag{2.13}$$

Conformal time is introduced and defined as $d\tau \equiv \frac{dt}{a(t)}$. The original time scale t will be called *physical time* from now on. The Hubble parameter also changes its form in the conformal time scale to

$$\mathcal{H} \equiv \frac{a'}{a}. \tag{2.14}$$

The primed variable denotes the conformal time derivative of that variable. This Hubble parameter in conformal time scale is related to the Hubble parameter in physical time scale such that $\mathcal{H} = aH$. In brief, the change in time scale will adjust the look of some equations but will not affect the physics of it whatsoever.

2.1.3 The Standard Model of Cosmology: (Flat) ΛCDM Model

Based on the FLRW model, we can assume a list of cosmic content that made up our universe. This gives us a variety of models, each of which predicts a different expansion history of the universe. For example, the *Einstein-de Sitter* (EdS) *model* assumes that the universe contains pressureless matter only. Nowadays, the model that best fits the observational data (see [9] for example) is the ΛCDM Model. The model assumed 4 major components of the universe, ordinary matter, cold dark matter (CDM), radiation, and cosmological constant as dark energy (Λ). The name came from the fact that energy-wise, the universe nowadays is occupied mainly by dark energy and cold dark matter. In particular, the Friedmann equation 2.10 can be manipulated with equation 2.9 into

$$H^2(a) = H_0\left[\Omega_{r,0}\left(\frac{a_0}{a}\right)^4 + \Omega_{m,0}\left(\frac{a_0}{a}\right)^3 + \Omega_{k,0}\left(\frac{a_0}{a}\right)^2 + \Omega_{\Lambda,0}\right], \tag{2.15}$$

where the density parameters are defined as

$$\begin{aligned} \Omega_i &= \frac{\rho_i}{\rho_{\text{crit}}} \; ; \; \rho_{\text{crit}} = \frac{3H^2}{8\pi G} \\ \Omega_k &= -\frac{k}{(aH)^2}, \end{aligned} \tag{2.16}$$

where i is the species of cosmic content: radiation, matter, or dark energy (Λ). The subscript "o" indicates that the quantity is evaluated at present. Notice that the sum of density parameters is unity at all times by definition. With this model, the density parameters, which are the energy contribution of each species to the expansion rate, can be estimated from cosmological surveys at different redshifts. As a result, the estimated present energy budget shares are roughly 70%, 25%, 5%, and <1% for dark energy, CDM, ordinary matter, and radiation, respectively. The contribution from global curvature is found to be negligibly small, $\Omega_{k,0} \sim 10^{-3}$ [9]. This fulfilled the point that was mentioned earlier when we discussed the geometrical type of spatial hypersurface. The choice of curvature parameter k is almost insignificant to the expansion rate. Judging from the dependence on a, its contribution to H has always been suppressed by other components throughout the history of the universe. Therefore, it is convenient and well-justified to simplify the geometry of space to be flat (Euclidean) in which there is no intrinsic curvature of the universe; the unperturbed geometry of the universe is assumed to be flat.

Another feature of this mixed-component model is the expansion history divides into different epochs, depending on the dominating component. Due to the difference in the equation of states, each type of cosmic content will evolve and induce an expansion rate differently. For instance, the energy density of ordinary/dark matter dilutes as a^{-3} and induces decelerated expansion, $a(t) \propto t^{-2/3}$, while the dark energy (Λ) stays constant and induces accelerated expansion, $a(t) \propto e^{Ht}$. By sequence, the universe underwent the radiation-dominated, matter-dominated, and currently in the dark energy-dominated era. Deep in each epoch, the expansion of the universe can be approximated by

$$a(t) \propto t^{\frac{2}{3(1+w)}} \quad \text{and} \quad a(t) \propto e^{Ht} \text{ for } w = -1. \tag{2.17}$$

Notice that the matter-dominated epoch is well-approximated by the EdS model since the universe energy budget is mainly contributed by matter. We will return to this point later when we discuss the evolution of matter fluid and tracers.

2.2 Cosmic Inflation Paradigm

In the last section, we discuss the basics of GR and how it is used to describe our universe's expansion history. Furthermore, it is responsible for forming structures that we can observe nowadays. Therefore, the large-scale structure is a direct probe to the theory of GR. However, the late time process is not the only source for the observed features. Those features of interest may lie within the initial condition of the universe itself before the late time evolution took place. This leads to the possibility to learn more about the physics before the Big Bang, the physics of inflation. In particular, the discovery of certain qualities of the universe's structure may help us constrain the possible model of inflation, telling us more about fundamental physics at a high energy scale. Before introducing the relevant characteristics, let us discuss some key aspects of inflation.

Inflation is the model of the universe's beginning introduced to explain the plotholes of the standard Hot Big Bang theory. The theory then proves itself by explaining the observational consequence and became one of the default assumed models of the very early phase of the universe. In the upcoming section, the motivation for the inflation proposal will be introduced.

2.2.1 The Standard Hot Big Bang: Explained and Unexplained

Based on the expansion history of ΛCDM model, we can discuss the thermodynamics throughout the cosmic timeline and infer the evolution of particles in the standard model. This study of thermal history gives rise to the so-called *Standard Hot Big Bang Theory*. Essentially, we have the explanation for the birth of particles in the standard model as the universe cools down. In particular, the universe starts with a high-temperature state, hence the 'hot' Big Bang, where all particles are tightly coupled together as a homogenized fluid, the particle soup. In the beginning, we suppose that there is some mechanism that produced asymmetry of baryonic number; there are more baryons than anti-baryons. Those two annihilate each other and are left with the baryon deficit that is what we observe nowadays. This is the process we call the *Baryongenesis* that provides us with the ingredients to form our universe. The expansion of the universe gradually cools down the temperature from which the universe underwent some phase transitions. At $T \sim 100$ GeV, the particles gain their masses via the Higgs mechanism including the weak interaction mediators, $W^{\pm}$ and Z bosons. This turned on the strength of the weak interaction; this process is called the electroweak phase transition. Below $T \sim 100$ MeV, the universe experienced the QCD phase transition where the strong interaction becomes important and

confined quarks together with gluons to form Hadrons. Down to around $T \sim 1$ MeV, the weak interaction between neutrinos and the rest of the particles becomes inefficient and much less than the expansion rate. This forced neutrino abundance to move out from the thermal equilibrium. This is the phenomenon called the *freeze-out*, decoupling the particle from the primordial plasma. Shortly after the neutrino decoupling, electrons and positrons annihilate each other and inject the energy into photon abundance through electromagnetic interaction, but not into the decoupled neutrinos. This causes the disparity between the photon and neutrino temperatures we observed. At $T \sim 100$ keV, *Big Bang nucleosynthesis (BBN)* is initiated where nuclei of elements lighter than Helium are created with protons and neutrons. The process filled the universe with free nuclei and electrons until $T \sim 1$ eV when they combined in the event called *Recombination*. At that time, the photon was no longer energetic enough to constantly ionize the Hydrogen atom so the abundance of free electrons dropped drastically. Inevitably, the Thomson scattering becomes disfavored and the photon decouples from the rest of the particle, free-streaming until now and got observed as the *cosmic microwave background* (CMB) radiation.

From this point, it is natural to think that the temperature of CMB should reflect the background temperature of the universe since the time of decoupling, after accounting for the cosmological redshift. The legacy of CMB observations concludes that the CMB temperature is very uniform with an effective average temperature of 2.73 Kelvin and one part in a hundred thousand of fluctuation. This suggests that the whole universe, at least in the observable patch, in that time is in thermal equilibrium as we have assumed when inferring the thermal history above. However, the expansion history fitted from the redshift observations constrains the age of the universe precisely, CMB is emitted around redshift $z \sim 1100$ (around 380 kyr after the Big Bang). Concerning the last scattering surface of CMB, it is impossible for light to travel around and cover the whole horizon, from the beginning to before the photon decoupling. This is contradictory since the heat transfer cannot go beyond the speed of light in a vacuum and the universe's thermal equilibrium is not secured. In other words, without any modification, we must live with the assumption that the universe starts with a homogeneous temperature state, which may appear unnaturally specified. This is the so-called *Horizon Problem* of the Standard Big Bang cosmology. One way to resolve this is to propose a mechanism that initially distributes the temperature. Therefore, inflation was proposed as a solution by assuming that the universe underwent accelerated expansion in the beginning which inflated the space rapidly. In this way, the region of thermal equilibrium can be arbitrarily stretched to the size of the CMB horizon just before the Hot Big Bang kicks in. This solves the horizon

problem without altering any of the Hot Big Bang storylines.

The Horizon Problem was not the only problem solved by inflation. Also, the flatness of the universe observed nowadays introduces the fine-tuning problem of the initial condition, the *Flatness Problem*. According to ΛCDM evolution discussed in section 2.1.3, the density parameter of intrinsic curvature, Ω_k, grows with the comoving Hubble horizon, $r_H = (aH)^{-1}$. Since the horizon has grown over time and inflated enormously from then to now, we expect an even flatter universe in the beginning. Considering how small $\Omega_k, 0$ is now, the initial curvature contribution must be very small. Moreover, the curvature nowadays must be very sensitive to the initial curvature energy fraction. Even a small change in initial Ω_k could alter the universe outcome drastically. Therefore, the initial condition must be carefully fine-tuned in order to arrive at the universe presently observed. Nicely, the accelerated expansion of inflation shrinks the Hubble horizon down in the beginning, suppressing Ω_k naturally. Conveniently, the amount of expansion we need to explain the Horizon Problem is sufficient to avoid this fine-tuning problem as well.

The last problem solved by inflation is the *Unwanted Relic Problem*. This issue is also known as the *magnetic monopole problem* since magnetic monopole is one of those unwanted relics. The story concerns the abundance of topological defects produced by the hypothetical spontaneous symmetry breaking (SSB) at a high energy scale. For example, the t'Hooft-Polykov magnetic monopole [44, 45] is a by-product from SSB of Grand Unified Theory (GUT) without U(1) symmetry to theory with U(1) symmetry. Other examples that can be found in the literature are cosmic strings, Domain Walls, and Textures. The existence of any of these can make the universe highly anisotropic and inhomogeneous. This is, again, mismatched with the observed isotropy of CMB. Inflation explained this with the iconic rapid expansion. The energy scale at which those SSBs occur was achieved deep in the inflationary period. Thus, the topological defects abundance is suppressed drastically by the expansion and becomes as less than one particle per one observable universe patch if they are ever produced at all.

All of these motivate the proposal of inflation by Alan Guth in 1981 [46] where he explains how the accelerated expansion merely solves all of the three problems mentioned above. However, Guth's model suffers from the Graceful Exit Problem; inflation cannot end with a high-temperature state for the Hot Big Bang, the super-cooling problem, or a sizable homogeneous region since it relies on the bubble nucleation mechanism to randomly occur in space. Shortly after, the problem is mitigated by the proposal of a new inflation model by two independent groups [47, 48]. The new model introduces the second-order phase transition which pushes the universe out of the false vacuum state. Thus, inflation is forced to end simultaneously across

the universe and does not occur randomly like the bubble nucleation anymore. However, the model is still stuck with the super-cooling problem and now has an additional problem in establishing the thermal equilibrium after the phase transition. This is because the interaction of the field in this model must be small. Hence, the inefficient heat transfer made the thermal equilibrium hard to establish. This problem is solved by the subsequent proposal of chaotic inflation by Linde in 1983 [49]. This model is robust for the fact that it does not rely on any phase transition. Hence, a strong interaction to distribute the heat across the space is unnecessary. This model is the first of the Large-field inflation kind where the field starts off at a high value and rolls towards a lower value. Another example of such a kind is the power-law inflation proposed by Lucchin and Matarrese in 1985 [50]. The hybrid model of inflation [51] was proposed following the supersymmetric model in particle physics theory where multiple fields existed simultaneously. This allows us to be more creative with the scenarios, for example, we can mix features of the phase transition (small-field) and the large-field models into one model. Other honourable mentions include natural inflation [52] and R^2 inflation [53] which have their pros and cons as a suitable model of inflation.

2.2.2 Kinematic Requirement of Inflation

The key property of inflation is that the expansion must be accelerated for a long enough time, at least to solve the Horizon and Flatness problem. This characteristic requires us to establish some condition to the matter equation of state dominating during the epoch. Let us consider the Friedmann equation 2.10 along with the evolution of energy density 2.9 to obtain the time dependence of the scale factor,

$$a(t) = a_0 \left[1 + \frac{3(1+w)}{2} H_0 (t - t_0)\right]^{\frac{2}{3(1+w)}}, \tag{2.18}$$

by assuming that there is a sole species of cosmic content that dominates during inflation. Let us be aware that the case of $w = -1$ is excluded from this formula and will give us an exponential growth scale factor instead. It is straightforward from this formula that the condition for the accelerated expansion $\ddot{a} > 0$ is $w < -\frac{1}{3}$. However, we expect inflation to end at some point so the third-order time derivative of $a(t)$ must be negative. This put the lower constraint $w > -1$ for the finite duration of this accelerated epoch.

2.2.3 Dynamic of Inflation

The expansion of space is driven by some kinds of matter as explained by the Friedmann equations 2.10 and 2.11. In turn, the kinematic of space affects the evolution of matter and this complete cycle forms a dynamical system hosted by inflation. Following the particle physicist approach, one may propose a field responsible for the accelerated expansion. A proper choice must respect the homogeneity and isotropy observed nowadays since the field must terminate and leave us with an appropriate initial condition for the Hot Big Bang, at least on the background level. One possible, perhaps the simplest, proposal is that inflation is dominated by a scalar field, called the *inflaton*, φ. This is because scalar is naturally directional-independent and we can require the field to be position-independent to respect the characteristics mentioned above. The dynamics of this field are presented by its action, which is written as

$$S = \int d\tau d^3x \sqrt{-g}\Big[\frac{1}{2}g^{\mu\nu}\partial_\mu\varphi\partial_\nu\varphi - V(\varphi)\Big], \tag{2.19}$$

where $V(\varphi)$ is the potential term of this field and $g \equiv \det(g_{\mu\nu})$. Note that we use the conformal metric here. Through the Euler-Lagrange equation, the equation of motion can be found,

$$\varphi'' + 2\mathcal{H}\varphi' + a^2 V_{,\varphi} = 0, \tag{2.20}$$

which is no other than the *Klein-Gordon equation*. The expression $V_{,\varphi} \equiv \frac{dV}{d\varphi}$ is the derivative of the potential with respect to the field. From Noether's theorem, the symmetry of a Lagrangian corresponds to a conserved quantity. In this case, it is the energy-momentum tensor which is written as

$$T_{\mu\nu} = \partial_\mu\varphi\partial_\nu\varphi + g_{\mu\nu}\left(\frac{1}{2}g^{\alpha\beta}\partial_\alpha\varphi\partial_\beta\varphi - V(\varphi)\right). \tag{2.21}$$

Since the field is homogeneous on the background level, the terms with the spatial derivative of the field vanish. Assuming that the inflaton field behaves like a perfect fluid, we can identify the background energy density and the pressure by comparing with equation 2.8,

$$\rho_\varphi = T^0_0 = \frac{1}{2}\Big(\frac{\varphi'}{a}\Big)^2 + V(\varphi), \tag{2.22}$$

$$P_\varphi = T^i_i = \frac{1}{2}\Big(\frac{\varphi'}{a}\Big)^2 - V(\varphi). \tag{2.23}$$

Here, we have a simple background scalar field that represents the matter in space-time. Next, we are going to discuss the conditions of the scalar field that drive the rapid expansion.

2.2.4 Slow-roll Conditions

Supposing that the inflaton field dominates the universe during inflation, some specifications must be imposed for the field to be responsible for the accelerated expansion. One way to achieve such an environment is to equip the field with slow-roll conditions. Essentially, the field is manipulated to develop slowly, a small kinematic term, compared to the latent potential energy that drives the expansion of space. As a result, inflation can occur with 1) accelerated expansion, and 2) a substantial period to solve the shortcomings of the Hot Big Bang theory. Let us introduce the parameters corresponding to those conditions. Firstly, we introduce the change in the expansion rate,

$$\epsilon \equiv \frac{d \ln H}{d \ln a} = -\frac{\dot{H}}{H^2}. \tag{2.24}$$

The first slow-roll condition is $\epsilon \ll 1$ to keep H varying slowly. In this way, the expansion is accelerated. On top of this, the first condition must be kept for a long enough time. Thus, it is required that $\left|\frac{d \ln \epsilon}{d \ln a}\right| \ll 1$. This leads to an introduction to the second parameter,

$$\eta \equiv -\frac{\ddot{\varphi}}{H\dot{\varphi}}, \tag{2.25}$$

where the second condition is satisfied when $\epsilon, |\eta| \ll 1$. By incorporating the Klein-Gordon equation 2.20, we can understand the parameter ϵ more as a fraction of kinetic energy over the total energy of the field. Thus, the first condition acts as a regulator that keeps the field rolling down the potential slowly, hence the name *slow-roll* inflation, whereas the second condition makes sure that the slow rolling is maintained for a while. Alternative definitions can be established with the help of Klein-Gordon equation 2.20 and Friedmann equations 2.10 and 2.11,

$$\epsilon_V \equiv \frac{M_{pl}^2}{2}\left(\frac{V_{,\varphi}}{V}\right)^2, \tag{2.26}$$

$$|\eta_V| \equiv M_{pl}^2 \frac{|V_{,\varphi\varphi}|}{V}, \tag{2.27}$$

which controls the shape of the potential itself to achieve the same dynamical conditions. We have defined $V_{,\varphi\varphi} \equiv \frac{d^2V}{d\varphi^2}$, representing the change of the potential term to the field. The slow-

roll potential requires $\epsilon_V \ll 1$ to keep the potential approximately constant and $|\eta_V| \ll 1$ to keep ϵ_V small. Keep in mind that these parameters are not the same as the previous ϵ and η which are often called the *Hubble slow-roll parameters*. Those parameters are used to represent the condition that keeps the Hubble parameter changing slowly. But, the parameters ϵ_V and η_V are used to create the condition that keeps the potential approximately flat. These parameters are called the *Potential slow-roll parameters*, judging if the given potential can lead to slow-roll inflation or not. These parameters can be related to each other as $\epsilon_V \approx \epsilon$ and $\eta_V \approx \epsilon + \eta$ during slow-roll inflation.

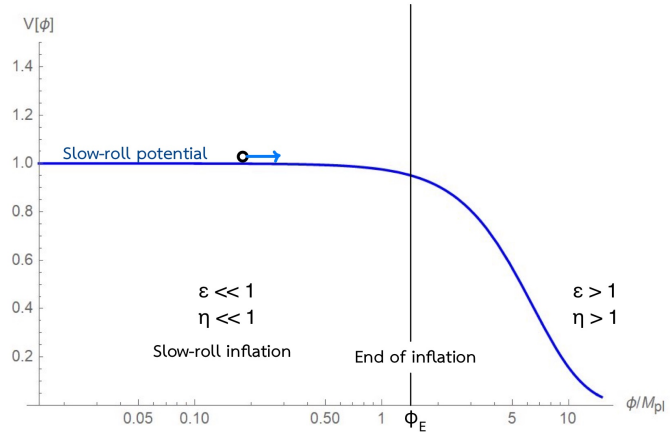

Figure 2.1: An illustration of the inflaton, ϕ, potential that drives the slow-roll inflation. In the context of slow-roll, the potential must be approximately flat to maintain an exponential expansion corresponding to small ϵ_V and η_V.

2.3 Cosmological Perturbation Theory

In the following discussion, inhomogeneity as a seed of cosmic structure will be introduced. In particular, perturbation of field and space-time geometry will play the main role and must be treated properly. This requires us to be careful about the number of degrees of freedom introduced into the system and their representation. In this section, we will discuss different ways to characterize those perturbative degrees of freedom in the context of GR.

One question that we can naturally ask before the discussion is "Why do we have to treat the perturbation in the GR regime?". The change in density is generally small in the perturbative regime and it would be significantly easier to treat our system in the Newtonian limit. However, the fact that we consider the situation on a large scale compared to the Hubble horizon makes

the GR effect significant. Let us consider the Poisson equation,

$$\nabla^2\Phi = 4\pi G\rho, \tag{2.28}$$

where Φ is the gravitational potential. Recall that this equation can be derived from the 00-component of the Einstein Field Equation 2.1 with the help of the *equivalence principle*. Note that the gravitational potential Φ and energy density ρ are treated as a perturbation from the background space. In the case of the FLRW background metric, we can develop the equation with the First Friedmann equation 2.10 on a flat geometry ($k = 0$) into

$$\nabla^2\Phi = \frac{3}{2}H^2\delta, \tag{2.29}$$

where $\delta = \frac{\delta\rho}{\rho_0}$ is the density contrast. ρ_0 is the background energy density responsible for the background expansion while $\delta\rho$ is a perturbation on it. From this equation, a scaling analysis can be done by considering

$$\frac{\Phi}{c^2} \sim \left(\frac{\lambda_{\text{phys}}}{\lambda_{\text{H}}}\right)^2 \delta \quad \text{where} \quad \lambda_{\text{H}} \sim \frac{c}{H}, \tag{2.30}$$

where λ_{phys} is the mode wavelength of Φ, corresponding to the scale on which we consider the system. λ_{H} is the Hubble Horizon radius. From the CMB observation [54], the density fluctuation in the early phase is in the order of $\delta \sim 10^{-5}$. However, as we will see later, the perturbation will be considered up to a scale much larger than the Hubble radius at the so-called s*uperhorizon limit*, $\frac{\lambda_{\text{phys}}}{\lambda_{\text{H}}} \gg 1$. This requires us to describe the perturbation with GR.

2.3.1 The Gauge Problem

An issue has to be addressed when dealing with perturbation in GR. The theory is covariance which means that a solution is identical under general diffeomorphism. In other words, the perturbation may manifest in different forms, depending on how the degree of freedom is represented, despite being of the same origin. This non-uniqueness of the solution is known as *the Gauge Problem*, the formal expression depends on how we represent the perturbation on the real spacetime. Mathematically, let us consider two manifolds: the background FLRW manifold, $\mathcal{M}_0$, and the real (perturbed) manifold, $\mathcal{M}$. Let ψ be a diffeomorphism one-to-one map of a point on $\mathcal{M}_0$, p, to $\psi(p)$ on $\mathcal{M}$. This corresponds to the *gauge choice*; ψ provides a certain representation of the perturbation on $\mathcal{M}$ with respect to the background $\mathcal{M}_0$. We

can define another gauge choice φ which maps the same point, p, to a different point $\varphi(p)$ on $\mathcal{M}$. These maps can be transformed into each other through the gauge transformation. In GR, since these correspondences are diffeomorphism, the solution of perturbation is identical regardless of the choice of gauge. Hence, the freedom to choose these maps sources the ambiguity of the perturbation's formal expression. There are two solutions to this problem. Firstly, we stick to a particular gauge and work with it until the end. This is called *gauge fixing*, after which the gauge transformation can be applied to have the results in different representations. Alternatively, we construct the *gauge-invariant* expression for the perturbation (degree of freedom) of interest. In this way, the expression is invariant under any gauge transformation, hence unambiguous.

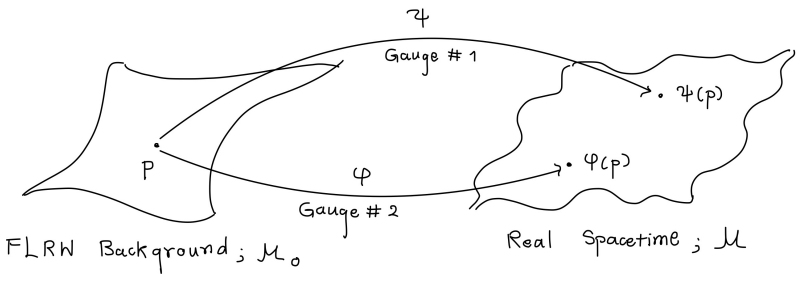

Figure 2.2: Gauge choices correspond to the diffeomorphism maps ψ and φ. These correspondences are one-to-one between the background FLRW manifold, $\mathcal{M}_0$, and the real (perturbed) manifold, $\mathcal{M}$.

A subtlety worth mentioning is that the choice of gauge is not the same as the choice of coordinates. Likewise, the gauge transformation is not a coordinate transformation. In particular, a gauge is chosen by specifying $\psi : \mathcal{M}_0 \longrightarrow \mathcal{M}$, whereas the choice of coordinates is the map from a point on a manifold to a point on the real coordinate space, $X : \mathcal{M} \longrightarrow \mathbb{R}^n$. The transformations gauge and coordinate are the change of maps ψ and X, respectively. This is important to stress since it may lead to some misinterpretation. The gauge transformation deals with the representation of perturbations only while the coordinate transformation transforms the way we measure the whole quantity, both background and perturbation. A general quantity that is invariant under coordinate transformation may host a perturbation that is not invariant under gauge transformation.

2.3.2 Gauge Transformation

We wish to explore what gauge transformation does to a mathematical object, like a tensor, defined on the manifolds. For generality, let us consider a tensor, T. Let us define the value

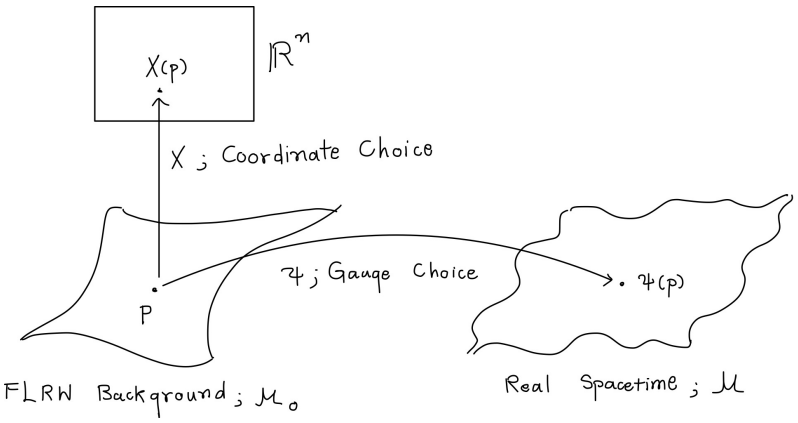

Figure 2.3: Comparison between the gauge and coordinate choices, ψ and X, as maps between points in the background and real manifolds, and in manifold and real coordinate space.

of it on the FLRW manifold, $\mathcal{M}_0$, to be the background value, T_0, at every point. Then, the tensor gauged to the real spacetime manifold, $\mathcal{M}$, will be perturbed with, ΔT, corresponding to the chosen gauge. Now, let us consider a single point on $\mathcal{M}$. A tensor realized on this point comprises the background value plus perturbation introduced by the gauge. However, this quantity can be the product of different gauges from different points in $\mathcal{M}_0$. But, since the tensors subjected to different gauges will arrive at the same point on $\mathcal{M}$, their real quantity (on real spacetime) can be compared to show the difference between gauges. For example, we can think of two gauges, ψ and φ, that map point p and q on $\mathcal{M}_0$ to the same point on $\mathcal{M}$, $\psi(p) = \varphi(q)$. Therefore, the gauge transformation can be realized as a one-to-one correspondence of different points in the background manifold. In particular, we will have to quantify the transformation, $q = \varphi^{-1}(\psi(p))$.

To measure this transformation, we take the coordinate choice X. We will discuss how to transport from p to q by exploiting the infinitesimal transformation on the chosen coordinate with a transformation parameter, λ. In linear order, it is written as

$$X^\mu(q) = X^\mu(p) + \lambda\xi^\mu|_p + \mathcal{O}(\lambda^2). \tag{2.31}$$

This is called the active coordinate transformation since the point on the manifold has been changed in this case. The transformation vector is defined by $\xi^\mu(X) = \frac{dX^\mu}{d\lambda}$. Equivalently, the transformation can be represented as a change in coordinate choice,

$$Y^\mu(q) = X^\mu(q) - \lambda\xi^\mu|_q + \mathcal{O}(\lambda^2), \tag{2.32}$$

which is called passive transformation. These two definitions are useful for discussing the transformation of T. The idea is we expect that the components of this tensor must be the same if it is transformed actively to another point on $\mathcal{M}_0$ and passively transform back with the same transformation vector and parameter, ξ^μ and λ. In particular, let T be a rank (m,n) tensor then the statement invokes $T^{\mu_1\cdots\mu_m}{}_{\nu_1\ldots\nu_n}(X(p)) = \tilde{T}^{\mu_1\cdots\mu_m}{}_{\nu_1\ldots\nu_n}(Y(q))$. This transportation allows us to compare the tensor associated with two background points, p and q. Exploiting chain rule leads to the first-order gauge transformation,

$$\tilde{T}^{\mu_1\cdots\mu_m}{}_{\nu_1\ldots\nu_n}(X(p)) = T^{\mu_1\cdots\mu_m}{}_{\nu_1\ldots\nu_n}(X(p)) + \mathcal{L}_\xi T^{\mu_1\cdots\mu_m}{}_{\nu_1\ldots\nu_n,\alpha}, \tag{2.33}$$

where the Lie derivative is defined as

$$\begin{aligned}\mathcal{L}_\xi T^{\mu_1\cdots\mu_m}{}_{\nu_1\ldots\nu_n,\alpha} =& T^{\mu_1\cdots\mu_m}{}_{\nu_1\ldots\nu_n,\alpha}\xi^\alpha \\ &- T^{\alpha\mu_2\ldots\mu_m}{}_{\nu_1\ldots\nu_n}\xi^{\mu_1}{}_{,\alpha}\cdots - T^{\mu_1\cdots\mu_{m-1}\alpha}{}_{\nu_1\ldots\nu_n}\xi^{\mu_n}{}_{,\alpha} \\ &+ T^{\mu_1\cdots\mu_m}{}_{\alpha\nu_2\ldots\nu_n}\xi^\alpha{}_{,\nu_1}\cdots + T^{\mu_1\cdots\mu_m}{}_{\nu_1\ldots\nu_{n-1}\alpha}\xi^\alpha{}_{,\nu_n},\end{aligned} \tag{2.34}$$

and the parameter λ is absorbed into ξ for simplicity. Here, we note that the coordinate derivative is shorthanded, $A_{,\alpha} \equiv \frac{dA}{dX^\alpha}$, and the tilde tensor, $\tilde{T}$, is the one that got transformed actively and passively. Notice that both T and T' in the formula are evaluated at the same coordinate $X(p)$. To discuss the perturbation of T in different gauges, we define the background value, T_0, on $\mathcal{M}_0$. This value can be passed through different maps to reach the point on $\mathcal{M}$; they are subjected to different gauges, ψ and φ. Mathematically, we can write the mapping as

$$\begin{aligned}\psi :& T_0 \longrightarrow T|_{\psi(p)} = T_0 + \Delta T, \\ \varphi :& T_0 \longrightarrow \tilde{T}|_{\varphi(q)=\psi(p)} = T_0 + \Delta\tilde{T}.\end{aligned} \tag{2.35}$$

We can link $T|_{\psi(p)}$ and $\tilde{T}|_{\varphi(q)=\psi(p)}$ together with the gauge transformation obtained earlier with the coordinate X. Hence, the gauge transformation of the perturbation is implied,

$$\Delta\tilde{T} = \Delta T + \mathcal{L}_\xi T, \tag{2.36}$$

where the tensor indices are omitted for the clarity of the expression. With this transformation, we can write the expression of perturbations from one gauge to the other. Let us remind ourselves that the transformation is induced by the infinitesimal vector, ξ. This is a crucial point which determines the degree of freedom we can remove by gauge fixing. In particular, ξ is a

4-vector. Therefore, we can remove 4 degrees of freedom. We will discuss this in more detail shortly.

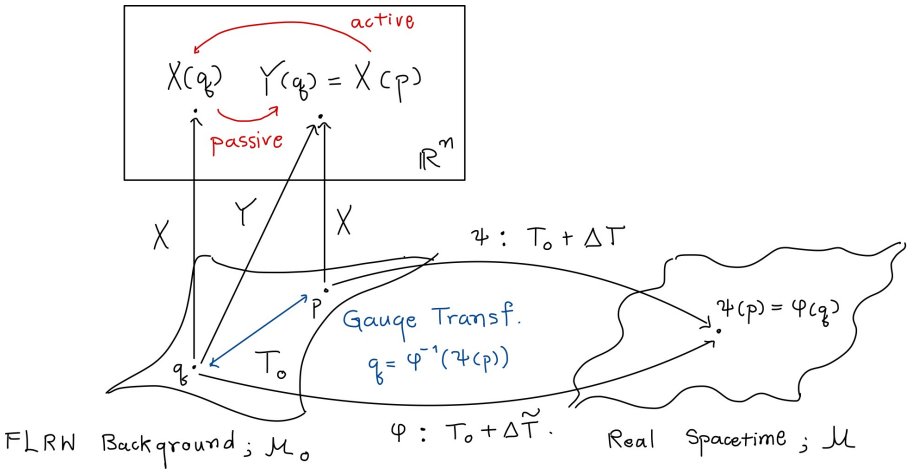

Figure 2.4: Summary of maps associated with the gauge transformation. X and Y are the coordinates where ψ and φ are the gauges. T_0 is the background value of the tensor where ΔT and $\Delta\tilde{T}$ are the perturbations associated with each gauge. In this picture, the gauge transformation can be viewed as a one-to-one correspondence between background point p and q which can be measured by mapping the points onto $\mathbb{R}^n$ and writing down the active and passive coordinate transformations.

2.3.3 Metric, Matter Perturbations, and SVT decomposition

Now that we have obtained the tool to control the perturbation in GR, we proceed to perturb the Einstein Equation. Let us start by generally perturbing each component of the metric tensor concerning the FLRW background,

$$\begin{aligned} g_{00} &= a^2(\tau)\left[1 + 2\sum_{r=1}^{\infty}\frac{1}{r!}\psi^{(r)}(\boldsymbol{x},\tau)\right], \\ g_{i0} &= a^2(\tau)\sum_{r=1}^{\infty}\frac{1}{r!}\omega_i^{(r)}(\boldsymbol{x},\tau) = g_{0i}, \\ g_{ij} &= a^2(\tau)\left\{\left[-1 + 2\sum_{r=1}^{\infty}\frac{1}{r!}\phi^{(r)}(\boldsymbol{x},\tau)\right]\delta_{ij} + \sum_{r=1}^{\infty}\frac{1}{r!}\chi_{ij}^{(r)}(\boldsymbol{x},\tau)\right\}, \end{aligned} \tag{2.37}$$

where $\psi^{(r)}$ and $\phi^{(r)}$ recalled the lapse and shift functions and $\chi_{ij}^{(r)}$ is a traceless tensor perturbation, i.e. $\chi_{ij}\delta^{ij} = 0$. For convenience, let us collect all orders of perturbation into single

functions,

$$\begin{aligned}
\psi(\boldsymbol{x},\tau) &= \sum_{r=1}^{\infty}\frac{1}{r!}\psi^{(r)}(\boldsymbol{x},\tau),\\
\phi(\boldsymbol{x},\tau) &= \sum_{r=1}^{\infty}\frac{1}{r!}\phi^{(r)}(\boldsymbol{x},\tau),\\
\omega_i(\boldsymbol{x},\tau) &= \sum_{r=1}^{\infty}\frac{1}{r!}\omega_i^{(r)}(\boldsymbol{x},\tau),\\
\chi_{ij}(\boldsymbol{x},\tau) &= \sum_{r=1}^{\infty}\frac{1}{r!}\chi_{ij}^{(r)}(\boldsymbol{x},\tau),
\end{aligned} \tag{2.38}$$

For the following discussion, it is useful to decompose the perturbation into the scalar, vector, and tensor parts entirely. In particular, the Helmholtz and Hodge theorems are applied to separate the divergence and solenoidal parts of vectors and tensors,

$$\begin{aligned}
\omega_i(\boldsymbol{x},\tau) &= \omega_{,i}(\boldsymbol{x},\tau) + \omega_i^{\perp}(\boldsymbol{x},\tau),\\
\chi_{ij}(\boldsymbol{x},\tau) &= \mathcal{D}_{ij}\chi(\boldsymbol{x},\tau) + \chi_{i,j}^{\perp}(\boldsymbol{x},\tau) + \chi_{j,i}^{\perp}(\boldsymbol{x},\tau) + \chi_{ij}^{TT}(\boldsymbol{x},\tau),
\end{aligned} \tag{2.39}$$

where $\mathcal{D}_{ij} \equiv \partial_i\partial_j - \frac{1}{3}\delta_{ij}\partial^2$. Here, the divergence parts are separated and described by scalar fields ω and χ for vector and tensor perturbations, respectively. Then, we are left with a divergenceless vector field $\omega^{\perp}$ by the Helmholtz theorem, i.e. $\partial_i\omega^i = 0$. For the tensor, the divergenceless part can be separated further into the longitudinal and transverse parts following the Hodge theorem. Namely, we have the longitudinal vector field $\chi_i^{\perp}$, i.e. ${\chi^{\perp}}^i{}_{,i} = 0$, and the transverse-traceless (TT) tensor field χ_{ij}^{TT}, i.e. $\delta^{ij}\chi_{ij}^{TT} = (\chi^{TT})^{ij}{}_{,i} = 0$. Finally, we have pure scalar (ψ, ϕ, ω, χ), vector ($\omega^{\perp\,i}$, $\chi^{\perp\,i}$), and tensor (χ^{TT}) perturbation modes. This is the so-called *SVT-decomposition* of the perturbation, which is useful to organize the perturbative degrees of freedom into scalar, vector, and tensor kinds. A nice thing about this categorization is each kind of metric perturbation is induced by the matter field of the same kind only. For example, the perturbation on the inflaton field, which is a scalar field, will activate the scalar metric perturbations ψ, ϕ, ω, χ at most.

Let us stop and check if we drop any degrees of freedom (d.o.f.) in the decomposition. Since the metric tensor is a symmetric 4×4 matrix, it has 10 degrees of freedom. These are initially represented by 2 scalars (ψ, ϕ), 1 vector (ω), and 1 symmetric and traceless tensor (χ). After SVT-decomposition, we split the generic vector and tensor into parts, subject to some con-

straint equations. In particular, the divergenceless vector field carries 2 degrees of freedom, having one removed by the constraint $\partial_i \omega^i = 0$. The removed degree of freedom transforms itself into the scalar field ω responsible for the divergence part. Similarly, 5 degrees of freedom of χ got split into 1 scalar (1 d.o.f.), 1 longitudinal vector (2 d.o.f.; 1 d.o.f. removed by ${\chi^{\perp}}^{i}{}_{,i} = 0$), and 1 TT-tensor, (2 d.o.f.; 1 d.o.f. removed by $\delta^{ij}\chi^{TT}_{ij} = 0$ and 3 d.o.f. is removed by $(\chi^{TT})^{ij}{}_{,i} = 0$). In summary, the number of degrees of freedom stays the same; the representations differ.

On the background level, the matter source field is assumed to behave like a perfect fluid (see equation 2.8). Let us rewrite the definition as

$$T_{\mu\nu} = \rho u_\mu u_\nu - P h_{\mu\nu} + \pi_{\mu\nu}, \tag{2.40}$$

where $h_{\mu\nu} = g_{\mu\nu} - u_\mu u_\nu$ is the metric tensor on a hypersurface orthogonal to the fluid velocity, i.e. $h_{\mu\nu}u^\nu = 0$. As a departure from the perfect fluid, $\pi_{\mu\nu}$ is the anisotropic stress tensor. Let us perturb each component of the fluid, including 2 scalars (ρ and P), a 4-vector (u_μ), and a tensor ($\pi_{\mu\nu}$), around the FLRW background. For scalars, we write

$$\begin{aligned} \rho(\boldsymbol{x},\tau) &= \rho_0(\tau) + \delta\rho(\boldsymbol{x},\tau) \quad ; \quad \delta\rho(\boldsymbol{x},\tau) = \sum_{r=1}^{\infty} \frac{1}{r!}\rho^{(r)}(\boldsymbol{x},\tau), \\ P\boldsymbol{x},\tau) &= P_0(\tau) + \delta P(\boldsymbol{x},\tau) \quad ; \quad \delta P(\boldsymbol{x},\tau) = \sum_{r=1}^{\infty} \frac{1}{r!}P^{(r)}(\boldsymbol{x},\tau), \end{aligned} \tag{2.41}$$

where the background quantities are denoted by a subscript "0" and related through the equation of state, $P_0 = w\rho_0$. Assuming that the universe is a thermodynamics system characterised by density (ρ), pressure (P) and entropy (S), the pressure can be written as a function $P = P(\rho, S)$. Thus, the perturbation can be described as

$$\delta P = \left.\frac{\partial P}{\partial \rho}\right|_S \delta\rho + \left.\frac{\partial P}{\partial S}\right|_\rho \delta S = c_s^2 \delta\rho + \delta P_{\text{non-ad}}, \tag{2.42}$$

where $c_s^2 \equiv \left.\frac{\partial P}{\partial \rho}\right|_S$ is the speed of sound and $\delta P_{\text{non-ad}} \equiv \left.\frac{\partial P}{\partial S}\right|_\rho \delta S$ is the non-adiabatic pressure term. A typical choice is $\delta P_{\text{non-ad}} = 0$; the universe is assumed to be an adiabatic system, having zero heat exchange with the environment which leads to a constant entropy. The fluid velocity

is perturbed around the static case in the comoving frame,

$$u^\mu \boldsymbol{x}, \tau) = \frac{1}{a(\tau)}\delta_0^\mu + \delta u^\mu(\boldsymbol{x}, \tau) \quad ; \quad \delta u^\mu(\boldsymbol{x}, \tau) = \frac{v^\mu}{a(\tau)} = \frac{1}{a(\tau)} \sum_{r=1}^{\infty} \frac{1}{r!} v^\mu_{(r)}(\boldsymbol{x}, \tau). \quad (2.43)$$

Let us discuss the degrees of freedom in δu^μ. A generic 4-vector would have 4 degrees of freedom for each component. However, the on-shell condition, $u_\mu u^\mu = 1$, removes 1 d.o.f., e.g. we can express v^0 in terms of the metric perturbations and the spatial components v^i. Hence, 3 d.o.f. are left. We can apply the SVT decomposition to v^i,

$$v^i(\boldsymbol{x}, \tau) = v_{,}{}^i(\boldsymbol{x}, \tau) + v^{\perp\, i}(\boldsymbol{x}, \tau), \quad (2.44)$$

where v is a scalar field whose spatial derivative is the divergence term and $v^{\perp\, i}$ is a divergenceless vector field, $v^{\perp\, i}{}_{i} = 0$. The anisotropic stress tensor is zero on the background level as isotropy is assumed in the FLRW universe. By construction, $\pi_{\mu\nu}$ can be chosen to be traceless and orthogonal to the fluid velocity, i.e. $\pi^\mu_\mu = \pi_{\mu\nu}u^\nu = 0$. This is because its trace and flux parallel to u^μ can be absorbed by ρ and P. Therefore, $\pi_{\mu\nu}$ inherits 5 degrees of freedom ($10 - 5$ from the constraints). The total number of perturbative d.o.f. is 10 as it should be for $T_{\mu\nu}$ which is a symmetric 4×4 matrix.

At the linear order of perturbation, we can fix the components $\pi_{0\mu} = 0$ without losing generality. This can be obtained by considering the orthogonality constraint $\pi_{\mu\nu}u^\nu = 0$ and neglecting the second or higher-order term of perturbations. Hence the perturbation from π is only in the spatial part π_{ij} which can be SVT-decomposed further into

$$\pi_{ij}(\boldsymbol{x}, \tau) = \mathcal{D}_{ij}\pi(\boldsymbol{x}, \tau) + \pi^\perp_{i,j}(\boldsymbol{x}, \tau) + \pi^\perp_{j,i}(\boldsymbol{x}, \tau) + \pi^{TT}_{ij}(\boldsymbol{x}, \tau). \quad (2.45)$$

Also, the on-shell condition on the linear level gives a direct correspondence between perturbations in the zeroth component of fluid velocity and the 00-th component of the metric tensor, $v^0 = \psi$.

2.3.4 Library of Gauges

The generic perturbations on the metric and matter sectors are composed of 10 d.o.f., distributed in the form of scalar, vector, and tensor fields. The ambiguity of perturbations in the GR framework allows us to adjust the value of those perturbations by transforming the gauge. In particular, the infinitesimal transformation of the gauge is translated into the language of

continuous coordinate transformation, altering the perturbation quantitatively. Such a transformation leads to different representations of the d.o.f. where one can choose which perturbations introduced generically to the metric and energy-momentum tensor can be removed. As a result, one will have diverse choices of gauges to fix, each associated with a different picture of how the universe is disturbed from its background.

Let us recall that the gauge transformation 2.36 is invoked by the infinitesimal transformation vector ξ^μ. This translation will be applied to each perturbation introduced in the last section. Mathematically,

$$\delta\tilde{g}_{\mu\nu} = \delta g_{\mu\nu} + \mathcal{L}_\xi g_{\mu\nu} \tag{2.46}$$

for the metric and

$$\delta\tilde{T}_{\mu\nu} = \delta T_{\mu\nu} + \mathcal{L}_\xi T_{\mu\nu} \tag{2.47}$$

for the matter sectors. Each choice of ξ^μ will lead us to a different gauge. A convenient exploitation is to fix some perturbations to zero by this transformation so fewer perturbations are to be dealt with. Hence, let us discuss how many SVT-decomposed perturbative variables we can remove. The transformation source ξ^μ can be decomposed as

$$\xi^\mu = (\xi^0, \xi^i)\ ;\ \xi^i = \xi^{,\,i} + \xi^{\perp\,i}. \tag{2.48}$$

The time component is a scalar (ξ^0) and the spatial component is a 3-vector that can be separated into the derivative of a scalar (ξ) and divergenceless vector field ($\xi^\perp$). Therefore, the gauge transformation can remove up to 2 scalar and 1 divergenceless vector perturbations in the SVT-decomposed picture. The following examples of gauges are characterized by the perturbations that were removed correspondingly.

Poisson Gauge

This gauge is also known as longitudinal or Conformal Newtonian gauge. The choice of this gauge is

$$\tilde{\omega} = \tilde{\chi} = \tilde{\chi}_i^\perp = 0. \tag{2.49}$$

This gauge removes some metric perturbations. In particular, the divergence part of 0μ-components and the divergence and solenoidal parts of ij-components. In other words, the perturbations to the 0μ and ij blocks of the metric are purely (divergenceless) vector and (TT-) tensor, respectively. A useful fact is the geometrical shear, $\sigma = -\omega + \frac{\chi'}{2}$, is zero. Also, the 00- and $0i$-components of the Einstein field equation 2.1 gives us the Poisson equation in FLRW uni-

verse,

$$\nabla^2\phi = 4\pi G a^2 \rho_0 \Delta_m, \tag{2.50}$$

where $\rho_0\Delta_m = \rho_0\delta - 3\mathcal{H}(\rho_0 + P_0)v$. The source of gravitational potential is the comoving density perturbation Δ which is a gauge-invariant variable (we will come back to this later).

Synchronous Gauge

The choice of this gauge is

$$\tilde{\psi} = 0. \tag{2.51}$$

This gauge removes a metric perturbation. In particular, the scalar perturbation on 00-component. Thus, the proper time of an observer at fixed spatial coordinates coincides with the cosmic time of the background FLRW metric. This gauge is often used with the *Orthogonal Gauge* which choose

$$\tilde{\omega} = \tilde{\omega}_i^{\perp} = 0, \tag{2.52}$$

additionally. Together, these two gauges create a picture where a constant-τ (spatial) hypersurface is always orthogonal to the line element of a stationary observer on background FLRW. In particular, the unit time-like vector yields $N^\mu = \frac{1}{a}(1, \mathbf{0})$. This gauge suffers from the residual gauge degree of freedom where the gauge transformation does not fix the degree of freedom completely; more than one choice of ξ^0 leads to $\tilde{\psi} = 0$. Accordingly, it is required to choose an initial function to fix the choice of ξ^0 and keep it in mind throughout the usage of this gauge.

Spatially Flat Gauge

This gauge is also known as the uniform curvature gauge. The choice of this gauge is

$$\tilde{\phi} = \tilde{\chi} = \tilde{\chi}_i^{\perp} = 0. \tag{2.53}$$

This gauge removes some metric perturbations. In particular, the entire perturbation of ij-components except the TT-tensor is removed. Thus, the spatial part of the metric resembles the one of the flat FLRW background metric. Let's consider the 3D-Ricci scalar compute with the first-order-perturbed metric,

$$R_{(3)}(\boldsymbol{x}, \tau) = \frac{6k}{a^2(\tau)} + \frac{12k}{a^2(\tau)}\hat{\phi}(\boldsymbol{x}, \tau) + \frac{4}{a^2(\tau)}\nabla^2\hat{\phi}(\boldsymbol{x}, \tau), \tag{2.54}$$

where $\hat{\phi}(\boldsymbol{x},\tau) = \phi(\boldsymbol{x},\tau) + \frac{1}{6}\nabla^2\chi(\boldsymbol{x},\tau)$ and k is the global curvature parameter introduced in section 2.1.1. In this gauge, $\hat{\phi} = 0$ and $R_{(3)}$ is a constant on a constant-τ hypersurface, hence the name uniform curvature gauge.

Comoving Gauge

The choice of this gauge is

$$\tilde{v} = \tilde{v}_i^{\perp} = 0. \tag{2.55}$$

This gauge removes some perturbations in the matter sector. In particular, the spatial components of the fluid velocity are unperturbed. This can be equipped further with

$$\tilde{\omega} = 0 \tag{2.56}$$

to have the *comoving orthogonal gauge*. In this picture, the fluid 4-velocity is orthogonal to the constant-τ hypersurface. In other words, since the energy density flux (or momentum density) is proportional to $v_i + w_i$, the divergence part of the flux is set to zero by the condition $v + w = 0$. Under this condition, the gauge-invariant comoving density perturbation introduced earlier takes the same form as the density contrast, $\Delta = \delta = \frac{\delta\rho}{\rho_0}$. Hence, the name comoving density perturbation to the gauge-invariant variable.

Uniform Density Gauge

The choice of this gauge is

$$\delta\tilde{\rho} = 0. \tag{2.57}$$

This gauge removes the density perturbation in the matter sector. Notice that another scalar and vector can be fixed to exploit the gauge transformation fully.

These gauge conditions may be limited to fixing 2 scalars and 1 divergenceless vector, but they can also be used with other dynamical requirements that further constrain the system. For example, in the orthogonal comoving gauge, both $v^{\perp}$ and $\omega^{\perp}$ cannot be removed simultaneously but the transformation. However, it can be a dynamic condition that suppresses the vector perturbation entirely. In particular, the absence of dissipation effect by anisotropic tensor implies that the vorticity, i.e. the perpendicular vector perturbations $v^{\perp} + \omega^{\perp}$, conserves along the fluid trajectory. Hence, it is suppressed by the universe's expansion and becomes negligible in the matter-dominated epoch. Another example is the application of the Poisson gauge. Typically, the vector and tensor perturbations are neglected from the picture. This is

possible since the vorticity is suppressed as explained earlier and the TT-tensor perturbation is uncoupled with the scalar part on the linear level. Therefore, with these features, the metric is simplified and perturbed only in the diagonal part with scalars. The anisotropic tensor is neglected (dynamical requirement) and only the divergence part of the fluid velocity exists with the density and pressure perturbations.

2.3.5 Gauge-Invariant Variables

As anticipated, another way to mitigate the gauge problem is to use gauge-invariant variables instead of the bare ones. Let us remind ourselves once again that this discussion is at linear-order gauge transformation. Thus, the variables introduced here are gauge-invariant only up to first-order transformation. The expressions discovered by Bardeen in 1980 [55] are the following.

Scalar Quantities

Let us start with the geometrical variables. The same logic follows where 4 d.o.f. can be reduced to 2 d.o.f. by gauge transformation. Hence, 4 scalar fields are combined into 2 expressions,

$$\begin{aligned} 2\Psi_A &\equiv 2\psi + 2\omega' + 2\frac{a'}{a}\omega - \chi'' + \frac{a'}{a}\chi', \\ 2\Phi_H &\equiv -2\phi - \frac{1}{3}\nabla^2\chi + 2\frac{a'}{a}\omega - \frac{a'}{a}\chi'. \end{aligned} \tag{2.58}$$

These are often called the *Bardeen potentials*. Notice that, in the gauge where $\omega = \frac{1}{2}\chi'$, the potentials reduce to $\Psi_A = \psi$ and $\Phi_H = -\phi - \frac{1}{6}\nabla^2\chi \propto R_{(3)}$ which are the lapse function and proportional to the spatial curvature, respectively.

Alternatively, more gauge-invariant expressions are constructed with the perturbations in the matter sector. The simplest form of velocity potential is

$$2V_s \equiv 2v + \chi'. \tag{2.59}$$

A gauge-invariant expression of density perturbation can be constructed by imagining a constant-τ hypersurface on which the matter lives. For example, we can require that the normal unit vector of the hypersurface, N^μ, always parallel to the fluid worldline; the metric is comoving

with the fluid trajectory. This is the same as writing $v = -\omega$. The expression can be invoked,

$$\Delta_m \equiv \delta\rho + \rho_0'(v + \omega), \tag{2.60}$$

which is called the *comoving-gauge density perturbation* since the expression reduces to the bare density perturbation in the comoving gauge. Notice that this is the same object introduced in the section 2.3.4 but without the Poisson gauge condition. The interpretation is that Δ_m is the perturbation amplitude in the (local) rest frame of the matter fluid. Alternatively, we can think of a hypersurface with no geometrical shear, as close as possible to the Newtonian-like time slicing. For the density perturbation induced on this surface, the gauge-invariant expression is

$$2\Delta_g \equiv 2\delta\rho + \rho_0'(2\omega + \chi'). \tag{2.61}$$

The question of to whether use the first or the latter depends on the preferred interpretation of the density perturbation; $\delta\rho$ can be applied in the comoving gauge or orthogonal zero-shear gauge.

Vector Quantities

The divergence-free vectors can be removed by 1. Hence, the 2 geometrical vector perturbations can be combined into one,

$$\Psi_i = \omega_i^{\perp} - \chi_i^{\perp}, \tag{2.62}$$

which represents the "frame-dragging" present in the Lense-Thirring effect for example. Another possibility which involves fluid velocity is

$$V_c^i = v_{\perp}^i + \left(\chi_{\perp}'\right)^i, \tag{2.63}$$

which is associated with the vorticity tensor of the fluid,

$$\omega_{\mu\nu} \equiv \frac{1}{2} h_\mu{}^\rho (u_{\rho;\sigma} - u_{\sigma;\rho}) h^\sigma{}_\nu, \tag{2.64}$$

where ";" denotes the covariant derivative and h is the metric tensor of a hypersurface orthogonal to the fluid velocity.

Tensor Quantities

Since the background metric has no TT-tensor part and the background perfect fluid is isotropic, the gauge transformation in linear order does not change the perturbations. Hence, χ_{ij}^{TT} and $\pi_{\mu\nu}$ are already gauge-invariant variable on the linear level.

2.4 Initial Condition From Inflation

One of the crucial predictions of inflation is the generation of initial inhomogeneity. This cosmic density fluctuation served as a seed for gravity to form the subsequent structure in our universe. The lack of this unevenness would result in a homogenized universe which is highly contradictory to the observation nowadays. Inflation explains that the quantum behaviour of the inflaton field is responsible for this initial perturbation. The ground-state fluctuation of the field was invoked in the early stage and stretched by the accelerated expansion later on. At that point, the field transits from quantum to classical state while preserving the quantum mechanically generated perturbation. These classical modes encoded themselves in the form of spatial curvature perturbation and became the seed of the Hot Big Bang era later on. This major process allows us to learn about inflation from the large-scale structure probe we can perform these days. This section will show how these fluctuations are produced.

2.4.1 Inflaton Perturbation On Flat Space-time

Let us recall the inflaton action 2.19 minimally coupled with gravity,

$$S = \int d\tau d^3x \sqrt{-g}\Big[\frac{M_{pl}^2}{2}R + \frac{1}{2}g^{\mu\nu}\partial_\mu\varphi\partial_\nu\varphi - V(\varphi)\Big]. \tag{2.65}$$

The key idea is to perturb the field with a small inhomogeneity, $\delta\varphi(\boldsymbol{x},\tau)$, on top of the homogeneous background field, $\varphi_0(\tau)$, as

$$\varphi(\boldsymbol{x},\tau) = \varphi_0(\tau) + \delta\varphi(\boldsymbol{x},\tau). \tag{2.66}$$

Then, we will study the dynamics of the perturbation during inflation to quantify the fluctuation once the field is quantized. However, GR requires us to equally perturb the space-time since any change in the matter sector will induce some variation in the geometry as well. In particular, the metric perturbations must be taken into account. Let us recall the metric per-

turbations under SVT decomposition (see equation 2.37 and 2.39),

$$\begin{aligned} g_{00} &= a^2(\tau)\,(1+2\psi)\,, \\ g_{i0} &= a^2(\tau)\left(\omega_{,i}+\omega_i^{\perp}\right) = g_{0i}, \\ g_{ij} &= a^2(\tau)\left[(-1+2\phi)\,\delta_{ij}+\mathcal{D}_{ij}\chi+\chi^{\perp}_{i,j}+\chi^{\perp}_{j,i}+\chi^{TT}_{ij}\right], \end{aligned} \tag{2.67}$$

where the argument $(\boldsymbol{x},\tau)$ is omitted for clarity. As discussed in the section 2.3.4, we can choose a gauge to simplify the calculation in a way that suits our focus. Here, we want to study the quantum behaviour of the inflaton field. For this purpose, it is convenient to work in the spatially flat gauge so that the scalar and the solenoidal vector perturbations in the spatial part of the metric are zero, $\phi = \chi = \chi^{\perp} = 0$. Additionally, more dynamical requirements are imposed in this simplest inflation model with one scalar field. First of all, the anisotropic stress is absent in this model, i.e. $\pi_{\mu\nu} = 0$; the only matter source is the inflaton field. Hence, the vector perturbations die quickly with the rapid expansion and are negligible. Then, the metric is reduced to

$$g_{00} = a^2(\tau)(1+2\psi)\ ,\ g_{i0} = g_{0j} = 0\ ,\ g_{ij} = a^2(\tau)\left(-\delta_{ij}+\chi^{TT}_{ij}\right). \tag{2.68}$$

For simplicity, we will assume $\psi = 0$ for now. This gives us a completely flat space-time which is an oversimplification. However, the resulting equation of motion will be the same with a slight modification which we will explain later.

Finally, in a linear regime, the equation of motion obtained for the TT-tensor is decoupled from the scalar part and propagates freely without the source term. Therefore, its presence is irrelevant to the discussion of scalar field dynamics. So, we neglect it for now. In conclusion, we have a flat FLRW metric in this gauge which is practically the same as the background space-time. Let us now proceed to perturb the action 2.65 and define a new variable, $u(\boldsymbol{x},\tau) = a(\tau)\delta\varphi(\boldsymbol{x},\tau)$. The result up to the second order in action is

$$\begin{aligned} S &= S^{(0)} + S^{(1)} + S^{(2)} \\ S^{(0)} &= \int d\tau d^3x \Big[\frac{1}{2}a^2(\varphi_0')^2 - a^4 V(\varphi_0)\Big] \\ S^{(1)} &= -\int d\tau d^3x\ a\Big[\varphi_0'' + 2\mathcal{H}\varphi_0' + a^2 V_{,\varphi}\Big]u \\ S^{(2)} &= -\int d\tau d^3x \Big[(u')^2 - (\nabla u)^2 + \left(\frac{a''}{a} - a^2 V_{,\varphi\varphi}\right)u^2\Big], \end{aligned} \tag{2.69}$$

where we have neglected the gravity action term for simplicity. Since space-time appeared unperturbed in this gauge, the metric has no perturbative dynamic to be discussed. If we include $\frac{M_{pl}^2}{2}R$ and vary the action concerning the scale factor, $a(\tau)$, the usual Friedmann equations 2.10 and 2.11 will be obtained. The zeroth-order action $S^{(0)}$ leads to the Klein-Gordon equation 2.20 as expected for the background dynamics. Consequently, the first-order action $S^{(1)}$ becomes zero. The linearized equation of motion of u can be obtained by varying the second-order action. The result is

$$u''(\boldsymbol{x},\tau) - \nabla^2 u(\boldsymbol{x},\tau) - \left(\frac{a''}{a} - a^2 V_{,\varphi\varphi}\right) u(\boldsymbol{x},\tau) = 0. \tag{2.70}$$

As a classical field, we can write the Fourier transformation of $u(\boldsymbol{x},\tau)$ as

$$u_{\boldsymbol{k}}(\tau) = \int d^3x \; u(\boldsymbol{x},\tau) e^{i\boldsymbol{k}\cdot\boldsymbol{x}}, \tag{2.71}$$

and the equation of motion in Fourier space reads

$$u''_{\boldsymbol{k}}(\tau) + \left(k^2 - \frac{a''}{a} + a^2 V_{,\varphi\varphi}\right) u_{\boldsymbol{k}}(\tau) = 0. \tag{2.72}$$

Note that the 3D Fourier transform is applied only to the spatial coordinates since the metric varies with time. The fact that we are working in the spatially flat gauge allows us to have flat spatial hypersurfaces at each constant time. In this case, expanding the perturbation with plane waves is possible. Otherwise, it must be replaced with the generalized solution of the Helmholtz equation,

$$\nabla^2_{cov} O_{\boldsymbol{k}} + k^2 O_{\boldsymbol{k}} = 0, \tag{2.73}$$

where ∇^2_{cov} is the Laplacian from covariant derivative. Notice that the operator reduces to ordinary Laplacian with flat space where the general solution would be plane waves as anticipated. This is one of the reasons why working in the spatially flat gauge is convenient for this discussion.

2.4.2 Classical Solutions of Inflaton Perturbation

Before translating the discussion into the context of the quantum fields, let us solve the equation of motion to understand the behaviour of the perturbation at different limits. In particular, the terms in the parenthesis of equation 2.72 suggest distinct behaviours of the field with

large and small wave numbers. From now on, we address 2 limiting scales; the *superhorizon limit* is where $k \ll \mathcal{H}$ and the *subhorizon limit* is where $k \gg \mathcal{H}$. To understand how these limits approximate the equation, let us manipulate it into a simpler form. The definitions of the slow-roll parameter ϵ and the (conformal) Hubble parameter (see equation 2.24 and 2.14) leads to

$$\epsilon = -\frac{\mathcal{H}'}{\mathcal{H}^2} = -\frac{1}{\mathcal{H}^2}\left(\frac{a'}{a}\right)' \longrightarrow \frac{a''}{a} = \mathcal{H}^2(2-\epsilon). \tag{2.74}$$

Furthermore, the second derivative of the potential with respect to the field is associated with the (potential) slow-roll parameter η_V (see equation 2.27) as

$$\eta_V = M_{pl}^2 \frac{V_{,\varphi\varphi}}{V} = \frac{V_{,\varphi\varphi}}{3H^2}\left(1-\frac{\epsilon}{3}\right)^{-1} \longrightarrow a^2 V_{,\varphi\varphi} = \mathcal{H}^2\eta_V(3-\epsilon), \tag{2.75}$$

where the Friedmann equations and scalar field energy density and pressure (2.10, 2.11, 2.22, 2.23) are implicitly used. An important remark is the second derivative of the potential is interpreted as an effective mass of the field, $V_{,\varphi\varphi} = m_\varphi^2$. Thus, the exact manipulation of the equation results in

$$u_{\boldsymbol{k}}''(\tau) + \left[k^2 - \mathcal{H}^2(\tau)(2-\epsilon+3\eta_V-\eta_V\epsilon)\right] u_{\boldsymbol{k}}(\tau) = 0. \tag{2.76}$$

During inflation, we expect the absolute value of the slow-roll parameters to be much less than 1. Therefore, the scale of the second term in the parentheses is pretty much determined by $\mathcal{H}$. The dependence on time is explicitly shown for $\mathcal{H}$ to emphasize that the presence of it makes the solution non-trivial.

Subhorizon limit

Let us consider the equation at the subhorizon scale, to begin with. In this case, the wave number dominates the size of the horizon, $k \gg \mathcal{H}$, and the equation can be approximated to the case of free-propagating plane waves,

$$u_{\boldsymbol{k}}''(\tau) + k^2 u_{\boldsymbol{k}}(\tau) = 0. \tag{2.77}$$

The normalized solution of this equation is well-known; it is

$$u_{\boldsymbol{k}}(\tau) = \frac{1}{\sqrt{2k}} e^{-ik\tau}, \tag{2.78}$$

where only the positive frequency solution is kept for the reason that will become clear when we quantize the field. This solution is simple also for the fact that the frequency is the same as the wave number; the field is effectively massless on a small scale seeing from the dispersion relation, $\omega_k^2 = k^2 + \cancelto{0}{m^2}$, regardless of the detailed structure of the field's potential. Hence, this solution holds for various models of inflation as long as the field is slow-rolling.

Superhorizon limit

For the superhorizon limit, the time-dependent part of the equation dominates the constant wave number. For a rough analysis now, let us go back to the previous form of the equation of motion 2.72. We know that the second derivative of the potential is at least the first order of the slow-roll parameter while $\frac{a''}{a}$ term is directly scaled as the horizon size. Thus, we neglect the potential term and the wave number and limit this discussion to the flat potential and superhorizon limits. In this case, we have

$$u_{\boldsymbol{k}}''(\tau) + \frac{a''}{a} u_{\boldsymbol{k}}(\tau) = 0. \tag{2.79}$$

The solution of this equation can be found in the power-law form of $a(\tau)$ as

$$u_{\boldsymbol{k}}(\tau) = A(k)a(\tau) + B(k)a^{-2}(\tau), \tag{2.80}$$

where $A(k)$ and $B(k)$ are functions of wave number as coefficients of growing and decaying modes, respectively. Recall that this perturbation relates to the actual field perturbation as $u_{\boldsymbol{k}}(\tau) = \delta a(\tau)\varphi_{\boldsymbol{k}}(\tau)$. Hence, the superhorizon evolution of the inflaton field perturbation is

$$\delta\varphi_{\boldsymbol{k}}(\tau) = A(k) + \cancelto{\text{decays}}{B(k)a^{-3}(\tau)} \approx A(k). \tag{2.81}$$

The expansion suppresses the decaying mode rapidly and the field perturbation becomes frozen in time. This result can be explained intuitively by the fact that the large-scale perturbation cannot be interfered with by any local physics going on within the horizon. The causality of physics requires that the interaction range between physical bodies must be well-contained in the Hubble sphere. Therefore, the perturbation on a scale much larger than that will remain unaltered regardless of what is happening within the horizon. However, as mentioned before, this is true only in the flat potential case and a more detailed analysis will show us that the solution can be slightly time-dependent up to the correction by the slow-roll parameter.

2.4.3 General Solutions in Quasi de-Sitter Spacetime

To find a general time-dependent solution to the perturbation, we have to write the coefficient of the equation 2.76 in terms of τ. In particular, the time evolution of the Hubble parameter during inflation can be written up to the linear order of the slow-roll parameter as

$$\mathcal{H}(\tau) \approx -\frac{1}{(1-\epsilon)\tau} \longrightarrow \mathcal{H}^2(\tau) \approx \frac{1}{\tau^2}(1+2\epsilon). \tag{2.82}$$

Therefore, the equation of motion can be approximated up to the linear order as

$$u''_{\boldsymbol{k}}(\tau) + \left[k^2 - \frac{2}{\tau^2}\left(1 + \frac{3}{2}\epsilon + \frac{3}{2}\eta_V\right)\right] u_{\boldsymbol{k}}(\tau) \approx 0. \tag{2.83}$$

Before proceeding from this point, the oversimplification must be lifted. As we have mentioned before, this analysis is oversimplified by the fact that we assume $\psi = 0$. The instalment of such a perturbative variable would have modified the action and given a different equation of motion for the inflaton perturbation. However, ψ is not a new degree of freedom but depends on $\delta\varphi'$ through the energy constraint from Einstein's Equation. Hence, the coupling term(s) between ψ and the inflaton field can be reorganized to obtain the usual form of the second-order action. The resulting modification is in the effective mass term, changing the coefficient of the slow-roll parameters.

Indeed, one can find the same equation of motion by choosing a different gauge. [17] decomposed the metric with Arnowitt–Deser–Misner (ADM) formalism instead of SVT formalism we used here and chose the comoving gauge. There, the scalar degree of freedom is parameterized with the spatial curvature perturbation, ζ (equivalent to ϕ in this thesis), and the field perturbation is gauged out. The equation of motion took the same form along with the following predictions. Alternatively, perhaps the most general, a gauge-invariant variable can be constructed. [56, 57] introduced the *Mukhanov-Sasaki variable* Q^φ that mixes the scalar field perturbation and spatial curvature perturbation,

$$Q^\varphi \equiv \delta\varphi + \frac{\varphi}{\mathcal{H}}\phi. \tag{2.84}$$

Then we can define $u_{\boldsymbol{k}}(\tau) \equiv \frac{Q^\varphi_{\boldsymbol{k}}(\tau)}{a(\tau)}$ in Fourier space and find the equation of motion of it like

before. The result would be

$$u_{\boldsymbol{k}}''(\tau) + \left[k^2 - \frac{2}{\tau^2}\left(1 + \frac{9}{2}\epsilon - \frac{3}{2}\eta_V\right)\right] u_{\boldsymbol{k}}(\tau) \approx 0, \tag{2.85}$$

where the only difference from the previous result is the expression in the parentheses. This gauge-invariant representation is more compromised when we discuss the translation of perturbation out of inflation. We expect the energy in the inflaton to decay into the standard model sector and reheat the universe after inflation. However, the perturbation on a superhorizon scale remains constant without decaying as explained before (see section 2.4.2). Hence, it is more feasible to think that the classical perturbation is saved as curvature perturbation after crossing the horizon and becomes the universe's inhomogeneity even if the inflaton field does not contribute to the energy budget anymore. Therefore, the Mukhanov-Sasaki variable is not only working on the subhorizon limit where the space is effectively flat and the field is fluctuating by quantum mechanics but also on the superhorizon limit where it becomes classical curvature perturbation.

With this level of approximation, the slow-roll parameters will be treated as constants. This is because their runnings are at the next order of perturbation. Hence, the equation can be written as *Bessel equation*,

$$u_{\boldsymbol{k}}''(\tau) + \left[k^2 + \frac{\nu^2 - \frac{1}{4}}{\tau^2}\right] u_{\boldsymbol{k}}(\tau) \approx 0, \tag{2.86}$$

by letting $\nu^2 = \frac{9}{4} + 9\epsilon - 3\eta_V$. To be precise, the usual form of the Bessel equation,

$$z^2 y''(z) + z y'(z) + \left(z^2 - \nu^2\right) y(z) = 0, \tag{2.87}$$

is obtained by letting $z = k\tau$ and $y(z) = u_{\boldsymbol{k}}(\tau)/\sqrt{\tau}$. Therefore, the exact solution is the linear combination of the Hankel functions of the first and second kinds, $H_\nu^{(1)}$ and $H_\nu^{(2)}$,

$$u_{\boldsymbol{k}}(\tau) = \sqrt{-\tau}\left[c_1(k) H_\nu^{(1)}(-k\tau) + c_2(k) H_\nu^{(2)}(-k\tau)\right], \tag{2.88}$$

where c_1 and c_2 are the coefficients that are found by matching to the subhorizon solution. Looking at the time evolution of the Hubble parameter discussed above, the parameter shrinks as inflation proceeds (conformal time increases from $-\infty$). Hence, this generic solution must return the subhorizon solution at the limit $-k\tau \longrightarrow \infty$, when the fluctuation is deep in the

horizon. In this case, the Hankel functions are approximately

$$H_\nu^{(1)}(-k\tau) \approx \sqrt{\frac{2}{-\pi k\tau}} e^{-i\left(k\tau+\frac{\pi}{2}\nu+\frac{\pi}{4}\right)} \quad \& \quad H_\nu^{(2)}(-k\tau) \approx \left(H_\nu^{(1)}(-k\tau)\right)^*. \tag{2.89}$$

The fact that we chose only the positive frequency solution for the subhorizon limit enforces $c_2 = 0$. Then, only c_1 is fixed with the normalization factor. The final solution reads

$$u_{\boldsymbol{k}}(\tau) = \frac{\sqrt{\pi}}{2}(-\tau)^{\frac{1}{2}} e^{i\frac{\pi}{2}\left(\nu+\frac{1}{2}\right)} H_\nu^{(1)}(-k\tau). \tag{2.90}$$

While we are at it, let us explore this exact solution's superhorizon limit and compare it to our previous analysis. Opposing to the subhorizon case, we will now consider the limit $-k\tau \longrightarrow 0$. In this limit, the Hankel function of the first kind is approaching the form,

$$H_\nu^{(1)}(-k\tau) \approx \sqrt{\frac{2}{\pi}} e^{-i\frac{\pi}{2}} 2^{\nu-\frac{3}{2}} \left(\frac{\Gamma(\nu)}{\Gamma(3/2)}\right) (-k\tau)^{-\nu}, \tag{2.91}$$

where Γ is the gamma function. This leads to the superhorizon solution,

$$u_{\boldsymbol{k}}(\tau) = \frac{1}{\sqrt{2k}}(-k\tau)^{\frac{1}{2}-\nu} \left(e^{i\frac{\pi}{2}\left(\nu-\frac{1}{2}\right)} 2^{\nu-\frac{3}{2}} \left(\frac{\Gamma(\nu)}{\Gamma(3/2)}\right)\right). \tag{2.92}$$

We can reinstall the scale factor to obtain the actual inflaton perturbation. We can exploit the approximation 2.82 to trade $a(\tau)$ with the (physical) Hubble parameter and conformal time while neglecting the correction from ϵ, i.e. $\tau \approx -(aH)^{-1}$. Recall that $\nu^2 = \frac{9}{4} + 9\epsilon - 3\eta_V$ so that $\nu = \frac{3}{2} + 3\epsilon - \eta_V + \mathcal{O}(2)$. Hence, the leading order of this solution can be obtained by assuming $2^{\nu-\frac{3}{2}} \approx \frac{\Gamma(\nu)}{\Gamma(3/2)} \approx 1$. Thus, the leading perturbation amplitude is

$$|\delta\varphi_{\boldsymbol{k}}(\tau)| = \frac{\sqrt{u_{\boldsymbol{k}}^* u_{\boldsymbol{k}}}}{a} = \frac{H}{\sqrt{2k^3}} \left(\frac{k}{\mathcal{H}}\right)^{\eta-2\epsilon}, \tag{2.93}$$

where we trade τ with $\mathcal{H}$ and ν back to the slow-roll parameters to associate this prediction with the features of inflation. Let us also recall the relation $\eta_V \approx \epsilon + \eta$. It is clear how the characteristics of space and field influence this prediction, the expansion rate and the mass of the inflaton field in particular. First of all, the fluctuation magnitude depends directly on the Hubble parameter, which reflects the energy scale of inflation (see Friedmann equation 2.10). Second of all, the running of the amplitude with the ratio $\frac{k}{\mathcal{H}}$ is introduced by the non-zero

slow-roll parameters. In the simplest case, one may assume a massless inflaton in perfect de Sitter space where the space eternally and exponentially expands. The amplitude loses the sense of comparison between itself and the Hubble horizon since the potential is flat and the space-time is conformal. Therefore, the dynamics are unchanged and the fluctuation becomes scale-invariant[1]. Nevertheless, this case is oversimplified since the expansion cannot be perfect de Sitter, otherwise the inflation will not end. Instead, a slight deviation is allowed where the universe slowly moves away from perfect de Sitter space; we have quasi-de Sitter expansion where the slow-roll parameters are small but nonzero. In this case, we retrieve the scale-dependence in the form of $\left(\frac{k}{\mathcal{H}}\right)^{-3\epsilon}$.

2.4.4 Quantum Fluctuations of Inflaton Field

The previous section has explained the evolution of the field fluctuations at different limits. The next question would be the origin of it. As already mentioned, the quantum behaviour of the field is significant in inflation. In this case, the fluctuation is probabilistic due to quantum uncertainty [58, 59, 60, 61]. Therefore, one should consider the statistics of the field rather than the deterministic classical picture. Intuitively, the rapid expansion stretched the quantum fluctuation of the field out. Then, these fluctuations curve the space-time creating the curvature perturbations. Thus, the quantum fluctuations of the field are the origin of the primordial fluctuations in inflation. As we mentioned before, the fluctuations are fully frozen at the superhorizon limit. These fluctuations should become classical at this limit. Thus, they become the classical fluctuations that seed the structure of the universe. Here, the statistics of the quantum fluctuations will be computed and show that it indeed becomes classical before inflation ends.

Field Quantization

To discuss the quantum behaviours, we must translate the classical description of the field into the language of quantum field theory. In particular, the inflaton field is promoted to a field operator and expanded with the creation and annihilation operators,

$$\hat{u}(\boldsymbol{x},\tau) = \int \frac{d^3k}{(2\pi)^3}\left[u_k(\tau)a_{\boldsymbol{k}}e^{i\boldsymbol{k}\cdot\boldsymbol{x}} + u_k^*(\tau)a_{\boldsymbol{k}}^\dagger e^{-i\boldsymbol{k}\cdot\boldsymbol{x}}\right], \tag{2.94}$$

[1] Notice that the k-dependence in the normalization factor is because the field is in Fourier space. The resulting variance in real space is scale-invariant.

where $u_k(\tau)$ and $u_k^*(\tau)$ are the classical solution obtained in the last section and its complex conjugate. The actual inflaton fluctuation is also promoted to an operator parallel to this by $\delta\hat{\phi} = \hat{u}/a(\tau)$. Notice that the subscript turns to k to indicate that the solution depends only on the magnitude of the wave vector and not the direction of it. We also define the conjugate momentum field by

$$\pi \equiv \frac{\partial \mathcal{L}}{\partial u} = u', \tag{2.95}$$

where $\mathcal{L}$ is the inflaton lagrangian (see action 2.19), and promote it to a quantum operator,

$$\hat{\pi}(\boldsymbol{x}, \tau) = \int \frac{d^3k}{(2\pi)^3} \left[u_k'(\tau) a_{\boldsymbol{k}} e^{i\boldsymbol{k}\cdot\boldsymbol{x}} + (u_k'(\tau))^* a_{\boldsymbol{k}}^\dagger e^{-i\boldsymbol{k}\cdot\boldsymbol{x}} \right]. \tag{2.96}$$

For canonical quantization, we invoke the commutation relations of creation and annihilation operators,

$$[a_{\boldsymbol{k}}, a_{-\boldsymbol{k'}}] = [a_{\boldsymbol{k}}^\dagger, a_{-\boldsymbol{k'}}^\dagger] = 0 \ ; \ [a_{\boldsymbol{k}}, a_{-\boldsymbol{k'}}^\dagger] = (2\pi)^3 \delta_D^{(3)}(\boldsymbol{k} + \boldsymbol{k'}), \tag{2.97}$$

where we use the convention $\hbar \equiv 1$. We can choose the normalization of the fields to satisfy the equal-time commutation relations,

$$[\hat{u}_{\boldsymbol{k}}(\tau), \hat{\pi}_{\boldsymbol{k'}}(\tau)] = i\delta_D^{(3)}(\boldsymbol{k} + \boldsymbol{k'}). \tag{2.98}$$

where the fields in Fourier space are written as

$$\begin{aligned} \hat{u}_{\boldsymbol{k}}(\tau) &= u_k(\tau) a_{\boldsymbol{k}} + u_k^*(\tau) a_{-\boldsymbol{k}}^\dagger, \\ \hat{\pi}_{\boldsymbol{k'}}(\tau) &= u_k'(\tau) a_{\boldsymbol{k}} + (u_k'(\tau))^* a_{-\boldsymbol{k}}^\dagger \end{aligned} \tag{2.99}$$

which means we must have the *Wronskian* of the mode functions that satisfies

$$W[u_k(\tau), u_k^*(\tau)] \times [a_{\boldsymbol{k}}, a_{-\boldsymbol{k'}}^\dagger] = \delta_D^{(3)}(\boldsymbol{k} + \boldsymbol{k'}), \tag{2.100}$$

where

$$W[u_k(\tau), u_k^*(\tau)] = -i(u_k(\tau)(u_k^*(\tau))' - u_k'(\tau) u_k^*(\tau)). \tag{2.101}$$

For the chosen commutation relations 2.97, it is required that $W[u_k(\tau), u_k^*(\tau)] = 1$ which fixes the normalization of the mode function $u_k(\tau)$. Notice that the positive-frequency-only solution (see equation 2.78) satisfies this normalization condition but is not the only one.

To build a system of energy level, the ground state must be defined. For a quantum field, the interpretation is the vacuum state is the ground state, having minimal excitation. Typically, the vacuum state is defined as a state that vanishes upon the application of the annihilation operator,

$$a_{\boldsymbol{k}} \left|0\right\rangle = 0. \tag{2.102}$$

Then, the excited quantum states in the Fock space are constructed by repeatedly applying the creation operators on the vacuum state,

$$\left|m_{\boldsymbol{k_1}}, n_{\boldsymbol{k_2}}, \ldots\right\rangle = \frac{1}{\sqrt{m!n!\ldots}} \left[\left(a^\dagger_{\boldsymbol{k_1}}\right)^m \left(a^\dagger_{\boldsymbol{k_2}}\right)^n\right]. \tag{2.103}$$

However, there is an ambiguity in the definition of creation and annihilation operators. Let us consider the mode expansion of the field operator 2.94 once again. We can define a new set of operators, $b_{\boldsymbol{k}}$ and $b^\dagger_{\boldsymbol{k}}$, that can be written as linear combinations of $a_{\boldsymbol{k}}$ and $a^\dagger_{\boldsymbol{k}}$,

$$\begin{aligned} b_{\boldsymbol{k}} &= \alpha_k a_{\boldsymbol{k}} + \beta^*_k a^\dagger_{-\boldsymbol{k}}, \\ b^\dagger_{\boldsymbol{k}} &= \alpha^*_k a^\dagger_{\boldsymbol{k}} + \beta_k a_{-\boldsymbol{k}}. \end{aligned} \tag{2.104}$$

Since the mode functions $u_k(\tau)$ is a solution from a linear differential equation, its linear combination is also a solution. Therefore, the field operator can also be expanded with this new set of creation and annihilation operators with a new mode function,

$$v_k(\tau) = \alpha_k u_k(\tau) + \beta_k u^*_k(\tau), \tag{2.105}$$

where the Wronskian condition, $W[v_k(\tau), v^*_k(\tau)] = 1$, fixes the normalization factor to $\left|\alpha_k\right|^2 - \left|\beta_k\right|^2 = 1$. Notice that even if $u_k(\tau)$ is chosen to have positive frequency only, the new mode function can be a mixture between both positive- and negative-frequency modes. As a result, we translate ourselves to a new set of mode functions and operators, from $a_{\boldsymbol{k}}$ and u_k to $b_{\boldsymbol{k}}$ and v_k, while keeping the field operator invariant. This is the so-called *Bogoliubov transformation* where α_k and β_k are the Bogoliubov coefficients. The issue is different creation and annihilation operators lead to different vacuum states which are not a vacuum of each other. For example,

$$\left\langle 0_{(b)}\right| b^\dagger_{\boldsymbol{k}} b_{\boldsymbol{k}} \left|0_{(b)}\right\rangle = 0 \text{ while } \left\langle 0_{(a)}\right| b^\dagger_{\boldsymbol{k}} b_{\boldsymbol{k}} \left|0_{(a)}\right\rangle \propto \left|\beta_k\right|^2. \tag{2.106}$$

Hence, the vacuum state of such a system is ambiguous and must be chosen as the system's ground state.

However, this is not the only issue. The fact that the dynamics of the field are discussed on a time-dependent background makes the definition of the vacuum state ambiguous. In particular, the amplitude of the general solution 2.88 is time-dependent thus the normalization condition $W[v_k(\tau), v_k^*(\tau)] = 1$ does not hold for every moment. Hence, we must also choose the time slice on which the normalized mode function and its associated annihilation operator are used to define the vacuum state of the system.

With this freedom, the preferable choice is the so-called *Bunch-Davies vacuum* [62] where the vacuum state at the beginning of inflation, $\tau \longrightarrow -\infty$. This corresponds to the subhorizon scale evolution where the space is approximately flat. For simplicity, we also keep only the positive frequency mode for the solution. These choices completely fix the vacuum state as a ground state of inflation where the normalized mode function is given by the solution 2.78 obtained previously.

Zero-point Mean and Variance of The Field

Now that we have the quantized field operator and its ground state, the expectation values can be computed that will characterise the statistics of the classical perturbation arising from this quantum behaviour. Let us start with the mean of this fluctuation, $\langle \delta\hat{\varphi} \rangle$. It must be zero by definition since the perturbation is defined as a deviation around the mean value of the field. Indeed, if one computes the expectation value, one finds the result,

$$\langle 0 | \, \hat{\varphi}(\boldsymbol{x}, \tau) \, | 0 \rangle = \frac{1}{a(\tau)} \langle 0 | \, \hat{u}(\boldsymbol{x}, \tau) \, | 0 \rangle = 0, \tag{2.107}$$

by the definition of the vacuum state and the orthogonality of the quantum state. However, the variance is nonzero. It is defined as $var\,[\delta\hat{\varphi}] = \langle \delta\hat{\varphi}^2 \rangle - \langle \delta\hat{\varphi} \rangle^2$. Since the mean is zero, the variance is directly equal to the expectation value of the squared field operator. For generality,

let us compute the expectation value of a product field at separation $\boldsymbol{r}$,

$$\begin{aligned}\xi_{\delta\varphi}(r) &\equiv \langle 0|\, \delta\hat{\varphi}^{\dagger}(\boldsymbol{x},\tau)\delta\hat{\varphi}(\boldsymbol{x}+\boldsymbol{r},\tau)\,|0\rangle \\ &= \frac{1}{a^2(\tau)}\int\frac{d^3k}{(2\pi)^3}\int\frac{d^3k'}{(2\pi)^3}e^{i\boldsymbol{k}\cdot(\boldsymbol{x}+\boldsymbol{r})}e^{-i\boldsymbol{k'}\cdot\boldsymbol{x}}u_k(\tau)u^*_{k'}(\tau)\,\langle 0|\,[\hat{a}_{\boldsymbol{k}},\hat{a}^{\dagger}_{\boldsymbol{k'}}]\,|0\rangle \\ &= \frac{1}{a^2(\tau)}\int\frac{d^3k}{(2\pi)^3}\int\frac{d^3k'}{(2\pi)^3}e^{i(\boldsymbol{k}-\boldsymbol{k'})\cdot\boldsymbol{x}}|u_k(\tau)|^2(2\pi)^3\delta^{(3)}_D(\boldsymbol{k}-\boldsymbol{k'})e^{i\boldsymbol{k'}\cdot\boldsymbol{r}} \\ &= \frac{1}{a^2(\tau)}\int\frac{d^3k}{(2\pi)^3}|u_k(\tau)|^2e^{i\boldsymbol{k}\cdot\boldsymbol{r}}.\end{aligned} \tag{2.108}$$

From this expression, the power spectrum can be defined as $P_u(k,\tau) = |u_k(\tau)|^2$ which relates to the power spectrum of $\delta\varphi$ as

$$P_{\delta\varphi}(k,\tau) = |\delta\varphi_k(\tau)|^2 = \frac{P_u(k,\tau)}{a^2(\tau)}. \tag{2.109}$$

The quantity $\xi_{\delta\varphi}(r)$ is the two-point correlation function of the inflaton field where we have found that its Fourier counterpart is the power spectrum $P_{\delta\varphi}(k)$. Alternatively, the power spectrum can be defined through the correlation function in Fourier space,

$$\langle\delta\varphi_{\boldsymbol{k}}\delta\varphi^*_{\boldsymbol{k'}}\rangle = \langle 0|\,\delta\hat{\varphi}_{\boldsymbol{k}}\delta\hat{\varphi}^{\dagger}_{\boldsymbol{k'}}\,|0\rangle = (2\pi)^3\delta^{(3)}_D(\boldsymbol{k}-\boldsymbol{k'})P_{\delta\varphi}(k). \tag{2.110}$$

Notice that both functions are isotropic in each space; they depend on the magnitude of r and k only. This is because inflaton is a scalar field so its perturbation has no preferred direction. Thus, the mode function $u_k(\tau)$ is isotropic, hence the power spectrum and the two-point correlation function. The variance of inflaton fluctuation is the two-point function with zero separation, $r = 0$. Hence, it is just a Fourier-space-volume integration over the power spectrum,

$$var\,[\delta\hat{\varphi}] = \left\langle\delta\hat{\varphi}^2\right\rangle = \int\frac{d^3k}{(2\pi)^3}P_{\delta\varphi}(k) = \int d\ln k\Delta_{\delta\varphi}(k), \tag{2.111}$$

where the dimensionless power spectrum is defined as $\Delta_{\delta\varphi}(k) \equiv \frac{k^3}{2\pi^2}P_{\delta\varphi}(k)$ which reflects the scale dependence of the field's variance. Let us compute the quantity at different times during inflation. From the solutions 2.78 and 2.93, the power spectrum on the subhorizon

and superhorizon scales are

$$\left(\frac{H}{2\pi}\right)^2 \xleftarrow{-k\tau\longrightarrow\infty} \Delta_{\delta\varphi}(k,\tau) \xrightarrow{-k\tau\longrightarrow 0} \left(\frac{H}{2\pi}\right)^2 \left(\frac{k}{\mathcal{H}}\right)^{2\eta-4\epsilon}. \tag{2.112}$$

To relate this prediction to the observable nowadays, it is useful to translate this into the statistics of curvature perturbation through the definition of a gauge-invariant variable, Mukhanov-Sasaki variable (see definition 2.84). In particular, the field fluctuation in spatially flat gauge is related to the curvature perturbation in comoving gauge as

$$\phi = -\frac{\mathcal{H}}{\varphi_0'}\delta\varphi. \tag{2.113}$$

With this, a new gauge-invariant variable can be constructed; the conserved curvature perturbation is defined as

$$\zeta \equiv -\phi - \mathcal{H}\frac{\delta\rho}{\rho_0'} = -\phi - \frac{\mathcal{H}}{\varphi_0'}\delta\varphi. \tag{2.114}$$

This quantity is more direct for interpreting the fluctuation that translated out of inflation since the curvature is where the perturbation got imprinted after inflation ended. The power spectrum of this quantity is then related to the field in spatially flat gauge as

$$\Delta_\zeta(k,\tau) = \left(\frac{\mathcal{H}}{\varphi_0'}\right)^2 \Delta_{\delta\varphi} \xrightarrow{-k\tau\longrightarrow 0} \left(\frac{H^2}{2\pi\dot{\varphi}_0}\right)^2 \left(\frac{k}{\mathcal{H}}\right)^{2\eta-4\epsilon}. \tag{2.115}$$

Horizon-Crossing Formalism

The solutions at subhorizon and superhorizon scales in 2.112 match at $k = \mathcal{H}$. This is the point of *horizon-crossing* where the fluctuation scale k^-1 matches the horizon scale $\mathcal{H}^-1$. After crossing the horizon, the mode function stops oscillating and decays by the scaling factor $(k/\mathcal{H})^{\eta-2\epsilon}$. Hence, $k = \mathcal{H}$ is a checkpoint where the fluctuation amplitude is fixed and conserved while living outside the horizon. After inflation, the horizon expands and the perturbation evolves and becomes relevant to physical processes within the Hubble sphere again after re-entering the horizon. We rely on this exact mechanism to learn about the physics of inflation since the transportation of unmodified fluctuation is ensured, playing an important role in the birth of the universe's structure.

Let us consider the horizon-crossing formalism in more detail. Schematically, as the Hubble sphere shrinks, each mode of perturbation becomes frozen from the large to small scale. After

every mode of interest reaches the superhorizon limit, their amplitudes (or the power spectrum) are different by the scaling factor. Hence, the power spectrum of each mode is typically evaluated at the horizon-crossing time of the pivot mode and multiplied by the mode ratio,

$$\Delta_\zeta(k) = \left(\frac{H^2}{2\pi\dot{\varphi}}\right)^2 \Big|_{\tau=k_*^{-1}} \left(\frac{k}{k_*}\right)^{2\eta-4\epsilon}, \tag{2.116}$$

where k_* is the pivot mode. Another alternative interpretation is that the fluctuation is scale-invariant before crossing the horizon and the power spectrum equal to $\left(\frac{H^2}{2\pi\dot{\varphi}}\right)^2$ for every mode. But then, each mode exits the horizon asynchronously and the frozen amplitude picks the value at a different moment of inflation, depending on its scale. Since the power spectrum is time-dependent, the frozen modes of fluctuation at the superhorizon limit differ by the ratio between their scales, owing that they exit the horizon at different times. The two interpretations give the same prediction in the end and which one to be preferred completely depends on one's taste.

2.4.5 Scale-dependent Power Spectrum

The prediction of the power spectrum gives some hint of the scale dependence in the curvature perturbation, relating the slow-roll parameters to the observable. A typical parameterization for measuring primordial scalar-mode power spectrum is

$$\Delta_\zeta(k) = A_s \left(\frac{k}{k_*}\right)^{n_s-1}, \tag{2.117}$$

where k_* is the pivot scale and A_s is the amplitude of the fluctuation at the length scale k_*^{-1}. n_s is the scalar spectral index, indicating the tilt of the power spectrum. The case where the power spectrum grows with k is denoted as blue tilt ($n_s > 1$) and the case where it declines with increasing k is denoted as red tilt ($n_s < 1$). By comparing this formula with the result of inflation 2.116, we have the predictions,

$$A_s = \Delta_\zeta(k_*) = \left(\frac{H^2}{2\pi\dot{\varphi}}\right)^2 \Big|_{\tau=k_*^{-1}} \quad \text{and} \quad n_s - 1 = 2\eta - 4\epsilon, \tag{2.118}$$

From the latest CMB power spectra analysis [63], the parameters are estimated,

$$\begin{aligned} n_s &= 0.9649 \pm 0.0042 \ (68\% \text{ CL.}) \\ \ln(10^{10} A_s) &= 3.044 \pm 0.0042 \ (68\% \text{ CL.}) \quad \text{at} \quad k_* = 0.05 \ \text{Mpc}^{-1} \end{aligned} \tag{2.119}$$

A crucial finding here is the spectrum is red-tilted with around 8σ confidence from $n_s = 1$. However, the dimensionless power spectrum Δ_ζ is often assumed to be scale-invariant for the fact that n_s is fairly close to 1. Hence, the power spectrum is often assumed to have k-dependence as $P_\zeta(k) \propto k^{-3}$ for simplicity.

2.4.6 Summary of The Process

Before moving on, let us review the whole process of initial condition generation once again. The simplest model of inflation suggests that the accelerated expansion was driven by a scalar field that dominates the energy budget of the universe, inflaton. For the slow-roll scenario, the kinematics of inflation and the dynamics of the field are regularized by the slow-roll parameters, quantifying the expansion rates and the shape of the field's potential. In the beginning, when space was minuscule, the quantum phenomena were relevant to the evolution of inflaton. The uncertainty of the observables invokes fluctuations in the homogeneous inflaton background field, producing a scale-invariant perturbation across the space (subhorizon limit). This perturbation induces some disturbance on the spatial curvature and the combination of both is gauge-invariant and hence a measurable physical quantity in linear order. They started to pick up some scale dependence while being stretched out by the expansion and became frozen once their length scale grew larger than the Hubble sphere (superhorizon limit). After inflation ends, the inflaton field loses its energy to the standard model sector. However, perturbations outside the horizon still prevail as curvature perturbations, encoding features of inflation. This has allowed us to study the physics of the early universe via the statistics of the structure we observe nowadays like the Cosmic Microwave Background or tracers like galaxies and dark matter halos. Until now, the CMB fluctuations are found to be Gaussian distributed agreeing with our simplest model.

But recently, primordial non-Gaussianity (PNG) has been the topic in the spotlight. The detection of it can reveal some new information about inflation beyond the linear theory. The ongoing efforts of PNG hunting exist in the next generation of surveys like CMB-S4 [64] and SPHEREx [24]. In the following sections, the relevance of PNG to the physics of inflation will be discussed and the method of detection via the statistics of tracers will be reviewed. Further-

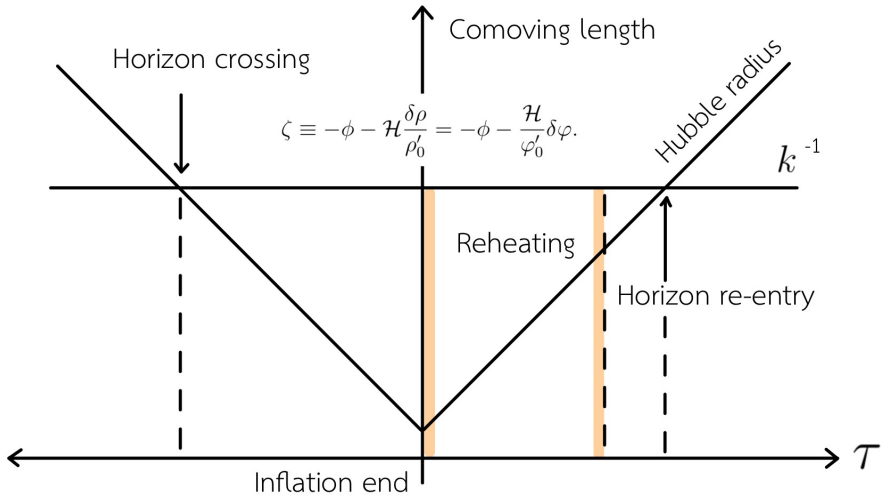

Figure 2.5: A schematic summary of the initial condition generation by inflation.

more, two independent studies have recently found a parity-violation signature in the statistics of galaxies, i.e. the four-point correlation function. The radical feature can widely rule out parity-conserving models of inflation if the detection is confirmed to be of a primordial origin. In the following section, the observational effects that may mimic such a signature will be quantified, clearing the path to the detection of primordial parity violation.

2.5 Primordial Non-Gaussianity from Inflation

The description of cosmological perturbation in inflation up until now is on the linear level. In particular, the second order in perturbations or more terms in the equations of motion are neglected and the discussed gauge transformation is valid up to the first order only. With this level of precision, the description of fluctuations' dynamics is limited at the free field level since the interaction terms are at least second-order in perturbations. Going beyond would require us to perturb the inflaton action to the third order, which will give an equation of motion in the second order, and the gauge description must be extended to the second order. The second-order equations of motion have been first obtained by [16]. In that paper, the production of non-Gaussianity (NG) by nonlinear dynamics has been discussed; Including the second-order perturbations allows the production of skewness in the fluctuations' statistics. Alternatively, [17] introduce the *in-in formalism*, borrowing the language of particle physics to compute the n-point correlation function of the fluctuations. The formalism allows us to split the Hamil-

tonian into the free and interaction parts. Since the state is evolved by using the free part of Hamiltonian, the linear solution can still be used along with the interaction Hamiltonian to compute the statistics higher than the variance. Therefore, NG is the probe of the fundamental interactions during inflation which allows us to describe the high energy physics beyond the free-field limit. This section will show different kinds of NG that can be produced from various models and some consistency relations that can be checked with the observation.

2.5.1 Gaussianity of Free Field

Let us recall some characteristics of Gaussian distribution. The probability distribution function (PDF) with zero mean is written as

$$\mathbf{G}(\zeta_g) = \frac{1}{\sigma\sqrt{2\pi}} e^{-\frac{\zeta_g^2}{2\sigma^2}}, \tag{2.120}$$

where ζ_g and σ are a Gaussian variable and the standard deviation of the distribution. In real situations, like in CMB or galaxies surveys, we expect that the fluctuation around the mean at each point was drawn from the underlying distribution dictated by the physics that generated it. To gain access to the true distribution function of such data, one of the ways is to measure the statistical moments from the spatially distributed perturbations, averaging over the survey volume. In other words, we can learn about the true PDF by interpreting the n-point correlation functions measured from the surveys. Fundamentally, the correlation function is computed from the PDF by

$$\langle \zeta^n \rangle = \int d\zeta \; \zeta^n \mathbf{G}(\zeta). \tag{2.121}$$

Notice that the PDF is characterised by variance only. One of the properties of Gaussian distribution is it can be fully characterized by just two quantities: mean and variance. All higher-order statistical moments can be specified with those two quantities and the distribution curve is symmetric about the mean. However, since the mean of perturbation is zero by definition, we expect only variance in the game and the distribution is symmetric around zero. Therefore, vanishing odd moments are expected. For example, there will be no skewness since the distribution is symmetric. Hence, if the theory gives the same feature, the distribution would be Gaussian around zero mean.

These statistical functions can be predicted by the theory of cosmological perturbation during inflation. The mean and variance of inflaton perturbation up to the linear order have been

computed in the last section by acting the vacuum state with the field operator. There, we find that the mean is indeed zero respecting the definition of field perturbation and the variance reflects the amplitude of the fluctuation. To obtain higher-order statistics in principle, the same procedure can be followed with more field operators. Let us consider the 3-point function,

$$\xi^{(3)}_{\delta\varphi}(\boldsymbol{r_1}, \boldsymbol{r_2}; \tau) \equiv \langle 0| \, \delta\hat{\varphi}(\boldsymbol{x}, \tau)\delta\hat{\varphi}(\boldsymbol{x} + \boldsymbol{r_1}, \tau)\delta\hat{\varphi}(\boldsymbol{x} + \boldsymbol{r_2}, \tau) \, |0\rangle = 0, \tag{2.122}$$

by using the linear solution 2.94. The function vanishes by the orthogonality of the quantum state. Notice that, for the same reason, the results can be extended to the higher-order ones. If the number of field operators is odd, its expectation value vanishes. Alternatively, the higher-order statistics can be distributed into lower-order ones by *Wick's theorem*,

$$T[\delta\hat{\varphi}(\boldsymbol{x_1}, \tau)\delta\hat{\varphi}(\boldsymbol{x_2}, \tau) \dots \delta\hat{\varphi}(\boldsymbol{x_{n-1}}, \tau)\delta\hat{\varphi}(\boldsymbol{x_n}, \tau)] = \sum_{\text{all possible contractions}} \overbrace{\delta\hat{\varphi}(\boldsymbol{x_1}, \tau)\delta\hat{\varphi}(\boldsymbol{x_2}, \tau)} \dots \overbrace{\delta\hat{\varphi}(\boldsymbol{x_{n-1}}, \tau)\delta\hat{\varphi}(\boldsymbol{x_n}, \tau)}, \tag{2.123}$$

where T is the time-ordering operator. The full formula of the theorem would have included the normal-ordered term without maximal contraction. However, they have vanished since we computed the expectation value with the vacuum state. Here, it is clear that an odd number of fields would lead to a multiplication of the mean $\langle\varphi\rangle$ which is zero. If the number of fields is even, the function can be described by products of two-point functions. These are the indications of a Gaussian distributed field which is exactly what one should expect from the free field.

One may conclude that the simplest single-field inflation predicts Gaussian distributed perturbation. Indeed, the latest constraint on non-Gaussianity from Planck CMB observation [23] agrees with this case, allowing deviation within a stringent boundary. However, this is not the case in general. Gaussian distribution is predicted here merely because we restrict the discussion to the linear order where the equation of motion is effectively free. Going beyond the first order, the interaction terms such as φ^3 are included in the action and will introduce nonlinearity to the dynamics of fluctuation. It is emphasized that this is not a modification to the simplest case; the model is just being treated more accurately in the context of perturbation theory. We will see the predicted amount of NG from the single-field model shortly.

2.5.2 Quantifying Non-Gaussianity: Small Deviation from Gaussianity

To understand why probing higher-order statistics is important beyond the linear theory in a model-independent manner, let us consider a true PDF $\mathbf{P}(\zeta)$ corresponding to the full theory of inflation. This PDF would be responsible for the statistics of initial fluctuations that we can access through the observations. Knowing the true form of this PDF would allow us to reconstruct the exact theory of inflation. In particular, the partition function can be written which is directly related to the action of the theory. We know from the CMB constraint [23] that the departure from Gaussian is small. Hence, the true PDF can be written as the Taylor series around the Gaussian PDF:

$$\mathbf{P}(\zeta) = \sum_{n=0}^{\infty} a_n \frac{d^n \mathbf{G}(\zeta_g)}{d\zeta_g^n}, \tag{2.124}$$

where a_n is the nth-order Taylor coefficient. After evaluating all of the derivatives, the series are chosen to be rearranged as[2]

$$\mathbf{P}(\zeta) = \mathbf{G}(\zeta_g)\Big[1 + \sum_{n=1}^{\infty} c_n He_n(\zeta_g/\sigma)\Big] \tag{2.125}$$

for convenience. The special function He_n is the nth-order *Hermite polynomial* and c_n is the corresponding coefficient in front of it. In this arrangement, c_n's are conveniently determined by using the orthogonality $He_n(\zeta)$,

$$\int dx\ He_n(x) He_m(x) e^{-x^2/2} = \sqrt{2\pi} n! \delta_{nm}. \tag{2.126}$$

From there, one finds that those coefficients are combinations of the statistical moments. Thus, probing higher-order statistics is effectively putting more precise corrections to the PDF and will unveil more insight into the full theory that sources this perturbation.

From now on, we will focus on how to model and predict the n-point correlation function of the perturbation. The exact way would start by writing the action of inflation once again. We wish to go beyond the linear theory and include interaction terms from the third-order or higher in the action as well. As mentioned before, the next step is either to find the nonlinear

[2] In general, any power series can be rearranged to series of Hermite polynomial.

equation of motion by studying the (nonlinear) cosmological perturbation theory [16] or using the in-in formalism to compute correlation functions directly from the interacting part of the Hamiltonian [17]. However, for the sake of simplicity of this work, we will follow the effective field redefinition. In general, we could write

$$\zeta = \zeta_g + \mathcal{F}_{NL}(\zeta_g), \tag{2.127}$$

where $\mathcal{F}_{NL}$ is some nonlinear function of the Gaussian variable. This is equivalent to saying that the real statistical variable drawn from the real PDF can be effectively described as the value drawn from the Gaussian PDF plus a correction from the nonlinear function of the Gaussian variable. s the deviation from Gaussianity is small, the nonlinear term is expected to be much smaller than the Gaussian variable. The formal expression of $\mathcal{F}_{NL}$ depends on the type of expected NG from inflation models of interest. This approach to quantifying NG is robust since it allows us to generalize the prediction of various inflation models into just a few models of field redefinition. For the first kind of NG, the model introduced in [19] is

$$\zeta(\boldsymbol{x}) = \zeta_g(\boldsymbol{x}) + \frac{3}{5} f_{NL}^{loc} \left[\zeta_g^2(\boldsymbol{x}) - \left\langle \zeta_g^2 \right\rangle\right] + \dots \,, \tag{2.128}$$

where ζ and ζ_g are the non-Gaussian and Gaussian variables. The time-dependent of the perturbation is omitted since the expression here is localised in time. f_{NL}^{loc} is the so-called nonlinear parameter since it captures the nonlinearity of the perturbation. This f_{NL}^{loc} is also known as the local nonlinear parameter for the fact that the expression is local on spatial coordinates. This model can capture the NG source by the local interaction in the action, e.g. φ^3, during inflation. From now on, the NG produced during inflation will be dubbed *Primordial* non-Gaussianity (PNG) to distinguish them from the NG introduced later after inflation ended, e.g. by late-time gravitational processes. As the deviation from Gaussianity is small, the nonlinear term is expected to be much smaller than the Gaussian variable. For the fluctuation around 10^{-5} [63], we then expect $\left|f_{NL}^{loc}\right| \ll 10^5$. We will use this model as an example to compute the prediction on the n-point functions.

2.5.3 N-point Correlation Function: Reload

Back to the discussion of mean and variance of perturbation during inflation, the power spectrum has been introduced as a Fourier counterpart of the two-point function. The same mathematical structure works the same for the higher-point function. Since we will be using

these functions as a main tool to compare theory with observation, let us revise the meaning of them once again.

Cosmological surveys typically aim to capture the field of fluctuations in a large-scale region. To obtain the n-point correlation function (NPCF), we effectively measure the fluctuations from n points in space, find the product, and find the average value of this product over the survey volume. For example, the two-point correlation function (2PCF) is the average of the product of the fluctuations at a certain separation,

$$\xi_\zeta(\boldsymbol{x};\boldsymbol{r}) = \langle \zeta(\boldsymbol{x})\zeta(\boldsymbol{x}+\boldsymbol{r})\rangle\,, \tag{2.129}$$

where $\boldsymbol{x}$ is the spatial position of the first fluctuation and the second one is located at $\boldsymbol{r}$ from the first one. Let us apply the cosmological principles to the statistical functions, i.e. isotropy and homogeneity. Homogeneity in this sense means that we expect the statistical properties of the fluctuation to be the same regardless of the point in space we are observing from. Hence, we can remove the dependence on $\boldsymbol{x}$ from the NPCF. The isotropy follows from the fact that we consider a scalar-mode fluctuation that has no preferred direction fundamentally. Hence, NPCF shall depend only on the size of the separation. In the end, we have the 2PCF as

$$\xi_\zeta(\boldsymbol{x};\boldsymbol{r}) \xrightarrow{\text{isotropy \& homogeneity}} \xi_\zeta(r). \tag{2.130}$$

Indeed, we observed the same properties when we computed the 2PCF from the linear theory (see discussion in section 2.4.4). As discussed in section 2.4.4, the Fourier counterpart of 2PCF is the power spectrum,

$$\xi_\zeta(r) = \int \frac{d^3k}{(2\pi)^3} P_\zeta(k) e^{i\boldsymbol{k}\cdot\boldsymbol{r}}, \tag{2.131}$$

where the power spectrum can be computed through

$$\langle \zeta_{\boldsymbol{k_1}}\zeta_{\boldsymbol{k_2}}\rangle = (2\pi)^3\delta_D^{(3)}(\boldsymbol{k_1}+\boldsymbol{k_2})P(k_1). \tag{2.132}$$

and the Fourier transform and the inverse Fourier transform of the field are

$$\begin{aligned} \zeta_{\boldsymbol{k}} &= \int d^3x\zeta(\boldsymbol{x})e^{-i\boldsymbol{k}\cdot\boldsymbol{x}}, \\ \zeta(\boldsymbol{x}) &= \int d^3k\zeta_{\boldsymbol{k}}e^{i\boldsymbol{k}\cdot\boldsymbol{x}}. \end{aligned} \tag{2.133}$$

This can be extended to the 3-point correlation function (3PCF) by including another field to the correlation functions; the fluctuations at 3 points in space are computed. Essentially, this is the lowest order of statistics indicating NG in the distribution since a Gaussian distribution predicts zero-odd NPCF. 3PCF is defined as

$$\xi_\zeta^{(3)}(r_1, r_2, \|\boldsymbol{r_1} + \boldsymbol{r_2}\|) = \langle \zeta(\boldsymbol{x})\zeta(\boldsymbol{x} + \boldsymbol{r_1})\zeta(\boldsymbol{x} + \boldsymbol{r_2})\rangle \,. \tag{2.134}$$

An important characteristic of 3PCF is that it forms a triangle configuration in space. As before, there exists a Fourier counterpart of 3PCF. To find that, we insert the inverse Fourier transform of the field into the ensemble average and gets

$$\xi_\zeta^{(3)}(r_1, r_2, \|\boldsymbol{r_1} + \boldsymbol{r_2}\|) = \int \frac{d^3k_1}{(2\pi)^3} \int \frac{d^3k_2}{(2\pi)^3} B_\zeta(k_1, k_2, \|\boldsymbol{k_1} + \boldsymbol{k_2}\|) \prod_{\sigma=1}^{2} e^{i\boldsymbol{k_\sigma}\cdot\boldsymbol{r_\sigma}} \tag{2.135}$$

where the bispectrum $B_\zeta(k_1, k_2, k_3)$ is computed from the correlation between three fields in Fourier space,

$$\langle \zeta_{\boldsymbol{k_1}} \zeta_{\boldsymbol{k_2}} \zeta_{\boldsymbol{k_3}} \rangle = (2\pi)^3 \delta_D^{(3)}(\boldsymbol{k_1} + \boldsymbol{k_2} + \boldsymbol{k_3}) B_\zeta(k_1, k_2, k_3). \tag{2.136}$$

Notice that the statistical homogeneity and isotropy have already been assumed in the expressions. The first point to realise is the mode vectors associated with the bispectrum also form a triangle in Fourier space, similar to what 3PCF have in real space. Secondly. the bispectrum vanishes if the fields $\zeta_{\boldsymbol{k}}$ were drawn from a Gaussian distribution. As usual, the four-point correlation function (4PCF) and its Fourier counterpart, the trispectrum $T_\zeta(k_1, k_2, k_3, k_4)$, are defined in the same manner,

$$\begin{aligned} &\xi_\zeta^{(4)}(r_1, r_2, r_3, \|\boldsymbol{r_1} + \boldsymbol{r_2} + \boldsymbol{r_3}\|) = \\ &\quad \int \frac{d^3k_1}{(2\pi)^3} \int \frac{d^3k_2}{(2\pi)^3} \int \frac{d^3k_3}{(2\pi)^3} T_\zeta(k_1, k_2, k_3, \|\boldsymbol{k_1} + \boldsymbol{k_2} + \boldsymbol{k_3}\|) \prod_{\sigma=1}^{3} e^{i\boldsymbol{k_\sigma}\cdot\boldsymbol{r_\sigma}} \end{aligned} \tag{2.137}$$

and

$$\langle \zeta_{\boldsymbol{k_1}} \zeta_{\boldsymbol{k_2}} \zeta_{\boldsymbol{k_3}} \zeta_{\boldsymbol{k_4}} \rangle = (2\pi)^3 \delta_D^{(3)}(\boldsymbol{k_1} + \boldsymbol{k_2} + \boldsymbol{k_3} + \boldsymbol{k_4}) T_\zeta(k_1, k_2, k_3, k_4). \tag{2.138}$$

These two quantities form a tetrahedral geometry in real and Fourier spaces. For this fact, 4PCF is the lowest-order statistic that its reflected configuration in the 3-dimensional space is distin-

guishable from the original configuration. Therefore, 4PCF is sensitive to the parity violation that may exist in the observable statistics. This useful property will become important in the upcoming chapter as a probe into a fundamental feature of gravity.

2.5.4 Local-Form Primordial Non-Gaussianity In Bispectrum

As anticipated, let us use the field redefinition 2.128 to compute the bispectrum of a non-Gaussian perturbation. From the Fourier transform of the field 2.133, we can write the field redefinition in Fourier space as

$$\zeta_{\boldsymbol{k}} = \zeta^g_{\boldsymbol{k}} + \frac{3}{5} f^{loc}_{NL} \int \frac{d^3k'}{(2\pi)^3} \left[\zeta^g_{\boldsymbol{k}'}\zeta^g_{\boldsymbol{k}-\boldsymbol{k}'} - \left\langle \zeta^g_{\boldsymbol{k}'}\zeta^g_{\boldsymbol{k}-\boldsymbol{k}'}\right\rangle\right] + \dots \,. \tag{2.139}$$

Then, by computing the 3PCF in Fourier space 2.136, we obtain the bispectrum,

$$B^{loc}_{\zeta}(k_1, k_2, k_3) = \frac{6}{5} f^{loc}_{NL} \left[P_\zeta(k_1)P_\zeta(k_2) + 2 \text{ perm.}\right], \tag{2.140}$$

where 2 perm. indicates other 2 similar term to $P_\zeta(k_1)P_\zeta(k_2)$ but permute the pair of mode vectors from the set $\{k_1, k_2, k_3\}$. In the computation, we exploit Wick's theorem 2.123 to distribute the correlation of 4 Gaussian fields into products of 2PCF. Then, we trade the Fourier space 2PCF with the power spectrum through equation 2.132. This formula gives us an estimator of the first kind of PNG, the local PNG, by measuring f^{loc}_{NL}. Notice that $f^{loc}_{NL} = 0$ corresponds to the Gaussian fluctuations case; the bispectrum is zero. An important feature of this kind of PNG is scale-independence. Namely, the resulting bispectrum picks the k-dependence from the product of the power spectrum only while other kinds of PNG will introduce additional scale-dependence. For $P_\zeta(k) \propto k^{-3}$, we have $B^{loc}_{\zeta}(k_1, k_2, k_3) \propto P^2_\zeta \propto (k_1 k_2)^{-3}$ in this case. Pictorially, the effect of NG bispectrum is equivalent to introducing *skewness* to the distribution of conserved curvature perturbation (see figure 2.6).

2.5.5 The Squeezed Limit And The Single-Field Consistency Relation

One of the important insights we can learn by measuring the local-form PNG is the number of active fields in inflation. Namely, there exists a consistency relation that holds for single-field inflation models only and the violation of it will rule out all single-field models regardless of the details. To introduce that relation, let us discuss a certain limit of the local PNG Bispectrum.

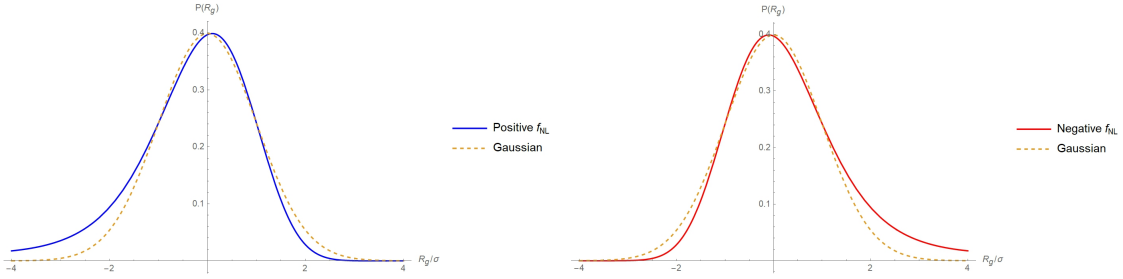

(a) Positive f_{NL} **(b)** Negative f_{NL}

Figure 2.6: The plot of probability density function when perturbed with parameter f_{NL}. In this case, the curves are (a) negatively skewed when f_{NL} is positive, and (b) positively skewed when f_{NL} is negative.

From the k-dependence discussed, we see that the power spectrum and bispectrum peak at a small k limit. This is beneficial for boosting the signal-to-noise ratio when estimating the f_{NL}^{loc}. Moreover, we obtained an interesting relation in this limit.

Recalling that the mode vectors of bispectrum resemble a triangle configuration in Fourier space, let us consider the case where one of the sides shrinks down and the other two sides degenerate, say $k_3 \ll k_1 \approx k_2 \approx k$. This is the so-called *squeezed bispectrum* where the local-PNG bispectrum 2.140 is approximately,

$$B_\zeta^{loc}(k_1 \approx k, k_2 \approx k, k_3 \longrightarrow 0) \approx \frac{12}{5} f_{NL}^{loc} P_\zeta(k) P_\zeta(k_3). \tag{2.141}$$

The expression of the bispectrum can be computed from a selected inflation model as well which we can take the same limit to compare with this effective field approach to NG. For single-field slow-roll inflation, we would expect f_{NL}^{loc} to depend on the slow-roll parameters since the higher-order interactions that sourced NG would be included in the inflaton potential $V(\varphi)$ which is parameterized by the slow-roll parameters. Indeed, [16] and [17] find the result, $f_{NL} = \frac{5}{6}(\eta - 2\epsilon)$. The result was extended to a general single-field model in [65] by relying on the fact that frozen long-mode perturbation modified the short-mode fluctuations within the horizon during inflation. This effect crucially requires the inflaton to be the only scalar degree of freedom so that its fluctuation is directly proportional to the curvature perturbation, which modified the short-mode power spectrum. If a new scalar field is introduced, the relation would not be direct and the following field correlation would not be valid. The method is nicely reviewed in [66] for more references. The result is

$$f_{NL}^{loc} = \frac{5}{12}(1 - n_s). \tag{2.142}$$

Notice that the local PNG is sourced by the scale dependence of the power spectrum; the local bispectrum vanishes for the scale-invariant primordial power spectrum ($n_s = 1$). Since [63] revealed the value of n_s to be very close to one, we would expect tiny $f_{NL}^{loc} \sim \mathcal{O}(10^{-2})$ for the single-field scenarios. The readers might wonder how can the prediction be confirmed if it is too tiny to detect. But, in reality, the point of this condition is how easy and powerful the violation of it is. As mentioned before, the parameter f_{NL}^{loc} can be large enough to be detectable, taking the value $f_{NL}^{loc} \ll 10^5$. This means it is possible to find the squeezed bispectrum in the observation. This will violate the condition and automatically rule out every single-field model, despite its details. The latest constraint from Planck's CMB observation [23] on f_{NL}^{loc} is

$$f_{NL}^{loc} = -0.9 \pm 5.1 \ (68\% \text{ CL.}), \tag{2.143}$$

which reduces the boundary to $f_{NL}^{loc} \sim \mathcal{O}(1)$. Thus, the consistency relation still holds. This is the first reason why an alternative probe of NG is important; the additional constraint from an independent source would complement the existing constraint on f_{NL}^{loc} and might invalidate the consistency relation eventually. The large-scale structure (LSS) probe like the galaxies' distribution is one of the strong candidates for producing a constraint at the same precision as CMB. Future surveys like SPHEREx [24] promise to constrain the parameter to around the order of 1. The theory and method used to determine the parameter from the LSS probe will be discussed in the next chapter.

2.5.6 The Zoo of Non-Gaussianities in The Bispectrum

The form of PNG in bispectrum has more variety than just the discussed local form. Other than the squeezed bispectrum, we can also have the bispectrum that is peaked at other configurations of mode vectors. For example, the equilateral bispectrum that peaks at $k_1 = k_2 = k_3$ (see figures 2.7b and 2.8b) and the enfolded or flattened shape that peaks at $k_1 = k_2 = k_3/2$ (see figures 2.7c and 2.8c) [67]. These signals are consequences of different inflation models inheriting different features and more than one model may produce the same kinds of bispectra. Hence, instead of categorising PNGs with their sourcing models, it is more compact to differentiate them by their peak limits. For instance, the bispectra from the Dirac-Bold-Infeld (DBI) model [68, 69] and the ghost inflation model [70] both peak at equilateral configuration. The model with the modified initial state of inflation [20, 21] produces the enfolded bispectrum. Also, some models produce a bispectrum that peaks at two configurations. For example, the single-field inflationary model with the Goldstone boson may produce a bispectrum that peaks

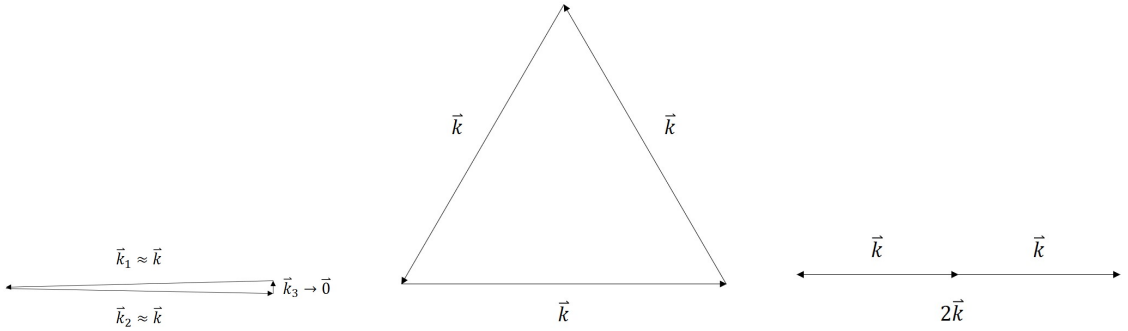

(a) Squeezed Bispectrum **(b)** Equilateral Bispectrum **(c)** Enfolded Bispectrum

Figure 2.7: Three examples of the mode vectors' configurations where the bispectrum peaks. 2.7a The squeezed bispectrum whose one of the mode vectors is squeezed down, $k_1 \approx k_2 \gg k_3 \longrightarrow 0$. 2.7b The equilateral bispectrum whose mode vectors are equal in size, $k_1 = k_2 = k_3$. 2.7c The enfolded bispectrum whose one of the mode vectors is double in length compared to the other two, $k_1 = k_2 = k_3/2$.

positively at the equilateral configuration and negatively at the folded configuration [22]. Also, the signal is orthogonal to both equilateral and squeezed forms, hence the name: orthogonal bispectrum. These different peak behaviours will introduce different kinds of scale dependence on the bispectrum which is important for the discussion of their detectability in the observation later.

In the context of data analysis, the bispectra from the catalogue of inflationary models that peak in the same configuration are generalised to a shape function. One shape function represents one kind of PNG regarding their peak limit. The following set of shape functions may not be directly obtained from the models of inflation but they are designed to be efficient in the numerical estimation of nonlinear parameters and are justified to be close to the bispectra given by the proposed models [71].

Equilateral Form NG [72]

$$B_\zeta^{equil}(k_1,k_2,k_3) = \frac{18}{5} f_{NL}^{equil} \Big[-\big(P_\zeta(k_1)P_\zeta(k_2) + 2\ perm.\big) - 2\big(P_\zeta(k_1)P_\zeta(k_2)P_\zeta(k_3)\big)^{2/3} + P_\zeta^{1/3}(k_1)P_\zeta^{2/3}(k_2)P_\zeta(k_3) + 5\ perm.\Big]. \tag{2.144}$$

Enfolded Form NG [20, 21]

$$B_\zeta^{en}(k_1,k_2,k_3) = \frac{18}{5} f_{NL}^{en}\Big[P_\zeta(k_1)P_\zeta(k_2) + 2\ perm. \\ + 3\big(P_\zeta(k_1)P_\zeta(k_2)P_\zeta(k_3)\big)^{2/3} \\ - P_\zeta^{1/3}(k_1)P_\zeta^{2/3}(k_2)P_\zeta(k_3) + 5\ perm.\Big]. \tag{2.145}$$

Orthogonal Form NG [22]

$$B_\zeta^{ortho}(k_1,k_2,k_3) = \frac{18}{5} f_{NL}^{ortho}\Big[-3\big(P_\zeta(k_1)P_\zeta(k_2) + 2\ perm.\big) \\ - 8\big(P_\zeta(k_1)P_\zeta(k_2)P_\zeta(k_3)\big)^{2/3} \\ + 3\big(P_\zeta^{1/3}(k_1)P_\zeta^{2/3}(k_2)P_\zeta(k_3) + 5\ perm.\big)\Big]. \tag{2.146}$$

Notice that the chosen templates, when $f_{NL}^{equil} = f_{NL}^{en} = f_{NL}^{ortho}$, are related through $B_\zeta^{ortho} = B_\zeta^{equil} - 2B_\zeta^{en}$.

Regarding the observational result, the amount of PNG of different kinds that exist in the initial condition is indicated by the nonlinear parameter f_{NL}^{equil}, f_{NL}^{en} and f_{NL}^{ortho} indicated in the functions above. Departure from zero of these parameters implies a non-zero bispectrum and hence the existence of NG. Up until now, the most stringent constraints on this parameter are provided by the CMB analysis where the latest result [23] indicates that

$$f_{NL}^{loc} = -0.9 \pm 5.1\ ,\ f_{NL}^{equil} = -26 \pm 47\ ,\ f_{NL}^{ortho} = -38 \pm 24$$

where the uncertainties are of 68% statistical confidence interval. The superscripts "loc", "equil" and "ortho" indicate that the parameters represent the bispectrum of squeezed, equilateral and orthogonal types respectively [3]. Even though the existence of NG of any kind is still not confirmed by the observational data (the absence of those parameters is still within the confidence interval), it cannot be denied as well. Therefore, it is beneficial to improve and find alternative

[3] It has been argued in [22] and [23] that the nonlinear parameter f_{NL}^{en} is directly proportional to $-f_{NL}^{ortho}$ due to the similar behaviour of the shape function. Hence, the estimation of it is omitted.

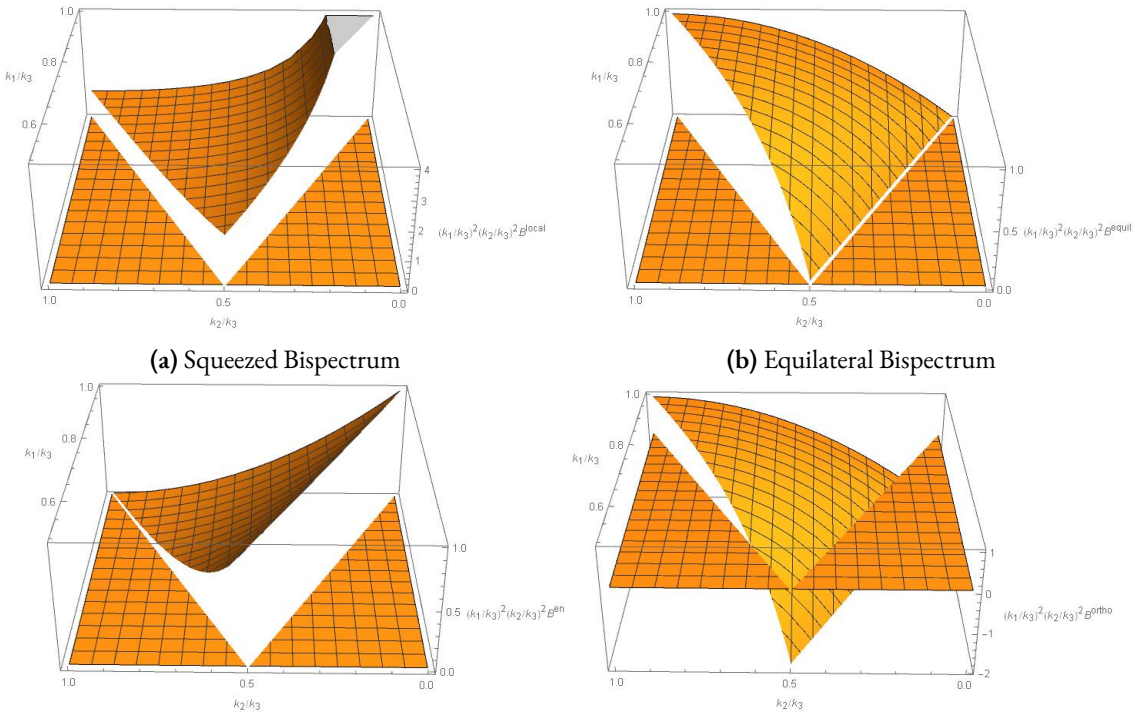

(a) Squeezed Bispectrum

(b) Equilateral Bispectrum

(c) Enfolded Bispectrum

(d) Orthogonal Bispectrum

Figure 2.8: The scale dependence of the shape functions for estimating the nonlinear parameter. Note that the corresponding nonlinear parameter f_{NL}'s are chosen to be 1 for visualization purposes. The squeezed bispectrum grows up to infinity at $k_2/k_3 \longrightarrow 0$ which corresponds to the squeezed limit. The equilateral and enfolded bispectra peak at $k_1/k_3 = k_2/k_3 = 1$ and $k_1/k_3 = k_2/k_3 = 0.5$ respectively. The orthogonal bispectrum has two peaks. The positive peak corresponds to the equilateral shape while the negative peak corresponds to the enfolded shape.

methods of estimation for these parameters. One such method is through the LSS data analysis such as the halo bias which will be discussed in this thesis.

2.5.7 Parity Symmetry of General Relativity

Let us spend a few words on the symmetry of this theory. One of the key features of GR, which is one of this thesis's main focuses, is *parity symmetry*. Generally, it is the symmetry of the left and right sides. By construction, the standard GR is a parity-conserving theory. In particular, the Einstein-Hilbert action is invariant under parity transformation, $\boldsymbol{x} \longrightarrow -\boldsymbol{x}$. Let us recall the action,

$$S_{GR} = \frac{M_{pl}^2}{2} \int d^4x \, \sqrt{-g}R = \int d^4x \, \mathcal{L}_{GR}. \tag{2.147}$$

The quantity in this action that may depend on the spatial coordinates is the metric tensor $g_{\mu\nu}$. The parity-invariant line element squared, ds^2, implies that 00- and ij-components of the metric tensor are parity invariant but the $i0$- and $0j$-components gain minus sign under parity transformation. Essentially, the spatial index is subjected to parity inversion while the time component is untouched. The Ricci scalar R is overall parity-conserving since it is constructed from the contraction of derivatives and metric tensors. Each parity-inverting spatial index is contracted with its pair and becomes parity-conserving overall. In fact, this property is already implied since R is a scalar[4]. Therefore, the standard GR Lagrangian is parity-conserving, $\mathbb{P}[\mathcal{L}_{GR}] = \mathcal{L}_{GR}$.

Moreover, there has been no concrete evidence of parity violation (PV) up until now. In particular, the clustering process of cosmological objects is expected to work the same even if the left and right sides of space are flipped. Also, one of the main predictions of the theory is the existence of gravitational waves (GW), transverse and traceless rank-2 tensor perturbation on the metric. GW has 2 degrees of freedom, corresponding to 2 polarizations by construction. Thus, the parity violation of GR can also manifest itself as a rotating polarization of GW. With the ongoing search, it is still undetermined if this circular polarization state of GW exists or not.

That being said, two recent independent analyses of the galaxy survey, Baryon Oscillation

[4] Actually, one still has to check if the quantity is a pseudo-scalar or not. A pseudo-scalar does not have explicit direction but gains a minus sign from the parity transformation. For example, a two-spinors contraction with γ^5 matrix, existing in weak interaction theory, is a pseudo-scalar. In this case, R is purely constructed from the space-time indices contractions so it is an actual space-time scalar.

Spectroscopic Survey (BOSS) DR12 LOWZ and CMASS, data claim the parity-violating feature in the galaxy distribution [1, 2]. In other words, they found evidence of parity violation in the galaxy distribution which may lead to some modification of GR. For instance, the parity-violating signature may exist in the universe's initial condition. Since the description of the fluctuation during inflation is based on GR, its modification could alter the production of the initial perturbation. An example of one such modification is the Chern-Simons gravity [13, 14] where a parity-violating term is introduced to the GR Lagrangian (see also [73] and references therein). However, before we conclude that the signature is of the fundamental origin, one has to be cautious about other effects that could mimic the parity violation and trick us into believing that the theory must be modified. This is one of the main discussions of this thesis; we seek to comprehend the complexity of large-scale structures and how they are observed to be able to model them correctly for the observation. This will be explained in detail later in the thesis.

3

Large Scale Structure Distribution

As the name of this thesis, we wish to probe the fundamental physics of inflation through the late-time observable. It is possible because the superhorizon evolution allows the curvature perturbation during inflation to become the initial condition of the universe in a well-preserved way. These curvatures induced an over- and under-dense region of the matter field according to GR. Hence, the information from inflation is imprinted on the distribution of matter in the late time universe. These matter fluctuations do not stay still; they evolve with the dynamics of space-time and their distribution pattern changes accordingly. Thus, the evolution of matter fluctuations must be studied to infer the initial condition by observing the large-scale structure (LSS) distribution. This chapter will start with the evolution of matter density before going into the discussion of *biased tracer*, which we will explain the meaning of it later.

3.1 Linear Evolution of Fluctuations

After the initial condition set up by inflation, the energy from the inflaton flows into the standard model sector and the universe is reheated. In the beginning, the universe is filled with radiation while the expansion cools down the cosmic content gradually. Since the energy of radiation dilutes the fastest, the matter becomes more important in the overall energy budget where the expansion trend changes. Now, the universe is dominated by dark energy which has not diluted during the whole history of the universe and the expansion is accelerated once again. Due to the evolving background expansion, the dynamics of the fluctuation in each

epoch are different. Moreover, the perturbations from inflation with different sizes re-enter the horizon at different times. So, the fluctuations on each scale underwent different evolution. This section will describe the evolution of fluctuations after the Big Bang on a large scale up to a linear regime.

To find the equations of motion of perturbation, we once again resort back to the (perturbed) Einstein Field Equation. We will start by discussing the linear evolution of the fluctuation which is well-approximated only when the fluctuation is still small. Further treatments will be introduced later for the formation of structures that need beyond the linear description. To study the gravitational evolution of matter density perturbation, it is convenient to use the Poisson gauge. This is because the metric perturbation ψ is closely related to the Newtonian gravitational potential. Moreover, we obtain a constraint equation which resembles the Poisson equation (see section 2.3.4). Let us recall the linearly perturbed metric in the Poisson gauge,

$$\begin{aligned} g_{00} &= a^2(\tau)(1+2\psi), \\ g_{i0} &= g_{0j} = 0, \\ g_{ij} &= -a^2(\tau)(1-2\phi)\delta_{ij}, \end{aligned} \tag{3.1}$$

where we neglect the pure vector perturbation according to the SVT decomposition, $\omega^{\perp}$, since they are suppressed in the initial condition as discussed in section 2.4. A global rotation field after inflation is needed to generate such a perturbation on a large scale. However, such a field or effect that contributes a significant amount of energy to alter the universe's structure has not been found yet. For simplicity, we will continue to assume that the transverse vector perturbations are negligible and the gravitational potential is the dominant source of the structure formation. With this simplification, the conformal part of the geometry resembles the weak-field limit of GR about Minkowski space-time, close to the Newtonian description of gravity.

The matter fluid is perturbed as in equation 2.40. However, we further simplify the situation by neglecting the anisotropic stress tensor $\pi_{\mu\nu}$. This quantity is approximately zero most of the time; in that standard Big Bang theory, only neutrino fluid can induce a substantial amount of $\pi_{\mu\nu}$ after decoupling but then gets suppressed in the MD epoch. Furthermore, the transverse part of fluid velocity is assumed to be zero for the same reason as $\omega^{\perp}$. For density perturbation, it is useful to define the density contrast,

$$\delta \equiv \frac{\delta\rho}{\rho_0} = \frac{\rho - \rho_0}{\rho_0}, \tag{3.2}$$

which is the perturbation compared to the background density. This quantity is dimensionless and is more versatile in describing the relative size of the perturbation to the environment in different epochs.

With this setup, the perturbed Einstein equations yield

$$\begin{aligned} \mathcal{D}_{ij}(\phi-\psi) &= 0 \\ \nabla^2\phi &= 4\pi G a^2 \rho_0 \Delta_m, \\ \phi' + \mathcal{H}\phi &= -4\pi G a^2(\rho_0 + P_0)v \\ \phi'' + 3\mathcal{H}\phi' + (2\mathcal{H}' + \mathcal{H}^2)\phi &= 4\pi G a^2 \delta P \end{aligned} \tag{3.3}$$

where $\rho_0\Delta_m = \rho_0\delta - 3\mathcal{H}(\rho_0+P_0)v$ is the comoving density perturbation expressed in Poisson gauge. The first two equations are nondynamical and the latter describes the evolution of the gravitational potential. Notice that, by the first constraint equation, ϕ and ψ are equal and interchangeable, thanks to the absence of $\pi_{\mu\nu}$. This is why ϕ can also be interpreted as the gravitational potential ψ. We continue by assuming the adiabaticity of the fluid, implying $\delta P = \frac{P_0'}{\rho_0'}\delta\rho$. For simplicity, we will consider the background dominated by a single component, i.e. deep into RD and MD epochs. Therefore, we can insert the equation of state $P_0 = wp_0$ to simplify the relation where w is a constant. We have $\delta P = w\delta\rho$ where the speed of sound reflects the background equation of state. After trading $\mathcal{H}^2$ and $\mathcal{H}'$ with the Friedmann equations and installing the equation of state, we obtain the equation of motion in Fourier space,

$$\phi_k'' + 3(1+w)\mathcal{H}\phi_k' + wk^2\phi_k = 0. \tag{3.4}$$

Since $\mathcal{H} = \mathcal{H}(\tau)$, this solution of this differential equation then depends on the background assumed; $\mathcal{H} = \frac{1}{\tau}$ for RD universe and $\mathcal{H} = \frac{2}{\tau}$ for MD universe. However, notice that the behaviours of ϕ_k changes concerning the comparison between the fluctuation's wavelength k^{-1} and the Hubble horizon size $\mathcal{H}^{-1}$. This suggests the disparity between superhorizon and subhorizon behaviours.

3.1.1 Gravitaional Potential: Superhorizon Solution

For superhorizon limit, $k \ll \mathcal{H}$, the equation 3.4 is approximated to

$$\phi_k'' + 3(1+w)\mathcal{H}\phi_k' \approx 0. \tag{3.5}$$

$w < 1$ and $\mathcal{H}$ is positive for both RD and MD backgrounds. Hence, there are two solutions to this equation: decaying and constant modes. We ignore the decaying mode since it would already be negligible compared to the continuous mode. The key point here is gravitational potential remains the same outside the horizon, whether the universe is RD or MD. This frozen perturbation is exactly what carried the initial condition out from inflation. Let us reconsider the definition of gauge-invariant conserved curvature perturbation 2.114 in the Poisson gauge. By using the Poisson equation, Friedmann equations, and the equation of state, we obtain

$$\zeta \equiv -\phi - \mathcal{H}\frac{\delta\rho}{\rho_0'} = -\frac{5+3w}{3+3w}\phi, \tag{3.6}$$

where we see that the quantity ζ is related to the initial gravitational potential that will become the initial condition of the universe after entering the horizon. Also, this implies that the initial gravitational potential stored outside the horizon takes different values in different epochs,

$$\phi_{RD} = -\frac{2}{3}\zeta \quad \text{and} \quad \phi_{MD} = -\frac{3}{5}\zeta. \tag{3.7}$$

A factor of $9/10$ appears after the transition from RD to MD era, $\phi_{MD} = \frac{9}{10}\phi_{RD}$.

3.1.2 Gravitaional Potential: General solution

To describe the evolution from the horizon entry, we will keep all terms in the equation 3.4. Thus, different background dynamics will alter the behaviour of the perturbation by changing $\mathcal{H}$ and w.

RD background

In RD era, $w = 1/3$ and $\mathcal{H} = 1/\tau$. Hence, the equation of motion takes the form,

$$\phi_k'' + \frac{4}{\tau}\phi_k' + \frac{k^2}{3}\phi_k = 0. \tag{3.8}$$

This equation can be manipulated into the Helmholtz equation,

$$x^2 y''(x) + 2xy'(x) + \left(x^2 - n(n+1)\right) y(x) = 0, \tag{3.9}$$

by letting $x = \frac{1}{\sqrt{3}}k\tau$ and $y(x) = x\phi_k(\tau)$ with $n = 1$. Thus, the solutions of gravitational potential on RD background are the spherical Bessel and the spherical Neumann functions,

$$\phi_k(\tau) = A_k \frac{j_1(x)}{x} + B_k \frac{n_1(x)}{x}, \tag{3.10}$$

where the x-dependence is kept for clarity. The first-order of these special functions takes a simple form of

$$\begin{aligned} j_1(x) &= \frac{\sin x}{x^2} - \frac{\cos x}{x}, \\ n_1(x) &= -\frac{\cos x}{x^2} - \frac{\sin x}{x}. \end{aligned} \tag{3.11}$$

By matching the superhorizon solution, $\phi_{RD}(x \longrightarrow 0) = -\frac{2}{3}\zeta_{in}$, we obtain the general solution for RD background,

$$\phi_k(\tau) = -2\zeta_{in}\left(\frac{\sin x - x\cos x}{x^3}\right). \tag{3.12}$$

It is clear that, once the potential enters the horizon during the RD epoch, it oscillates and decays by time as $\sim x^{-2} \propto \tau^{-2} \propto a^{-2}$. The physical explanation is that radiation does not cluster. Thus, when the universe is filled with radiation, the gravitational potential cannot assemble the cosmic content since the radiation pressure keeps them away from each other. So, the potential is solely diluted by the expansion.

MD background

In MD era, $w = 0$ and $\mathcal{H} = 2/\tau$. Hence, the equation of motion takes a simpler form,

$$\phi_k'' + \frac{6}{\tau}\phi_k' = 0. \tag{3.13}$$

The solutions of this equation are decay and constant power-law modes,

$$\phi_k(\tau) = C_k + D_k\tau^{-5}. \tag{3.14}$$

Neglecting the decay mode as usual, we have constant gravitational potential at all scales in the MD epoch. This is because the pressure is zero for pressureless dust and the potential clusters the cosmic content together which strengthens it in turns. Therefore, the potential can

maintain its magnitude even in an expanding space.

3.1.3 Linear Evolution of Cold Dark Matter

We arrive at the main focus of this thesis: the evolution of matter. The distribution of this fluid is the key to the formation of structure since it creates gravitational potential at the over-dense region, pulling themselves together and forming a virialized object. In other words, the structures observed nowadays are essentially tracers of underlying matter distribution. Therefore, the dynamics in each epoch must be described to understand the distribution pattern at each moment. We study cold dark matter (CDM) here because it is the dominating component of matter, owing more than 5 times more energy than baryons. Also, its dynamics are relatively easy to model since it is sensitive to gravitational interaction only, at least after decoupling deep in the RD epoch.

Generally, we can trade the gravitational potential with the matter density contrast in the equation 3.5 and obtain the equation of motion for matter perturbation. However, there is another way to obtain the equation of motion for matter; the conservation of energy-momentum tensor gives 4 equations,

$$T^{\mu\nu}{}_{;\nu} = 0. \tag{3.15}$$

By using the same setup, we obtain the relativistic continuity and Euler equations,

$$\begin{aligned} \delta' + 3\mathcal{H}\left(\frac{\delta P}{\delta\rho} - \frac{P_0}{\rho_0}\right)\delta &= \left(1 + \frac{P_0}{\rho_0}\right)(3\phi' - \boldsymbol{\nabla}\cdot\boldsymbol{v}) \\ \boldsymbol{v}' + \mathcal{H}\boldsymbol{v} - 3\mathcal{H}\frac{P_0'}{\rho_0'}\boldsymbol{v} &= -\frac{\boldsymbol{\nabla}\delta P}{\rho_0 + P_0} - \boldsymbol{\nabla}\psi \end{aligned} \tag{3.16}$$

This method is nice since we are sure that CDM does not interact with other fluids and its conservation can be written independently. Thus, we have the decoupled dynamical equations from the start. Let us substitute the characteristics of CDM: pressureless, $P_0 = \delta P = 0$. The equations reduced to

$$\begin{aligned} \delta_m' + \boldsymbol{\nabla}\cdot\boldsymbol{v}_m - 3\phi' &= 0 \\ \boldsymbol{v}_m' + \mathcal{H}\boldsymbol{v}_m &= -\boldsymbol{\nabla}\phi, \end{aligned} \tag{3.17}$$

where we also insert the zero gravitational slip constraint, $\psi = \phi$. By taking the spatial deriva-

tive of the Euler equation and substituting the continuity equation, we have

$$\delta_m'' + \mathcal{H}\delta_m' = \nabla^2\phi. \tag{3.18}$$

We wish to trade the gravitational potential with the density fluctuations to obtain the equation of motion for δ_m. From the Poisson equation, this potential is sourced by all species of cosmic content, including radiation and matter mainly during the RD and MD period. Therefore, the coupling with radiation fluctuation δ_r is expected. However, the contribution of it is irrelevant for the following reasons. During the RD epoch, we already see that the gravitational potential sourced by the dominating radiation decayed like $\sim (k\tau)^{-2}$. By taking the Laplacian to the solution 3.12, we can infer through the Poisson equation that the radiation density oscillates around zero in RD. In the MD era, the gravitational potential is constant. But, since the radiation does not cluster, the fluctuation oscillates around a new equilibrium set by the stationary potential. Thus, radiation on average would not contribute stably to gravitational potential in a time scale much longer than the oscillation period; there is no long-living shift. All these discussions can be explicitly shown by writing down the radiation fluid equations. Hence, the Poisson equation can be practically written as

$$\nabla^2\phi \approx 4\pi G a^2 \rho_{0,m}\Delta_m \approx \frac{3}{2}\mathcal{H}^2\delta_m + 3\mathcal{H}(\phi' + \mathcal{H}\phi). \tag{3.19}$$

Notice that, at this point, we can already infer the superhorizon evolution of density contrast. Since the potential is stationary outside the horizon and $k \ll \mathcal{H}$, we can neglect the Laplacian and time derivative of ϕ. Then, one finds that $\delta_m \propto -\phi$ remains constant in time at superhorizon limits, both in the RD and MD epochs. However, the magnitude of the comoving density contrast Δ_m grows like $(k\tau)^2$ outside the horizon. In the subhorizon limit $k \gg \mathcal{H}$, we see earlier that the potential either decays like $(k\tau)^{-2}$ during RD or stays constant during MD. Therefore, we can neglect $3\mathcal{H}(\phi_k' + \mathcal{H}\phi_k)$ when comparing to $k^2\phi_k$,

$$\nabla^2\phi \approx 4\pi G a^2 \rho_{0,m}\delta_m \quad ; \quad \text{Subhorizon limit.} \tag{3.20}$$

An interesting implication is the density perturbation in the Comoving and Poisson gauges are the same on a scale deep in the horizon. This shows that the gauge ambiguity is lifted when we translate from a large scale, where the GR effect is important, to a small scale, where Newtonian gravity is effective enough, as we have discussed at the beginning of section 2.3. In this case, the evolution of δ_m and Δ_m coincide. The following discussion will be dedicated to the behaviour

inside the horizon. The final equation of motion yields

$$\delta_m'' + \mathcal{H}\delta_m' - 4\pi G a^2 \rho_{0,m}\delta_m \approx 0. \tag{3.21}$$

For a two-component universe, we can use the Friedmann equation 2.10 to write the time-dependent conformal Hubble parameter as

$$\mathcal{H}^2 = \mathcal{H}_0^2 \frac{\Omega_{m,0}^2}{\Omega_{r,0}} \left(\frac{1}{y} + \frac{1}{y^2}\right), \tag{3.22}$$

where $y = a/a_{eq}$ and a_{eq} is the scale factor at $\rho_m = \rho_r$. Insert this into the equation and change variables to give us the so-called *Mészáros equation* [74],

$$\delta_m''(y) + \frac{2+3y}{2y(1+y)}\delta_m'(y) - \frac{3}{2y(1+y)}\delta_m(y) = 0. \tag{3.23}$$

The solutions of this equation are

$$\delta_m \propto \begin{cases} 2+3y \\ -(2+3y)\ln\left(\frac{\sqrt{1+y}+1}{\sqrt{1+y}-1}\right) + 6\sqrt{1+y} \end{cases}. \tag{3.24}$$

This solution smoothly describes the evolution of matter density from the RD to the MD epochs. Let us focus on the growing mode in each era. The solution in deep RD can be found by considering $y \ll 1$; the matter perturbation growing mode is logarithmic, $\delta_m \propto \ln(a/a_{eq})$. In the MD epoch ($y \gg 1$), the perturbation grows linearly, $\delta_m \propto a/a_{eq}$. This disparity of evolution in the RD and MD periods implies scale dependence in the observed matter distribution in the deep MD epoch. This follows from the fact that the fluctuations at each scale enter the horizon at different times. Recalling the horizon crossing criterion, $k = \mathcal{H}$, we can define the scale that enters at $a = a_{eq}$ as k_{eq}.

To understand how this post-process introduces scale dependence, let us indicate the time stamps in perturbation evolution with mode k. Initially, the density perturbation lives outside the horizon where it stays constant in time (but depends on k). Then, the perturbation enters the horizon at $k = \mathcal{H}$ corresponding to some scale factor $a = a_k$. From this point, the perturbation starts to grow, with the trend depending on the epoch in which the perturbation crosses the horizon. Then, the perturbation reaches the time of observation; let us say we are

observing the structure at $a = a_{obs}$. The summary of evolution would be

$$k^{3/2}\phi_k = \text{constant} \xrightarrow{\text{Horizon-crossing}} \delta_{k=\mathcal{H}} \propto \phi_{k=\mathcal{H}} \propto k^{-3/2} \xrightarrow{\text{time evolution}} \delta_k(a_{obs}), \tag{3.25}$$

where the subhorizon evolution is divided into two cases,

$$\delta_k(a_{obs}) = \begin{cases} \ln\left(\frac{a_{eq}}{a_k}\right)\left(\frac{a_{obs}}{a_{eq}}\right)\delta_{k=\mathcal{H}} & \text{;Enter in RD} \\ \left(\frac{a_{obs}}{a_k}\right)\delta_{k=\mathcal{H}} & \text{;Enter in MD} \end{cases}. \tag{3.26}$$

Notice that we assume a scale-independent dimensionless power spectrum of ζ so that $k^3|\zeta_k|^2$ is constant which is equivalently $\zeta_k \propto \phi_k \propto k^{-3/2}$. The relation between ϕ and δ is given by the Poisson equation. To recognize the dependence on k of δ_k, we recall that the horizon crossing time a_k depends on k from the relation $k = \mathcal{H}$. It can be inferred from the growing rate of $\mathcal{H}$ that a_k is proportional to k^{-1} and k^{-2} for the mode entering in the RD and MD epochs, respectively. Hence, the final k-dependence can be written as

$$\delta_k(a_{obs}) \propto \begin{cases} k^{-3/2}\ln\left(\frac{k}{k_{eq}}\right) & \text{;Enter in RD} \\ k^{1/2} & \text{;Enter in MD} \end{cases}. \tag{3.27}$$

This is the so-called *Mészáros effect*, the post-process that introduces dependence on k to the scale-invariant initial condition. By computing the matter power spectrum, we obtain the famous prediction,

$$P_m(k) \propto \begin{cases} k^{-3}\left(\ln\left(\frac{k}{k_{eq}}\right)\right)^2 & ; k > k_{eq} \\ k & ; k < k_{eq} \end{cases}, \tag{3.28}$$

where $k_{eq} = 0.073\Omega_m h^2$ Mpc^{-1} is the scale entering the horizon at matter-radiation equality time. The proportionality shows that the amplitude of density fluctuation on a small scale grows as the cubic length scale $(1/k)^3$ but decreases inversely $(1/k)^{-1}$ after passing the scale $1/k_{eq}$ on a larger scale (see figure 3.1)

Typically, this effect is captured by introducing the transfer function, $T(k)$, which may have various definitions throughout the literature. In this thesis, a certain definition is adopted,

$$\phi_{\boldsymbol{k}} = \frac{3}{5}T(k)\zeta_{\boldsymbol{k}}{}^{1}. \tag{3.29}$$

[1] The factor $\frac{3}{5}$ is there for historical reasons, It came from the relation between the primordial Bardeen poten-

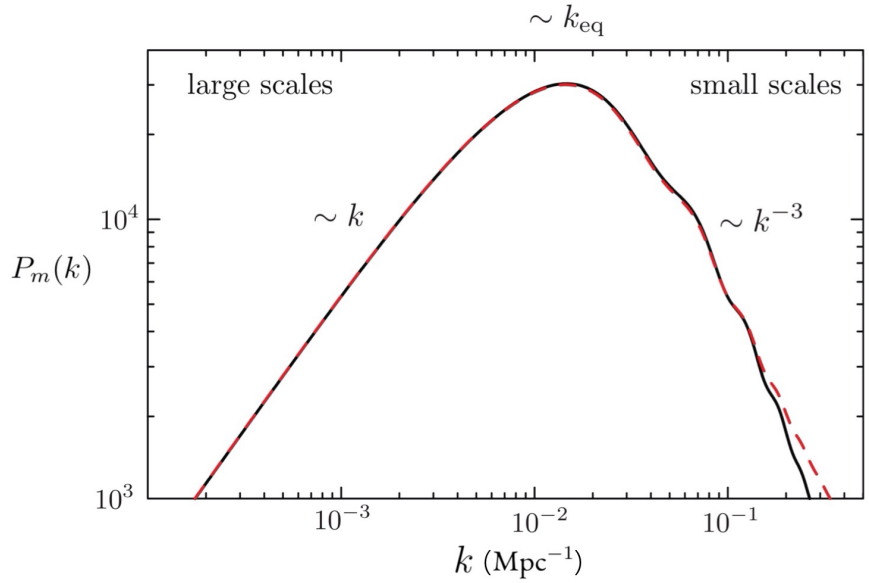

Figure 3.1: Scale dependence of matter density power spectrum. The thick black line presents the prediction by linear theory as being done here. The red dashed line is the prediction with non-linear corrections. This plot is taken from the *Cosmology Part III Mathematical Tripos* lecture note, D. Baumann.

The relation describes the modification of the gravitational potential ϕ rather than the density fluctuation. This is the effect discussed above without passing the potential through the Poisson equation. In particular, the solutions 3.12 tells us that $\phi_k \propto k^{-7/2}$ and solution 3.14 tells us that ϕ_k stays constant after crossing the horizon, suggesting that it keep the k-dependence like $\phi_k \propto k^{-3/2}$ from the primordial perturbation. It is important to stress that this is not exactly an equal-time relation; $\Phi_{\boldsymbol{k}}$ is the value in the matter-dominated epoch but $\zeta_{\boldsymbol{k}}$ is a stochastic value provided by inflation. The transfer function here is merely a separation of scale dependence caused by the Mészáros effect from the whole modification. To complete the description, the linear growth factor $D(a)$, encoding the linear evolution part to an arbitrary observation time, must be included. In the MD epochs, $D(a) \propto a$ (see solution 3.24 and the following discussion). The Poisson equation is then used to translate from potential to density contrast. The final form is

$$\delta_{\boldsymbol{k}}(a) = \frac{2}{5}\frac{k^2 T(k) D(a)}{\Omega_m H_0^2}\zeta_{\boldsymbol{k}}. \tag{3.30}$$

Notice that the formula returns identical asymptotic k-dependence as solution 3.27. This will be the starting point for the formation of the structure in the following section.

tial and the curvature perturbation that enter the horizon during the matter-dominated era [75].

3.2 Nonlinear Evolution of the Cold Dark Matter

The linear evolution of dark matter density on the superhorizon and subhorizon scales has been discussed in the last section. There, the Mészáros effect is found which is the first modification on density perturbation introduced by the dynamics after inflation we see. Ending the discussion, we conclude that the linear density perturbation is growing linearly with the scale factor in the MD epoch (see solution 3.24). This suggests one important issue: the linear perturbation will become inaccurate at some point in the late time universe. Later on, we will discuss the structure formation during the MD era which will require the nonlinear description of perturbation evolution. Hence, let us focus on the universe with the MD background. Generally, we write

$$\begin{aligned} \delta_{\boldsymbol{k}}(\tau) &= \sum_{n=1}^{\infty} \delta_{\boldsymbol{k}}^{(n)}(\tau), \\ \theta_{\boldsymbol{k}}(\tau) &= \sum_{n=1}^{\infty} \theta_{\boldsymbol{k}}^{(n)}(\tau), \end{aligned} \tag{3.31}$$

in Fourier space. From this point, **the subscript "$\boldsymbol{m}$" is dropped** from the matter background density and density contrast for clarity. Here, we see the appearance of fluid velocity perturbation: $\theta = \boldsymbol{\nabla} \cdot \boldsymbol{v}$ is the fluid velocity divergence. Previously, the fluid velocity was not explicitly discussed because its divergence is directly proportional to the density contrast as a linear solution on the MD background, $\delta_m' = -\boldsymbol{\nabla} \cdot \boldsymbol{v}_m$. In other words, we expect the same solution for $\delta_{\boldsymbol{k}}^{(1)}(\tau)$ and $\theta_{\boldsymbol{k}}^{(1)}(\tau)$. The nonlinearity starts from the second-order and beyond which are the aim of this section.

3.2.1 Collisionless Self-Gravitating CDM Fluid Equations

To do so, let us write the fluid equations for CDM again, but this time in a nonlinear regime. It is hard to follow the previous procedure; fully nonlinear cosmological perturbation theory would require us to consider the gauge problem and derive the equation of motion from Einstein's equation or conservation of energy-momentum tensor order by order. Hence, we follow a simpler analysis. We have seen the gauge ambiguity vanish on the subhorizon limit where the Poisson equation takes the same form as in Newtonian gravity (see equation 3.20 and the discussion above it). Hence, Newtonian gravity is not a bad approximation as we will consider structures much smaller than the horizon scale. Furthermore, CDM is assumed to interact

only with gravity. We see from the previous section that the source of gravitational potential is matter (see equation 3.19 and the discussion above it). Since CDM is the major contributor of matter in our universe, CDM fluid is effectively gravitating itself. These assumptions reduce our description of CDM perturbation to a collisionless self-gravitating fluid on an expanding background. With a non-relativistic space-time, the Lagrangian of such a particle can be easily written as

$$\mathcal{L} = \frac{1}{2}m\left\|\dot{\boldsymbol{x}}_{\text{phys}}(\boldsymbol{x},t)\right\|^2 - m\Phi(\boldsymbol{x},t), \tag{3.32}$$

where m is the mass of the CDM particle and $\boldsymbol{x}$ refers to comoving coordinates. The potential Φ is different from ϕ encountered previously. This quantity is rather defined as the background potential responsible for the expansion with the perturbation part,

$$\Phi = \Phi_b + \phi \quad ; \quad \Phi_b = \frac{2}{3}\pi G\rho_0\|\boldsymbol{x}\|^2. \tag{3.33}$$

The background potential is matched from the Friedmann equation 2.10 as an energy constraint of the static object on comoving coordinates. As in Newtonian gravity, the potential is constrained by the Poisson equation,

$$\nabla^2\Phi = -4\pi G a^2\rho, \tag{3.34}$$

where the Laplacian is constructed from the spatial derivative on the comoving coordinates. With the defined potential, the background part of the Poisson equation vanishes. So, the part can be removed and the equation is left with the perturbation part,

$$\nabla^2\phi = -4\pi G a^2\rho_0\delta, \tag{3.35}$$

Recall that $\boldsymbol{x}_{\text{phys}} = a(t)\boldsymbol{x}$ so that the Lagrangian can be written as

$$\mathcal{L}(\boldsymbol{x},\dot{\boldsymbol{x}}) = \frac{1}{2}ma^2(t)\|\dot{\boldsymbol{x}}\|^2 - m\phi(\boldsymbol{x},t), \tag{3.36}$$

where we exploit the symmetry of Lagrangian and use the canonical transformation, $\mathcal{L} \longrightarrow \mathcal{L} + \frac{d\Psi}{dt}$ with $\Psi = \frac{1}{2}ma\dot{a}\|\boldsymbol{x}\|^2$, with the help from the Friedmann equation 2.10. With this Lagrangian, we can the conjugate momentum of the system as

$$\boldsymbol{p} = \boldsymbol{\nabla}_{\dot{x}}\mathcal{L} = ma\boldsymbol{v}, \tag{3.37}$$

where the peculiar velocity is $\boldsymbol{v} = \dot{\mathbf{x}}$. The equation of motion is the Euler-Lagrange equation,

$$\dot{\boldsymbol{p}} = \boldsymbol{\nabla}\mathcal{L} \longrightarrow \frac{d\boldsymbol{v}}{dt} + H\boldsymbol{v} = -\frac{1}{a}\boldsymbol{\nabla}\phi, \tag{3.38}$$

which is the Euler equation in the Lagrangian picture of fluid. Alternatively, we can discuss the Hamiltonian mechanics. By Legendre transformation, we can change the dynamical variables $(\boldsymbol{x}, \dot{\boldsymbol{x}}) \longrightarrow (\boldsymbol{x}, \boldsymbol{p})$ and write a Hamiltonian define on phase space,

$$\mathbf{H}(\boldsymbol{x}, \boldsymbol{p}, t) = \frac{p^2}{2ma} + m\phi(\boldsymbol{x}, t), \tag{3.39}$$

and the equation of motion can be computed from the Hamilton equations.

The situation can also be analysed statistically since we are interested in the collective phenomena of CDM particles rather than the motion of a single particle. Generally, we can now consider the phase space evolution of the distribution function. Let us recall the evolution equation in phase space,

$$\hat{\mathbb{L}}[f] = \hat{\mathbb{C}}[f], \tag{3.40}$$

where f is the phase space distribution. The left-hand side of the equation is the *Liouville operator* $\hat{\mathbb{L}}$, returning is the change along the phase space trajectory. The right-hand side is the collision operator, encoding the change due to particle interactions. In the case of CDM, the collision is assumed to vanish since it only interacts with gravitational potential, causing a change in momentum. Hence, the situation falls into the case of *Louisville theorem*; the phase space distribution function is conserved along the phase space trajectory,

$$\hat{\mathbb{L}}[f] = \frac{df}{d\lambda} = 0, \tag{3.41}$$

where λ is the affine parameter of the trajectory curve. For $f = f(\boldsymbol{x}, \boldsymbol{p}, t)$, we obtain the so-called *Vlasov-Poisson* equation,

$$\frac{df}{dt} + \frac{\boldsymbol{p}}{ma^2} \cdot \boldsymbol{\nabla} f - m\boldsymbol{\nabla}\phi \cdot \boldsymbol{\nabla}_{\boldsymbol{p}} f = 0, \tag{3.42}$$

where the potential ϕ is sourced through the Poisson equation 3.35. It is hard to solve for the distribution function exactly from this equation. Luckily, we do not have to do so to obtain the statistical quantities. Those characteristics can be obtained by finding the moment solutions

of this equation. Namely, the mass density and fluid velocity are defined as

$$\begin{aligned}\rho(\boldsymbol{x},t) &= \frac{m}{a^3}\int d^3p\; f(\boldsymbol{x},\boldsymbol{p},t)\\ \boldsymbol{v}(\boldsymbol{x},t) &= \frac{1}{ma}\frac{\int d^3p\;\boldsymbol{p}f(\boldsymbol{x},\boldsymbol{p},t)}{\int d^3p\; f(\boldsymbol{x},\boldsymbol{p},t)}\end{aligned} \tag{3.43}$$

Notice that the fluid description also changes from the Lagrangian picture to the Eulerian picture since we are no longer tracking the motion of each particle. Rather, we define statistical quantities on a static coordinate through moments of the distribution function. For instance, the fluid velocity is not the time-derivative of the coordinates like in the Lagrangian picture but rather a vector field defined on phase space. Before proceeding, let us assume isotropy of the distribution function $f = f(\boldsymbol{x}, p, t)$ since we do not expect the distribution of particles to depend on the direction of its momentum. The equation of motion of the zeroth moment can be obtained by integrating the Vlasov-Poisson equation over the momentum volume,

$$\frac{\partial\rho}{\partial t} + 3H\rho + \frac{1}{a}\boldsymbol{\nabla}\cdot(\rho\boldsymbol{v}) = 0, \tag{3.44}$$

which is the continuity equation of fluid on an expansion coordinate. We neglect $\int d^3p\;\boldsymbol{\nabla}_{\boldsymbol{p}}f$ by the isotropy of f. The density in this equation can be split into the background and perturbation parts, $\rho = \rho_0(1+\delta)$. The background matter density is expected to dilute as a^{-3} (see equation 2.9) so we have the background part as $\dot{\rho}_0 + 3H\rho_0 = 0$. Therefore, the continuity equation above is left with just the perturbation part,

$$\frac{\partial\delta}{\partial t} + \frac{1}{a}\boldsymbol{\nabla}\cdot[(1+\delta)\boldsymbol{v}] = 0 \tag{3.45}$$

The first moment can be found by $\int d^3p\;\boldsymbol{p}$ (3.42),

$$\frac{\partial v^i}{\partial t} + Hv^i + \frac{1}{a}\left(v^i\frac{\partial}{\partial x^i}\right)v^i = -\frac{1}{a}\frac{\partial\phi}{\partial x^i} - \frac{1}{a\rho}\frac{\partial}{\partial x^i}\left[\rho\Pi^{ij}\right], \tag{3.46}$$

where the velocity dispersion tensor is defined as

$$\Pi^{ij} = \frac{\int d^3p\; p^ip^jf(\boldsymbol{x},\boldsymbol{p},t)}{\int d^3p\; f(\boldsymbol{x},\boldsymbol{p},t)} - v^iv^j, \tag{3.47}$$

and the indices notation for 3D vectors and tensors is used here. Notice that the velocity dis-

persion is sourced by the pressure of the fluid in the isotropic case, $\Pi^{ij} = P\delta^{ij}$, which is zero for pressureless CDM. Hence, the last term is neglected. Considering the equations 3.44 and 3.46, the scale factor always appears where the spatial derivative is. This is because fluid is on an expanding coordinate. The factor can be absorbed by rescaling the time into the conformal time so the coordinate is conformal to a static flat (Minkowski) space-time. The final set of fluid equations is

$$\begin{aligned} \frac{\partial \delta}{\partial \tau} + \boldsymbol{\nabla} \cdot [(1+\delta)\boldsymbol{v}] &= 0, \\ \frac{\partial \boldsymbol{v}}{\partial \tau} + (\boldsymbol{v} \cdot \boldsymbol{\nabla})\, \boldsymbol{v} + \mathcal{H}\boldsymbol{v} &= -\boldsymbol{\nabla}\phi, \\ \nabla^2 \phi &= \frac{3}{2}\Omega_m \mathcal{H}^2 \delta, \end{aligned} \tag{3.48}$$

where the last equation is non-dynamical and comes from the Poisson equation 3.19 modified with the Friedmann equation 2.10. It is important to emphasize that no linear approximation has been done in this derivation. These equations are obtained by separating the background and disturbance parts. The existing and well-known background dynamics are used to remove the background part of the equations and all nonlinear terms of inhomogeneous quantity are well-kept.

Another worth mentioning is the continuity and Euler equations in this case can be written in terms of convective time derivative, $\frac{D}{D\tau} = \frac{\partial}{\partial \tau} + \boldsymbol{v} \cdot \boldsymbol{\nabla}$,

$$\begin{aligned} \frac{D\delta}{D\tau} + \theta(1+\delta) &= 0, \\ \frac{D\boldsymbol{v}}{D\tau} + \mathcal{H}\boldsymbol{v} &= -\boldsymbol{\nabla}\phi. \end{aligned} \tag{3.49}$$

Notice that the Euler equation matches the equation of motion 3.38 obtained earlier if we go back to the physical time scale and reduce the convective derivative to the partial derivative. Indeed, the convective time derivative in the Euler description turns into the partial time in the Lagrangian fluid description.

The Euler and Poisson equations can be combined to remove ϕ from the picture. To do so, we take a spatial derivative to the Euler equation. The result is

$$\frac{\partial \theta}{\partial \tau} + \mathcal{H}\theta + \frac{3}{2}\Omega_m \mathcal{H}^2 \delta = -v^i \partial_i \theta - \partial_i v^j \partial_j v^i. \tag{3.50}$$

Then, we have a system of two nonlinear fluid equations with 2 degrees of freedom: the fluid density and velocity. From this point, we can solve the system order by order of perturbation to obtain the nonlinear evolution of CDM fluid. It is useful to move to the Fourier space since it is easier to order the structure by its scale. So, the (inverse) Fourier transformation of the quantities are

$$\begin{aligned}
\delta(\boldsymbol{x},\tau) &= \int \frac{d^3k}{(2\pi)^3}\delta_{\boldsymbol{k}}(\tau)e^{-i\boldsymbol{k}\cdot\boldsymbol{x}},\\
\boldsymbol{v}(\boldsymbol{x},\tau) &= \int \frac{d^3k}{(2\pi)^3}\boldsymbol{v}_{\boldsymbol{k}}(\tau)e^{-i\boldsymbol{k}\cdot\boldsymbol{x}},\\
\theta(\boldsymbol{x},\tau) &= \int \frac{d^3k}{(2\pi)^3}\theta_{\boldsymbol{k}}(\tau)e^{-i\boldsymbol{k}\cdot\boldsymbol{x}}.
\end{aligned} \tag{3.51}$$

Notice that the relation $\theta = \boldsymbol{\nabla}\cdot\boldsymbol{v}$ implies that $\boldsymbol{v}_{\boldsymbol{k}} = i\frac{\boldsymbol{k}}{k^2}\theta_{\boldsymbol{k}}$ in Fourier space. These transformations can be plugged into the first equation of 3.48 and equation 3.50 to obtain the equations in Fourier space,

$$\begin{aligned}
&\frac{\partial\delta_{\boldsymbol{k}}(\tau)}{\partial\tau} + \theta_{\boldsymbol{k}}(\tau) =\\
&\qquad -\int_{\boldsymbol{k_1}}\int_{\boldsymbol{k_2}} \delta_D^{(3)}(\boldsymbol{k}-\boldsymbol{k_1}-\boldsymbol{k_2})\alpha(\boldsymbol{k_1},\boldsymbol{k_2})\theta_{\boldsymbol{k_1}}(\tau)\delta_{\boldsymbol{k_2}}(\tau),\\
&\frac{\partial\theta_{\boldsymbol{k}}(\tau)}{\partial\tau} + \mathcal{H}(\tau)\theta_{\boldsymbol{k}}(\tau) + \frac{3}{2}\Omega_m(\tau)\mathcal{H}^2(\tau)\delta_{\boldsymbol{k}}(\tau) =\\
&\qquad -\int_{\boldsymbol{k_1}}\int_{\boldsymbol{k_2}} \delta_D^{(3)}(\boldsymbol{k}-\boldsymbol{k_1}-\boldsymbol{k_2})\beta(\boldsymbol{k_1},\boldsymbol{k_2})\theta_{\boldsymbol{k_1}}(\tau)\theta_{\boldsymbol{k_2}}(\tau),
\end{aligned} \tag{3.52}$$

where we use the notation $\int_{\boldsymbol{k}} \equiv \int \frac{d^3k}{(2\pi)^3}$ for clarity. The kernels are defined as

$$\alpha(\boldsymbol{k_1},\boldsymbol{k_2}) = \frac{\boldsymbol{k_1}\cdot(\boldsymbol{k_1}+\boldsymbol{k_2})}{k_1^2} \quad \text{and} \quad \beta(\boldsymbol{k_1},\boldsymbol{k_2}) = \frac{\|\boldsymbol{k_1}+\boldsymbol{k_2}\|^2(\boldsymbol{k_1}\cdot\boldsymbol{k_2})}{2k_1^2k_2^2}. \tag{3.53}$$

The system is conveniently presented in partial differential equations (PDE) of time. All time-dependent functions are indicated with the argument.

3.2.2 Standard Perturbation Theory (SPT) Approach

The system 3.52 can be solved perturbatively where the solution can be obtained order by order (see expansion 3.31). In particular, the lower-order solutions are used to solve for the

next-order solutions. Notice that the right-hand side of the equations 3.52 hosts the nonlinear contribution which will be substituted with the solutions from the previous order. Our starting point would be on the linear level where we can neglect the right-hand side of the equations completely. The solutions are expected to match the linear evolution on the subhorizon scale discussed in the last section. Since the linear part of the system is already satisfied, the second-order PDEs can be obtained by extending the approximation up to the second-order in perturbation. Then, the linear solution enters the second-order system via the nonlinear terms which we can then solve. The procedures then repeat for higher-order solutions. So, we would expect the PDEs of the nth-order solution to be

$$\begin{aligned}
&\frac{1}{\mathcal{H}}\frac{\partial\delta^{(n)}_{\boldsymbol{k}}(\tau)}{\partial\tau}+\frac{\theta^{(n)}_{\boldsymbol{k}}(\tau)}{\mathcal{H}}= \\
&\quad-\sum_{m=1}^{n-1}\int_{\boldsymbol{k_1}}\int_{\boldsymbol{k_2}}\delta^{(3)}_D(\boldsymbol{k}-\boldsymbol{k_1}-\boldsymbol{k_2})\alpha(\boldsymbol{k_1},\boldsymbol{k_2})\frac{\theta^{(m)}_{\boldsymbol{k_1}}(\tau)}{\mathcal{H}}\delta^{(n-m)}_{\boldsymbol{k_2}}(\tau), \\
&\frac{1}{\mathcal{H}}\frac{\partial}{\partial\tau}\left(\frac{\theta^{(n)}_{\boldsymbol{k}}(\tau)}{\mathcal{H}}\right)+\left(\frac{\mathcal{H}'}{\mathcal{H}^2}+1\right)\left(\frac{\theta^{(n)}_{\boldsymbol{k}}(\tau)}{\mathcal{H}}\right)+\frac{3}{2}\Omega_m\delta^{(n)}_{\boldsymbol{k}}(\tau)= \\
&\quad-\sum_{m=1}^{n-1}\int_{\boldsymbol{k_1}}\int_{\boldsymbol{k_2}}\delta^{(3)}_D(\boldsymbol{k}-\boldsymbol{k_1}-\boldsymbol{k_2})\beta(\boldsymbol{k_1},\boldsymbol{k_2})\frac{\theta^{(m)}_{\boldsymbol{k_1}}(\tau)}{\mathcal{H}}\frac{\theta^{(n-m)}_{\boldsymbol{k_2}}(\tau)}{\mathcal{H}},
\end{aligned} \tag{3.54}$$

where we manipulate the equations such that $\theta^{(n)}_{\boldsymbol{k_1}}(\tau)$ is normalized by $\mathcal{H}$. A quick inspection would tell us that the PDEs at each order are nonlinear so it is nontrivial to solve. But, let us explore some possibilities step by step. Looking at the system again, there are only time derivatives and $\boldsymbol{k}$ is nondynamical. So, we may expect a solution of each order with the time-dependent part factored out from the mode-dependent coefficient. However, the nonlinearity of the integral term prevents us from factoring the k-dependence part out from the PDEs. If possible, a nontrivial choice of separation would be needed to solve the equations. Before that, let us apply some approximation to the PDEs to simplify the situation.

SPT On A Fixed Background Cosmology

Before that, let us manipulate the equations further. The linear growth factor of the CDM density perturbation is introduced in the last section where we found $D(a)\propto a$ in the deep MD epoch. As we want to be general and stay on a ΛCDM, let us define the growth rate

parameter,

$$f \equiv \frac{d\ln D}{d\ln a} = \frac{1}{\mathcal{H}}\frac{d\ln D}{d\tau}. \tag{3.55}$$

Equivalently, $D(a) \propto a^f$. For the EdS universe, we expect $f = 1$ as we have found earlier for deep MD epoch. Therefore, the PDEs take the forms,

$$\begin{aligned}
\frac{\partial\delta^{(n)}_{\boldsymbol{k}}(\tau)}{\partial\ln D} + \frac{\theta^{(n)}_{\boldsymbol{k}}(\tau)}{\mathcal{H}f} &= \\
-\sum_{m=1}^{n-1}\int_{\boldsymbol{k_1}}\int_{\boldsymbol{k_2}} \delta_D^{(3)}(\boldsymbol{k}-\boldsymbol{k_1}-\boldsymbol{k_2})\alpha(\boldsymbol{k_1},\boldsymbol{k_2})\frac{\theta^{(m)}_{\boldsymbol{k_1}}(\tau)}{\mathcal{H}f}\delta^{(n-m)}_{\boldsymbol{k_2}}(\tau), & \\
\frac{\partial}{\partial\ln D}\left(\frac{\theta^{(n)}_{\boldsymbol{k}}(\tau)}{\mathcal{H}f}\right) + \frac{1}{f}\left(\frac{\mathcal{H}'}{\mathcal{H}^2}+1\right)\left(\frac{\theta^{(n)}_{\boldsymbol{k}}(\tau)}{\mathcal{H}f}\right) + \frac{3}{2}\frac{\Omega_m}{f^2}\delta^{(n)}_{\boldsymbol{k}}(\tau) &= \\
-\sum_{m=1}^{n-1}\int_{\boldsymbol{k_1}}\int_{\boldsymbol{k_2}} \delta_D^{(3)}(\boldsymbol{k}-\boldsymbol{k_1}-\boldsymbol{k_2})\beta(\boldsymbol{k_1},\boldsymbol{k_2})\frac{\theta^{(m)}_{\boldsymbol{k_1}}(\tau)}{\mathcal{H}f}\frac{\theta^{(n-m)}_{\boldsymbol{k_2}}(\tau)}{\mathcal{H}f}. &
\end{aligned} \tag{3.56}$$

As mentioned in the last section, the fluid equations are built in the deep MD epoch where Ω_m is very close to one. On a ΛCDM background, Ω_m is time-dependent as the universe translates through different eras, from the RD to ΛD epochs. However, we can approximate Ω_m as a constant for a timescale much smaller than the entire MD period. Notice that this also implies a constant growth rate f since the background parameters are unchanged. This simplification is equivalent to asking for a fixed background cosmology. Of course, this is not true in the well-accepted ΛCDM universe model and we will comment on this later. Let us solve this system in the linear order. In that case, we neglect the integral terms since they are nonlinear,

$$\begin{aligned}
\frac{\partial\delta^{(1)}_{\boldsymbol{k}}(\tau)}{\partial\ln D} + \frac{\theta^{(1)}_{\boldsymbol{k}}(\tau)}{\mathcal{H}f} &= 0, \\
\frac{\partial}{\partial\ln D}\left(\frac{\theta^{(1)}_{\boldsymbol{k}}(\tau)}{\mathcal{H}f}\right) + \frac{1}{f}\left(\frac{\mathcal{H}'}{\mathcal{H}^2}+1\right)\left(\frac{\theta^{(1)}_{\boldsymbol{k}}(\tau)}{\mathcal{H}f}\right) + \frac{3}{2}\frac{\Omega_m}{f^2}\delta^{(1)}_{\boldsymbol{k}}(\tau) &= 0.
\end{aligned} \tag{3.57}$$

By the first equation, $\delta^{(1)}_{\boldsymbol{k}}(\tau) \propto D(\tau)$ implies the linear solution,

$$\theta^{(1)}_{\boldsymbol{k}}(\tau) = -\mathcal{H}f\delta^{(1)}_{\boldsymbol{k}}(\tau). \tag{3.58}$$

After substituting the solution into the second PDE, we obtain a constraint,

$$\frac{1}{f}\left(\frac{\mathcal{H}'}{\mathcal{H}^2}+1\right)=\frac{3}{2}\frac{\Omega_m}{f^2}-1. \tag{3.59}$$

Therefore, we can rewrite the PDEs for the nth-order perturbation as

$$\begin{aligned}
&\frac{\partial\delta_{\boldsymbol{k}}^{(n)}(\tau)}{\partial\ln D}+\frac{\theta_{\boldsymbol{k}}^{(n)}(\tau)}{\mathcal{H}f}=\\
&-\sum_{m=1}^{n-1}\int_{\boldsymbol{k_1}}\int_{\boldsymbol{k_2}}\delta_D^{(3)}(\boldsymbol{k}-\boldsymbol{k_1}-\boldsymbol{k_2})\alpha(\boldsymbol{k_1},\boldsymbol{k_2})\frac{\theta_{\boldsymbol{k_1}}^{(m)}(\tau)}{\mathcal{H}f}\delta_{\boldsymbol{k_2}}^{(n-m)}(\tau),\\
&\frac{\partial}{\partial\ln D}\left(\frac{\theta_{\boldsymbol{k}}^{(n)}(\tau)}{\mathcal{H}f}\right)+\left(\frac{3}{2}\frac{\Omega_m}{f^2}-1\right)\left(\frac{\theta_{\boldsymbol{k}}^{(n)}(\tau)}{\mathcal{H}f}\right)+\frac{3}{2}\frac{\Omega_m}{f^2}\delta_{\boldsymbol{k}}^{(n)}(\tau)=\\
&-\sum_{m=1}^{n-1}\int_{\boldsymbol{k_1}}\int_{\boldsymbol{k_2}}\delta_D^{(3)}(\boldsymbol{k}-\boldsymbol{k_1}-\boldsymbol{k_2})\beta(\boldsymbol{k_1},\boldsymbol{k_2})\frac{\theta_{\boldsymbol{k_1}}^{(m)}(\tau)}{\mathcal{H}f}\frac{\theta_{\boldsymbol{k_2}}^{(n-m)}(\tau)}{\mathcal{H}f}.
\end{aligned} \tag{3.60}$$

Notice that the linear-order solutions factor their time dependence out as linear growth factor $D(\tau)$. In particular, the solutions are written as

$$\begin{aligned}
\delta_{\boldsymbol{k}}^{(1)}(\tau)&=D(\tau)\delta_{\boldsymbol{k}}^{(1)},\\
\theta_{\boldsymbol{k}}^{(1)}(\tau)&=-\mathcal{H}(\tau)fD(\tau)\theta_{\boldsymbol{k}}^{(1)},
\end{aligned} \tag{3.61}$$

where $\delta_{\boldsymbol{k}}^{(1)}=\theta_{\boldsymbol{k}}^{(1)}$ at the first order. These solutions will be substituted into the second-order equations to solve for the next-order solution. The crucial point is the equations are *homogeneous* in $D(\tau)$. Thus, we can always factor the time dependence out. Moreover, the nonlinearity of the integral term suggests that the time dependence of the nth-order solution is $D^n(\tau)$. Therefore, we re-write the order expansion more conveniently,

$$\begin{aligned}
\delta_{\boldsymbol{k}}(\tau)&=\sum_{n=1}^{\infty}D^n(\tau)\delta_{\boldsymbol{k}}^{(n)},\\
\theta_{\boldsymbol{k}}(\tau)&=-\mathcal{H}(\tau)f\sum_{n=1}^{\infty}D^n(\tau)\theta_{\boldsymbol{k}}^{(n)}.
\end{aligned} \tag{3.62}$$

Let us emphasize that this factorization of time dependence is possible because we assume constants Ω_m and f. The assumption made the equation homogeneous in the growth factor so the

solution can be ordered with the power-law time-dependent factor. Now that the evolution part is known, we need the solutions for mode-dependence amplitudes. The factorization of time dependence would leave the system with constraint equations where the integral of lower-order solutions solves the next-order amplitudes. Thus, the solutions can be solved iteratively starting from the known linear solutions. Then, it is realized that all higher-order solutions are merely multiple first-order density solutions integrated against a kernel,

$$\begin{aligned}\delta^{(n)}_{\boldsymbol{k}} &= \int_{\boldsymbol{q_1}} \cdots \int_{\boldsymbol{q_n}} \delta^{(3)}_D \left(\boldsymbol{k} - \sum_{i=1}^{n} \boldsymbol{q_i} \right) F^{(s)}_n(\boldsymbol{q_1}, \ldots, \boldsymbol{q_n}) \delta^{(1)}_{\boldsymbol{q_1}} \ldots \delta^{(1)}_{\boldsymbol{q_n}}, \\ \theta^{(n)}_{\boldsymbol{k}} &= \int_{\boldsymbol{q_1}} \cdots \int_{\boldsymbol{q_n}} \delta^{(3)}_D \left(\boldsymbol{k} - \sum_{i=1}^{n} \boldsymbol{q_i} \right) G^{(s)}_n(\boldsymbol{q_1}, \ldots, \boldsymbol{q_n}) \delta^{(1)}_{\boldsymbol{q_1}} \ldots \delta^{(1)}_{\boldsymbol{q_n}}.\end{aligned} \tag{3.63}$$

where the superscript "(s)" denotes a symmetrized-in-k's kernel. This follows from the fact that a kernel solved from the constraint equations will get symmetrized by $\delta^{(1)}_{\boldsymbol{q_1}} \ldots \delta^{(1)}_{\boldsymbol{q_n}}$ in the end. With these ansatzes, we can solve for the kernels from the equations 3.60. The recursion relations are

$$\begin{aligned}F_n(\boldsymbol{q_1}, \ldots, \boldsymbol{q_n}) &= \left[\left(2n + 3\frac{\Omega_m}{f^2} \right) (n-1) \right]^{-1} \sum_{m=1}^{n-1} G_m(\boldsymbol{q_1}, \ldots, \boldsymbol{q_m}) \\ &\left[2\beta(\boldsymbol{k_1}, \boldsymbol{k_2}) G_{n-m}(\boldsymbol{q_{m+1}}, \ldots, \boldsymbol{q_n}) + \left(2n + 3\frac{\Omega_m}{f^2} - 2 \right) \alpha(\boldsymbol{k_1}, \boldsymbol{k_2}) F_{n-m}(\boldsymbol{q_{m+1}}, \ldots, \boldsymbol{q_n}) \right], \\ G_n(\boldsymbol{q_1}, \ldots, \boldsymbol{q_n}) &= \left[\left(2n + 3\frac{\Omega_m}{f^2} \right) (n-1) \right]^{-1} \sum_{m=1}^{n-1} G_m(\boldsymbol{q_1}, \ldots, \boldsymbol{q_m}) \\ &\left[2n\beta(\boldsymbol{k_1}, \boldsymbol{k_2}) G_{n-m}(\boldsymbol{q_{m+1}}, \ldots, \boldsymbol{q_n}) + 3\frac{\Omega_m}{f^2} \alpha(\boldsymbol{k_1}, \boldsymbol{k_2}) F_{n-m}(\boldsymbol{q_{m+1}}, \ldots, \boldsymbol{q_n}) \right],\end{aligned} \tag{3.64}$$

where $\boldsymbol{k_1} = \sum_{i=1}^{m} \boldsymbol{q_i}$ and $\boldsymbol{k_2} = \sum_{i=m+1}^{n} \boldsymbol{q_i}$. Let us also recall that $\boldsymbol{k} = \boldsymbol{k_1} + \boldsymbol{k_2}$ according to solutions 3.63. Notice that the first-order kernels are trivial,

$$F_1 = G_1 = 1. \tag{3.65}$$

The kernel obtained from this formula is bare and can be symmetrized by

$$\begin{aligned} F_n^{(s)}(\boldsymbol{q_1},\ldots,\boldsymbol{q_n}) &= \frac{1}{n!}\sum_{\sigma} F_n(\boldsymbol{q_1},\ldots,\boldsymbol{q_n}), \\ G_n^{(s)}(\boldsymbol{q_1},\ldots,\boldsymbol{q_n}) &= \frac{1}{n!}\sum_{\sigma} G_n(\boldsymbol{q_1},\ldots,\boldsymbol{q_n}), \end{aligned} \tag{3.66}$$

where σ denotes all permutations of set $\{\boldsymbol{q_1},\ldots,\boldsymbol{q_n}\}$.

Solution on Einstein-de Sitter Background

Let us use this framework to obtain the second-order solution as an example. Typically, the situation is simplified to a pure EdS universe, representing the deep MD epoch. In this case, the universe is occupied solely by matter ($\Omega_m = 1$) and the linear growth factor is $D(a) \propto a$ ($f = 1$). Moreover, the scale factor grows like τ^2 and the Hubble parameter takes the form $\mathcal{H} = 2/\tau$. Hence, the expansion can be written as

$$\begin{aligned} \delta_{\boldsymbol{k}}(\tau) &= \sum_{n=1}^{\infty} a^n(\tau)\delta_{\boldsymbol{k}}^{(n)}, \\ \theta_{\boldsymbol{k}}(\tau) &= -\mathcal{H}(\tau)\sum_{n=1}^{\infty} a^n(\tau)\theta_{\boldsymbol{k}}^{(n)}. \end{aligned} \tag{3.67}$$

The second-order kernels are obtained by substituting the first-order kernels 3.65 into the recursion relations 3.64 with the specification of the EdS universe. Then, the kernels are symmetrized through the formula 3.66. The results are

$$\begin{aligned} F_2^{(s)}(\boldsymbol{q_1},\boldsymbol{q_2}) &= \frac{5}{7} + \frac{2}{7}\frac{(\boldsymbol{q_1}\cdot\boldsymbol{q_2})^2}{q_1^2 q_2^2} + \frac{\boldsymbol{q_1}\cdot\boldsymbol{q_2}}{2}\left(\frac{1}{q_1^2}+\frac{1}{q_2^2}\right), \\ G_2^{(s)}(\boldsymbol{q_1},\boldsymbol{q_2}) &= \frac{3}{7} + \frac{4}{7}\frac{(\boldsymbol{q_1}\cdot\boldsymbol{q_2})^2}{q_1^2 q_2^2} + \frac{\boldsymbol{q_1}\cdot\boldsymbol{q_2}}{2}\left(\frac{1}{q_1^2}+\frac{1}{q_2^2}\right). \end{aligned} \tag{3.68}$$

These kernels are then used to compute the mode-dependent part of the second-order solutions $\delta_{\boldsymbol{k}}^{(2)}$ and $\theta_{\boldsymbol{k}}^{(2)}$ through formulae 3.63. We obtain the full second-order solution with the time evolution factor (see expansions 3.67). Let us point out that the numerical coefficients in the kernels depend on the background cosmology, i.e. the factor Ω_m/f^2 seen earlier. Hence, those numbers are valid only for the EdS background and will take different values for $\Omega_m \neq 1$.

A crucial simplification we have made in the last section is asking Ω_m to be a constant; we fixed the background cosmology. It is well-known that the best model of the universe is the ΛCDM model (see section 2.1.3) which has an evolving background where the density parameters change with time. Reinstalling time-dependence to Ω_m would have sabotaged the homogeneity in the linear growth factor of PDEs 3.60 and the time evolution factorization of the ansatzes 3.62 would not work. However, we can still follow the same logic and write slightly more complicated expansions. Let us reconsider the computation of solutions. The first-order solution can still be split into time evolution and mode dependence as obtained in section 3.1.3. This is because the linear-order equations 3.57 are homogeneous in $\delta^{(1)}_{\mathbf{k}}$ and $\theta^{(1)}_{\mathbf{k}}$ and the derivative operator only cares about the time evolution of the solution. Hence, the mode-dependence part can be factored out and the linear growth factor is obtained by integrating the remaining equations. The second-order solutions are non-trivial to obtain. The inhomogeneity in $D(\tau)$ prevents us from factoring out the time dependence from the equation completely like before. However, the factorized form of the first-order solution ensures the separation of time-dependent function at some level of the solution. Indeed, $D^2(\tau)$ can still be nicely factored out from the integral. So, we can at least use the separation of variables, $\delta^{(2)}_{\boldsymbol{k}}(\tau) = D_2(\tau)\delta^{(2)}_{\boldsymbol{k}}$ and $\theta^{(2)}_{\boldsymbol{k}}(\tau) = D_2(\tau)\theta^{(2)}_{\boldsymbol{k}}$, to solve the PDEs. The second-order growth factor D_2 is obtained by integrating PDEs and the mode-dependent part is obtained from the following constraint equations. The third-order solution can be solved with the same method as the second-order. The story is more complicated at higher order; there is more than one integral term on the right-hand side of the PDEs. Each contribution is equipped with a different combination of time-dependent factors. For instance, the fourth-order equations would have the integrals with $\delta^{(2)}\delta^{(2)}$ and $\delta^{(3)}\delta^{(1)}$ which will give different time dependence. The naive separation of variables cannot be used anymore. Instead, the solutions are factorized as $\delta^{(2)}_{\boldsymbol{k}}(\tau) = \sum_m^{n-1} D_{m,n-m}(\tau)\delta^{(m,n-m)}_{\boldsymbol{k}}$ and $\theta^{(2)}_{\boldsymbol{k}}(\tau) = \sum_m^{n-1} D_{m,n-m}(\tau)\theta^{(m,n-m)}_{\boldsymbol{k}}$. In this way, the equations can be separated into multiple PDEs with their own integral contribution which can be solved independently. For instance, in the fourth-order solution, the growth factor $D_{2,2}(\tau)$ can be integrated from the PDEs with $\delta^{(2)}\delta^{(2)}$ integral term while $D_{3,1}(\tau)$ is obtained separately from the PDEs with $\delta^{(1)}\delta^{(3)}$. Each growth factor will have its mode dependence part, $\delta^{(m,n-m)}_{\boldsymbol{k}}$ and $\theta^{(m,n-m)}_{\boldsymbol{k}}$ with the personalised kernels $F_{(m,n-m)}$ and $G_{(m,n-m)}$. The set of solutions grows rapidly from the fixed background case and will not be computed in this thesis. [76] pointed out that the EdS background is not a bad approximation. $f \approx \Omega_m^{0.55}$

on ΛCDM background with the accuracy of linear growth factor $D(\tau)$ down to $< 1\%$ level at any time in range $\Omega_m \in [0.01, 1]$, which is well-approximated by EdS expansion.

3.3 Introduction to Biased Tracer

Direct observation of the underlying matter distribution is hard since our detection is limited to electromagnetic waves. Not all region in space emits a detectable signal and a full map of matter in the universe is still to be achieved. However, nature is still kind enough to leave us with some observable. Astronomical objects like galaxies are detectable and the recent catalogues contain millions of them [77, 78]. This large number of objects allows us to perform a feasible statistical analysis to learn about their underlying distribution. Let us define the (comoving) number density contrast,

$$\delta_g(\boldsymbol{x}) \equiv \frac{\delta n_g(\boldsymbol{x})}{\bar{n}_g} = \frac{n_g(\boldsymbol{x}) - \bar{n}_g}{\bar{n}_g}, \tag{3.69}$$

analogue to the matter density contrast. $n_g(\boldsymbol{x})$ is the comoving tracer number density while $\bar{n}_g$ is the average number density. By construction, the mean of this quantity (one-point function; $\langle \delta_g \rangle$) is zero. This is the statistical quantity of interest from which we will compute the NPCF. As usual per cosmological probes, the limitation of observation over space forced us to infer the ensemble average quantity from averaging over survey volume. This means there are 2 hypotheses to be adopted. Firstly. the homogeneity and isotropy of the underlying ensemble are assumed so that the sample at different points and directions are drawn from the same ensemble. Secondly, the observed sample of tracers is a fair sample that represents the ensemble well. With these two hypotheses, we expect the *ergodicity* over space of the tracer samples that the statistics inferred from averaging over the observable sky will be a good representation of the real distribution. Equivalently, the probability of finding an object P in a volume element δV is given by

$$P = \bar{n}_g V. \tag{3.70}$$

The probability here is position- and directional-independent, emphasizing the statistical homogeneity and isotropy. So, no matter from which area you are sampling the population of the galaxy, the measured statistics will be the same. We anticipate that more details on the statistics of the tracer will be presented in section 3.5.

A slight complication is that these objects do not represent the matter distribution directly.

The structure formation and clustering process are complicated and the number of tracers may not be directly proportional to the level of matter over density; the nonlinearity of gravity could spoil the proportionality. Moreover, the galaxy's formation rate can depend heavily on physics other than gravity like the local radiation field [79, 80, 81]. For tracers like dark matter halo, not all over-dense regions collapse into halo. These complications and many more are why these observed objects are *biased tracers* of the matter distribution. The connection between these biased tracers and the density distribution is crucial to mapping the universe's structure at different times, unlocking the window to infer the initial condition and fundamental physics of inflation that came with it.

Before continuing the discussion, let us clarify the different species of biased tracers. In this thesis, there are two kinds of tracers discussed:

- **Dark Matter Halo:** This is a hypothetical virialized region of dark matter enclosing smaller sub-structures inside. Since dark matter is not luminous, the halo cannot be directly observed by using electromagnetic waves. However, the halo is over-dense in matter and creates a gravitational potential well bounding other visible objects like galaxies inside them. Therefore, it can be identified by applying the halo finding algorithm to the distribution of galaxies such as the Friends-of-Friends (FoF) [82] and spherical-overdensity (SO) [83] algorithms. and Theoretically, the object is formed by the collapse of an over-dense region. Therefore, the statistic of the DM halo is associated with the statistics of underlying matter via the collapse theory which will be discussed shortly.

- **Galaxies:** They can be observed directly thanks to their electromagnetic wave emission. So, the identification is much less complicated than the DM halo and the number of this kind of tracer is much larger. However, their statistics are harder to model. Unlike DM halo whose formation is dominated by gravitational process, the formation of galaxies is a very complex process and can depend on many environmental factors other than gravity itself. Thus, we will not attempt to build the theory bottom-up but rather write an effective biased relation of the density fields (more detail later).

In this section, the theory of biased tracers and the statistics of them will be presented.

3.3.1 Origin Of Bias Parameter

As anticipated, the population of tracers is biased compared with the matter density distribution. This fact is first discovered in the distribution of a rich cluster of galaxies. The sample of the galaxy clusters from the Abell catalogue [27] was statistically analysed where the spatial correlation function $\xi_{cluster}$, which is associated with the probability of finding a pair of clusters at

a given separation length r, can be estimated [84, 85]. The same method was also applied to the population of galaxies to obtain the same function for galaxies ξ_{galaxy}. However, the results were misaligned. Regarding the power-law model of the correlation function, $\xi(r) = (r/r_*)^\gamma$, the characteristic correlation length of clusters, $r_{*cluster} \approx 25h^{-1}$ Mpc, is significantly smaller than of galaxies, $r_{*galaxy} \approx 50 - 100h^{-1}$ Mpc, while the exponent γ for clusters and galaxies are comparable, about $-1.7 \sim 1.8$. Shortly after, N. Kaiser suggests that, if the clusters were formed in the over-dense region, ξ_{galaxy} is "biased" from the underlying matter density fluctuation. Mathematically, it can be written as

$$\xi_{cluster}(r) = b^2 \xi_R(r), \tag{3.71}$$

where b is the bias parameter and $\xi_R(r) \equiv \langle \delta_R(\vec{x}) \delta_R(\vec{x}+\vec{r}) \rangle$ is the spatial correlation function of the smoothed linear density contrast. It was soon realized, upon the rise of the Standard Cold Dark Matter (sCDM) model, that even the galaxies themselves are not a good representative of the matter distribution. Nowadays, the ΛCDM model, which is a widely accepted model for our universe, accurately predicts the two-point correlation function of the matter density [15]. Hence, by measuring the function of galaxies or clusters from surveys, the bias parameter can be estimated. This is the key parameter affected by NG which will be studied in the upcoming sections. This is one of the methods by which the LSS survey is able to put a constraint on NG.

3.3.2 General Bias Expansion

We would like to establish an effective bias model for the tracer's population. The model will consist of the physical effect that may play a role in altering the tracer's population. In particular, we expect an expansion of the form,

$$\delta_g(\boldsymbol{x}, \tau) = \sum_{\mathcal{O}} (b_{\mathcal{O}}(\tau) + \varepsilon_{\mathcal{O}}(\boldsymbol{x}, \tau)) \mathcal{O}(\boldsymbol{x}, \tau) + \varepsilon(\boldsymbol{x}, \tau), \tag{3.72}$$

where $\mathcal{O}$ is a physical operator representing quantity that the tracer's number density depends on. For example, the matter density contrast, δ, is straight-forwardly one of those operators (see section 3.3.1). Each operator is accompanied by a bias parameter, $b_{\mathcal{O}}$, indicating the strength of the dependence of tracer density on that physics. For instance, a large bias parameter for δ would suggest that the tracer's population is largely amplified from the matter density contrast. A positive bias parameter would imply that the tracer is more crowded in the over-dense region and the opposite for negative bias. This effective expansion allows us to discuss the statistical

relation between tracers and relevant physical quantity. The relation of 2PCF in section 3.3.1 can be written from a model like $\delta_g(\boldsymbol{x}, \tau) = b_1(\tau)\delta(\boldsymbol{x}, \tau)$.

The nature is more complex than just a linear model of density contrast. The key is to explore every possible physics that could affect the tracer's population. Then, the bias parameters are left to be free and will be constrained by the correlation functions computed from the surveys. This is a general idea of how we learn about the galaxies' distribution and relevant physics. Though the set of relevant operators is gigantic, some can be less important than others depending on the scale. For example, the term at higher order becomes less important on a sufficiently large scale where perturbation theory is valid. Moreover, some non-local effects are suppressed at a large scale. For example, baryonic physics like the Baryon Acoustics Oscillation (BAO) feature is averaged out if we consider a minimum scale much larger than the BAO length scale. Finally, a sensible effective deterministic bias expansion can be written when the scale of interest is specified. However, we allow some degree of randomness to the bias coefficients and the tracer's population, capturing by $\varepsilon_{\mathcal{O}}(\boldsymbol{x}, \tau)$ and $\varepsilon(\boldsymbol{x}, \tau)$ respectively. These terms host the small-scale physics that are ignored in the deterministic expansion. Even though we must include them, they are completely random, thus uncorrelated to the deterministic part and with each other. The discussion of these stochastic terms is beyond the scope of this thesis and will not be explored in detail.

In the following section, we will explore the effect of gravitational physics on the tracer distribution. In particular, the evolution of the tracer number density under gravitational influence will be considered to identify the relevant operators in the bias expansion.

3.4 Conserved Evolution of Biased Tracers

For simplicity, the conservation of the tracer number is assumed; We will consider the situation where tracers are not created or destroyed along the trajectory. A population of it formed instantaneously at time τ_* and has been comoving with matter fluid until arbitrary time τ. This is a dramatic simplification since the number of tracers has always been changing throughout the universe's history. This issue will be addressed later by assuming multiple formation times. For the time being, let us write the conservation equation of the tracer fluid as the continuity equation,

$$\frac{D}{D\tau}\delta_g = \theta(1 + \delta_g) \tag{3.73}$$

The underlying CDM is described as an ideal, pressureless fluid with curl-free velocity. The suppression of vorticity on a large scale is well-justified by observation where CMB is dominated by scalar mode rather than vector or tensor. Indeed, these are the same assumptions we made for the collisionless self-gravitating CDM fluid where we assume an isotropic phase space distribution function (see section 3.2.1). The equations governing the dynamics of such a fluid are the continuity and Euler (momentum) equations (see equations 3.48),

$$\begin{aligned} \frac{D}{D\tau}\delta &= \theta(1+\delta), \\ \frac{D\theta}{D\tau} + \mathcal{H}\theta &= -\partial_i v^j \partial_j v^i - \frac{3}{2}\Omega_m \mathcal{H}^2 \delta, \end{aligned} \tag{3.74}$$

where the terms in the Euler equation are from expansion dilution, convective term, and gravitational pull. Notice that θ is the same as in equation 3.73 since the comoving condition is assumed[2]. This is true only for a sufficiently large patch where gravitational force dominates in the dynamics of tracers and the equivalent principle holds.

These equations govern the evolution of the conserved tracer and matter fluid. The idea is now the following. We propose the bias expansion of tracer density at the formation time as an initial condition. By solving these evolution equations, we will have the bias expansion at an arbitrary time given that the fluids are conserved and comoving. As you may see, these equations are nonlinearly coupled. Hence, one could expect a nonlinear evolution from them. $\delta_g(\tau)$ can be solved perturbatively with respect to the initial condition $\delta_g(\tau_*) \equiv \delta_{g*}$. There are two equivalent ways to do so. First, we integrate the continuity equations directly. Secondly, we iteratively solve equations 3.73 and 3.74 with a joint perturbative solution. At the end of each way, we will have a different formal expression but they describe the same physics.

Another important equation is the Poisson equation (see equations 3.48),

$$\nabla^2 \phi = \frac{3}{2}\Omega_m \mathcal{H}^2 \delta, \tag{3.75}$$

that relates the gravitational potential with the matter density distribution. As we will see later, the tidal field is also a relevant quantity in the game which is defined as

$$K_{ij} = \frac{2}{3\Omega_m \mathcal{H}^2}\partial_i \partial_j \phi - \frac{1}{3}\delta_{ij}\delta \equiv \mathcal{D}_{ij}\delta \quad ; \quad \mathcal{D}_{ij} \equiv \left(\frac{\partial_i \partial_j}{\nabla^2} - \frac{1}{3}\delta_{ij}\right). \tag{3.76}$$

[2] this condition breaks down if we consider a small-scale tracer where non-gravitational forces can significantly influence the galaxy trajectory, suggesting the so-called *velocity bias*.

Notice that K_{ij} is nothing more than the traceless part of $\partial_i \partial_j \phi$.

Lagrangian coordinates, Eulerian coordinates, and Fluid Trajectory

Before proceeding from this point, it is important to understand the concept of Lagrangian and Eulerian descriptions of fluid. The Lagrangian picture describes fluid as the motion of a parcel labelled with its position $\boldsymbol{q}(\tau)$, as in classical mechanics where the state of the system is defined on the configuration space. In this way, the coordinates deform and follow the trajectory of the parcel, removing the peculiar velocity in the direction of the flow. The convective derivative of a physical quantity is solely the time derivative since the parcel is stationary on the Lagrangian coordinates. The price to pay is that the spatial derivative involves the coordinates' deformation. In the Eulerian picture, the coordinates are fixed and the fluid parcel flows through the observed volume instead. The fluid velocity is now a field defined on the coordinate and time-dependent, $\boldsymbol{v}(\boldsymbol{x}, \tau)$. In this way, the convective derivative includes the velocity term, concerning the fluid flow. However, the spatial derivative has no deformation since the spatial coordinate is fixed. Imposing an equal number of tracers in the parcel, We can write the relation between the Lagrangian and the Eulerian volumes as

$$V^L = (1 + \delta^{(L)})V, \tag{3.77}$$

where V^L and V is the Lagrangian and Eulerian volumes respectively. $\delta^{(L)}$ is the matter density contrast in that parcel computed with the Lagrangian volume. For example, a larger region of a proto-halo in Lagrangian space in the initial condition shrinks down to the final Eulerian volume to form the halo which occupies a smaller space. By the definition of halo density contrast,

$$1 + \delta_g = \frac{N_g/V}{\bar{n}_g}, \tag{3.78}$$

where N_g is the number of tracers in the parcel, we can infer a relation between the tracer density contrast in Lagrangian and Eulerian spaces, δ_g and $\delta_g^{(L)}$, as

$$1 + \delta_g = (1 + \delta_g^{(L)})(1 + \delta^{(L)}). \tag{3.79}$$

The tracer density in each space would have its bias expansion with the parameter defined on the corresponding space. Hence, we now have a set of Eulerian bias and Lagrangian bias parameters, associated with the expansion of δ_g and $\delta_g^{(L)}$, respectively. However, they are related through

the relation 3.79. As an example, let us consider the linear bias, $\delta_g = b_1\delta$ and $\delta_g^{(L)} = b_1^{(L)}\delta^{(L)}$,

$$1 + \delta_g = 1 + (1 + b_1^{(L)})\delta + \mathcal{O}(\delta^2). \tag{3.80}$$

Note that, in first-order, the density contrasts in Lagrangian and Eulerian space are interchangeable, $\delta^{(L)} = \delta + \mathcal{O}(\delta^2)$. We can infer the relation of linear bias between both spaces as $b_1 = 1 + b_1^{(L)}$. Notice that if the tracer is uniformly distribution in the Lagrangian space, $b_1^{(L)} = 0$, they are unbiased relative to the underlying matter, $b_1 = 1$.

This relation of the higher-order bias parameters can be inferred by expanding the bias relation to higher-order. Also, the Lagrangian space density $\delta^{(L)}$ must be properly transformed into the Eulerian density δ. Essentially, the initial density of Lagrangian and Eulerian spaces are the same. Then, the Eulerian density evolves according to the fluid equations (see section 3.2), displacing and growing with time, i.e. they hold equal value and start at the same position $\boldsymbol{q}$. However, the Lagrangian density is not subjected to fluid displacement as the coordinate is fixed. Thus, it only evolves with time according to the growth factor. Therefore, the relation between the density contrasts can be described with the time evolution-excluded SPT solutions 3.63. By solving and inverse the relations, we can substitute $\delta^{(L)}$ with δ to the desired order and obtain the Eulerian bias parameter in terms of the Lagrangian ones. For example, if we assume spherical symmetry where the tidal field is absent[3], the bias of operator δ^2 is transformed as

$$b_2 = 2(1 + c_2)b_1^{(L)} + b_2^{(L)}. \tag{3.81}$$

The constant c_2 depends on the background cosmology, as we have discussed in section 3.2.2. For example, $c_2 = -\frac{17}{21}$ for the EdS background. A full-detail analysis with general background cosmology and no spherical symmetry assumed is presented in [86, 87].

Furthermore, [88] point out that these fluid dynamics descriptions can be associated with different gauges in general relativity in the second order. The Lagrangian picture is similar to the comoving-synchronous gauge for the fact that it removes the fluid velocity. Thus, the vector modes are removed such that the line element is comoving with the matter fluid. Furthermore, the spatial coordinates are laid on an equal-time hyper-surface, fixing the 00-component perturbation to zero. However, the spatial components of the metric are allowed to be non-diagonal, deforming with time. On the other hand, the Eulerian description fixes the spatial part of the metric to always be diagonal but allows the vector perturbation in the $0i$-components instead.

[3] Notice that this corresponds to the spherical collapse scenario.

This is the Poisson gauge or the total matter gauge dubbed in [88]. Note that the space is still defined on the same equal-time hypersurface.

Mathematically, the initial position on both coordinates is identical; $\boldsymbol{q}$ refers to the initial Lagrangian position. The Eulerian position represents the trajectory of the fluid parcel on fixed coordinates $\boldsymbol{x}_{\text{fl}}(\boldsymbol{q},\tau)$ which depends on the initial position and time. We can relate the two as $\boldsymbol{x}_{\text{fl}}(\boldsymbol{q},\tau) = \boldsymbol{q} + \boldsymbol{s}(\boldsymbol{q},\tau)$ where the $\boldsymbol{q}$ is time-independent and serves as an initial condition of the trajectory on the Eulerian picture. $\boldsymbol{s}(\boldsymbol{q},\tau)$ is the fluid displacement. In other words, the Lagrangian picture encoded the fluid flow in the deformation of coordinates. On the other hand, the Eulerian picture explicitly shows the flow with the fluid velocity $\boldsymbol{v} = \dot{\mathrm{s}}(\boldsymbol{q},\tau)$ on fixed coordinates, varying fluid position. In this picture, the fluid parcel is kicked by peculiar gravitational potential and the equation of motion is realized,

$$\left(\frac{\partial^2}{\partial\tau^2} + \mathcal{H}\frac{\partial}{\partial\tau}\right)\boldsymbol{s}(\boldsymbol{q},\tau) = -\nabla\Phi(\boldsymbol{q}+\boldsymbol{s}(\boldsymbol{q},\tau),\tau). \tag{3.82}$$

At linear approximation, the continuity equation in the Eulerian picture implies $\dot{\delta}^{(1)} = -\nabla\cdot\boldsymbol{v}^{(1)}$ so the fluid displacement at linear order can be expressed as

$$\boldsymbol{s}^{(1)}(\boldsymbol{q},\tau) = \boldsymbol{x}^{(1)}_{\text{fl}}(\boldsymbol{q},\tau) - \boldsymbol{q} = -\frac{\boldsymbol{\nabla}}{\nabla^2}\delta^{(1)}(\boldsymbol{q},\tau), \tag{3.83}$$

where $\frac{\boldsymbol{\nabla}}{\nabla^2}$ is an operator inverse Fourier transformed from $-i\frac{\boldsymbol{k}}{k^2}$. This also implies that the time evolution of $\boldsymbol{s}^{(1)}$ depends on the linear growth factor as well as $\delta^{(1)}$. This will be used when we discuss the second-order perturbative solution in the next section. In the following discussions, we will see the advantages and disadvantages of both pictures.

3.4.1 Solution From The Continuity equation

We can exploit the fact that both fluids are comoving, i.e. they admit the same θ and write

$$\frac{1}{1+\delta_g}\frac{D}{D\tau}\delta_g = \frac{1}{1+\delta}\frac{D}{D\tau}\delta, \tag{3.84}$$

from equations 3.73 and the continuity equation of 3.74. From now on, It is convenient to work in the Lagrangian description because a convective derivative can be treated as a partial derivative. In this way, the equation above can be integrated easily. However, one must keep in mind that we will be working on the Lagrangian coordinates $\boldsymbol{q} = \boldsymbol{x}(\tau) - \boldsymbol{s}(\boldsymbol{q},\tau)$, where

$\boldsymbol{s}(\boldsymbol{q},\tau)$ is the Lagrangian displacement, instead of the Eulerian coordinates $\boldsymbol{x}$.

By using the chain rule, we can integrate the equation along the fluid trajectory and obtain

$$\ln\left(\frac{1+\delta_g(\boldsymbol{x}_{\mathrm{fl}}(\tau),\tau)}{1+\delta(\boldsymbol{x}_{\mathrm{fl}}(\tau),\tau)}\right)=\ln\left(\frac{1+\delta_g(\boldsymbol{x}_{\mathrm{fl}}(\tau_*),\tau_*)}{1+\delta(\boldsymbol{x}_{\mathrm{fl}}(\tau_*),\tau_*)}\right), \tag{3.85}$$

where we introduce the fluid trajectory in Eulerian coordinate $\boldsymbol{x}_{\mathrm{fl}}(\tau)$ such that $\boldsymbol{x}_{\mathrm{fl}}(\tau=0)=\boldsymbol{q}$. This is equivalent to setting the initial condition for the Lagrangian displacement of the fluid trajectory to be $\boldsymbol{s}(\boldsymbol{q},\tau=0)=0$. τ_* refers to the time of tracer formation[4]. It is important to emphasize that the position of the fluid parcel is also changing even if the equation is integrated over time. This is because we integrate with the Lagrangian picture; the Lagrangian coordinates $\boldsymbol{q}$ are unchanged but the coordinates $\boldsymbol{x}_{\mathrm{fl}}$ are deforming with the fluid displacement $\boldsymbol{s}(\boldsymbol{q},\tau)$. The interpretation of this solution is the density ratios of tracer and matter are equal for the conserved evolution. As an example, we will expand this to the second order of perturbation,

$$\begin{aligned}1+\delta_g^{(1)}+\delta_g^{(2)}=1+\delta^{(1)}-\delta_*^{(1)}+\delta_{g*}^{(1)}\\ \delta^{(2)}-\delta_*^{(2)}++\delta_{g*}^{(2)}+[\delta_*^{(1)}]^2+\delta^{(1)}\delta_*^{(1)}+[\delta^{(1)}-\delta_*^{(1)}]\delta_{g*}^{(1)},\end{aligned} \tag{3.86}$$

where the quantity denoted with "$*$" is evaluated at time τ_*. We will also perturb δ concerning the Lagrangian displacement and time evolution. In an unperturbed FLRW metric, $\boldsymbol{x}_{\mathrm{fl}}$ is constant in a comoving frame. Thus, the Lagrangian displacement is the first-order perturbation by itself as discussed above. Hence, we will need only the linear perturbation of it to discuss the second-order solution. It is written as

$$\boldsymbol{x}_{\mathrm{fl}}(\tau_*)=\boldsymbol{x}_{\mathrm{fl}}(\tau)+\boldsymbol{s}(\boldsymbol{q},\tau_*)-\boldsymbol{s}(\boldsymbol{q},\tau)=\boldsymbol{x}_{\mathrm{fl}}(\tau)-\left(\frac{D_*}{D}-1\right)\boldsymbol{s}^{(1)}(\boldsymbol{x}_{\mathrm{fl}},\tau)+\ldots, \tag{3.87}$$

where the time evolution of $\boldsymbol{s}^{(1)}$ is captured by the linear growth factor of the density perturbation $D(\tau)$ in the short-hand notation $*$ as usual. This follows from the solution 3.83 where $\boldsymbol{s}_{\boldsymbol{k}}^{(1)}(\tau)=i\frac{\boldsymbol{k}}{k^2}\delta^{(1)}(\tau)\propto D(\tau)$ in Fourier space. The position argument of $\boldsymbol{s}^{(1)}$ is interchangeable between $\boldsymbol{x}\longleftrightarrow\boldsymbol{q}$ since the term is already at the first order by $\boldsymbol{s}^{(1)}$. Therefore, the perturbed density is

$$\delta^{(1)}-\delta_*^{(1)}=\left(1-\frac{D_*}{D}\right)\delta^{(1)}+\left(1-\frac{D_*}{D}\right)\frac{D_*}{D}\boldsymbol{s}^{(1)}\cdot\nabla\delta^{(1)}. \tag{3.88}$$

[4]Keep in mind that we assume instantaneous formation. In a more detailed description, the formation is not instantaneous and the formation time could refer to the point of half-mass assembly or others.

The time evolution is the first term while the second term presents the fluid displacement effect. The last ingredient is the initial bias expansion of the galaxy number density. We recall the general bias expansion 3.72. For generality, we will include 3 operators: δ, δ^2 and $K_{ij}K^{ij}$. The first operator is motivated by Kaiser's introduction of the bias parameter (see section 3.3.1). We already see δ^2 emerging in the perturbative solution 3.86 so it is included. The introduction of $K_{ij}K^{ij}$ may seem a bit vague here but it will be clear later on why. Essentially, the solution suggests the dependence on $\delta^{(2)}$ which turns out to contain the tidal field contribution by solving through SPT (see the kernels 3.68). This tells us that the dependence on the tidal field of the tracer population will be inevitably induced by gravitational evolution. Therefore, it is also included in the initial bias expansion for completeness of the description. At the formation time, the perturbative expansion is then written up to the second order of perturbation as

$$\begin{aligned}\delta_g^{(1+2)}(\boldsymbol{x}_*,\tau_*) =& b_1^*\left[\delta^{(1)}+\delta^{(2)}\right](\boldsymbol{x}_*,\tau_*)+\varepsilon^*(\boldsymbol{x}_*,\tau_*)+\frac{1}{2}b_2^*\left[\left(\delta^{(1)}\right)_*\right]^2\\ &+b_{K^2}^*\left[\left(K_*^{(1)}\right)_{ij}\left(K_*^{(1)}\right)^{ij}\right].\end{aligned} \tag{3.89}$$

Notice that every operator here is locally observable, depending on one point in space only. The tidal field exists in this expansion only from the second order since the lowest order operator which is directional-independent is $K^2 = K_{ij}K^{ij}$. For now, we did not include the stochastic term ε_δ in the first term to motivate that the conserved evolution will automatically induce such a term. Equations 3.88 and 3.89 are substituted into equation 3.86 to obtain the final tracers density contrast,

$$\begin{aligned}\delta_g =&\delta_g^{(1)}+\delta_g^{(2)}\quad\text{where}\\ \delta_g^{(1)} =&\left(1+\frac{D_*}{D}[b_1^*-1]\right)\delta^{(1)}+\varepsilon^*\\ \delta_g^{(2)} =&\left\{1+\left(\frac{D_*}{D}\right)^2[b_1^*-1]\right\}\delta^{(2)}+\left\{\frac{D_*}{D}[b_1^*-1]+\left(\frac{D_*}{D}\right)^2[b_1^*-1]+\frac{1}{2}b_2^*\left(\frac{D_*}{D}\right)^2\right\}[\delta^{(1)}]^2\\ &+b_{K^2}^*\left(\frac{D_*}{D}\right)^2\left[K^{(1)}\right]^2+\left(\frac{D_*}{D}-1\right)\frac{D_*}{D}[b_1^*-1]\boldsymbol{s}^{(1)}\cdot\nabla\delta^{(1)}-\left(\frac{D_*}{D}-1\right)\varepsilon^*\delta^{(1)}\\ &+\left(\frac{D_*}{D}-1\right)\boldsymbol{s}^{(1)}\cdot\nabla\varepsilon^*.\end{aligned} \tag{3.90}$$

The biases are factored out such that their evolution is clear to be seen. Notice that all quantities are evaluated at $(\boldsymbol{x},\tau)$ except ε^*. This expression can be manipulated further by substituting

the expression of $\delta^{(2)}$ inferred from the SPT (see solution 3.63 and second-order kernels 3.68). By assuming the EdS background, it can be written as

$$\delta^{(2)}(\boldsymbol{x},\tau) = \frac{17}{21}[\delta^{(1)}]^2 + \frac{2}{7}[K^{(1)}]^2 - \boldsymbol{s}^{(1)}\cdot\nabla\delta^{(1)}, \tag{3.91}$$

recalling the definition of the tidal field 3.76 and the first-order fluid displacement 3.83. As discussed in section 3.2.2, the numerical factors in this expression depend on the chosen background cosmology. After substituting this into the results and rearranging the terms, one obtains the relation,

$$\begin{aligned}\delta_g^{(1+2)} = {} & b_1^E\left[\delta^{(1)}+\delta^{(2)}\right] + \varepsilon + \frac{1}{2}b_2^E\left[\delta^{(1)}\right]^2 + b_{K^2}^E[K^{(1)}]^2 \\ & - \left(\frac{D_*}{D}-1\right)\varepsilon^*\delta^{(1)} + \left(\frac{D_*}{D}-1\right)\boldsymbol{s}^{(1)}\cdot\nabla\varepsilon^*,\end{aligned} \tag{3.92}$$

where we introduce the Eulerian bias parameters defined as

$$\begin{aligned} b_1^E &= 1 + \frac{D_*}{D}[b_1^* - 1] \\ b_2^E &= b_2^*\left(\frac{D_*}{D}\right)^2 + \frac{8}{21}\left(1-\frac{D_*}{D}\right)[b_1^E - 1] \\ b_{K^2}^E &= b_{K^2}^*\left(\frac{D_*}{D}\right)^2 - \frac{2}{7}\left(1-\frac{D_*}{D}\right)[b_1^E - 1]. \end{aligned} \tag{3.93}$$

One can see that the tracer distribution becomes less biased over time; the fraction $\frac{D_*}{D}$ decreases as τ increases. Another interesting point is the absence of $\boldsymbol{s}\cdot\nabla\delta$ deterministic bias. Notice that it has been removed once we admitted the SPT solution of $\delta^{(2)}$. The explanation is tracers are set to be comoving with the matter fluid and gravitational interaction obeys the equivalence principle. Hence, the tracers cannot be displaced away from the flow trajectory. At first, the term appears because we perturbed only $\delta^{(1)}$ without realising the second-order contribution, which is inconsistent. In reality, the fluid displacement induces the change in δ at the second order as well and the terms are cancelled out. Finally, we return to the point mentioned before; the stochastic contribution $\varepsilon^*\delta$ naturally appears at second-order. This implies the stochastic contribution to b_1. Realistically, the formation time distribution must be known to take this interaction into account. Then, the stochastic contribution to the first-order bias can be analytically averaged over that distribution. Instead of proposing a model for this, ε_δ is introduced as a free parameter.

The stochastic term $\boldsymbol{s}^{(1)} \cdot \nabla \varepsilon^*$ appears because ε^* is defined on the formation time slice, at a specific Eulerian position. Hence, the fluid displacement shall capture the spatial dependence of the stochastic field. However, in the limit of large-scale bias, the stochastic field is effectively spatial-independent. This is because the field represents the small-scale effects, uncorrelated at a long separation. In other words, it is completely described by the spatial-independent one-point statistic. Therefore, the term vanishes and does not introduce a new bias operator.

As anticipated, the solution also implies the emergence of tidal field dependence. Suppose the initial bias expansion has $b^*_{K^2} = 0$, i.e. the tidal field is irrelevant to the tracers' formation. At a later time, the dependence on the tidal field is still induced by gravitational evolution. This suggests the tidal field squared operator in the bias expansion. The associated bias parameter $b^E_{K^2}$ is left as a free parameter because the prediction above depends on the chosen background cosmology and relies on the conservation of the tracer number.

Realistic Tracer Sample: Formation time Distribution

There is an additional complication when applying this parameterization to a realistic catalogue of tracers. Each tracer can form at a different time. Hence, the measurement must be the weighted average,

$$b_{\mathcal{O}}(\tau) = \int d\tau_* \mathcal{P}(\tau_*) b^E_{\mathcal{O}}(\tau | \{b^*_{\mathcal{O}'}\}, \tau_*), \tag{3.94}$$

where $\mathcal{P}(\tau_*)$ is the formation time PDF. The same relation applies to the stochastic terms. $\mathcal{P}(\tau_*)$ is unknown and complicate to model. Hence, it is hard to analytically infer the set of bias parameters from one redshift to another. However, the expansion can still be consistently used to infer the correct (Eulerian) description at each redshift as long as we allow them to be an arbitrary function of time. A similar case is when the appearance of $\varepsilon^* \delta$ at the second-order evolution implies an additional bias parameter. In other words, rather than a single ε^*, a realistic sample at a redshift admits many formation times (hence many ε^*) from which the average value is measured. Hence, the effective ε_δ was introduced as a free function of time.

3.4.2 Joint Perturbative Solution

As anticipated, another way to obtain the evolution of the bias expansion is to solve the set of equations 3.73 and 3.74 simultaneously. As demonstrated by the last calculation, one must keep in mind that the fluid displacement will also be counted as a first-order perturbation. However, it is irrelevant in the context of bias as we have seen in the previous approach; we

are under the assumption of comoving tracers and matter and the physics of biased tracers must be translational-invariant. Thus, it will be convenient to organize those contributions when evolving the perturbative expansion. One possible treatment is using the Lagrangian Perturbation Theory (LPT) where, instead of constructing the operator from local observable, the relevant quantity to the tracer population is the deformation tensor defined as

$$M_{ij} \equiv \partial_{q,i} s_j. \tag{3.95}$$

The evolved matter density can then be written as

$$1 + \delta(\boldsymbol{x}, \tau) = |1 + \boldsymbol{M}|^{-1}_{\boldsymbol{q},\tau}, \tag{3.96}$$

assuming that $\delta \longrightarrow 0$ as $\tau \longrightarrow 0$ (initial density on Lagrangian space) and the matter density at $(\boldsymbol{x}, \tau)$ is given by a single parcel streamed from the past (single-stream regime). We can also write a similar relation for tracers. In other words, the evolution of δ is now characterized by the deformation of the Lagrangian volume. We can use this relation to obtain a similar relation as equation 3.85 through the continuity equations 3.73 and in 3.74,

$$\ln \left[\frac{|1 + \boldsymbol{M}_g|}{|1 + \boldsymbol{M}|} \right]_{\boldsymbol{q},\tau} = \ln \left[\frac{|1 + \boldsymbol{M}_g|}{|1 + \boldsymbol{M}|} \right]_{\boldsymbol{q},\tau_*}. \tag{3.97}$$

Notice that we do not have to worry about the fluid trajectory anymore since the deformation tensor is evaluated on the Lagrangian coordinate by definition. Thus, no fluid displacement term will be introduced by the perturbative evolution and all of them are well-contained by M_{ij}. The initial bias relation up to the second order is

$$\begin{aligned} |1 + \boldsymbol{M}_g(\boldsymbol{q}, \tau_*)|^{-1} =& b^*_{\mathrm{Tr}\{M\}} \mathrm{Tr}\{\boldsymbol{M}\} + b^*_{\mathrm{Tr}\{M^2\}} \mathrm{Tr}\{\boldsymbol{M}\boldsymbol{M}\} + b^*_{(\mathrm{Tr}\{M\})^2} (\mathrm{Tr}\{\boldsymbol{M}\})^2 \\ &+ \varepsilon^* + \varepsilon^*_{\mathrm{Tr}\{M\}} \mathrm{Tr}\{\boldsymbol{M}\} + \dots . \end{aligned} \tag{3.98}$$

Note that operators constructed from M_{ij} in LPT can be converted to linear combinations of the standard observable operators like before. Hence, the bias expansions are equivalent. However, they are not equal in order by order of perturbation, e.g. second-order standard operators can come from the first-order Lagrangian operator.

Another treatment is integrating the set of equations along the fluid flow as before [89, 90, 91]. However, the difference from SPT is that rather than perturbatively solving the equation,

we find Green's function of this system of equations and use it to collect the source contribution along the fluid flow. Mathematically, it is written as

$$\boldsymbol{\Psi}(\boldsymbol{x},\tau) = \boldsymbol{A}(\tau,\tau_*)\cdot\boldsymbol{\Psi}(\boldsymbol{x}_*,\tau_*) + \int_{\tau_*}^{\tau} d\tau' \boldsymbol{A}(\tau,\tau')\boldsymbol{S}(\boldsymbol{x}_{\rm fl}(\tau'),\tau'), \tag{3.99}$$

where $\boldsymbol{A}$ is the green function of this system of equations 3.73 and 3.74 and $\boldsymbol{S}$ is the source terms matrix. The corresponding equation of motion is

$$\frac{D}{D\tau}\boldsymbol{\Psi} = -\boldsymbol{\sigma}\cdot\boldsymbol{\Psi} + \boldsymbol{S}, \tag{3.100}$$

where

$$\boldsymbol{\Psi}(\boldsymbol{x},\tau) = \begin{pmatrix} \delta_g(\boldsymbol{x},\tau) \\ \delta(\boldsymbol{x},\tau) \\ \frac{\theta(\boldsymbol{x},\tau)}{\mathcal{H}(\tau)} \end{pmatrix} ;\ \boldsymbol{\sigma}(\tau) = \begin{pmatrix} 0 & 0 & 1 \\ 0 & 0 & 1 \\ 0 & \frac{3}{2}\Omega_m(\tau)\mathcal{H}(\tau) & \mathcal{H}(\tau) + \frac{\mathcal{H}'(\tau)}{\mathcal{H}(\tau)} \end{pmatrix} ;$$
$$\boldsymbol{S}(\boldsymbol{x},\tau) = \begin{pmatrix} -\delta_g(\boldsymbol{x},\tau)\theta(\boldsymbol{x},\tau) \\ -\delta(\boldsymbol{x},\tau)\theta(\boldsymbol{x},\tau) \\ -|\boldsymbol{\nabla}\boldsymbol{v}|^2(\boldsymbol{x},\tau)/\mathcal{H}(\tau) \end{pmatrix}.$$

The Green's function can be found by solving

$$\left(\frac{D}{D\tau} + \boldsymbol{\sigma}\cdot\right)\boldsymbol{A}(\tau,\tau_*) = \mathbb{I}_{3\times3}\delta(\tau-\tau_*) \quad \text{where} \quad \boldsymbol{A}(\tau,\tau) = \mathbb{I}_{3\times3}. \tag{3.101}$$

$\mathbb{I}_{n\times n}$ denotes $n\times n$ identity matrix. For Einstein-de Sitter (EdS) model, $\Omega_m = 1$ and $a(\tau)\propto\tau^2$, the Green's function takes the form,

$$\boldsymbol{A}(\tau,\tau_*) = \begin{pmatrix} 1 & -1 & 0 \\ 0 & 0 & 0 \\ 0 & 0 & 0 \end{pmatrix} + \begin{pmatrix} 0 & 3/5 & -2/5 \\ 0 & 3/5 & -2/5 \\ 0 & -3/5 & 2/5 \end{pmatrix}\left(\frac{D}{D_*}\right) + \begin{pmatrix} 0 & 2/5 & 2/5 \\ 0 & 2/5 & 2/5 \\ 0 & 3/5 & 3/5 \end{pmatrix}\left(\frac{D}{D_*}\right)^{-3/2}. \tag{3.102}$$

The meaning of equation 3.99 is the solution breaks down into two parts. The first part is the propagation of the initial state. The second part is the interaction along the flow obtained by integrating Green's function with the source term along the fluid trajectory. The linear solution is obtained by neglecting the integral, which starts at the second order by construction. Indeed, one finds that it matches the SPT solution of the matter fluid (see first-order solution 3.65).

This is expected since the solution must be identical regardless of the procedure, as anticipated before. In particular, it is nothing else than the linear evolution of the perturbations on the EdS background where δ_g and δ follow the linear growth factor $D(\tau) = a(\tau)$ and the velocity divergence $\theta = -\dot{D}(\tau)\delta$ is negative by the collapsing pressureless matter.

The first-order solution can then be used to solve for the second-order solution, and so on. One detail to be addressed here is the third component of the source term can be written in terms of δ and K via the perturbed continuity equation. To do so, the Eulerian coordinates $\boldsymbol{x}$ derivative must be transformed as

$$\partial^i = ([\mathbb{I} + \boldsymbol{M}]^{-1})^i_j \partial^j_q, \tag{3.103}$$

where ∂^j_q is the Lagrangian coordinates derivative operator. Then, we exploit that the fluid velocity is the convective time derivative of the fluid displacement to expand the source term in the order of $\boldsymbol{s}$. The expression up to the second order is

$$\partial^i_x v^j = (1 + \partial^i_q s_k \partial^k_q)\dot{s}^j + \mathcal{O}(3), \tag{3.104}$$

which can be computed by using the solution of the previous order. For example, $\boldsymbol{s}^{(1)} = -\frac{\nabla}{\nabla^2}\delta^{(1)}$, where the first-order solution is $\delta^{(1)} = a(\tau)\delta^{(1)}_*$, is used to write the second-order source term. Thus, the solution is completely free of any displacement term. Indeed, this is the advantage of this approach. No fluid displacement term will be explicit by expressing the solution with quantity evaluated on the Lagrangian coordinates. However, we can directly use them to write the Eulerian bias expansion without worrying about displacement terms. This is because, even if those terms are installed to move the results from the Lagrangian to the Eulerian position, they cancel themselves completely in the equal-time (Eulerian) bias expansion. We have seen this explicitly before in the previous approach when we substituted $\delta^{(2)}$ into the perturbative series of δ_g. There, we see how the translation term was cancelled on the second order. This is expected because the physics of biased tracer is translational-invariant and fluid displacement should not construct a new (deterministic) operator in the expansion.

3.4.3 Evolution on General Background Cosmology

As discussed for SPT of CDM fluid, the realistic background cosmology is evolving. Therefore, it is advisable to extend the analysis beyond the EdS background. We follow the same

re-parameterization of equations 3.60 on equations 3.100 to obtain

$$\frac{D}{D\ln D}\tilde{\boldsymbol{\Psi}} = -\tilde{\boldsymbol{\sigma}}\cdot\tilde{\boldsymbol{\Psi}} + \tilde{\boldsymbol{S}}, \tag{3.105}$$

where

$$\tilde{\boldsymbol{\Psi}}(\boldsymbol{x},\tau) = \begin{pmatrix}\delta_g\\ \delta\\ \tilde{\theta}\end{pmatrix} \quad ; \quad \tilde{\boldsymbol{\sigma}}(\tau) = \begin{pmatrix}0 & 0 & 1\\ 0 & 0 & 1\\ 0 & \frac{3}{2}\frac{\Omega_m}{f^2} & \frac{3}{2}\frac{\Omega_m}{f^2}-1\end{pmatrix} \quad ; \quad \tilde{\boldsymbol{S}}(\boldsymbol{x},\tau) = \begin{pmatrix}-\delta_g\tilde{\theta}\\ -\delta\tilde{\theta}\\ -|\boldsymbol{\nabla}\tilde{\boldsymbol{v}}|^2\end{pmatrix}$$

$$\frac{D}{D\ln D} \equiv \frac{\partial}{\partial\ln D} + \tilde{\boldsymbol{v}}\cdot\boldsymbol{\nabla} \quad ; \quad \tilde{\boldsymbol{v}} \equiv (\mathcal{H}f)^{-1}\boldsymbol{v} \quad ; \quad \tilde{\theta} \equiv \boldsymbol{\nabla}\cdot\tilde{\boldsymbol{v}}.$$

Let us recall that the definition of growth rate 3.55 and its identity 3.59 are used in obtaining the above. The structure of the equation is preserved and the form of $\tilde{\boldsymbol{\sigma}}$ returns to the one in equation 3.100 in the EdS case. Therefore, the solution can be found following the same procedure but with the dependence on $D(\tau)$ rather than τ. This will become more complicated if Ω_m and f are functions of time as the solution will not be ordered with the power-law of growth factor (see discussion in section 3.2.2). Instead, the time dependence at each order diverse into a set of $D_{m,n-m}$. Nevertheless, the EdS background is a decent approximation as discussed according to [76].

3.4.4 Third- and higher-order Solutions

Let us stick with the EdS approximation. By any approaches mentioned above, we can perturbatively solve for the higher-order solution at will. The solution up to the third order of perturbation has been obtained in [92] where a new bias operator appeared,

$$O^{(3)}_{\rm td} \equiv \frac{8}{21}K^{(1)\,ij}\mathcal{D}_{ij}\left[(\delta^{(1)})^2 - \frac{3}{2}(K^{(1)})^2\right]. \tag{3.106}$$

Recall that the derivative operator $\mathcal{D}_{ij}$ is defined in equation 3.76. Note that this operator is still of the local kind despite the derivative operator. This is because $\mathcal{D}_{ij}$ is scale-dependent by construction ($\propto k^0$ in Fourier space). However, it is not locally expressible in terms of δ and K_{ij}. Therefore, the appearance of this operator indicates that our operators in the Eulerian bias expansion are insufficient, following the previous discussion on the local tidal field squared operator, $K_{ij}K^{ij}$. This new operator is now included in the expansion. Following

[92], we could alternatively add the velocity shear $\mathcal{D}_{ij}\theta$ as a new relevant quantity to construct this third-order operator. This trend continues to the higher order. At the fourth order and so on, velocity shear is no longer sufficient to describe the tracer population. New relevant operators will keep appearing and inevitably be included in the expansion. However, they will be of the higher order which can be truncated at some level of consideration. Then, it is unnecessary to find the operators in all order practically.

3.4.5 Building Library of Physical Operator

Previously, we have discussed how the conserved evolution invokes new operators, K_{ij} and O_{td}, in the bias expansion for consistency. It is natural to expect that, beyond the third order, more operators will appear and the the bias expansion will keep growing. The question we will try to address in this section is "Is there a way to construct a complete dictionary of the bias expansion at any desirable order of perturbation?". A nice proposal of recursion relation is presented in [91] and reviewed in section 2 of [28]. In their argument, the number conservation in the evolution of tracers is abandoned to reflect the realistic tracer population which can form and merge along the trajectory. However, the set of operators is not unique and one can find a clever way to re-order the operators more conveniently depending on the purpose. The choice of operators is similar to the choice of basis to parameterize the population of tracers. For example, [93] also propose an alternative way to build the bias expansion where every possible local expression that could be built from perturbatively solving the fluid equation is listed. Then, the extra degrees of freedom are removed by the equivalence principle, i.e. Galilean symmetry. More variety of bias expansions are also proposed in [94, 95, 96].

3.5 Statistics of Tracer: N-point Correlation Function

We have discussed the statistics of curvature perturbation as the initial condition in the section 2.5.3. Now, it is the turn of tracers; the statistical quantity of discrete objects like tracer distribution must be addressed. The situation differs from the continuous field of curvature perturbation ζ. The tracer is a point-like object labelled with its position in space. Therefore, counting the tracer in a fixed volume will give us the probability of finding a tracer rather than an autocorrelation function. For example, the probability is given by the equation 3.70. However, the physics of LSS was discussed in the language of density contrast. In particular, the

bias relation connects δ with δ_g where we expect the statistics to be translated. Therefore, this section will review the connection between counting probability and the statistics of the continuous field.

Let us use the definition of the probability 3.70 to define the mean number of object s found in a finite volume V as

$$\langle N \rangle = \bar{n}_g V. \tag{3.107}$$

Then, the 2PCF is defined to quantify the excess probability of finding objects at two positions in space simultaneously. Let us first write the probability in the case of no correlation. If we assume an identical Poisson process at each point in space, then the probability of finding an object in any infinitesimal volume can be written as

$$\delta P = \bar{n}_g \delta V. \tag{3.108}$$

Notice that resuming the expression gives the equation 3.70. If the stochastic process in infinitesimal volumes δV_1 and δV_2 are independent, then the joint probability is the product of the probabilities at each point,

$$\delta P_{12} = \delta P_1 \delta P_2 = \bar{n}_g^2 \delta V_1 \delta V_2 \quad \text{(Uncorrelated Poisson Points)}, \tag{3.109}$$

This is the case of uniform Poisson statistics where each volume element is uncorrelated. Hence, the two-point correlation, $\xi_g(\|\boldsymbol{r_2} - \mathbf{r}_1\|)$, is the additional part of the expression above,

$$\delta P_{12} = \delta P_1 \delta P_2 = \bar{n}_g^2 (1 + \xi_g(\|\boldsymbol{r_2} - \boldsymbol{r_1}\|)) \delta V_1 \delta V_2. \tag{3.110}$$

Notice that the correlation function depends on the norm of the separation vector between the volume elements, $r_{12} = \|\boldsymbol{r_2} - \boldsymbol{r_1}\|$. This is enforced by statistical isotropy where the statistics should not be directional-dependent.

Let us consider the number density contrast 3.69 as a continuous density function on space. The 2PCF is naively computed by

$$\begin{aligned} \xi_g(r_{12}) &= \langle \delta_g(\boldsymbol{r_1}) \delta_g(\boldsymbol{r_2}) \rangle \\ &= \frac{\langle [n_g(\boldsymbol{r_1}) - \bar{n}_g][n_g(\boldsymbol{r_2}) - \bar{n}_g] \rangle}{\bar{n}_g^2} \\ \langle n_g(\boldsymbol{r_1}) n_g(\boldsymbol{r_2}) \rangle &= \bar{n}_g^2 [1 + \xi_g(r_{12})]. \end{aligned} \tag{3.111}$$

Comparing with equation 3.110, we see a clear similarity. This is because introducing a non-zero correlation is equivalent to assuming a non-uniform Poisson process over the sky. In particular, $n_g(\boldsymbol{r})$ is drawn from an ensemble and defines the probability of finding an object at $\boldsymbol{r}$,

$$\delta P(\boldsymbol{r}) = n_g(\boldsymbol{r})\delta V. \tag{3.112}$$

Notice that the mean number of objects computed from this still satisfies the equation 3.107. The joint probability can be found by averaging the product of single-point probability,

$$\begin{aligned} \delta P_{12} &= \langle \delta P(\boldsymbol{r_1})\delta P(\boldsymbol{r_2})\rangle \\ &= \langle n_g(\boldsymbol{r_1})n_g(\boldsymbol{r_2})\rangle\, \delta V_1 \delta V_2 \\ &= \bar{n}_g^2[1+\xi_g(r_{12})]\delta V_1 \delta V_2. \end{aligned} \tag{3.113}$$

The computation automatically returns the joint probability in the correlated case. Therefore, we conclude that the density contrast field 2PCF is the excess probability of finding the tracers simultaneously at two points with r_{12} separation.

The three- and higher-point correlation functions follow; They are computed from δ_g. The difference is just the interpretation in the context of finding probability. For example, the 3PCF yields

$$\begin{aligned} \xi^{(3)}(r_{12}, r_{23}, r_{13}) &= \langle \delta_g(\boldsymbol{r_1})\delta_g(\boldsymbol{r_2}\delta_g(\boldsymbol{r_3})\rangle \\ \langle n_g(\boldsymbol{r_1})n_g(\boldsymbol{r_2})n_g(\boldsymbol{r_3})\rangle &= \bar{n}_g^3[1+\xi_g(r_{12})+\xi_g(r_{23})+\xi_g(r_{13})+\xi_g^{(3)}(r_{12}, r_{23}, r_{13})]. \end{aligned} \tag{3.114}$$

This structure of statistical function is divided into two parts: the *disconnected* and the *connected*. Essentially, the 2PCFs in this probabilistic quantity are dubbed the disconnected part since they depend on just one separation length and do not connect every point. The last term of 3PCF is called the connected 3PCF since it depends on every possible connection of 3 points. This structure carries on to the higher NPCF where we can categorize the contributions neatly. Notice that all disconnected contributions are the lower NPCFs. Therefore, a higher-order NPCF is unlocked every time the higher joint probability is probed.

The Wiener-Khinchin Theorem

We have seen that the power spectrum is the Fourier transform of 2PCF in real space in the context of quantum field theory. In section 2.5.3, we generalize it to the classical ensemble

of conserved curvature perturbation. However, we never explicitly mention why such a correspondence is true in the real observation where ergodicity is assumed to infer ensemble average from real space average. Let us argue that the same structure also applies to the statistics of tracers. In particular, the *Wiener-Khinchin Theorem* plays a major role here. Essentially, the theorem states that the auto-correlation of a stationary random process[5], i.e. its correlation functions are time translational-invariant, has a spectral decomposition given by the power spectral density of that process. The theorem is applied to real space instead of temporal space. Since the statistics of tracers are assumed to be homogeneous, i.e. spatial translational-invariant, the NPCFs are expected to have Fourier counterparts as spectral decomposition. Let us verify this by computing the power spectrum with the Fourier transform number density contrast,

$$\begin{aligned} P_g(\boldsymbol{k}) &= V^{-1}\left\langle|\delta_{g,\boldsymbol{k}}|^2\right\rangle = V^{-1}\left\langle\delta_{g,\boldsymbol{k}}\delta^*_{g,\boldsymbol{k}}\right\rangle \\ &= V^{-1}\int d^3x_1 e^{i\boldsymbol{k}\cdot\boldsymbol{x_1}}\int d^3x_2 e^{-i\boldsymbol{k}\cdot\boldsymbol{x_2}}\left\langle\delta_g(\boldsymbol{x_1})\delta_g(\boldsymbol{x_2})\right\rangle, \end{aligned} \tag{3.115}$$

where V is the real space volume[6]. Here, we will insert the 2PCF in the form $\xi_g(\boldsymbol{r})$ where $\boldsymbol{r} = \boldsymbol{x_2} - \boldsymbol{x_1}$. It is emphasized that the statistical homogeneity assumption enters the analysis here. So that,

$$\begin{aligned} V^{-1}\int d^3x_1 e^{i\boldsymbol{k}\cdot\boldsymbol{x_1}}\int d^3x_2 e^{-i\boldsymbol{k}\cdot\boldsymbol{x_2}}\left\langle\delta_g(\boldsymbol{x_1})\delta_g(\boldsymbol{x_2})\right\rangle &= \int d^3r\xi_g(\boldsymbol{r})e^{i\boldsymbol{k}\cdot\boldsymbol{r}}\frac{\int d^3x_2 e^{i\boldsymbol{k}\cdot\boldsymbol{x_2}}e^{-i\boldsymbol{k}\cdot\boldsymbol{x_2}}}{V} \\ P_g(\boldsymbol{k}) &= \int d^3r\xi_g(\boldsymbol{r})e^{i\boldsymbol{k}\cdot\boldsymbol{r}}. \end{aligned} \tag{3.116}$$

So, we have the correspondence as anticipated. Typically, the statistics are also assumed to be isotropy. Hence, a further simplification is,

$$P_g(k) = \int d^3r\xi_g(r)e^{i\boldsymbol{k}\cdot\boldsymbol{r}}, \tag{3.117}$$

where the directional dependence is taken out. The inverse Fourier transformation followed,

$$\xi_g(r) = \int \frac{d^3k}{(2\pi)^3}P_g(k)e^{-i\boldsymbol{k}\cdot\boldsymbol{r}}, \tag{3.118}$$

[5] wide-sense-stationary random process to be precise. But, a strictly stationary process is also included in this theorem.

[6] This term comes from $(2\pi)^3\delta_D^{(3)}(\boldsymbol{0}) = \int d^3x e^{i\boldsymbol{o}\cdot\boldsymbol{x}} = V$.

The same correspondence and proof can also be shown for higher NPCF of this statistical homogeneous and isotropic system.

4

Probing Non-Gaussianity With Halo Bias

The first fundamental physics probed by LSS that will be discussed in this thesis is the Primordial non-Gaussianity (PNG) from inflation. The signal potentially reveals the fundamental features of inflation such as the interactions, number, or even speed of propagation of the active fields. For more details, we invite the reader to revise the chapter 2. As discussed in chapters 3, the statistics of inflation translate into the LSS distribution which we can probe nowadays, i.e. the biased tracer distribution. In this section, we review the effect of non-Gaussian initial conditions on the scale dependence of halo bias.

4.1 Structure Formation: DM Halo Collapse Theory

Let us discuss briefly the formation of DM halo from the over-dense region. As time passes, the perturbation will soon grow large enough for the nonlinear effect to become important. In particular, the mode couplings in the integral terms of equations 3.60 become comparable to other linear terms. Therefore, the next-order perturbations solved from the recursion relation of kernel 3.64 are as large as the order before. Hence, the perturbative description of density perturbation breaks down for structure formation where $\delta > 1$. There are several attempts to go beyond the perturbative regime and describe the collapsing process. let us start with a simplified description, *the spherical collapse*, which assumes that the virialized objects are collapsed with spherical symmetry.

The goal is to be able to indicate when and where the collapse happens. To do so, it is crucial

to know how much over-density is needed. This value will serve as a bar for our linear description of δ beyond which the halo is formed. Firstly, let us define a spherical region with a radius of choice R. We will attempt to determine if the matter in this region will collapse into an object or not. The choice of R is important since it is associated with the resulting mass of the object. In this case, the radius can be derived from the dark matter halo's mass of interest. For example, our Milky Way galaxy is hosted by a dark matter halo of mass around $10^{12} M_{\odot}$[97]. Galaxy surveys also suggest that the dark matter halo has a mass ranging from $10^{10} M_{\odot}$ (dwarf galaxy) [98, 99] to $10^{14} M_{\odot}$ (galaxy clusters) [100]. δ is then coarse-grained using the window function as

$$\delta_R(\boldsymbol{x}, z) = \int d^3y\, \delta(\boldsymbol{y}, z) W_R(\|\boldsymbol{x} - \boldsymbol{y}\|), \tag{4.1}$$

where δ_R is the smoothed density contrast field and $W_R(|\boldsymbol{x} - \boldsymbol{y}|)$ is the spherical top-hat window function defined as

$$W_R(\|\boldsymbol{x} - \boldsymbol{y}\|) = \begin{cases} \frac{3}{4\pi R^3} & ; \|\boldsymbol{x} - \boldsymbol{y}\|^2 \leq R^2 \\ 0 & ; \text{elsewhere} \end{cases}. \tag{4.2}$$

Let us consider the space within this over-dense region. To study its evolution, the area will be treated as a local FLRW closed universe and apply the Friedmann equations. By solving the resulting parametric equations, it is evident that the space initially expands then turns around and collapses into the center. The interpretation is that, as the over-density increases, the gravitational force becomes strong enough to pull the matter back toward each other within a finite time t_{col}. In reality, the collapsing matter will virialize into a halo which takes approximately the same time as t_{col}. Knowing this fact, one could hypothetically assume that the linear regime is still valid and compute the growing linear density contrast at t_{col}. The result is

$$\delta(t = t_{col}) = \delta_c \approx 1.686. \tag{4.3}$$

This number is false since the situation we are considering now involves a large over-density when the region is collapsing. Hence, the linear theory cannot be applied here. However, this is useful as we are dealing with linear perturbation only need to know where the object is formed. Hence, we can heuristically say that, if $\delta_R \geq \delta_c$, the matter in that region collapses and virializes into an object. The process described here is called the *spherical collapse theory* where the object is assumed to form from the matter content inside a spherical region. This criterion was used in [27] and [101]. This will become a basic assumption for the upcoming mathematical

formulation for the halo population.

Since we will be working with the coarse-grained matter density field, the window function is applied to equation 3.30. Accordingly, we have

$$\delta_{\boldsymbol{k};R}(z) = \frac{2}{5}\frac{k^2\tilde{W}_R(kR)T(k)D(z)}{\Omega_m H_0^2}\zeta_{\boldsymbol{k}} \equiv \mathcal{M}_R(k,z)\zeta_{\boldsymbol{k}}, \tag{4.4}$$

where $\tilde{W}_R$ is the Fourier transformed window function,

$$\tilde{W}_R(kR) = \frac{3}{(kR)^3}[\sin(kR) - (kR)\cos(kR)], \tag{4.5}$$

and all transformation factors are collected into the function $\mathcal{M}_R(k,z)$ for later convenience.

Beyond this simplified description, the Zel'dovich approximation [102] is one such way to go beyond the linear equation of motion in the Lagrangian picture. In this approximation, the gravitational potential provides an initial kick to the motion of δ. Then, δ is assumed to undergo inertial motion rather than resting at its initial position. When this is used to set the initial condition for structure formation, the over-dense region will undergo *ellipsoidal collapse*. The difference is the tidal field that is taken into account and the spherical symmetry is not secure anymore. This approximation is accurate and widely used for setting the initial condition for structure formation. However, we can ignore this complication since we are only interested in identifying the collapsed region and not the details of the halo formation process. For our proposes, the only relevant difference that ellipsoidal collapse makes is modifying the threshold over density, δ_c, according to the initial tidal field (see [103]). This will be well-captured by the following analysis where we do not assume a numerical value for δ_c and the dependence of tracers population on the tidal field will be introduced.

4.1.1 Halo Mass Function

A crucial dependence of halo formation is the radius of the collapse region. Equation 4.4 tells us that the filtered density tends to take a smaller value as the radius is larger. This makes sense because a larger averaging volume would bring the filtered matter density closer to the background value. Hence, the density contrast will approach zero as the radius grows. We will show that this corresponds to increasing the halo mass. Since all of the matter in the region will end up in the halo, the filter size here coincides with the resulting halo mass. Accordingly, we

may relabel the function with mass M instead of R since it has a one-to-one relation as

$$M = \frac{4}{3}\pi\rho_0 R^3, \tag{4.6}$$

for this spherical filter. The size of the window function increases with interested halo mass. Therefore, the profile of δ_R changes according to the mass of the resulting halo. This will change the number of the regions where $\delta_R \geq \delta_c$ and the haloes with different mass have unequal population. In particular, the number of high-mass haloes should be less than the low-mass ones.

Under some assumption, let us formulate the halo distribution across a range of masses. The halo population of the mass between M and $M + dM$ can be written as

$$N(M) - N(M + dM) = \frac{dN}{dM}dM \tag{4.7}$$

where $N(M)$ is the number of halo of mass M. Notice that the order of subtraction is chosen such that the quantity is positive since the population decreases as the mass increases. Furthermore, by multiplying M on both sides, the relation can be presented in terms of the total mass of the halo population in the range of $[M, M + dM]$ instead,

$$M\frac{dN}{dM}dM = m(M) - m(M + dM). \tag{4.8}$$

In 1974, W. H. Press and P. Schechter proposed a formalism to obtain the halo number density [104]. They postulate that the probability of $\delta_M \geq \delta_c$ is equal to the mass fraction contained in halos with mass greater than M. Mathematically, it is written as

$$\frac{m_{\geq M}(M)}{m_{tot}} = \int_{\delta_c}^{\infty} d\delta_M \, \mathbf{P}(\delta_M), \tag{4.9}$$

where $m_{\geq M}$ is the mass locked inside the haloes with mass greater than or equal to M, m_{tot} is the total mass in the universe, and $\mathbf{P}(\delta_M)$ is the probability distribution function (PDF) of δ_M. Notice that, if we take a derivative with respect to M on $m_{\geq M}$ and multiply with mass fraction dM, the right-hand side of the equation 4.9 is obtained. Therefore,

$$M\frac{dN}{dM}dM = -m_{tot}\frac{d}{dM}\left[\int_{\delta_c}^{\infty} d\delta_M \, \mathbf{P}(\delta_M)\right] dM. \tag{4.10}$$

Finally, we substitute the relation $m_{tot} = \rho_0 V_{tot}$, where V_{tot} is the volume of the universe and define the halo number density $n(M) = \frac{N(M)}{V_{tot}}$. The result is

$$\frac{dn}{dM} dM = -2 \frac{\rho_0}{M} \frac{d}{dM} \left[\int_{\delta_c}^{\infty} d\delta_M \, \mathbf{P}(\delta_M) \right] dM, \tag{4.11}$$

where $\frac{dn}{dM} dM$ is the halo mass function representing the number density of the halo with mass in the range of $[M, M + dM]$. The fudge factor 2 is introduced by hand to the relation which is later addressed to be a cure to the so-called *cloud-in-cloud problem*. The problem concerns the formation of the halo at different scales; it is possible that the over-density in a region with a smaller mass is enclosed and collapsed in a region with a larger mass hence creating a redundancy in the halo counting. The solution to this problem was later proposed by J. R. Bond, S. Cole, G. Efstathiou and N. Kaiser in 1990 [105]. Instead, they derived the halo mass function through the Excursion set formalism that considers the mass hierarchy of halo formation. In particular, the formation of a halo with high mass is prioritized and counted before the low mass type. Roughly speaking, The randomness of the variable δ_M is formulated using the Markovian random walk which starts from infinitely large mass to zero mass. The first up crossing through the δ_c bar will dictate the mass of the halo that forms from that variable. In this formalism, the fudge factor appears naturally.

Furthermore, the expression can be manipulated by using the chain rule. The result is

$$\frac{dn}{d \ln M} = \frac{\rho_0}{M} \nu f(\nu) \frac{d \ln \nu}{d \ln M}, \tag{4.12}$$

where $\nu \equiv \frac{\delta_c}{\sigma_M}$ is the normalized variable and $\sigma_M^2 = \langle \delta_M^2(x) \rangle$ is the variance of δ_M distribution. The function $f(\nu)$ is defined as

$$f(\nu) = 2 \sigma_M \mathbf{P}(\nu). \tag{4.13}$$

This relation is useful because it connects the underlying distribution of matter density to the dark matter halo number density which the galaxy population can trace. It is evident that the kind of statistics of δ_M impacts how haloes are distributed across the sky, suggesting a connection for studying early cosmology, i.e. building a model that gives well-fitted halo mass function.

It is worth mentioning that, up until now, the spherical collapse is assumed. This is not exactly the case in reality since the Zel'dovich approximation precisely predicted the ellipsoidal

collapse instead. Accordingly, the model was improved in 1999 by R. K. Sheth, H. J. Mo and G. Torman [106]. In this case, the critical density δ_c depends on the mass of the resulting halo causing some modifications on the halo mass function. For simplicity, we will neglect those changes and use only the expression for the spherical collapse in this review.

4.2 Theoretical Prediction of Halo Bias Parameter: Threshold Bias

In this section, we will go through the timeline of theoretical developments starring the halo bias parameter, focusing on the threshold bias. The story began when N. Kaiser realised that the misalignment in the two-point correlation function of galaxies and clusters from the Abell catalogue could be theoretically explained (see section 3.3.1 and the paper [27]). Similar but not the same as the Press-Schechter mass function (see section 4.1.1), he formulates that the average cluster number density equals the probability of $\delta_R \geq \delta_c$. By assuming a Gaussian-distributed δ_R, he computed the two-point correlation function of the clusters with the linear bias parameter. This marks the first theoretical prediction of the parameter. The parameter was then regarded as the threshold bias since it was formulated from the collapse threshold theory (see section 4.1). Not long after, the formalism was extended to the case of non-Gaussian δ_R by S. Matarrese, F. Lucchin and S. A. Bonometto using the path-integral formalism [107]. The discussion of the halo bias correction in section 4.3 will be based on their theoretical work.

4.2.1 Threshold Bias with Gaussian Prior

By adopting the collapse criterion of the Press-Schechter theory discussed in section 4.1, we can write an ansatz for halo number density as

$$n_h(\boldsymbol{q}) = \Theta(\delta_R(\boldsymbol{q}) - \delta_c) \tag{4.14}$$

where Θ is the Heaviside step function and $\boldsymbol{q}$ is a position defined on the Lagrangian coordinate. Even though the superscript (L) is omitted, let us remind you that the density here is defined in Lagrangian space. Thus, the criterion here is for indicating the *proto-halo*, the progenitor region that will collapse into a halo later. But, by conservation of the tracer number, the proto-halo number and the resulting halo number are the same. Notice that we have implicitly specified the halo mass by choosing R. This means we are considering the population of the halo with

the corresponding mass computed from equation 4.6 only, in contrast to what we have done when formulating the Press-Schechter mass function (see section 4.1.1). Accordingly, we can compute the ensemble average of halo number density with the associated mass at position $\boldsymbol{q}$ by

$$\langle n_h(\boldsymbol{q})\rangle = \int_{-\infty}^{\infty} d\delta_R\, \Theta(\delta_R(\boldsymbol{q}) - \delta_c)\mathbf{P}(\delta_R) = \int_{\delta_c}^{\infty} d\delta_R\, \mathbf{P}(\delta_R). \tag{4.15}$$

where $\langle . \rangle$ represents the ensemble average operation. Note that n_h has the same meaning as tracer number density n_g but specifically for DM halo. To proceed from this point, the distribution of δ_R must be specified. For simplicity, we will assume Gaussian-distributed δ_R at every point in space. The probability distribution function (PDF) can be written as

$$\mathbf{P}(\delta_R) = \frac{1}{\sqrt{2\pi}\sigma_R} e^{-\delta_R^2/2\sigma_R^2}. \tag{4.16}$$

This is indeed not a bad assumption since the initial distribution of fluctuation from inflation is found to be close to Gaussian hence the filtered density contrast also is. In the upcoming sections, we will present the attempt to go beyond this assumption by introducing small non-Gaussianity and the results here will serve as the zeroth order of the next discussion. Nevertheless, we will first proceed with the Gaussian case for now. Accordingly, the mean yields

$$\langle n_h \rangle = \bar{n}_h \frac{1}{2} \mathbf{erfc}\left(\frac{\nu}{\sqrt{2}}\right), \tag{4.17}$$

where **erfc** is the complementary error function. Notice that the mean is now independent of the Lagrangian position since we assume the homogeneity in the space of the PDF. We can extend this result to the higher-order statistical moment by using the multi-variate Gaussian PDF,

$$\langle n_h(\boldsymbol{q}_1) \dots n_h(\boldsymbol{q}_N)\rangle = \int_{\delta_c}^{\infty} d\delta_R(\boldsymbol{q}_1) \cdots \int_{\delta_c}^{\infty} d\delta_R(\boldsymbol{q}_N)\, \mathbf{G}(\{\delta_R(\boldsymbol{q}_N)\}), \tag{4.18}$$

where $\{\delta_R(\boldsymbol{q}_N)\}$ represents the set of variables $\delta_R(\boldsymbol{q}_1), \dots, \delta_R(\boldsymbol{q}_N)$ and

$$\mathbf{G}(\{x_N\}) = \frac{1}{(2\pi)^{N/2}|C|^{1/2}} e^{-\frac{1}{2}\sum_{ij} x_i (C^{-1})_{ij} x_j} \tag{4.19}$$

is the multivariate Gaussian PDF. The covariance matrix is defined as $C_{ij} = \langle x_i x_j \rangle$, a collection of the two-point correlation functions between variables. To discuss the halo bias, the

relation between tracer discrete statistics and continuous density contrast NPCF is recalled. In particular, the 2CPF follows the relation 3.111,

$$\xi_h(r) = \frac{\langle (n_h(\boldsymbol{q}) n_h(\boldsymbol{q}+\boldsymbol{r})\rangle}{\bar{n}_h^2} - 1. \tag{4.20}$$

Notice that the 2PCF only depends on the norm of separation displacement r. This follows from the assumption of an isotropic universe. The function is first analytically computed by N. Kaiser in 1984 [27] and elaborated in [108, 109] shortly after. The result is

$$1 + \xi_h(r) = \sqrt{\frac{2}{\pi}} \left[\mathbf{erfc}\left(\frac{\nu}{\sqrt{2}}\right)\right]^{-2} \int_\nu^\infty d\nu\, e^{-\nu^2/2} \mathbf{erfc}\left(\frac{\nu - \nu\hat{\xi}_R(r)}{\sqrt{2(1-\hat{\xi}_R^2(r))}}\right), \tag{4.21}$$

where $\hat{\xi}_R(r) = \frac{\langle \delta_R(\boldsymbol{q})\delta_R(\boldsymbol{q}+\boldsymbol{r})\rangle}{\sigma_R^2}$ is the normalized two-point correlation function regarding the filtered matter density distribution. Since the matter correlation drops with increasing separation length (see section 3.3.1), it is reasonable to assume $\hat{\xi}_R(r) \ll 1$ at a large scale. This is the approximation that was used in the above-mentioned papers and also in [101]. In this case, we can expand the result in the power series of ξ_R as

$$\xi_h(r) = \sum_{N=1}^{\infty} \frac{1}{N!} \left(b_N^{(L)}\right)^2 (\xi_R(r))^N, \tag{4.22}$$

where $b_N^{(L)}$ is the bias parameter of the N-th order. The superscript L is present to emphasize that this parameter is of the set-up with Lagrangian coordinates. Note that the Lagrangian bias must be transformed into the Eulerian bias to compare with the observation since the observed matter distribution is in Eulerian space. Such a transformation is discussed in section 3.4. The parameter is obtained as

$$b_N^{(L)} = 2\left[\mathbf{erfc}\left(\frac{\nu}{\sqrt{2}}\right)\right]^{-1} \frac{e^{\nu^2/2}}{\sigma_R^N} \pi^{-1/2}\, 2^{-N/2}\, \mathbf{H}_{N-1}(\nu/\sqrt{2}), \tag{4.23}$$

where $\mathbf{H}$ denoted the physicists' Hermite polynomials. The expression can be further simplified by the *high peak limit*, $\nu \gg 1$. This limit corresponds to the case where the critical density δ_c is much higher than the amplitude of the matter fluctuation σ_R which is justified by the fact that we are in the perturbative regime of matter density where $|\delta| \ll 1$ therefore

$\sigma_R \sim |\delta| \ll \delta_c = 1.686$. This result is

$$b_N^{(L)} \xrightarrow{\nu \gg 1} \frac{\nu^N}{\sigma_R^N} + \mathcal{O}(\nu^{N-1}). \tag{4.24}$$

This approximation allowed us to write the 2PCF as

$$\xi_h(r) \xrightarrow{\nu \gg 1} \mathbf{exp}\left(\frac{\nu^2}{\sigma_R^2}\xi_R(r)\right) - 1. \tag{4.25}$$

This is the result N. Kaiser presented in his paper. Later, when we introduce a small NG to the prior, this result will serve as a leading contribution to the bias with a small correction from NG.

4.2.2 The MLB Approach To Halo Bias With Non-Gaussian Prior

We should work with non-Gaussian matter density fluctuation for many reasons instead of a simple Gaussian distribution. One of the reasons is numerous models of inflation produce non-Gaussianity which is still not ruled out by the observation as discussed in section 2.5.6. Hence, it is possible that the initial distribution provided by inflation is not precisely Gaussian. In fact, the nonlinearity of general relativity can naturally introduce NG to the distribution of matter even though inflation gave exactly Gaussian prior (this will be discussed later in section 4.3.1). Another reason is $-1 \leq \delta < \infty$ by definition while a Gaussian variable can hold any real value in the range $[-\infty,\infty]$. This mismatch of domains may not be a severe problem in the small perturbation regime, $|\delta| \ll 1$ but it indicates that Gaussian distribution is fundamentally not suitable in describing δ. For these reasons, it is therefore crucial to have a description for the halo bias that starts with non-Gaussian distribution. In 1986, S. Matarrese, F. Lucchin and S. A. Bonometto presented an approach to the large-scale matter distribution using the path-integral formalism [107]. They did not make any assumption about the kind of prior distribution and started with a generic PDF.

Using the path-integral formalism, we treat δ as a random field defined on a three-dimensional Lagrangian space. With the existence of external source J, the partition function is written as

$$\mathbf{Z}[J] = \int [\mathcal{D}\delta(\boldsymbol{q})]\ \mathbf{P}\left[\delta(\boldsymbol{q})\right] e^{i\int d^3q\, J(\boldsymbol{q})\delta(\boldsymbol{q})}, \tag{4.26}$$

where $\mathcal{P}\left[\delta(\boldsymbol{q})\right]$ is PDF defined in the functional space of $\delta(\boldsymbol{q})$ and the path-integral measure is

chosen such that the resulting probability is normalized to 1. It is important to mention that the generating functional $\ln \mathbf{Z}[J]$ can be written in a Taylor series expansion where the functional derivative terms are defined as the connected correlation functions $\xi_c^{(N)}$. Hence, given a complete set of $\xi_c^{(N)}$, the partition function is specified and the exact underlying distribution function is revealed.

As before, the matter density contrast field must be smoothed with the window function characterized by the radius R (see equation 4.1). Therefore, the correlation function of the smoothed field reads

$$\xi_R^{(N)}(\{\boldsymbol{q}_N\}) = \int \Big\{\prod_{r=1}^{N} d^3y_r \, W_R\big(|\boldsymbol{q}_r - \boldsymbol{y}_r|\big)\Big\}\xi^{(N)}(\{\boldsymbol{y}_N\}), \tag{4.27}$$

where $\xi^{(N)}(\{\boldsymbol{y}_N\}) = \langle \delta(\boldsymbol{y}_1)\dots\delta(\boldsymbol{y}_N)\rangle$ is the N-point correlation function of density contrast field and the notation $\{a_N\} = a_1, \dots, a_N$ is adopted for cleanness of the expression. The halo number density field is defined as equation 4.14. To study the halo bias, the (disconnected) correlation function of it must be computed. We will proceed by, first, computing the joint probability of exceeding the threshold defined as

$$\Pi_{\nu,R}^{(N)}(\{\boldsymbol{q}_N\}) = \Big\langle \prod_{r=1}^{N} n_h(\boldsymbol{q}_r)\Big\rangle = \int [\mathcal{D}\delta]\ \mathbf{P}\left[\delta(\boldsymbol{q})\right] \prod_{r=1}^{N}\Big\{\Theta(\delta_R(\boldsymbol{q}_r) - \nu\sigma_R)\Big\} \tag{4.28}$$

where the subscripts ν, R indicate that the quantity is computed with respect to the chosen parameter ν and the filter radius R. The quantity will later be used to compute the (disconnected) correlation function,

$$\xi_{\nu,R}^{(N)}(\{\boldsymbol{q}_N\}) = \Big\langle \prod_{r=1}^{N}\big[n_h(\boldsymbol{q}_r)/\langle n_h\rangle\big]\Big\rangle - 1 = \frac{\Pi_{\nu,R}^{(N)}}{\big[\Pi_{\nu,R}^{(1)}\big]^N} - 1. \tag{4.29}$$

The joint probability is computed by manipulating the Heaviside step function and defining an external field associated with the window function from which we can re-construct the partition function. The corresponding generating functional can then be expanded by the connected correlation function $\xi_c^{(n)}$,

$$\ln \mathbf{Z}[J] = \sum_{n=1}^{\infty} \frac{i^n}{n!} \int d^3y_1 \cdots \int d^3y_n \, \xi_c^{(n)}(\{\boldsymbol{y}_n\}) J(\boldsymbol{y}_1)\dots J(\boldsymbol{y}_n). \tag{4.30}$$

With some manipulation, the cluster expansion is utilized and we arrive at the final expression,

$$\Pi^{(N)}_{\nu,R} = \sum_{L=0}^{\infty} \sum_{\{m_L\}} \left\{ \prod_{n=2}^{L} \prod_{\{r_n\}=1}^{N} \left[\frac{1}{m_{n,\{r_n\}}!} \left(\frac{w^{(n)}_{R,\{r_n\}}}{n!} \right)^{m_{n,\{r_n\}}} \right] \prod_{r=1}^{N} a_{m_r}\left(\nu/\sqrt{2}\right) \right\}, \quad (4.31)$$

where

$$w^{(n)}_{R,\{r_n\}} = \begin{cases} 0 & ; n = 1 \textbf{ or } n = 2 \text{ where } r_1 = r_2 \\ \xi^{(n)}_R(\{\boldsymbol{q}_n\})/\sigma^n_R & ; \textit{other} \text{ n} \end{cases}, \quad (4.32)$$

and

$$\begin{aligned} a_0(z) &= \frac{1}{2}\mathbf{erfc}(z), \\ a_m(z) &= \pi^{-1/2} 2^{-m/2} e^{-z^2} \mathbf{H}_{m-1}(z) \text{ for } m > 0. \end{aligned} \quad (4.33)$$

The $L = 0$ term contributes 1 to the series. The set $m_L = m_1, \ldots, m_L$ consist of all non-negative integers satisfying $\sum_{n=1}^{L} n m_n = L$ and $m_{n,\{r_n\}}$ refers to non-negative integers satisfying $\sum_{n=1}^{N} m_{n,\{r_n\}} = m_n$. The process of series expansion and the definition of the summation indices introduced some indeterminate contributions 0^0 in this final expression. Those will be taken to be 1 since it actually corresponds to $e^0 = 1$ contribution. The complete derivation is provided in Appendix A.1.

Given the set of connected correlation functions, every order of the joint probability can be specified which can be used to determine the complete set of disconnected correlation functions $\xi^{(N)}_{\nu,R}$. This connects the theory with the observation since $\xi^{(N)}_{\nu,R}$ is the statistical quantities that can be constrained by the observational data.

Another important result of the paper is the cross-correlation function between objects with different parameters ν and R, (ν_1, R_1) and (ν_2, R_2). It can be written as

$$\xi^{(2)}_{\nu_1,R_1;\nu_2,R_2}(\boldsymbol{q}_1, \boldsymbol{q}_2) + 1 = \left\langle \frac{n_{h;\nu_1,R_1}(\boldsymbol{q}_1) n_{h;\nu_2,R_2}(\boldsymbol{q}_2)}{\langle n_{h;\nu_1,R_1}\rangle \langle n_{h;\nu_2,R_2}\rangle} \right\rangle = \frac{\Pi^{(2)}_{\nu_1,R_1;\nu_2,R_2}}{\Pi^{(1)}_{\nu_1,R_1} \times \Pi^{(1)}_{\nu_2,R_2}}. \quad (4.34)$$

The procedure of deriving $\Pi^{(2)}_{\nu_1,R_1;\nu_2,R_2}$ is similar to how we obtain the expression 4.31. The

result is

$$\xi^{(2)}_{\nu_1,R_1;\nu_2,R_2}(\boldsymbol{q}_1,\boldsymbol{q}_2) = -1 + \sum_{L=0}^{\infty}\sum_{\{m_L\}}\left\{\prod_{n=2}^{L}\prod_{j=0}^{n}\left[\frac{1}{m_{n,j}!}\left(\frac{w^{(n)}_{[R_1:j,R_2:n-j]}}{j!(n-j)!}\right)^{m_{n,j}}\right] a_m\big(\nu_1/\sqrt{2}\big)a_{L-m}\big(\nu_2/\sqrt{2}\big)\right\}\Bigg/\left[\Pi^{(1)}_{\nu_1,R_1}\times\Pi^{(1)}_{\nu_2,R_2}\right], \tag{4.35}$$

where $\Pi^{(1)}_{\nu_1,R_1}$ and $\Pi^{(1)}_{\nu_2,R_2}$ are determined by equation 4.31 and the new function is defined as

$$w^{(n)}_{[R_1:j,R_2:n-j]} = \begin{cases} 0 & ;n=1 \textbf{ or } n=2 \text{ where } j=1 \\ \xi^{(n)}_{[R_1:j,R_2:n-j]}\Big/\sigma^j_{R_1}\sigma^{n-j}_{R_2} & ;\textit{other} \text{ n} \end{cases}, \tag{4.36}$$

where

$$\xi^{(n)}_{[R_1:j,R_2:n-j]}(\boldsymbol{q}_1,\boldsymbol{q}_2) = \int\prod_{r=1}^{j}d^3y_r\,W_{R_1}(|\boldsymbol{q}_1-\boldsymbol{y}_r|)\prod_{s=1}^{n-j}d^3y_s\,W_{R_2}(|\boldsymbol{q}_2-\boldsymbol{y}_s|)\xi^{(n)}(\{\boldsymbol{y}_n\}). \tag{4.37}$$

The derivation of this expression will be explained in detail in appendix A.2.

These overwhelmingly long expressions will be simplified by the *high peak limit*, $\nu \gg 1$, as we have used in section 4.2.1. This allowed us to simplify the function a_n by substituting them with their asymptotic form,

$$a_m(\nu/\sqrt{2}) \xrightarrow{\nu\gg1} (2\pi)^{-1/2}\nu^{(m-1)}e^{-\nu^2/2}. \tag{4.38}$$

Accordingly, the mean becomes

$$\Pi^{(1)}_{\nu,R} = (2\pi\nu^2)^{-1/2}e^{-\nu^2/2}\mathbf{exp}\left(\sum_{n=3}^{\infty}\nu^n\frac{w^{(n)}_R}{n!}\right). \tag{4.39}$$

The two-point cross-correlation function becomes

$$\xi^{(2)}_{\nu_1,R_1;\nu_2,R_2}(\boldsymbol{q}_1,\boldsymbol{q}_2) = -1 + \mathbf{exp}\left\{\sum_{n=2}^{\infty}\sum_{j=1}^{n-1}\nu_1^j\nu_2^{n-j}\frac{w^{(n)}_{[R_1:j,R_2:n-j]}}{j!(n-j)!}\right\}, \tag{4.40}$$

and the two-point correlation function with the same filter scale and biasing parameter be-

comes

$$\xi^{(2)}_{\nu,R}(\boldsymbol{q}_1,\boldsymbol{q}_2) = -1 + \mathbf{exp}\left\{\sum_{n=2}^{\infty}\sum_{j=1}^{n-1}\left(\frac{\nu}{\sigma_R}\right)^n \frac{\xi^{(n)}_R\left([\boldsymbol{q}_1\, j\ times], [\boldsymbol{q}_2\ n\text{-}j\ times]\right)}{j!(n-j)!}\right\}, \tag{4.41}$$

where there is a repetition of positions in the argument of $\xi^{(n)}_R$.

Let us discuss this latest expression. If the underlying distribution is the zero-mean Gaussian, the partition function is specified with just two-point correlation functions and there is no contribution from the higher-order connected correlation function. In this case, the expression is reduced to the expression 4.25 which is derived in the Gaussian prior case. With the presence of a small NG, the higher-order connected correlation functions are non-zero but their contribution would be much smaller than the two-point contribution. In other words, the Gaussian expression is the leading term of this expression.

To study the linear bias, let us expand the expression up to the linear order of exponential,

$$\xi^{(2)}_{\nu,R}(\boldsymbol{q}_1,\boldsymbol{q}_2) = \left(\frac{\nu}{\sigma_R}\right)^2 \xi^{(2)}_R(\boldsymbol{q}_1,\boldsymbol{q}_2) + \left(\frac{\nu}{\sigma_R}\right)^3 \xi^{(3)}_R(\boldsymbol{q}_1,\boldsymbol{q}_1,\boldsymbol{q}_2) + \dots, \tag{4.42}$$

where we have used the rotational invariance of the NPCF, $\xi^{(3)}_R(\boldsymbol{q}_1,\boldsymbol{q}_1,\boldsymbol{q}_2) = \xi^{(3)}_R(\boldsymbol{q}_2,\boldsymbol{q}_2,\boldsymbol{q}_1)$. The first term is identical to the contribution in the Gaussian case and the following terms are interpreted as corrections to the leading Gaussian term.

A worth-mentioning clarification is that the NPCF contribution is not an analogy of loop correction in particle physics. We will see shortly that, in Fourier space, the bispectrum contribution is integrated with a cut-off at low- and high-k and may be confused with the loop correction in quantum field theory. Despite their close appearances, they are different because the NG contribution cannot be normalized like the loop correction. In brief, the NG contribution induces a new physical operator in the bias expansion, the Bardeen potential ϕ [110, 111],

$$b_\phi f_{NL}\phi \in \delta_g, \tag{4.43}$$

where b_ϕ is the Bardeen potential bias parameter degenerated with the nonlinear parameter f_{NL}. Hence, it cannot be removed by shifting the operators induced by gravitational evolution, e.g. δ, K^2, and O_{td}. Meanwhile, the loop correction arising from those operators can be renormalized and will not appear explicitly in the physical bias expansion [112].

4.3 Non-Gaussian Correction to Halo Bias

Looking at the expression 4.42, we see how NG affects the statistics of large-scale structures. As constrained by the observations, NG is, if any exists, small. We have discussed in section 2.5.6 that the leading contribution from NG is the three-point function and the significance lowers for the higher N-point functions. Therefore, one can choose to truncate the series of corrections in the order of interest. The three-point function or bispectrum correction has been studied by S. Matarrese and L. Verde in 2008 [29] for the local NG and then extended to the equilateral and folded NG in the subsequent year [30]. Not long after, J. Gong and S. Yokoyama studied the correction up to the four-point function or the trispectrum [33]. It is also worth mentioning that N. Dalal et al. (2007) [31] and A. Taruya, K. Koyama and T. Matsubara (2008) [32] also explored the correction in the same order but with different approaches. The first paper estimates the correction from the local ansatz (see equation 2.128) by splitting the linear and quadratic contribution of the ansatz. The derivation in it was carefully investigated in [113, 114] with the so-called *peak-background split* (PBS) approach. The second work made use of the so-called *local biasing* series which is based on the perturbation theory. In this section, we will derive the correction based on the threshold bias we have discussed in section 4.2.

The Fourier transform of equation 4.42 truncated at three-point contribution reads

$$P_h(k) = b_L^2 P_m(k) + b_L^3 \int \frac{d^3k'}{(2\pi)^3} B_m(k, k', |\boldsymbol{k} + \boldsymbol{k}'|) \tag{4.44}$$

where $b_L = b_1^{(L)} = \nu/\sigma_M$[1] and the subscript h and δ denoting the statistical quantity of the halo number density and the filtered density contrast respectively. Since NG is small, the bispectrum contribution is much smaller than the first term. Therefore, the expression is comparable to

$$P_h(k) = \big(b_L + \Delta b_L\big)^2 P_m(k) \approx \big(b_L + 2 b_L \Delta b_L\big) P_m(k), \tag{4.45}$$

where $\Delta b_L \ll b_L$ is the bias correction. Hence, we can write the correction from the bispectrum as

$$\Delta b_L(k) = \frac{b_L^2}{2P_m(k)} \int \frac{d^3k'}{(2\pi)^3} B_m(k, k', |\boldsymbol{k} + \boldsymbol{k}'|). \tag{4.46}$$

[1] Recall that the parameters radius R and mass M have one-to-one correspondence (see the discussion at the beginning of section 4.1.1).

Notice that the correction is scale-dependent; only $\boldsymbol{k}'$ got integrated out. To write the expression in terms of the primordial spectra, we recall the relation 4.4. Let us consider the structure at present where the redshift factor z is zero where the linear growth function is normalized $D(z = 0) = 1$. With respect to the definition of the power spectrum and bispectrum, the function $\mathcal{M}_M(k) \equiv \mathcal{M}_M(k, z = 0)$ will be inserted into the equation as

$$\Delta b_L(k) = \frac{b_L^2}{2P_\zeta(k)\mathcal{M}_M(k)} \int \frac{d^3k'}{(2\pi)^3} \mathcal{M}_M(k')\mathcal{M}_M(|\boldsymbol{k} + \boldsymbol{k}'|)B_\zeta(k, k', |\boldsymbol{k} + \boldsymbol{k}'|). \quad (4.47)$$

Alternatively, the convenient form for numerical calculation reads

$$\Delta b_L(k) = \frac{b_L^2}{8\pi^2\mathcal{M}_M(k)} \int_0^\infty dk' \, (k')^2 \mathcal{M}_M(k') P_\zeta(k') \int_{|k-k'|}^{k+k'} dz \left(\frac{q}{kk'}\right) \mathcal{M}_M(q) \frac{B_\zeta(k, k', q)}{P_\zeta(k)P_\zeta(k')}, \quad (4.48)$$

where we substitute $q = \|\boldsymbol{k} + \boldsymbol{k}'\|$. This formula is robust because The bispectrum, which represents NG in the initial condition, can be chosen according to the scenario of interest. Different kinds of it were discussed in section 2.5.6 and their corresponding bias corrections will be studied in the upcoming section.

With all the necessary ingredients, this formula can be used to estimate and study the behaviour of the bias correction with a caveat. The boundary of the integral over modes may be a little bit misleading. The horizon scale and the filter size limit the integration boundary. In particular, the variable k corresponds to the separation length r used to compute ξ_h (or $\xi_{\nu,R}$). This length defines the separation distance between objects which collapse from individual regions. By definition, all masses in the collapse region defined as a sphere of radius R will be concentrated into one object only. Therefore, it is irrational to consider the scale $k \gtrsim 1/R$ because it would mean we correlate overlapping collapse regions where the intersection is ill-defined. Moreover, we ignore the contribution from outside the horizon which became part of the background in the local universe. Therefore, the numerical integration of all bispectrum configurations is bounded by the inverse horizon and filter scale constraints.

4.3.1 Scale Dependence of The Correction

As shown in equation 4.47, the correction to the bias parameter is scale-dependent. When considering different forms of bispectrum, the correction may exhibit distinct varying behaviours

through scales. This reflects their detectability, i.e. size of the correction compared to the basic contribution, on various observational scales and gives character to the signals derived from different kinds of NG. This section will present and discuss their scale dependence. In particular, the results in [30] will be re-evaluated but also with the orthogonal bispectrum introduced earlier in section 2.5.6. Accordingly, the detectability of the correction is presented by

$$\beta_M(k) = \frac{1}{\delta_c}\frac{\Delta b_L}{b_L} = \frac{1}{8\pi^2\sigma_M^2\mathcal{M}_M(k)}\mathbf{I}_M(k), \tag{4.49}$$

where

$$\mathbf{I}_M(k) = \int_0^\infty dk'\,(k')^2\mathcal{M}_M(k')P_\zeta(k')\int_{|k-k'|}^{k+k'} dz\left(\frac{q}{kk'}\right)\mathcal{M}_M(q)\frac{B_\zeta(k,k',q)}{P_\zeta(k)P_\zeta(k')}, \tag{4.50}$$

which is a fraction of the correction with respect to the Gaussian bias. Thus, a particular NG is easily detected at a scale k if it yields high $\beta_M(k)$. The subscript "M" is indicated here to remind us that the correction is mass dependence from the filter function. The list of the templates for bispectra of each kind of NG reviewed in 2.5.6 will be used to compute the function $\beta(k)$ and discuss their detectability accordingly. However, prior to that, we will discuss one important type of NG which is not of a primordial kind but also contributes a correction to bias as well.

NG from the nonlinearity of GR

Regarding the theory of general relativity (GR), the equations of motion of cosmological perturbations are obtained from the Einstein Field Equation. Once the perturbations are studied up to the second order, it is evident that the nonlinear correction term introduces NG to the matter density distribution during the matter-dominated era. In particular, the perturbation that was in the superhorizon limit re-enters the horizon and affects the structure formation. With the horizon re-entry, the intrinsic PNG that was carried by the frozen perturbation is injected into the statistics of the large-scale structure. However, it is stressed that even in the absence of intrinsic PNG[2], the nonlinearity still introduces NG to the curvature perturbation. This effect was studied by N. Bartolo, S. Matarrese and A. Riotto in 2003 [117] where it gives

[2] This does not necessarily mean the one produced by inflation but by other possible scenarios beforehand as well [115, 116]

a negative contribution to the bispectrum as

$$B_{\zeta}^{GR}(k_1, k_2, k_3) = \frac{6}{5} f_{NL}^{GR}(k_1, k_2, k_3) P_{\zeta}(k_1) P_{\zeta}(k_2) + 2\ perm., \tag{4.51}$$

where $2\ perm.$ refers to the same term as before but permuting between $\{k_1, k_2, k_3\}$ and

$$f_{NL}^{GR}(k_1, k_2, k_3) = -\frac{5}{3}\left(1 - \frac{5}{2}\frac{k_1 k_2 \cos\theta_{12}}{k_3^2}\right), \tag{4.52}$$

where θ_{12} is the angle between $\boldsymbol{k}_1$ and $\boldsymbol{k}_2$ [30]. The equation 4.52 can be obtained by computing the three-point function of density contrast from equation 7 in [117] in Fourier space where only the term depends on conformal time squared is considered since it corresponds to the horizon re-entered perturbation. Furthermore, to consider the standard inflation scenario with no PNG, the parameter a_{nl} in the equation is set to 1.

The function $\beta(k)$ is evaluated for the newly discussed NG from the nonlinearity of GR and the shapes of PNG discussed in section 2.5.6, and plotted in figure 4.1. As an example, the following result is evaluated concerning the population of the dark matter halo with mass $10^{12} M_{\odot}$ which corresponds to the smoothing scale $R \sim 1h^{-1}$ Mpc. Therefore, the relevant scale in the plot is below $k \sim 1h$ Mpc^{-1} (a more accurate threshold is presented in the figure). We also introduce a long mode cut-off to the integral domain at the horizon scale $r_H = (cH_0)^{-1} \sim 5 \times 10^3 h^{-1}$ Mpc. Let us emphasize that the description of halo bias used here is valid only on a large scale. So, the results are only sensible at the linear scale and the separation is much larger than the Lagrangian radius of the halo, roughly speaking at $k < 10^{-1}h$ Mpc^{-1}. .

On the scale of around 10^{-4} to 10^{-1} hMpc^{-1}, it is evident that NG correction from the nonlinearity of GR is the largest. Among all shapes of intrinsic PNG, the local form NG would contribute the largest correction where the scale dependence is almost identical to the GR bias correction. The numerical analysis found that the correction by GR nonlinearity is bigger than the local form by the factor $5/3 \sim 1.6$ (see figure 4.1). This can be traced back to equation 4.52 where the factor in front of the parenthesis is exactly $5/3$. The tail (high k) of the GR correction plot is lifted from the *1.6local* line. This is because the term subtracted from 1 in the parenthesis (see equation 4.52) supports the overall value when integrated over all triangle configurations of mode vectors. It is important to emphasize that the GR correction is negative and is present regardless of the existence of PNG. This means the bias correction from the local

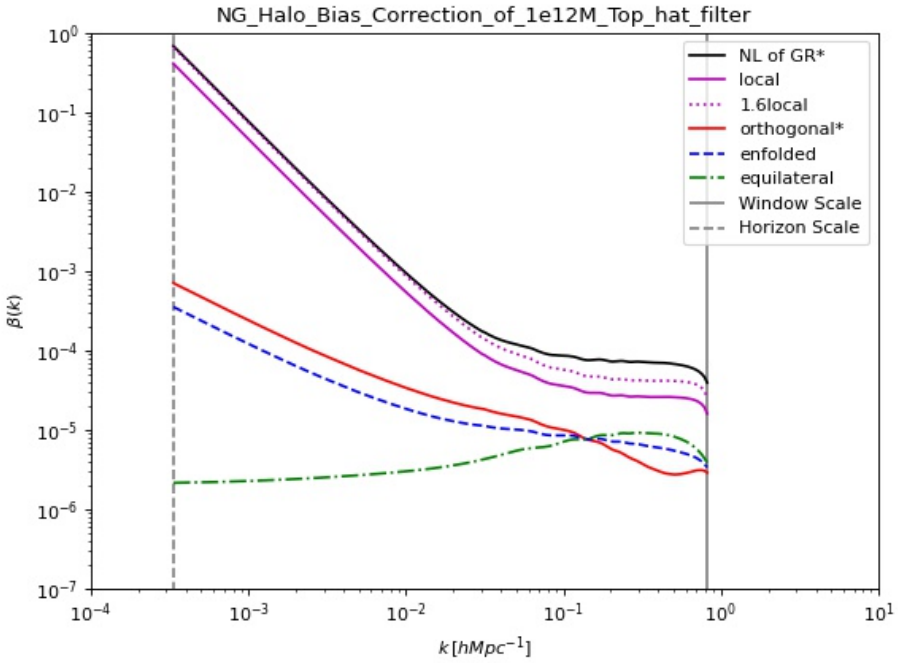

Figure 4.1: This plot presents the scale-dependent halo corrections as a consequence of different kinds of NG including the nonlinearity of GR (black solid line), local form NG (purple solid line), orthogonal form NG (red solid line), enfolded form NG (blue dashed line), and equilateral form NG (green dot-dashed line). For visualization purposes, the sign of the corrections indicated with * (NL of GR and orthogonal) is flipped from negative to positive in this plot. The nonlinear parameters of each shape are set to $f_{NL}^{loc} = f_{NL}^{equil} = f_{NL}^{en} = f_{NL}^{ortho} = 1$. It is numerically estimated that, at low k, the GR correction is larger than the local NG correction by a factor of ~ 1.6 which is illustrated by the dotted purple line compared to the GR correction line. It is also evident that the combination $2\beta_{en} - \beta_{equil}$ resembles the flipped orthogonal correction $-\beta_{ortho}$ which is shown by the light blue dotted line on top of the red solid line.

form, along with other shapes, could either add or subtract the existing contribution from GR depending on the sign of nonlinear parameters f_{NL}^{loc}, f_{NL}^{equil}, and f_{NL}^{orth}. The equilateral NG contributes the least correction to the halo bias and is the only contribution that grows with k while others decrease.

It is also worth mentioning that the correction of the equilateral and enfolded NG resemble the one of the orthogonal NG, as $\beta_{orth} = \beta_{equil} - 2\beta_{en}$ (see dotted light blue line in figure 4.1, recall that the graph of the orthogonal correction is flipped from negative to positive). This can be traced back to the relation of the bispectra themselves. From the definition of templates in section 2.5.6 and the plots in figure 2.8, it is evident that, when $f_{NL}^{loc} = f_{NL}^{equil} = f_{NL}^{orth}$, these

bispectra of these shapes are related as $B_\zeta^{ortho} = B_\zeta^{equil} - 2B_\zeta^{en}$. Since the integral in equation 4.47 is linear in B_ζ, this proportion propagates throughout the formula and persists in the final result.

To constrain the nonlinear parameters f_{NL}'s, the resulting formulae of scale-dependent halo bias corrections are applied to the data from galaxy surveys such as the Baryon Oscillation Spectroscopic Survey (BOSS) as a part of Sloan Digital Sky Survey (SDSS) (recently in [118, 119, 120, 121]). It is important to mention that, for the galaxy observation at the redshift factor $z \neq 0$, the linear growth factor must be reinstalled into the formula. This will not alter the scale dependence we have discussed since it will contribute just a constant multiplicative factor to the bias correction. Hence, it is ignored in this review for its irrelevance to the main discussion. Examples of estimation results are $f_{NL}^{loc} = -33 \pm 28$ [121], $f_{NL}^{equil} = 2 \pm 212$ and $f_{NL}^{ortho} = 126 \pm 72$ [120] where all uncertainties are of 68% confidence interval. Compared to the latest CMB result [23], the uncertainties of these recent results still fully cover those of CMB results and thus do not provide any new information about NG. However, numerous improvements can be made to the data analysis pipeline of the LSS survey. Several adjustments have gradually been made and it is clear that the constraint provided by this technique became narrower throughout the past years [119]. Thus, the study is still of great interest and potentially gives a competing result with the CMB analysis in the future. Furthermore, the new generation of LSS surveys is equipped with better instruments and promises to bring a tighter constraint to the table. For example, SPHEREx survey [24] forecast the f_{NL}^{loc} estimation with the uncertainty at the order of 1. It is also possible to exploit radio signal data from the Square Kilometer Array (SKA) observatory to constrain f_{NL}^{loc} through scale-dependent bias and achieving a similar level of precision [26, 25].

4.3.2 Mass Dependence of The Detectability Function

The plot 4.1 shows the detectability function from the Halo with mass $10^{12} M_\odot$ only. However, the halo mass can vary widely (see discussion in paragraph 2 of section 4.1) which will alter the window function $\tilde{W}_M$, and the function $\mathcal{M}_M$ and σ_M, consequently. Before going into the discussion, let us show the mass comparison of each kind of NG in figure 4.2.

From the figures, the revealed mass dependence at a large scale can be divided into two groups: those with larger detectability at a higher mass, and a lower mass. The first group includes the Local and NL of GR types. The rest belong to the second group. These behaviours are translated from the mass dependence of σ_M and the cut-off of the integral over k's existing

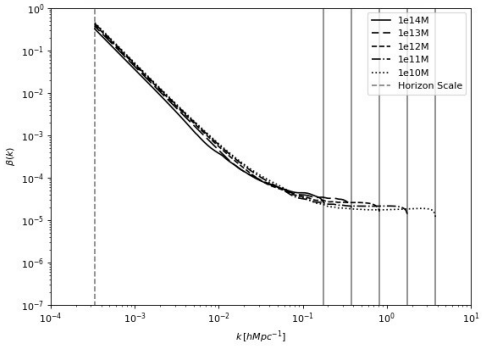

(a) Local Bispectrum

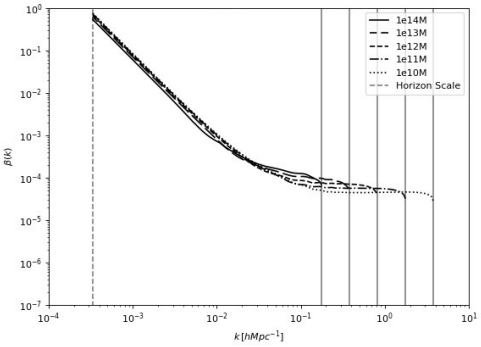

(b) Nonlinearity of GR (NL of GR) Bispectrum

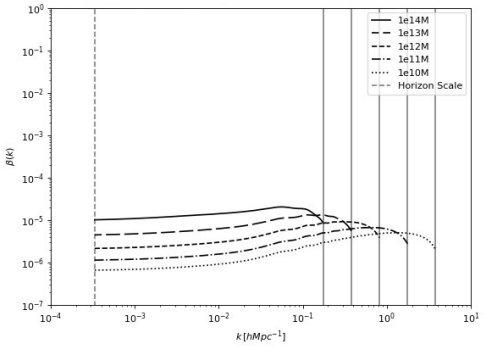

(c) Equilateral Bispectrum

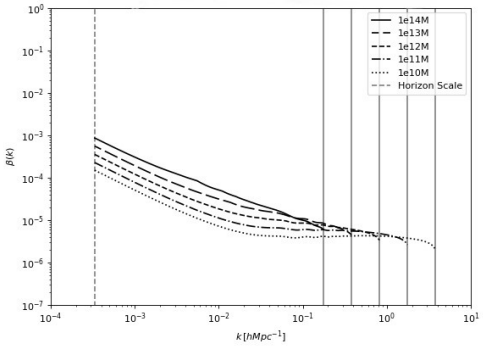

(d) Enfolded Bispectrum

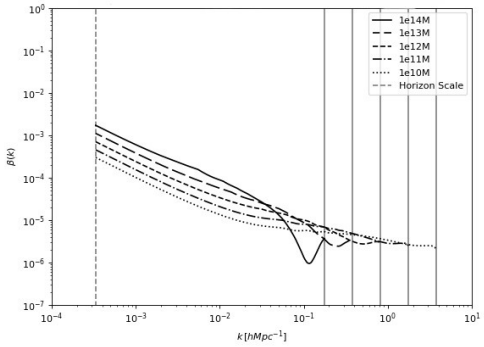

(e) Orthogonal Bispectrum

Figure 4.2: Comparison of scale dependence detectability functions at different halo mass. The range of masses, $\log(M/M_\odot) \in [10, 11, 12, 13, 14]$, are presented for the Local, Equilateral, Enfolded and Orthogonal kind of bispectrum along with the bispectrum introduced by the nonlinearity of GR (NLGR). At a large scale, the signals of local and NL of GR types with a lower halo mass are larger but not at an appreciable level. The Equilateral, Enfolded and Orthogonal kinds exhibit a noticeable mass dependence opposite to the prior two.

in the definition of β_M. In particular, σ_M decreases with growing mass since the width of the window function in the integral,

$$\sigma_M^2 = \int d^3k \; \tilde{W}_M(kR) P_m(k), \tag{4.53}$$

contracts down. Therefore, the prefactor $1/\sigma_M^2$ caused the detectability to increase with growing mass. This effect can be seen clearly in the second group including Equilateral, Enfolded, and Orthogonal types (see figures 4.2c, 4.2d, and 4.2e). However, a slight mass dependence of the two prior types is the opposite. The explanation lies in the integral term of equation 4.49, $\mathbf{I}_M(k)$. Considering at a small k, the local and NL of GR bispectra peak at large k'. Thus, the extension of window functions by lower mass in the integral contributes significantly to the numerator, unlike the other types with peak limits at the comparable size of k and k'. Therefore, the mass dependence flipped at a large scale for local and NL of GR types (see figures 4.2a and 4.2b) but not at a significant level since both the integral and the prefactor grow significantly with decreasing mass.

4.3.3 Other choices of Window Function

The interpretation of collapse theory depends on the shape of the window function. Different choice has their pros and cons which must be taken into account when using them. For example, the top-hat filter in real space sharply truncates the contribution at radius R. However, the function extends to infinity in Fourier space which may be problematic when a high k contribution is unneeded. Thus, the filter must be chosen properly to match the purpose of each study. Three choices of the window function, including the top hat in real space, are explored in this thesis. The other two popular choices are the Gaussian and sharp k-space filters (top-hat in Fourier space). In Fourier space, the Gaussian type is defined as

$$\tilde{W}_{Gauss}(kR) = \mathbf{exp}\left\{-\frac{(kR)^2}{2}\right\}, \tag{4.54}$$

and the sharp k-space type is defined as

$$\tilde{W}_{sharpk}(kR)) = \begin{cases} 1 & ; kR \leq 1 \\ 0 & ; kR > 1 \end{cases}. \tag{4.55}$$

As it turns out, no difference in the results is found among these window functions. The replicated plots with the Gaussian and sharp k-space window functions are shown Appendix B.

5

Probing Parity Violation With Four-point Correlation Function

One of the starting points of the physical model building is the *symmetry*. This fundamental feature imposes rules that should be respected by the object in the theory. Mainly, there are two types of symmetry: continuous and discrete symmetries. A continuous symmetry such as Poincaré symmetry dictates the dynamics by appointing the conserved quantity via the *Noether's theorem*. A discrete symmetry such as parity symmetry regulates the properties of the objects and the interactions between them. Typically, the choice of these symmetries is empirical; the specific properties of nature are assumed. Namely, a consistent theory can be built by appointing a set of symmetries. Then, its prediction is compared with the experiments and observations to test the assumption on those symmetries. Such tests are powerful since a certain kind of symmetry may be a building block of many models. Disapproval of one symmetry could lead to the abandonment of numerous theories.

This section focuses on the *parity symmetry*. Essentially, it is a mirror symmetry where the theory must be invariant under the flipping of the left and right sides of the space. Mathematically, a parity-conserving object O is invariant under parity transformation,

$$\mathbb{P}[O(\boldsymbol{x_1}, \boldsymbol{x_2}, \ldots, \boldsymbol{x_n})] = O(-\boldsymbol{x_1}, -\boldsymbol{x_2}, \ldots, -\boldsymbol{x_n}) = O(\boldsymbol{x_1}, \boldsymbol{x_2}, \ldots, \boldsymbol{x_n}), \tag{5.1}$$

where $\boldsymbol{x_1}, \boldsymbol{x_2}, \ldots, \boldsymbol{x_n}$ are spatial coordinates. Generally, a parity conserving theory is the the-

ory with the Lagrangian that is invariant under parity transformation, $\mathbb{P}[\mathcal{L}] = \mathcal{L}$. For example, GR respects parity symmetry since the Einstein-Hilbert action is invariant under parity transformation (see section 2.5.7). Therefore, it is expected that the physical products from the standard GR must be the same under the alteration of left and right.

This includes the galaxy distribution because its initial condition from inflation and the mechanism after are both based on GR theory. So, it is natural to think that the galaxy distribution should respect the parity symmetry. However, recent analyses found contradictory results. [1] and [2] independently found a deficit value in the galaxy's 4PCF compared with its mirror counterpart, reflecting a parity violation in LSS. This finding can be ground-breaking since it would suggest that GR is fundamentally a parity-violating theory. For example, some high-energy parity-violating modifications play a notable role in producing density fluctuation during inflation. Hence, the LSS is already parity-violating initially. However, observing LSS is complicated. The galaxy map gathered from the sky is subjected to the *projection effects* which may manipulate the position of galaxies in such a way that parity violation appears artificially. One such effect is the Redshift Space Distortion (RSD) effect; The galaxy's redshift (radial distance) estimation is distorted by its peculiar velocity via the relativistic Doppler effect. The role of this effect has been recently pointed out in [3]. They computed the galaxy trispectrum with the RSD effect including GR correction with which they concluded that the emerged parity violation could explain parts of the signature found in [1, 2]. This thesis will extend the analysis by including the so-called *wide-angle effect*: the establishment of multiple LOS for each galaxy for the NPCF at large separations in the sky. Moreover, we revise the averaging over the survey volume in real space as a technique to compute 4PCF (see section 3.5) as it will remove the parity violation from RSD in the observed trispectrum in the end.

Why Probing PV with 4PCF?

Let us spend a few words on why we have to resort to 4PCF to probe for PV in galaxy distribution. In general, it is less computationally expensive to probe lower-order statistics such as 2PCF or 3PCF. However, as mentioned in section 3.5, the ensemble average of galaxies are accessed through averaging over the survey volume. Therefore, a certain configuration of galaxies is indistinguishable if it can be achieved by three-dimensional spatial rotating of another configuration. With this in mind, we can see geometrically why 2PCF and 3PCF cannot probe PV through the galaxy survey. In particular, the geometry of 2PCFs and 3PCFs are line and triangle of separations in space, respectively. When the parity transformation reflects the lateral(s) of the shape, the three-dimensional rotation can always transform them back to the original

shape. This is because they are one- and two-dimensional geometries. However, 4PCF forms a tetrahedral which is a three-dimensional shape and the reflected configuration is not achievable by the rotation (see figure 5.1). Therefore, the parity-odd mode exists at the lowest-order statistic of 4PCF.

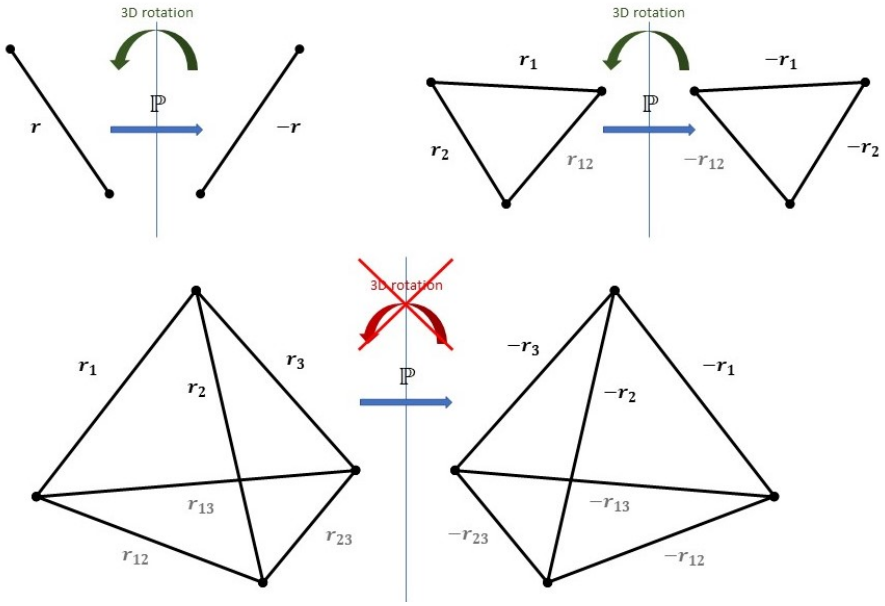

Figure 5.1: Pictorial Explanation of Parity distinguishability of 4PCF. Note that the reflected configurations are rotated for easy illustration.

5.1 Redshift Space Distortion (RSD) Effect

This observational effect concerns the radial distance of the observed galaxy. The inevitable fact about astrophysical surveys is that the sky is two-dimensional while the real universe is spatially three-dimensional. In other words, the observed ground is a projection of cosmic volume on a spherical surface. Thus, while the angles (θ, φ) of the galaxy on spherical coordinates can be indicated directly from the sky, the radial position or the depth (r) is estimated by its redshift instead. The universe's expansion causes the so-called *cosmological redshift* through the Hubble law, which depends on the distance between the galaxy and the observer. For an object with a low redshift factor, the proper distance is linearly proportional to the factor,

$$\chi(z) = \int \frac{dz}{H(z)} \xrightarrow{\text{low}z} z = H(z)\chi + \mathcal{O}(z^2). \tag{5.2}$$

However, the degeneracy with other kinds of redshift is unavoidable. Apart from cosmological redshift, special relativity implies the relativistic Doppler effect where the electromagnetic waves received by the observer are redshifted by the source's and observer's velocity projection on the straight LOS connecting the two. For galaxies clustering on a large scale, peculiar velocity is induced by the gravitational interaction. [34] first investigate the effect on a linear scale where the peculiar velocity is small. The simultaneous infall of matter creates a squashing pattern along the LOS. For a higher velocity in the nonlinear virializing process, the distribution stretched along the LOS, creating the Finger-of-god (FOG) pattern [35]. These effects are nicely combined and formalized in [36]. To construct the mathematical description, let us start with writing the redshift space radial distance,

$$s = \frac{z}{H} = r + \frac{\boldsymbol{v}_g \cdot \hat{\mathbf{r}}}{H}, \tag{5.3}$$

where r is the real space radial distance, $\boldsymbol{v}_g$ is the galaxy's peculiar velocity, and $\hat{\mathbf{r}}$ is the LOS. The second term with peculiar velocity is the relativistic Doppler effect term which we have assumed the magnitude peculiar velocity to be much less than the speed of light $v_g \ll c$ and neglected the term of order $\mathcal{O}(v_g^2)$ or more (notice that we set $c \equiv 1$). With this modification on the side, we consider the projection effect. As a spatial distortion, RSD does not change the number of galaxies but changes the number density via deforming the volume element. In particular,

$$dN_g = n_g(\boldsymbol{x}) d^3x = n_{g,s}(\boldsymbol{s}) d^3s, \tag{5.4}$$

where $n_{g,s}$ is the galaxies number density in redshift space. The density is then transformed from real space by the Jacobian determinant,

$$\det J = \left| \frac{d^3s}{d^3x} \right| = \frac{s^2 \partial s}{x^2 \partial x} = \left[1 + \frac{1}{H} \frac{\partial}{\partial r} (\boldsymbol{v}_g \cdot \hat{\mathbf{r}}) \right] \left[1 + \frac{\boldsymbol{v}_g \cdot \hat{\mathbf{r}}}{Hr} \right]^2 . \tag{5.5}$$

By neglecting the term with velocity squared, we obtain the transformation,

$$n_{g,s}(\boldsymbol{s}) = n_g(\boldsymbol{x}) \left[1 - \frac{1}{H} \frac{\partial}{\partial r} (\boldsymbol{v}_g \cdot \hat{\mathbf{r}}) - 2 \frac{\boldsymbol{v}_g \cdot \hat{\mathbf{r}}}{Hr} \right] . \tag{5.6}$$

Let us mention that the last term in the square bracket is neglected in [34] since it is much smaller than the term before in the small angle approximation. This is a fair simplification for galaxy survey in the 20th century where the galaxy sample is taken from a small angular space

in the sky. In particular, the scaling of the terms are

$$\frac{\frac{1}{H}\frac{\partial}{\partial r}\left(\boldsymbol{v}_g\cdot\hat{\mathbf{r}}\right)}{2\frac{\boldsymbol{v}_g\cdot\hat{\mathbf{r}}}{Hr}}\sim kR\gg 1 \text{ For small angle surveys.} \tag{5.7}$$

where R is the survey depth and k is the mode of number density contrast field. For a small-angle survey, feasible n-point statistics can be extracted at small separations of galaxies only, hence $kR\gg 1$. Therefore, the last term can be neglected. However, the current and future surveys are capturing the sky with a wider angle and the term cannot be neglected anymore [38, 122]. For example, the data from the Baryon Oscillation Spectroscopic Survey (BOSS) allow [1] to probe 4PCF with the arm separation of $20-160\ h^{-1}$Mpc at the redshift $0.2-0.7$ (corresponds to the proper radial distance of $\sim\ 800\ -\ 2500$ Mpc) which results in $kR\ \sim\ 0.01\ -\ 0.25$. Therefore, the term must be kept for this purpose. Then, the number density contrast can be computed by

$$1+\delta_{g,s}=(1+\delta_g)\left[1-\frac{1}{H}\frac{\partial}{\partial r}\left(\boldsymbol{v}_g\cdot\hat{\mathbf{r}}\right)-2\frac{\boldsymbol{v}_g\cdot\hat{\mathbf{r}}}{Hr}\right]\frac{\bar{n}_g(r)}{\bar{n}_g(s)}. \tag{5.8}$$

The fraction of mean number density appears in this case. Since the correction from the Doppler effect is small, we can expand

$$\bar{n}_g(s)=\bar{n}_g(r)+\frac{\partial\bar{n}_g}{\partial r}(\boldsymbol{v}_g\cdot\hat{\mathbf{r}})+\mathcal{O}(v_g^2). \tag{5.9}$$

Therefore, we have the final transformation [123, 124],

$$\delta_{g,s}(\boldsymbol{s})=\delta_g(\boldsymbol{x})-\left[\frac{1}{H}\frac{\partial}{\partial r}\left(\boldsymbol{v}_g\cdot\hat{\mathbf{r}}\right)+\alpha_{nwt}(r)\frac{\boldsymbol{v}_g\cdot\hat{\mathbf{r}}}{r}\right], \tag{5.10}$$

where $\alpha_{nwt}(r)\equiv\frac{\partial\ln r^2\bar{n}_g}{\partial\ln r}$ is the Newtonian redshift amplitude. Notice that the effect of gravity in the analysis up until now is in Newtonian approximation. In the full GR consideration, α_{GR} is complicated since a series of effects could alter the observed number density [125]. [124] have discussed three groups of effects in the GR context in section 4: geometry and mode coupling, Doppler lensing, and acceleration terms. There is also an additional effect from the gravitational potential that appears only in the full GR context [125, 126]. However, this is an extra complication ignored in this thesis as the value of α_{GR} is irrelevant for introducing parity violation to 4PCF; we consider the amplitude as some constant α for simplicity. Different val-

ues of α may be associated with a data set with certain properties as pointed out in [124, 127] and references therein. This is because the function depends only on redshift and does not introduce directional dependence to the tracer population. Thus, it cannot source PV on its own. Also, let us assume that the galaxies members of NPCF are at around the same redshift so we can assume α to be the same for every $\delta_{g,s}$. This is not a crude assumption since the redshift difference between 2 tracers in redshift space is suppressed by $\Delta z \sim H\Delta r/c$ where Δr is a proper displacement between tracers projected along LOS. Hence, considering the 4PCF with $\mathcal{O}(100)$ Mpc arm lengths would result in a minuscule redshift difference between members. Therefore, they are subjected to roughly the same value of α. The main focus rather goes to the cosine factor from $\boldsymbol{v}_g \cdot \hat{\mathbf{r}}$ which we will see shortly how it may introduce some asymmetry.

Let us consider the Fourier transform of $\delta_{g,s}(\boldsymbol{s})$,

$$\delta_{\boldsymbol{k}}^{g,s} = \int d^3s e^{i\boldsymbol{k}\cdot\boldsymbol{s}} \left\{ \delta_g(\boldsymbol{x}) - \left[\frac{1}{H}\frac{\partial}{\partial r}\left(\boldsymbol{v}_g \cdot \hat{\mathbf{r}}\right) + \alpha \frac{\boldsymbol{v}_g \cdot \hat{\mathbf{r}}}{r} \right] \right\} \tag{5.11}$$

We wish to express this in terms of the real space density to see the modification introduced by RSD. To do so, we assume a small distortion term as usual and expand the exponential factor concerning the expression 5.3,

$$\begin{aligned} e^{i\boldsymbol{k}\cdot\boldsymbol{s}} &= e^{i\boldsymbol{k}\cdot\boldsymbol{x}} e^{ik\mu\left(\frac{\boldsymbol{v_g}\cdot\hat{\boldsymbol{r}}}{H}\right)} \\ &= e^{i\boldsymbol{k}\cdot\boldsymbol{x}} \sum_{n=0}^{\infty} \frac{1}{n!} \left[ik\mu \left(\frac{\boldsymbol{v_g}\cdot\hat{\boldsymbol{r}}}{H} \right) \right]^n , \end{aligned} \tag{5.12}$$

where we define the cosine factor $\mu \equiv \hat{\boldsymbol{k}} \cdot \hat{\boldsymbol{s}}$[1]. Then, the density and velocity are inverse Fourier-transformed (similar to equations 3.51). For later convenience, the velocity will be expressed with velocity divergence, $\theta_g = i\boldsymbol{k} \cdot \boldsymbol{v_g}$, instead. The final result is

$$\begin{aligned} \delta_{\boldsymbol{k}}^{g,s} = \sum_{n=1}^{\infty} \frac{(k\mu)^{n-1}}{(n-1)!} \int_{\boldsymbol{k_1}} \cdots \int_{\boldsymbol{k_n}} \delta_D^{(3)} \left(\boldsymbol{k} - \sum_{i=1}^{n} \boldsymbol{k_i} \right) \prod_{\sigma=2}^{n} \left[\frac{\mu_\sigma}{k_\sigma} \frac{\theta_{g,\boldsymbol{k_\sigma}}}{H} \right] \\ \left[\delta_{g,\boldsymbol{k_1}} - \left(\mu_1^2 - i\frac{4\pi\alpha}{k_1^3}\mu_1 \right) \frac{\theta_{g,\boldsymbol{k_1}}}{H} \right] . \end{aligned} \tag{5.13}$$

Note that the product term vanishes for $n = 1$ and $\mu_\sigma \equiv \hat{\boldsymbol{k}}_{\boldsymbol{\sigma}} \cdot \hat{\mathbf{s}}$. Let us discuss the modifications introduced by the RSD effect. The product of velocity divergence coming out from the

[1] Notice that $\hat{s} = \hat{r}$

plane wave factor expansion is the nonlinear FOG effect. Notice that those higher-order terms become more important with larger θ_g. In the second square bracket, we observe two shifting terms. The one proportional to μ_1^2 is the well-known Kaiser effect whereas the other is the wide-angle redshift term. The term becomes important for large modes (low k_1) as anticipated, Interestingly, it is proportional to $i\mu_1$ rather than μ_1^2 like the Kaiser term. This dependence is the key to PV mimicry of the RSD effect, similar to what has been discussed in [3] for the GR effect encoded in the parameter α_{GR}.

As usual, we would like to predict the galaxy's NPCF concerning the underlying matter's NPCF. The galaxy number density contrast will be connected to the matter density contrast through the (Eulerian) bias expansion 3.72. The galaxy's velocity divergence will be assumed to equal the matter fluid velocity divergence on a large scale through the equivalence principle, $\theta_g = \theta$. One may wonder if these transitions can introduce PV. By construction, the bias expansion is a true scalar expression with no directional dependence. Thus, it is not possible that the expansion will introduce PV, at least with this effective bias model on a large scale where standard GR gravity dominates the system. The fact that we assume equal velocities also prevents any directional dependence entering through the so-called *velocity bias*. Therefore, we conclude that the PV signature will not emerge from this part. The fact that we will consider the 4PCF force us to consider the bias expansion up to the third-order,

$$\delta_g = b_1\delta + b_2\delta^2 + b_3\delta^3 + b_{K^2}K_{ij}K^{ij} + b_{K^3}K^i{}_jK^j{}_kK^k{}_i + b_{td}O_{td}^{(3)}, \tag{5.14}$$

where the tidal field K_{ij} and the third-order tidal operator $O_{td}^{(3)}$ are defined in equations 3.76 and 3.106, respectively. The argument is omitted; the bias parameters are time-dependent (redshift-dependent) and the operators depend on both position and redshift. However, we will ignore the time dependence as we have assumed roughly equal-redshift galaxies in 4PCF. All terms can be expressed in Fourier space with the density field(s) δ integrating against a k-dependent kernel. Lastly, δ and θ are solved perturbatively through SPT of fluid equations in section 3.2.2 where the solutions at each order are obtained by integrating the first-order density $\delta_{\boldsymbol{k}}^{(1)}$ against Fourier space kernels F_n and G_n (see equations 3.63 and the recursion relation of kernels after). For fixed background cosmology (see section 3.2.2), the final result can be rearranged as

$$\delta_{\boldsymbol{k},\mu}^{g,s}(\tau) = \sum_{n=1}^{\infty} D^n(\tau)\delta_{\boldsymbol{k},\mu}^{g,s\,(n)}, \tag{5.15}$$

where

$$\delta^{g,s\,(n)}_{\boldsymbol{k},\mu} = \int_{\boldsymbol{k_1}} \cdots \int_{\boldsymbol{k_n}} \delta_D^{(3)} \left(\boldsymbol{k} - \sum_{i=1}^{n} \boldsymbol{k_i} \right) S^{(n)}(\boldsymbol{k_1}, \ldots, \boldsymbol{k_n}, \mu_1, \ldots, \mu_n) \delta^{(1)}_{\boldsymbol{k_1}} \ldots \delta^{(1)}_{\boldsymbol{k_n}}, \tag{5.16}$$

and $S^{(n)}$ is the nth redshift space kernel. The solution of kernels up to the third order can be found in Appendix C. From this point, we ignore the time evolution factor for simplicity since it will not source PV and we are under the assumption that galaxies in the considered 4PCF are at roughly the same redshift. Hence, we set $D(\tau) \equiv 1$ for convenience[2]. Let us discuss the mathematical structure of the kernel for future discussion. For PV searching, we are interested in the cosine term $\mu_\sigma = \hat{\boldsymbol{k}}_{\boldsymbol{\sigma}} \cdot \hat{\boldsymbol{r}}$. This is because the parity transformation would change $\mathbb{P}[\hat{\boldsymbol{k}}_{\boldsymbol{\sigma}}] = -\hat{\boldsymbol{k}}_{\boldsymbol{\sigma}}$ but leave the LOS unchanged, Therefore, $\mathbb{P}[\mu_\sigma] = -\mu_\sigma$. Notice that the norm and the dot product of k_σ's are invariant under parity transformation. Therefore, the redshift space kernel at any order can be reorganized as a polynomial of μ_σ's,

$$S^{(n)}(\boldsymbol{k_1}, \ldots, \boldsymbol{k_n}, \mu_1, \ldots, \mu_n) = \sum_{\{\alpha_n\}} s_n^{\{\alpha_n\}}(\boldsymbol{k_1}, \ldots, \boldsymbol{k_n}) \mu_1^{\alpha_1} \ldots \mu_n^{\alpha_n}, \tag{5.17}$$

where $\{\alpha_n\} = \alpha_1, \ldots, \alpha_n$ is a set of summation indices that are the exponents of μ_σ's and $s_n^{\{\alpha_n\}}$ is a parity-invariant mode-dependent coefficient for each monomial of μ_σ's. This expression will become useful shortly.

5.2 Redshift Space Trispectrum with Plane Parallel Limit

The trispectrum of galaxy number density can be computed from

$$\left\langle \delta^{g,s}_{\boldsymbol{k_1},\mu_1} \delta^{g,s}_{\boldsymbol{k_2},\mu_2} \delta^{g,s}_{\boldsymbol{k_3},\mu_3} \delta^{g,s}_{\boldsymbol{k_4},\mu_4} \right\rangle = \delta_D^{(3)} \left(\boldsymbol{k_1} + \boldsymbol{k_2} + \boldsymbol{k_3} + \boldsymbol{k_4} \right) T_{g,s}(\boldsymbol{k_1}, \ldots, \boldsymbol{k_4}, \mu_1, \ldots, \mu_4). \tag{5.18}$$

Let us recall that the delta function ensures the homogeneity of statistics. Notice that we abandon the statistical isotropy by the LOS dependence. However, this will later be reinstalled by the averaging over the observed volume. Also, the time dependence is neglected as it will be constant as discussed shortly before. Similar to what we have discussed for 2PCF and 3PCF

[2] This is the case for the present time and will not be the same for other redshift samples. Nonetheless, it will be a constant.

in section 3.5, the trispectrum is divided into the disconnected and connected contributions. The two leading connected contributions are

$$T^c_{g,s}(\boldsymbol{k_1},\ldots,\boldsymbol{k_4},\mu_1,\ldots,\mu_4) = T^{3111}_{g,s} + T^{2211}_{g,s}, \tag{5.19}$$

where

$$\begin{aligned} T^{3111}_{g,s} =& 6S^{(3)}(\boldsymbol{k_2},\boldsymbol{k_3},\boldsymbol{k_4})S^{(1)}(\boldsymbol{k_2})S^{(1)}(\boldsymbol{k_3})S^{(1)}(\boldsymbol{k_4})P_m(k_2)P_m(k_3)P_m(k_4) \\ &+ 3 \text{ perm.}, \end{aligned} \tag{5.20}$$

and

$$\begin{aligned} T^{2211}_{g,s} =& 4S^{(1)}(\boldsymbol{k_3})S^{(1)}(\boldsymbol{k_4})P_m(k_3)P_m(k_4) \\ &\Big[S^{(2)}(\boldsymbol{k_{13}},\boldsymbol{k_3})S^{(2)}(\boldsymbol{k_{24}},\boldsymbol{k_4})P(k_{13}) + S^{(2)}(\boldsymbol{k_{14}},\boldsymbol{k_4})S^{(2)}(\boldsymbol{k_{23}},\boldsymbol{k_3})P(k_{14})\Big] \\ &+ 5 \text{ perm.}. \end{aligned} \tag{5.21}$$

Note that $\boldsymbol{k_{ij}} \equiv \boldsymbol{k_i} + \boldsymbol{k_j}$ and unbolded vectors are the norm of them. $T^{3111}_{g,s}$ and $T^{2211}_{g,s}$ are essentially computed from the contribution $\left\langle \delta^{(3)}_{g,s}\delta^{(1)}_{g,s}\delta^{(1)}_{g,s}\delta^{(1)}_{g,s}\right\rangle$ and $\left\langle \delta^{(2)}_{g,s}\delta^{(2)}_{g,s}\delta^{(1)}_{g,s}\delta^{(1)}_{g,s}\right\rangle$, respectively. Note that we omit μ_σ's from the argument of the redshift kernels but keep in mind that every $\boldsymbol{k_\sigma}$ is always accompanied by μ_σ in the argument. The permutation terms can be written by switching the position in the arguments of mode vectors around from $\boldsymbol{k}_1$ to $\boldsymbol{k}_4$. So, $T^{3111}_{g,s}$ have 3 more permuted terms by selecting 3 modes out of 4 modes and $T^{2211}_{g,s}$ have 5 more permuted termed by selecting 2 modes out of 4 modes. The calculations of these contributions have been done systematically in [37] where the reader is highly recommended to have a look. There, the alpha term in equation 5.13 is not included and only Kaiser and FOG effect were present. Without going into the detailed calculation, one can tell from the expression 5.17 that the Trispectrum can also be reorganized as

$$T^c_{g,s}(\boldsymbol{k_1},\ldots,\boldsymbol{k_3},\mu_1,\ldots,\mu_3) = \sum_{\alpha_1,\alpha_2,\alpha_3} t^{\alpha_1,\alpha_2,\alpha_3}(\boldsymbol{k_1},\boldsymbol{k_2},\boldsymbol{k_3})\mu_1^{\alpha_1}\mu_2^{\alpha_2}\mu_3^{\alpha_3}. \tag{5.22}$$

Notice that we reduce the argument of the trispectrum to 3 pairs of mode vector and cosine factor. This is because the homogeneity controlled by the delta function enforces the quadrilateral condition $\boldsymbol{k_4} = -\boldsymbol{k_{123}}$. Assuming a single LOS for all modes, the cosine factor can also be written as $\mu_4 = \frac{k_1\mu_1+k_2\mu_2+k_3\mu_3}{k_{123}}$. This single LOS assumption is the *plane-parallel limit*

where we assume that the LOS of each galaxy is approximately the same. However, one might notice that this contradicts the introduction of the α_{nwt} term in equation 5.10 where we assume a wide-angle survey. This issue will be addressed in the upcoming section where the LOS geometry treatment due to a wide angle is employed. From this point, let us ignore this fact and process as if plane-parallel approximation is active.

5.3 Isotropic 4PCF with Plane Parallel Limit: PV-Free Estimator

One important step of galaxy statistical analysis is the averaging over the survey volume. This is an inevitable procedure that gives us access to the ensemble average by assuming the ergodicity of the galaxies sample (see section 3.5) In particular, the 4PCF estimator is

$$\hat{\zeta}(\boldsymbol{r_1}, \boldsymbol{r_2}, \boldsymbol{r_3}) = \int \frac{d^3s}{V_s} \delta_{g,s}(\boldsymbol{s}) \delta_{g,s}(\boldsymbol{s} + \boldsymbol{r_1}) \delta_{g,s}(\boldsymbol{s} + \boldsymbol{r_2}) \delta_{g,s}(\boldsymbol{s} + \boldsymbol{r_3}), \tag{5.23}$$

where $\boldsymbol{s}$ is the position of the first galaxy, which is also used as a major LOS of 4PCF, and $\boldsymbol{r_1}$, $\boldsymbol{r_2}$ and $\boldsymbol{r_3}$ are the position of the other 3 galaxies with respect to the first. If this estimator of ensemble-averaged 4PCF is unbiased, then taking the ensemble average of this expression will give us

$$\hat{\zeta}(\boldsymbol{r_1}, \boldsymbol{r_2}, \boldsymbol{r_3}) = \int \frac{d^3s}{V_s} \zeta(\boldsymbol{s}; \boldsymbol{r_1}, \boldsymbol{r_2}, \boldsymbol{r_3}), \tag{5.24}$$

where $\zeta(\boldsymbol{s}; \boldsymbol{r_1}, \boldsymbol{r_2}, \boldsymbol{r_3}) = \langle \delta_{g,s}(\boldsymbol{s}) \delta_{g,s}(\boldsymbol{s} + \boldsymbol{r_1}) \delta_{g,s}(\boldsymbol{s} + \boldsymbol{r_2}) \delta_{g,s}(\boldsymbol{s} + \boldsymbol{r_3}) \rangle$. Notice that the ensemble average version is allowed to be anisotropic by LOS dependence but it got removed in the final measurement by the fact that we obtain prediction from averaging over the survey volume. Crucially, this process will erase the PV signature that comes with μ since the factor would have already been averaged out. Let us see this mathematically by writing the Fourier transform of 4PCF,

$$\zeta(\boldsymbol{s}; \boldsymbol{r_1}, \boldsymbol{r_2}, \boldsymbol{r_3}) = \int_{\boldsymbol{k_1}} \int_{\boldsymbol{k_2}} \int_{\boldsymbol{k_3}} T^c_{g,s}(\boldsymbol{k_1}, \ldots, \boldsymbol{k_3}, \mu_1, \ldots, \mu_3) \mathbf{exp} \left(i \sum_{\sigma=1}^{3} \boldsymbol{k_\sigma} \cdot \boldsymbol{r_\sigma} \right), \tag{5.25}$$

following from the Wiener-Khinchin Theorem (see section 3.5) where $\boldsymbol{k_s} = \boldsymbol{k_4} = -\boldsymbol{k_{123}}$. Substituting the expression 5.22 gives us

$$\hat{\zeta}(\boldsymbol{r_1}, \boldsymbol{r_2}, \boldsymbol{r_3}) = \sum_{\alpha_1,\alpha_2,\alpha_3} \int_{\boldsymbol{k_1}} \int_{\boldsymbol{k_2}} \int_{\boldsymbol{k_3}} t^{\alpha_1,\alpha_2,\alpha_3}(\boldsymbol{k_1}, \boldsymbol{k_2}, \boldsymbol{k_3}) \mathbf{exp}\left(i \sum_{\sigma=1}^{3} \boldsymbol{k_\sigma} \cdot \boldsymbol{r_\sigma} \right) \int \frac{s^2 ds}{V_s} \int d\Omega_s \, \mu_1^{\alpha_1} \mu_2^{\alpha_2} \mu_3^{\alpha_3}. \tag{5.26}$$

Let us consider the last integral. It is the only part that may introduce PV to the isotropic estimator. However, we will show that the parity-odd contribution is removed by averaging over LOS. Let us start by expanding the dot product,

$$\begin{aligned} \mu_\sigma^{\alpha_\sigma} &= (\hat{\boldsymbol{k}}_{\boldsymbol{\sigma}} \cdot \hat{\boldsymbol{s}})^{\alpha_\sigma} \\ &= \sum_{j=1}^{\alpha_\sigma} c_j^{(\alpha_\sigma)} \mathcal{P}_j(\hat{\boldsymbol{k}}_{\boldsymbol{\sigma}} \cdot \hat{\boldsymbol{s}}), \end{aligned} \tag{5.27}$$

where $\mathcal{P}_j$ is the jth-order *Legendre polynomial*. Then, through the *spherical harmonic addition theorem*, we have

$$\mu_\sigma^{\alpha_\sigma} = \sum_{j_\sigma=1}^{\alpha_\sigma} c_{j_\sigma}^{(\alpha_\sigma)} \frac{4\pi}{2j_\sigma + 1} \sum_{m_{j_\sigma}=-j_\sigma}^{j_\sigma} Y_{j_\sigma,m_{j_\sigma}}(\hat{\boldsymbol{k}}_{\boldsymbol{\sigma}}) Y^*_{j_\sigma,m_{j_\sigma}}(\hat{\boldsymbol{s}}), \tag{5.28}$$

where Y_{j,m_j} is the (j, m_j)-order spherical harmonic function. With this decomposition, let us consider the averaging over the line of sight integral,

$$\int d\Omega_s \, \mu_1^{\alpha_1} \mu_2^{\alpha_2} \mu_3^{\alpha_3} = (4\pi)^3 \sum_{j_1,j_2,j_3} \sum_{m_{j_1},m_{j_2},m_{j_3}} \frac{c_{j_1}^{(\alpha_1)} c_{j_2}^{(\alpha_2)} c_{j_3}^{(\alpha_3)}}{(2j_1+1)(2j_2+1)(2j_3+1)} Y_{j_1,m_{j_1}}(\hat{\boldsymbol{k}}_{\boldsymbol{1}}) Y_{j_2,m_{j_2}}(\hat{\boldsymbol{k}}_{\boldsymbol{2}}) Y_{j_3,m_{j_3}}(\hat{\boldsymbol{k}}_{\boldsymbol{3}}) \int d\Omega_s Y^*_{j_1,m_{j_1}}(\hat{\boldsymbol{s}}) Y^*_{j_2,m_{j_2}}(\hat{\boldsymbol{s}}) Y^*_{j_3,m_{j_3}}(\hat{\boldsymbol{s}}). \tag{5.29}$$

The last integral is the so-called *Gaunt integral*,

$$\begin{aligned}\mathcal{G}^{j_1,j_2,j_3}_{m_{j_1},m_{j_2},m_{j_3}} &\equiv \int d\Omega_s Y^*_{j_1,m_{j_1}}(\hat{\boldsymbol{s}}) Y^*_{j_2,m_{j_2}}(\hat{\boldsymbol{s}}) Y^*_{j_3,m_{j_3}}(\hat{\boldsymbol{s}}) \\ &= \sqrt{\frac{(2j_1+1)(2j_2+1)(2j_3+1)}{4\pi}} \begin{pmatrix} j_1 & j_2 & j_3 \\ 0 & 0 & 0 \end{pmatrix} \begin{pmatrix} j_1 & j_2 & j_3 \\ m_{j_1} & m_{j_2} & m_{j_3} \end{pmatrix},\end{aligned} \tag{5.30}$$

where the parenthesis terms are the *Wigner 3-j symbol*. The symbol yields some constant coefficient with constraints on the indices. In particular, the second symbol imposes the following constraints,

$$\begin{aligned} &1)\ m_{j_1} + m_{j_2} + m_{j_3} = 0 \\ &2)\ |j_1 - j_2| \leq j_3 \leq j_1 + j_2 \text{ (Triangle inequality)}, \end{aligned} \tag{5.31}$$

and owe a transformation,

$$\begin{pmatrix} j_1 & j_2 & j_3 \\ -m_{j_1} & -m_{j_2} & -m_{j_3} \end{pmatrix} = (-1)^{j_1+j_2+j_3} \begin{pmatrix} j_1 & j_2 & j_3 \\ m_{j_1} & m_{j_2} & m_{j_3} \end{pmatrix}. \tag{5.32}$$

Therefore, the first symbol with zero m_j's implies a constraint $j_1 + j_2 + j_3 =$ even. This will become important shortly. For clarity let us write the averaging integral in terms of the isotropic basis function,

$$\int d\Omega_s\, \mu_1^{\alpha_1} \mu_2^{\alpha_2} \mu_3^{\alpha_3} = (4\pi)^3 \sum_{j_1,j_2,j_3} \mathcal{C}^{\alpha_2,\alpha_1,\alpha_3}_{j_1,j_2,j_3} \mathcal{P}_{j_1,j_2,j_3}(\hat{\boldsymbol{k}}_{\boldsymbol{1}}, \hat{\boldsymbol{k}}_{\boldsymbol{2}}, \hat{\boldsymbol{k}}_{\boldsymbol{3}}), \tag{5.33}$$

where the isotropic basis function [128] is defined as

$$\begin{aligned}\mathcal{P}_{j_1,j_2,j_3}(\hat{\boldsymbol{k}}_{\boldsymbol{1}}, \hat{\boldsymbol{k}}_{\boldsymbol{2}}, \hat{\boldsymbol{k}}_{\boldsymbol{3}}) =& (-1)^{j_1+j_2+j_3} \sum_{m_{j_1},m_{j_2},m_{j_3}} \begin{pmatrix} j_1 & j_2 & j_3 \\ m_{j_1} & m_{j_2} & m_{j_3} \end{pmatrix} \\ & Y_{j_1,m_{j_1}}(\hat{\boldsymbol{k}}_{\boldsymbol{1}}) Y_{j_2,m_{j_2}}(\hat{\boldsymbol{k}}_{\boldsymbol{2}}) Y_{j_3,m_{j_3}}(\hat{\boldsymbol{k}}_{\boldsymbol{3}}),\end{aligned} \tag{5.34}$$

and the coefficients are

$$\mathcal{C}^{\alpha_2,\alpha_1,\alpha_3}_{j_1,j_2,j_3} = \frac{c^{(\alpha_1)}_{j_1} c^{(\alpha_2)}_{j_2} c^{(\alpha_3)}_{j_3}}{\sqrt{4\pi(2j_1+1)(2j_2+1)(2j_3+1)}} \begin{pmatrix} j_1 & j_2 & j_3 \\ 0 & 0 & 0 \end{pmatrix}. \tag{5.35}$$

The isotropic basis is useful for indicating the parity-odd and parity-even contributions. In particular, the spherical harmonic is parity-odd when the index j is odd. Therefore, the basis is parity-odd when $j_1 + j_2 + j_3 =$ odd and parity-even otherwise. Then, having a non-zero coefficient $\mathcal{C}_{j_1,j_2,j_3}^{\alpha_2,\alpha_1,\alpha_3}$ when the sum of angular momentum indices is an odd number is direct evidence of PV in 4PCF. In fact, this is how [1, 2] determine the existence of PV from the BOSS galaxy dataset. They compared the estimated coefficients with mock datasets with no PV and found up to 7.1σ different statistically.

However, the coefficient 5.35 is constrained with $j_1 + j_2 + j_3 =$ even by the zero-m_j's Wigner 3-j symbol. Therefore, all parity-odd contributions are non-existing. This follows from the averaging of LOS pointed out in Appendix G of [37]. This is very powerful since one could consider the RSD as detailed as one wants but the potential PV by introducing LOS will be removed regardless. We may conclude here that the RSD in the plane-parallel limit cannot inject PV into the observed galaxy 4PCF.

5.4 Wide-angle Effect: Theoretical Comeback (?)

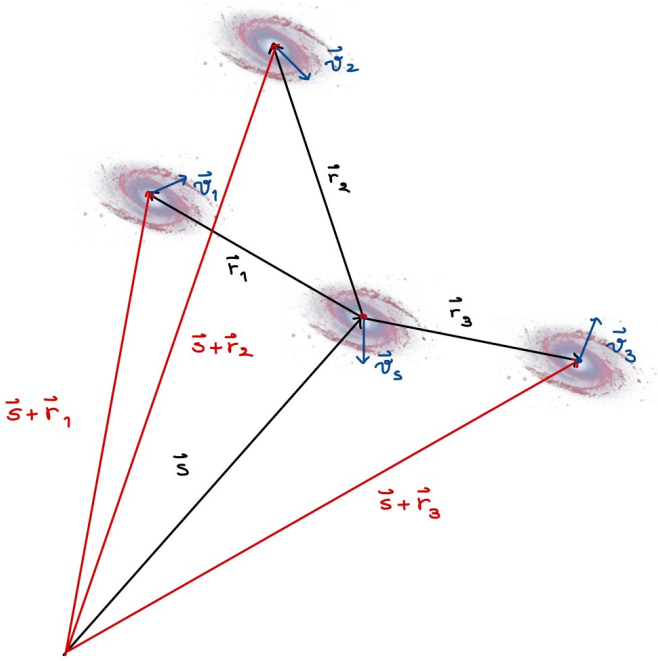

Figure 5.2: Geometry of local LOS for each galaxy in 4PCF.

As anticipated at the end of section 5.2, the single LOS assumption (plane-parallel) is crude. This is because the arm lengths, r_1, r_2, and r_3, can be significant compared to the radial distance s for modern surveys (see the discussion above equation 5.10). Therefore, multiple LOS must be employed in the calculation. Let us consider the configuration of 4 galaxies once again; the first galaxy is at the position $\boldsymbol{s}$ from the observer and the other three galaxies' positions are indicated with $\boldsymbol{r_1}$, $\boldsymbol{r_2}$, and $\boldsymbol{r_3}$ with respect to the first galaxy (see figure 5.2). Hence, the LOS of the first galaxy is $\hat{\boldsymbol{s}}$ as usual. However, the LOS of the others are (see [39] and reference therein),

$$\widehat{\boldsymbol{s}+\boldsymbol{r_\sigma}} = \frac{\boldsymbol{s}+\boldsymbol{r_\sigma}}{\|\boldsymbol{s}+\boldsymbol{r_\sigma}\|} \quad , \quad \sigma \in \{1,2,3\}. \tag{5.36}$$

The norm can be computed from $\|\boldsymbol{s}+\boldsymbol{r_\sigma}\| = \sqrt{s^2+r_\sigma^2+2sr_\sigma(\hat{\boldsymbol{s}}\cdot\hat{\boldsymbol{r}}_{\boldsymbol{\sigma}})}$. At the first level, let us expand the LOS up to first-order correction,

$$\widehat{\boldsymbol{s}+\boldsymbol{r_\sigma}} = \hat{\boldsymbol{s}} + \frac{r_\sigma}{s}\left[\hat{\boldsymbol{r}}_{\boldsymbol{\sigma}} - \hat{\boldsymbol{s}}(\hat{\boldsymbol{s}}\cdot\hat{\boldsymbol{r}}_{\boldsymbol{\sigma}})\right] + \mathcal{O}\left(\frac{r_\sigma^2}{s^2}\right). \tag{5.37}$$

Notice that the correction becomes important when r_σ is a sizable fraction of s. With this personalized LOS, the cosine factor of each galaxy is

$$\begin{aligned}
\mu'_\sigma &= \hat{\boldsymbol{k}}_{\boldsymbol{\sigma}}\cdot\widehat{\boldsymbol{s}+\boldsymbol{r_\sigma}} \\
&= \hat{\boldsymbol{k}}_{\boldsymbol{\sigma}}\cdot\hat{\boldsymbol{s}} + \frac{r_\sigma}{s}\left[\hat{\boldsymbol{k}}_{\boldsymbol{\sigma}}\cdot\hat{\boldsymbol{r}}_{\boldsymbol{\sigma}} - (\hat{\boldsymbol{k}}_{\boldsymbol{\sigma}}\cdot\hat{\boldsymbol{s}})(\hat{\boldsymbol{s}}\cdot\hat{\boldsymbol{r}}_{\boldsymbol{\sigma}})\right] \\
&= \mu_\sigma + \frac{r_\sigma}{s}\left[\hat{\boldsymbol{k}}_{\boldsymbol{\sigma}}\cdot\hat{\boldsymbol{r}}_{\boldsymbol{\sigma}} - \mu_\sigma(\hat{\boldsymbol{s}}\cdot\hat{\boldsymbol{r}}_{\boldsymbol{\sigma}})\right],
\end{aligned} \tag{5.38}$$

where the first galaxy still have the same factor as $\hat{\boldsymbol{k}}_{\boldsymbol{s}}\cdot\hat{\boldsymbol{s}}$. We will use prime to denote the corrected LOS and keep the unprimed factor for the usual single-LOS approximation. This correction forces us to reconsider the product of cosine factors in the expansion 5.22. In particular,

$$\begin{aligned}
\mu_s^{n_s}(\mu'_1)^{n_1}(\mu'_2)^{n_2}(\mu'_3)^{n_3} =& \mu_s^{n_s}\mu_1^{n_1}\mu_2^{n_2}\mu_3^{n_3} \\
&+ \frac{r_3}{s}n_3\left[\hat{\boldsymbol{k}}_{\boldsymbol{3}}\cdot\hat{\boldsymbol{r}}_{\boldsymbol{3}} - \mu_3(\hat{\boldsymbol{s}}\cdot\hat{\boldsymbol{r}}_{\boldsymbol{3}})\right]\mu_3^{n_3-1}\mu_s^{n_s}\mu_1^{n_1}\mu_2^{n_2} \\
&+ 2\text{ perm.} + \mathcal{O}\left(\frac{r_\sigma^2}{s^2}\right),
\end{aligned} \tag{5.39}$$

where the 2 permutation terms are obtained by cyclic replacement of indices 1, 2, and 3. As before, we can trade $\mu_s = \frac{k_1\mu_1+k_2\mu_2+k_3\mu_3}{k_{123}}$ to reduce that number of cosine factors. In this

relation, more cosine factors appeared through the LOS correction. For clarity, we let $\rho_\sigma = \hat{\boldsymbol{k}}_{\boldsymbol{\sigma}} \cdot \hat{\boldsymbol{r}}_{\boldsymbol{\sigma}}$ and $\nu_\sigma = \hat{\boldsymbol{s}} \cdot \hat{\boldsymbol{r}}_{\boldsymbol{\sigma}}$. Therefore, the expansion must be re-ordered in the new form,

$$T^c_{g,s}(\boldsymbol{k_1}, \ldots, \boldsymbol{k_3}, \mu_1, \ldots, \mu_3) = \sum_{\{\alpha_9\}} t'^{\{\alpha_9\}}(\boldsymbol{k_1}, \boldsymbol{k_2}, \boldsymbol{k_3}) \times \mu_1^{\alpha_1}\mu_2^{\alpha_2}\mu_3^{\alpha_3}\nu_1^{\alpha_4}\nu_2^{\alpha_5}\nu_3^{\alpha_6}\rho_1^{\alpha_7}\rho_2^{\alpha_8}\rho_3^{\alpha_9}. \tag{5.40}$$

Let us pause and ponder about the validity of this expansion. Despite starting from first-order LOS correction, this expression works up to an arbitrary correction order. This is because the cosine factors will always be introduced as power-law and form a power-law monomial after expanding. Therefore, the following discussion holds up to the validity of Taylor's expansion in any order. As apparent, these new geometrical quantities are the new challengers that may introduce PV to the 4PCF. However, we will argue in the next section that they will not produce any PV in the end.

For later convenience, the dot product between modes in $t'^{\{\alpha_9\}}$ are separated out and yields a new expansion,

$$T^c_{g,s}(\boldsymbol{k_1}, \ldots, \boldsymbol{k_3}, \mu_1, \ldots, \mu_3) = \sum_{\{\alpha_{12}\}} \tilde{t}^{\{\alpha_{12}\}}(k_1, k_2, k_3)\kappa_{12}^{\alpha_{10}}\kappa_{23}^{\alpha_{11}}\kappa_{13}^{\alpha_{12}} \times \mu_1^{\alpha_1}\mu_2^{\alpha_2}\mu_3^{\alpha_3}\nu_1^{\alpha_4}\nu_2^{\alpha_5}\nu_3^{\alpha_6}\rho_1^{\alpha_7}\rho_2^{\alpha_8}\rho_3^{\alpha_9}. \tag{5.41}$$

where $\kappa_{ij} = \hat{\boldsymbol{k}}_{\boldsymbol{i}} \cdot \hat{\boldsymbol{k}}_{\boldsymbol{j}}$. This is possible because we know that the products existing in the trispectrum are also power-law like other cosine factors. In this way, the coefficient is isotropic and surely not a parity-violating part. Then, the next section will assess whether the cosine factors will leave any PV behaviour after the Fourier transformation back to 4PCF.

5.5 Isotropic Wide-angle 4PCF: Still PV-Free

Following the procedure in obtaining equation 5.26, we obtain the estimator for with wide-angle effect,

$$\hat{\zeta}(\boldsymbol{r_1}, \boldsymbol{r_2}, \boldsymbol{r_3}) = \sum_{\{\alpha_{12}\}} \int_{\boldsymbol{k_1}} \int_{\boldsymbol{k_2}} \int_{\boldsymbol{k_3}} \tilde{t}^{\{\alpha_{12}\}}(k_1, k_2, k_3)\kappa_{12}^{\alpha_{10}}\kappa_{23}^{\alpha_{11}}\kappa_{13}^{\alpha_{12}}\rho_1^{\alpha_7}\rho_2^{\alpha_8}\rho_3^{\alpha_9} \exp\left(i\sum_{\sigma=1}^{3} \boldsymbol{k}_{\boldsymbol{\sigma}} \cdot \boldsymbol{r}_{\boldsymbol{\sigma}}\right) \int \frac{s^2 ds}{V_s} \int d\Omega_s \, \mu_1^{\alpha_1}\mu_2^{\alpha_2}\mu_3^{\alpha_3}\nu_1^{\alpha_4}\nu_2^{\alpha_5}\nu_3^{\alpha_6}. \tag{5.42}$$

Let us consider the LOS integral first. We follow the same decomposition of cosine factors as in section 5.3. In particular, the factor $\mu_\sigma^{\alpha_\sigma}$ follows the decomposition 5.28. Similarly, the other cosine factors are proportional to the sum of spherical Harmonics products as

$$\begin{aligned}
\nu_a^{\alpha_\sigma} &= \sum_{j_\sigma=1}^{\alpha_\sigma} c_{j_\sigma}^{(\alpha_\sigma)} \frac{4\pi}{2j_\sigma+1} \sum_{m_{j_\sigma}=-j_\sigma}^{j_\sigma} Y_{j_\sigma,m_{j_\sigma}}(\hat{\boldsymbol{r}}_{\boldsymbol{a}}) Y^*_{j_\sigma,m_{j_\sigma}}(\hat{\boldsymbol{s}}), \\
\rho_a^{\alpha_\sigma} &= \sum_{j_\sigma=1}^{\alpha_\sigma} c_{j_\sigma}^{(\alpha_\sigma)} \frac{4\pi}{2j_\sigma+1} \sum_{m_{j_\sigma}=-j_\sigma}^{j_\sigma} Y_{j_\sigma,m_{j_\sigma}}(\hat{\boldsymbol{r}}_{\boldsymbol{a}}) Y^*_{j_\sigma,m_{j_\sigma}}(\hat{\boldsymbol{k}}_{\boldsymbol{a}}), \\
\kappa_{ab}^{\alpha_\sigma} &= \sum_{j_\sigma=1}^{\alpha_\sigma} c_{j_\sigma}^{(\alpha_\sigma)} \frac{4\pi}{2j_\sigma+1} \sum_{m_{j_\sigma}=-j_\sigma}^{j_\sigma} Y_{j_\sigma,m_{j_\sigma}}(\hat{\boldsymbol{k}}_{\boldsymbol{a}}) Y^*_{j_\sigma,m_{j_\sigma}}(\hat{\boldsymbol{k}}_{\boldsymbol{b}}).
\end{aligned} \tag{5.43}$$

Essentially, the LOS integral will capture a product of spherical harmonics from μ's and ν's. Hence, the term in the summation over spherical harmonics indices will be proportional to

$$\int d\Omega_s \prod_{n=1}^{6} Y^*_{j_n,m_{j_n}}(\hat{\boldsymbol{s}}). \tag{5.44}$$

As shown in Appendix D, this integral is non-vanishing only if

$$\sum_{n=1}^{6} j_n = \text{even} \quad \text{and} \quad \sum_{n=1}^{6} m_{j_n} = 0. \tag{5.45}$$

The integral over Ω_{k_a}'s capture product of $Y^*_{j_n,m_{j_n}}(\hat{\boldsymbol{k}}_{\boldsymbol{a}})$ and will impose similar constraints to the angular momentum indices. Before that, let us also expand the plane wave factors with the *Rayleigh Expansion*,

$$e^{i\boldsymbol{k}_{\boldsymbol{\sigma}}\cdot\boldsymbol{r}_{\boldsymbol{\sigma}}} = 4\pi \sum_{l_\sigma m_\sigma} i^{l_\sigma} j_{l_\sigma}(kr) Y_{l_\sigma,m_\sigma}(\hat{\boldsymbol{r}}_{\boldsymbol{\sigma}}) Y^*_{l_\sigma,m_\sigma}(\hat{\boldsymbol{k}}_{\boldsymbol{\sigma}}). \tag{5.46}$$

So, the constraint picked up by the integration will also include these indices in the plane wave factor. In particular, the resulting constraints are

$$\begin{aligned} j_1 + j_7 + l_1 + j_{10} + j_{12} &= \text{even} \quad \text{from} \quad \int d\Omega_{k_1}, \\ j_2 + j_8 + l_2 + j_{10} + j_{11} &= \text{even} \quad \text{from} \quad \int d\Omega_{k_2}, \\ j_3 + j_9 + l_3 + j_{11} + j_{12} &= \text{even} \quad \text{from} \quad \int d\Omega_{k_3}. \end{aligned} \tag{5.47}$$

Now that we have all the constraints, let us assess the estimator's parity. To do so, we will collect the spherical harmonics that depend on the arm directions, $\hat{\boldsymbol{r}}_{\mathbf{1}}$, $\hat{\boldsymbol{r}}_{\mathbf{2}}$, and $\hat{\boldsymbol{r}}_{\mathbf{3}}$, and consider their parity transformation. After evaluating all integrals in the equation 5.42, the estimator is proportional to

$$\begin{aligned} \hat{\zeta}(\boldsymbol{r}_{\mathbf{1}}, \boldsymbol{r}_{\mathbf{2}}, \boldsymbol{r}_{\mathbf{3}}) \propto \sum_{\{\alpha_{12}\}} \sum_{\{j_{12}, m_{j_{12}}\}}^{\{\alpha_{12}\}} \sum_{\{l_3, m_3\}} & Y_{j_7, m_{j_7}}(\hat{\boldsymbol{r}}_{\mathbf{1}}) Y_{j_8, m_{j_8}}(\hat{\boldsymbol{r}}_{\mathbf{2}}) Y_{j_9, m_{j_9}}(\hat{\boldsymbol{r}}_{\mathbf{3}}) \\ & \times Y_{j_4, m_{j_4}}(\hat{\boldsymbol{r}}_{\mathbf{1}}) Y_{j_5, m_{j_5}}(\hat{\boldsymbol{r}}_{\mathbf{2}}) Y_{j_6, m_{j_6}}(\hat{\boldsymbol{r}}_{\mathbf{3}}) \\ & \times Y_{l_1, m_1}(\hat{\boldsymbol{r}}_{\mathbf{1}}) Y_{l_2, m_2}(\hat{\boldsymbol{r}}_{\mathbf{2}}) Y_{l_3, m_3}(\hat{\boldsymbol{r}}_{\mathbf{3}}). \end{aligned} \tag{5.48}$$

Let us recall that the parity transformation is $\mathbb{P}[\hat{\zeta}(\boldsymbol{r}_{\mathbf{1}}, \boldsymbol{r}_{\mathbf{2}}, \boldsymbol{r}_{\mathbf{3}})] = \hat{\zeta}(-\boldsymbol{r}_{\mathbf{1}}, -\boldsymbol{r}_{\mathbf{2}}, -\boldsymbol{r}_{\mathbf{3}})$ and the parity transformation of spherical harmonic function is $Y_{l,m}(-\hat{\boldsymbol{r}}) = (-1)^l Y_{l,m}(\hat{\boldsymbol{r}})$. Therefore, the estimator will be pure of parity-even terms if we can show that the sum of angular momentum indices,

$$S = \sum_{n=4}^{9} j_n + \sum_{\sigma=1}^{3} l_\sigma, \tag{5.49}$$

is always even. This can be shown by adding all indices constraints, 5.45 and 5.47, together and obtain,

$$S + 2\sum_{n=1}^{3} j_n + 2\sum_{\sigma=10}^{12} j_\sigma = \text{even} \longrightarrow S = \text{even}. \tag{5.50}$$

Hence, we have shown explicitly that the parity-odd modes are removed by averaging LOS even with the wide-angle correction.

Let us end this discussion with some caveats. This result is derived from the trispectrum with wide-angle correction by Taylor's series. Whether a similar conclusion is reached for the

exact form of LOS correction is beyond the scope of this derivation and remains a challenge for future work. Secondly, the estimator assumes a fair sample of galaxies distributed across the sky and that the surveys are able to achieve full-sky coverage. The details about the survey-related potential systematics are assessed in [1] where no significant systematics are found. Thirdly, the prediction here relies on the SPT (see section 3.2.2) which is valid above the nonlinear scale but deep under the horizon scale, where the dynamics of the matter fluid are dominated by Newtonian gravity. In this scale, the galaxies are also assumed to comoving with the matter fluid and the bias expansion is built from gravitational evolution only. However, since the bias expansion is a true scalar relation, it will always be parity-invariant. Otherwise, a nonstandard parity-odd operator may be constructed from a pseudo-scalar, such as a dot product against the angular momentum. One of the few possible ways to introduce PV into the 4PCF now is the primordial trispectrum from inflation. In other words, the PV signature may already exist in the universe's initial condition generated by inflation, suggesting that some physical mechanism breaks parity symmetry in the high-energy regime. For example, since the cosmological perturbation theory is based on GR, one may think of some high-energy modification of GR which is parity-violating. We invite the reader to see section 2.5.7 for more details.

6

Summary and Conclusion

This thesis discusses how fundamental features of inflation can be inferred from cosmological probes like the Large-scale Structure (LSS). We have explored how General relativity (GR) is constitutional to the cosmological model of the universe. Particularly, the expansion of the universe is merely a consequence of cosmic content's existence in space-time as described by the Friedmann equations. Consistent with several redshift surveys, the ΛCDM model is regarded as the best universe model to describe the expansion history. By studying the universe's thermodynamics and the behaviours of the particle standard model sector, one established the Standard Hot Big Bang Theory for the production of known particles nowadays. However, some shortcomings exist in the theory and later invoke the introduction of the cosmic inflation model. The dynamics and its state-of-the-art predictions are reviewed. In particular, inflation gave the initial seeds for the subsequent cosmic structure by the quantum fluctuation of the scalar field called inflaton. Once again, we resort to GR to describe the perturbation on the cosmological scale; the cosmological perturbation theory is discussed. The process in which the fluctuations become the initial condition after inflation ends is also reviewed. In particular, we show how the fluctuations at the superhorizon limit are conserved and translated out from inflation. For the simplest single-field model of inflation, where inflaton completely dominates the energy budget of inflation, the resulting density fluctuation will be very close to Gaussian. Adding more features to the model increases the departure from Gaussian in a predictable fashion; the Hunt for primordial non-Gaussianity (PNG) begins, quantified by the nonlinear parameter, f_{NL}. For example, a local self-interaction of inflaton and a non-canonical kinetic

term of the inflaton Lagrangian induce local and equilateral PNG, respectively. Each type of PNG is associated with a different peak limit of the primordial bispectrum. For example, the local PNG causes a peak of bispectrum at the squeezed limit where one of the three associated modes is very small compared to the others. Hence, measuring these amplitudes would reveal the degree of importance of those corresponding features. Moreover, some models come with a constraint on those parameters with other observables. For example, Local PNG produced by single-field models should respect the single-field consistency relation, equating the local-type f_{NL} to the scale dependence of the primordial power spectrum (the scalar spectral index). Hence, the measurement of f_{NL} could also rule some models out if the consistency check failed. Another fundamental feature of interest is the parity symmetry of GR. While the standard GR is parity-conserving, recent analyses found a parity violation (PV) in the galaxy's four-point correlation function (4PCF). If the observed PV are of the initial condition, a modification of GR at a high energy level is suggested.

We present how the anticipated observables, PNG and PV, can be probed from the galaxy distribution. The evolution of the fluctuation after re-entering the horizon is reviewed at the linear perturbation level. There, the transfer function is introduced to encode the modification of the density fluctuation from the initial curvature perturbation due to its linear evolution. The description is extended to the nonlinear regime with the standard perturbation theory (SPT). Due to the complexity of GR in a nonlinear regime, the Newtonian description of gravity is used instead with a smaller validity scale (much smaller than the horizon scale). Moreover, since Cold Dark Matter (CDM) is the main contributor to the matter density and only interacts with the gravitational field, the CDM fluid is assumed to be collisionless and self-gravitating. It is also noted that Einstein-de Sitter (EdS) background cosmology is an accurate assumption predicting the time evolution of perturbations down to 1% uncertainty. The SPT approach allows the nth-order solution to be written as a product of n linear density perturbation integrated against a kernel computing from the recursion relation. With the multiplication of the transfer function, the matter N-point statistics can be connected to the primordial ones. However, since CDM cannot be observed directly with electromagnetic waves, the distribution of galaxies is used to trace the underlying matter distribution instead. However, the galaxies' number over/under-density is not a direct reflection of the matter dispersion but rather a biased one. This motivates the theory of biased tracer where the tracer's population is described by the effective bias expansion consisting of the physical operators and the associated bias parameters. The physical operator represents the quantity affecting the galaxy distribution and the bias parameter tells us the degree of dependence. In this thesis, the operators are invoked

by the conserved gravitational evolution of tracers where we extend the expansion up to the third-order operator. Then, we discuss the discrete statistics of the tracer and how they can be related to the continuous density field statistics.

With the complete relation from inflation to galaxy distribution, the estimator for the fundamental features of inflation can be constructed. We review the probing on PNG from the scale-dependent Dark Matter (DM) Halo bias. Essentially, a DM halo is a hypothetical virialized region of dark matter which creates a large potential well, hosting some smaller structures, such as clusters of galaxies, inside. Unlike galaxies, the formation of DM halo is much simpler to explain thanks to the sole gravitational interaction of DM. We review the spherical collapse theory and comment on some extensions where we find the critical linear density δ_c. The Press-Schechter theory tells us that the place where a halo formed is indicated by the filtered over-density exceeding the threshold δ_c. Accordingly, the population of halos is found to be mass-dependent described by the halo mass function. Moreover, the influence of PNG on the halo bias parameter is discussed as one of the main focuses of this thesis. With the same threshold criterion and the high-peak assumption, the MLB approach obtained the corrected power spectrum by the bispectrum. The effect also promotes the Bardeen gravitational potential as an operator in the effective bias expansion. Crucially, the bias corrections due to non-Gaussianities (NG) are scale-dependent. Hence, the observed halo power spectrum will gain a small but detectable scale-dependent correction. Each type of PNG will introduce a distinct scale dependence to the power spectrum. On top of PNGs, we also discuss the NG introduced by the nonlinearity of GR neglected previously by studying the late-time evolution with Newtonian gravity. On a valid linear scale ($k \lesssim 0.1h^{-1}$ Mpc), the detectability of the GR effect is the highest, of 1.6 times more than the local PNG. The equilateral, folded, and orthogonal types are less detectable. We also point out the degeneracy of signals; the bispectrum of the latter three types are related by $B_\zeta^{ortho} = B_\zeta^{equil} - 2B_\zeta^{en}$ assuming the same amplitude. By changing the halo mass associated with the window function, the mass dependence of correction is realized. While the local and GR types do not hold an appreciable level of mass dependence, the other three types demonstrate a notable change. We identify that the dependence originated from the mass-dependent variance of filtered density fluctuation. We also find that the choice of window functions does not noticeably affect the prediction.

Lastly, the PV in the galaxy 4PCF is discussed in response to the findings from two independent analyses from BOSS DR12 galaxy data [1, 2]. In particular, this thesis assesses the potential of the redshift space distortion (RSD) effect in mimicking the PV signature in 4PCF. While the parity-violating trispectrum has been predicted in the literature (see [3]), it has not

been investigated explicitly if the averaging of the line of sight (LOS) will clean the artificial PV from the isotropic 4PCF estimator, as used in [1, 2]. It is found that, even with the wide-angle effect, the PV introduced anisotropically by RSD will eventually be removed by averaging LOS. Therefore, the isotropic estimator of 4PCF remains unbiased in the parity-odd mode. However, some caveats must be taken into account. This thesis only considers the LOS correction with Taylor's expansion. The exact treatment remains an open task for future work. Other survey-related effects are not considered in this thesis but are already well-investigated in [1]. The result merely indicates that the estimator used in the analyses is not biased by RSD and the detected signature must be of other origin. One of the possibilities left is the PV are produced in inflation where possible high-energy modifications of GR are active. One such adjustment that induces PV in the initial condition of the universe is the *Chern-Simon* gravity active during inflation.

A

MLB Derivations in Path Integral Approach

A.1 Joint Probability

Starting from the definition of the joint probability (see equation 4.28),

$$\Pi^{(N)}_{\nu,R}(\{\vec{q}_N\}) = \int [\mathcal{D}\delta]\ \mathbf{P}\left[\delta(\vec{q})\right] \prod_{r=1}^{N} \Big\{\Theta(\delta_R(\vec{q}_r) - \nu\sigma_R)\Big\}, \tag{A.1}$$

where we recall the short-hand notation $\{a_N\} = a_1, \ldots, a_N$. The integral forms of the Heaviside step function, $\Theta(a-b) = \int_b^\infty d\alpha\, \delta(a-\alpha)$, and the Dirac delta, $\delta(a-\alpha) = (2\pi)^{-1}\int_{-\infty}^{\infty} d\phi\, \mathbf{exp}\{i\phi[a-\alpha]\}$, are substituted into the equation where the filtered field δ_R is unpacked into window function, W_R, and the density contrast, δ. After some rearrangement, we have

$$\begin{aligned}
\Pi^{(N)}_{\nu,R} =& (2\pi)^{-N} \int_{\nu\sigma_R}^{\infty} d\alpha_1 \cdots \int_{\nu\sigma_R}^{\infty} d\alpha_N \int_{-\infty}^{\infty} d\phi_1 \cdots \int_{-\infty}^{\infty} d\phi_N\, e^{-i\sum_{r=1}^{N}\phi_r\alpha_r} \\
& \left\{ \int [\mathcal{D}\delta]\ \mathbf{P}\left[\delta(\vec{q})\right] e^{i\int d^3y \left(\sum_{r=1}^{N}\phi_r W_R(|\vec{q}-\vec{y}|)\right)\delta(\vec{y})} \right\} \\
=& (2\pi)^{-N} \int_{\nu\sigma_R}^{\infty} d\alpha_1 \cdots \int_{\nu\sigma_R}^{\infty} d\alpha_N \int_{-\infty}^{\infty} d\phi_1 \cdots \int_{-\infty}^{\infty} d\phi_N\, e^{-i\sum_{r=1}^{N}\phi_r\alpha_r}\, \mathbf{Z}[J^*].
\end{aligned} \tag{A.2}$$

Notice that the expression in the bracket resembles the partition function with an external field defined as

$$J^*(\vec{q},\{\vec{y}_N\}) = \sum_{r=1}^{N} \phi_r W_R(|\vec{q}-\vec{y}_r|). \tag{A.3}$$

Then, we can utilize the generating functional (see equation 4.30) and write an expansion of the partition function as

$$\begin{aligned}\mathbf{Z}[J^*] &= \mathbf{exp}\left\{\sum_{n=1}^{\infty}\frac{i^n}{n!}\int d^3y_1\cdots\int d^3y_n\,\xi_c^{(n)}(\{\vec{y}_n\})J^*(\vec{q}_1,\{\vec{y}_N\}_1)\ldots J^*(\vec{q}_n,\{\vec{y}_N\}_n)\right\}\\ &= \mathbf{exp}\left\{\sum_{n=1}^{\infty}\frac{i^n}{n!}\sum_{\{r_n\}=1}^{N}\xi_R^{(n)}(\{\vec{q}_n\})\phi_{r_1}\ldots\phi_{r_n}\right\}\end{aligned} \tag{A.4}$$

where $\xi_R^{(n)}(\{\vec{q}_n\})$ is the correlation function of the filtered field (see equation 4.27). The subscript "c" is omitted but the correlation functions here are the connected kind by the definition. The summation $\sum_{\{r_n\}=1}^{N}$ is a shorthand notation for $\sum_{r_1=1}^{N}\sum_{r_2=1}^{N}\cdots\sum_{r_n=1}^{N}$. The expansion is then substituted into the joint probability expression where we will perform some mathematical trick as follows. The expression is arranged as

$$\Pi_{\nu,R}^{(N)} = (2\pi)^{-N}\int_{\nu\sigma_R}^{\infty}\{d\alpha_N\}\int_{-\infty}^{\infty}\{d\phi_N\}\,\mathbf{exp}\left\{\sum_{n=1}^{\infty}\frac{i^n}{n!}\sum_{\{r_n\}=1}^{N*}\xi_R^{(n)}(\{\vec{q}_n\})\phi_{r_1}\ldots\phi_{r_n}\right\}\chi_{\nu,R} \tag{A.5}$$

where the summation $\sum_{\{r_n\}=1}^{N*}$ excludes the terms $n=2$ where $r_1=r_2$ which are the terms with σ_R^2. Those excluded terms are encapsulated in $\chi_{v,R}$ defined as

$$\chi_{\nu,R}(\{\alpha_N\},\{\phi_N\}) = \mathbf{exp}\left\{-i\sum_{r=1}^{N}\phi_r\alpha_r - \frac{1}{2}\sigma_R^2\sum_{r=1}^{N}\phi_r^2\right\}. \tag{A.6}$$

Notice that this function has useful properties,

$$\begin{aligned} i\frac{\partial}{\partial\alpha_{r_j}}\chi_{\nu,R} &= \phi_{r_j}\chi_{\nu,R},\\ \int_{-\infty}^{\infty}\{d\phi_N\}\,\chi_{\nu,R} &= (2\pi)^{N/2}\sigma^{-N}\mathbf{exp}\left\{-\frac{1}{2}\sum_{r=1}^{N}\frac{\alpha_r^2}{\sigma_R^2}\right\}.\end{aligned} \tag{A.7}$$

We, therefore, applied the first property to exchange ϕ_{r_j} in the exponent with $i\frac{\partial}{\partial\alpha_{r_j}}$ after which the integral similar to the second property arises in the equation and can be evaluated. The result reads

$$\Pi^{(N)}_{\nu,R} = (2\pi)^{-N/2}\int_{\nu}^{\infty}\{d\alpha_N\}\,\mathbf{exp}\left\{\sum_{n=2}^{\infty}(-1)^n\sum_{\{r_n\}=1}^{N}\frac{w^{(n)}_{R,\{r_n\}}}{n!}\prod_{j=1}^{n}\frac{\partial}{\partial\alpha_{r_j}}\right\}\mathbf{exp}\left\{-\frac{1}{2}\sum_{r=1}^{N}\alpha_r^2\right\}, \tag{A.8}$$

where $w^{(n)}_{R,\{r_n\}}$ is defined as

$$w^{(n)}_{R,\{r_n\}} = \begin{cases} 0 & ;n=1 \textbf{ or } n=2 \text{ where } r_1=r_2 \\ \xi^{(n)}_R(\{\vec{q}_n\})/\sigma_R^n & ;\textit{other} \text{ n} \end{cases}. \tag{A.9}$$

$n=0$ term is absent by definition of the density contrast, $\langle\delta\rangle=0$, and $n=2$ terms where $r_1=r_2$ are zero since they were taken to form $\chi_{\nu,R}$ previously. Next, let us consider the exponential term,

$$\mathbf{exp}\left\{\sum_{n=2}^{\infty}\sum_{\{r_n\}=1}^{N}(\dots)_{n,\{r_n\}}\right\} = \prod_{n=2}^{\infty}\prod_{\{r_n\}=1}^{N}\sum_{m_{n,\{r_n\}}=0}^{\infty}\left\{\frac{1}{m_{n,\{r_n\}}!}\left[(\dots)_{n,\{r_n\}}\right]^{m_{n,\{r_n\}}}\right\},$$

where we use Taylor's expansion and the index $m_{n,\{r_n\}}$ is indicated by the subscript corresponding to each exponential term in the product. To write the expression of $\Pi^{(N)}_{\nu,R}$ in series rather than products, we utilize the so-called "cluster expansion" to exchange the position of sum and product operators,

$$\prod_{n=2}^{\infty}\prod_{\{r_n\}=1}^{N}\sum_{m_{n,\{r_n\}}=0}^{\infty}(\dots) = \sum_{L=0}^{L}\sum_{\{m_L\}}\prod_{n=1}^{\infty}\prod_{\{r_n\}=1}^{N}(\dots), \tag{A.10}$$

where the members of set $m_L = m_1,\dots,m_L$ are non-negative integers satisfying $\sum_{n=1}^{L} nm_n = L$ and $m_{n,\{r_n\}}$ refers to non-negative integers satisfying $\sum_{n=1}^{N} m_{n,\{r_n\}} = m_n$. However, there are some caveats. Firstly, the term $L=0$ is taken to be 1 since it corresponds to the first term of the exponential expansion. Secondly, it is possible that $\left[(\dots)_{n,\{r_n\}}\right]^{m_{n,\{r_n\}}}$ yields 0^0 when both base and exponent are zero simultaneously. This kind of indeterminate form that appeared in the expression will be taken as 1 since the zero base term was simply expanded from $\mathbf{exp}(0)$ which equals 1 by definition. Then, we recall the definition of the (physicists')

Hermite polynomial,

$$\left(\frac{\partial}{\partial x}\right)^n e^{-x^2} = (-1)^n \mathbf{H}_n(x) e^{-x^2}. \tag{A.11}$$

This will be applied to $\frac{\partial}{\partial \alpha_{r_j}}$ which is acting on the Gaussian-like exponential on the back of the expression. After factoring $\frac{\partial}{\partial \alpha_{r_j}}$ out, we have

$$\Pi_{\nu,R}^{(N)} = \sum_{L=0}^{L} \sum_{\{m_L\}} \left\{ \prod_{n=1}^{\infty} \prod_{\{r_n\}=1}^{N} \frac{1}{m_{n,\{r_n\}}!} \left[\frac{w_{R,\{r_n\}}^{(n)}}{n!}\right]^{m_{n,\{r_n\}}} \right.$$
$$\left. \prod_{r=1}^{N} \left((2\pi)^{-1/2} \int_{\nu}^{\infty} d\alpha_r \, (-1)^{-m_r} \left(\frac{\partial}{\partial \alpha_r}\right)^{m_r} \mathbf{exp}\left\{-\frac{1}{2}\sum_{r=1}^{N} \alpha_r^2\right\} \right) \right\}. \tag{A.12}$$

As a consequence of factoring out the partial derivative, a new index m_r is defined as

$$m_r = \sum_{n=1}^{L} \sum_{\{r_n/r_1\}=1}^{N} (m_{n,r_1,r_2,\ldots,r_n} + m_{n,r_2,r_1,\ldots,r_n} + \cdots + m_{n,r_n,r_1,\ldots,r_1}), \tag{A.13}$$

where $\ldots$ refers to other terms in which one of the indices $\{r_n\}$ exchanges it position with r_1 in the front and $\{r_n/r_j\} = r_1, r_2, \ldots, r_{j-1}, r_{j+1}, \ldots, r_n$. Note that the role of r_1 in the summation can practically be played by any in $\{r_n\}$ without changing the meaning of m_r. For term $m_r = 0$, the integral evaluates to the complementary error function. To evaluate other terms, we utilize the fundamental rule of calculus where we sacrifice one order of the derivative. The remaining orders of the derivatives will transform into Hermite polynomial through equation A.11. The final result reads

$$\Pi_{\nu,R}^{(N)} = \sum_{L=0}^{\infty} \sum_{\{m_L\}} \left\{ \prod_{n=2}^{L} \prod_{\{r_n\}=1}^{N} \left[\frac{1}{m_{n,\{r_n\}}!} \left(\frac{w_{R,\{r_n\}}^{(n)}}{n!} \right)^{m_{n,\{r_n\}}} \right] \prod_{r=1}^{N} a_{m_r}\left(\nu/\sqrt{2}\right) \right\}, \tag{A.14}$$

where

$$\begin{aligned} a_0(z) &= \frac{1}{2}\mathbf{erfc}(z), \\ a_m(z) &= \pi^{-1/2} 2^{-m/2} e^{-z^2} \mathbf{H}_{m-1}(z) \text{ for } m > 0. \end{aligned} \tag{A.15}$$

A.2 Cross-correlation Function

According to the equation 4.34,

$$\xi^{(2)}_{\nu_1,R_1;\nu_2,R_2}(\vec{q}_1,\vec{q}_2) = -1 + \frac{\Pi^{(2)}_{\nu_1,R_1;\nu_2,R_2}}{\Pi^{(1)}_{\nu_1,R_1} \times \Pi^{(1)}_{\nu_2,R_2}}, \tag{A.16}$$

we have to compute $\Pi^{(1)}_{\nu,R}$ and $\Pi^{(2)}_{\nu_1,R_1;\nu_2,R_2}$ in order to obtain the cross-correlation function. The first one can be easily obtained by considering the case $N = 1$ of equation 4.31. The second one is evaluated from

$$\Pi^{(2)}_{\nu_1,R_1;\nu_2,R_2} = \int [\mathcal{D}\delta]\ \mathbf{P}\left[\delta(\vec{q})\right]\ \Theta(\delta_{R_1}(\vec{q}_r) - \nu_1\sigma_{R_1}) \times \Theta(\delta_{R_2}(\vec{q}_r) - \nu_2\sigma_{R_2}). \tag{A.17}$$

The idea of derivation follows what has been done in appendix A.1. The main difference is the external field is instead defined as

$$J^*(\vec{q},\vec{y}_1,\vec{y}_2) = \phi_1 W_R(|\vec{q}-\vec{y}_1|) + \phi_2 W_R(|\vec{q}-\vec{y}_2|), \tag{A.18}$$

and the expanded partition function yields

$$\mathbf{Z}[J^*] = \mathbf{exp}\left\{\sum_{n=1}^{\infty}\frac{i^n}{n!}\sum_{\{r_n\}=1}^{N}\xi^{(n)}_{[R_1:j,R_2:n-j]}(\vec{q}_1,\vec{q}_2)\phi_1^j\phi_2^{n-j}\right\}, \tag{A.19}$$

where

$$\xi^{(n)}_{[R_1:j,R_2:n-j]}(\vec{q}_1,\vec{q}_2) = \int\prod_{r=1}^{j} d^3y_r\, W_{R_1}(|\vec{q}_1-\vec{y}_r|)\prod_{s=1}^{n-j} d^3y_s\, W_{R_2}(|\vec{q}_2-\vec{y}_s|)\xi^{(n)}(\{\vec{y}_n\}). \tag{A.20}$$

Along the same line as before, the terms $\sigma^2_{R_1}\phi_1^2$ and $\sigma^2_{R_2}\phi_2^2$ in the exponent are factored out to complete the square with the other exponentials. The ϕ_1 and ϕ_2 in the exponent get transformed into derivatives after which we can integrate the leftover variables out by the Gaussian integral. Finally, we apply the cluster expansion and collect some terms into the function a (see

definition A.15). After substituting all of the ingredients, the final result is

$$\xi^{(2)}_{\nu_1,R_1;\nu_2,R_2}(\vec{q}_1,\vec{q}_2) = -1 + \sum_{L=0}^{\infty}\sum_{\{m_L\}}\left\{\prod_{n=2}^{L}\prod_{j=0}^{n}\left[\frac{1}{m_{n,j}!}\left(\frac{w^{(n)}_{[R_1:j,R_2:n-j]}}{j!(n-j)!}\right)^{m_{n,j}}\right]\right. \\ \left. a_m\big(\nu_1/\sqrt{2}\big)\,a_{L-m}\big(\nu_2/\sqrt{2}\big)\right\} \Bigg/ \left[\Pi^{(1)}_{\nu_1,R_1}\times\Pi^{(1)}_{\nu_2,R_2}\right]. \tag{A.21}$$

B

Scale-dependent Halo Bias Detectability With Different Window Functions

This appendix presents the plots of NG correction detectability from the scale-dependent bias with Gaussian and sharp k-space filters (equation 4.54 and 4.55, respectively) instead of the top-hat filter. The plots of the Gaussian filter are shown in figure B.1 and the plots of the sharp-k filter are shown in figure B.2

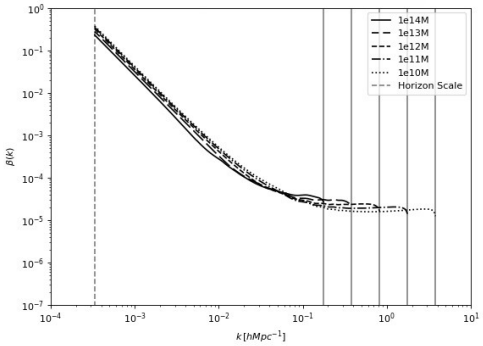

(a) Local Bispectrum

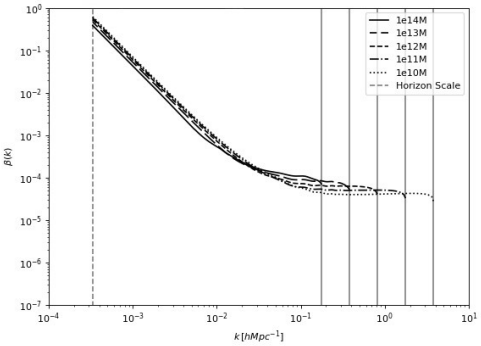

(b) Nonlinearity of GR (NL of GR) Bispectrum

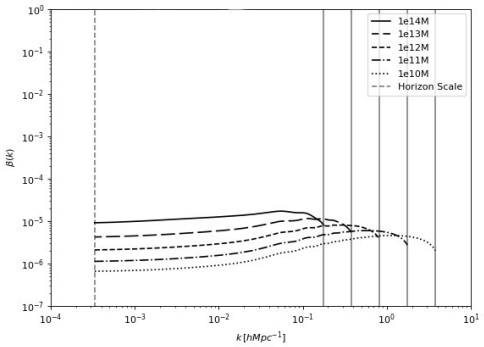

(c) Equilateral Bispectrum

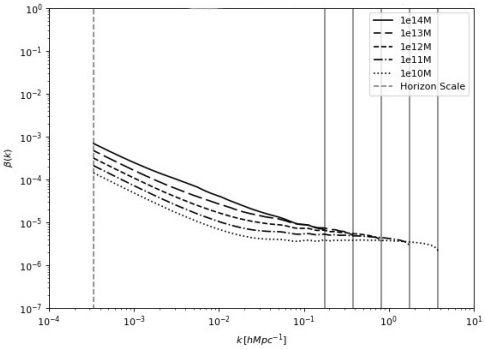

(d) Enfolded Bispectrum

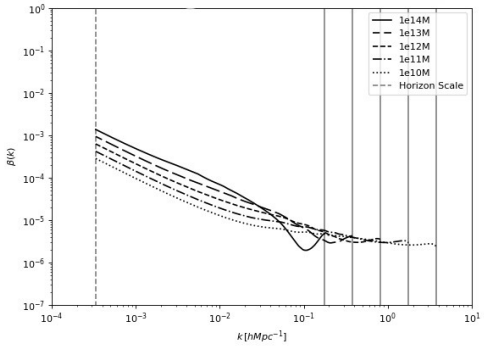

(e) Orthogonal Bispectrum

Figure B.1: Comparison of scale dependence detectability functions at different halo mass with Gaussian Filter.

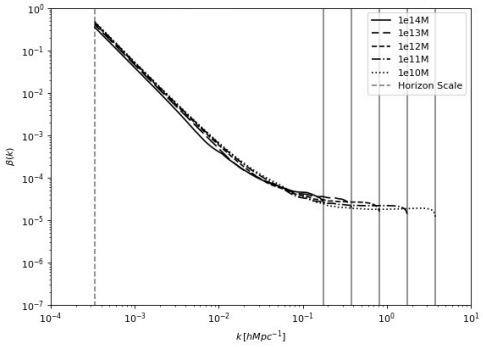

(a) Local Bispectrum

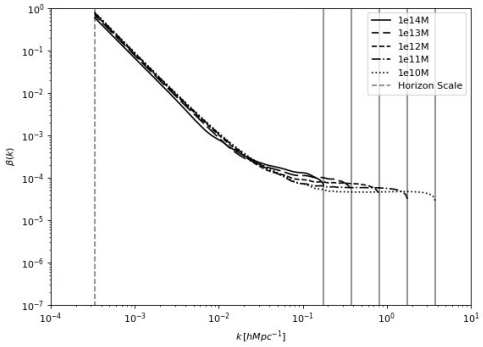

(b) Nonlinearity of GR (NL of GR) Bispectrum

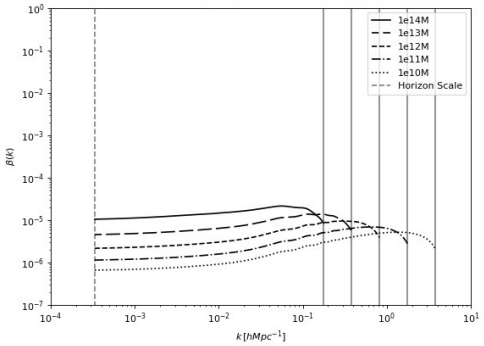

(c) Equilateral Bispectrum

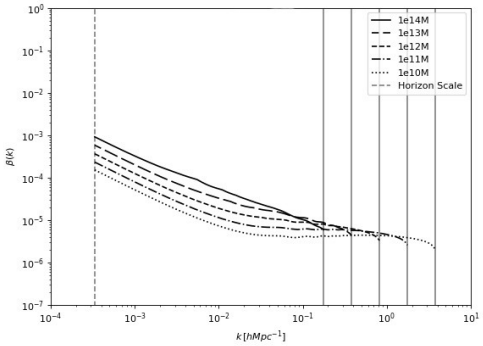

(d) Enfolded Bispectrum

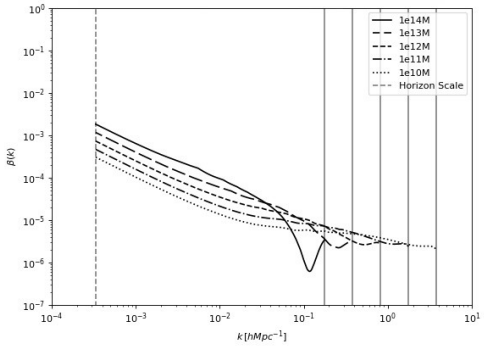

(e) Orthogonal Bispectrum

Figure B.2: Comparison of scale dependence detectability functions at different halo mass with Sharp-k Filter.

C

Redshift Space Kernels

As anticipated in section 5.1, the kernels for the number density contrast solution at up to the third order. We start by writing equation 5.14 in Fourier space,

$$\begin{aligned}\delta^g_{\boldsymbol{k}} =& b_1\delta_{\boldsymbol{k}} + b_2\mathbf{Cov}[\delta^2]_{\boldsymbol{k}} + b_3\mathbf{Cov}[\delta^3]_{\boldsymbol{k}} + b_{K^2}\mathbf{Cov}[K_{ij}K^{ij}]_{\boldsymbol{k}} \\ &+ b_{K^3}\mathbf{Cov}[K^i{}_jK^j{}_kK^k{}_i]_{\boldsymbol{k}} + b_{td}O^{(3)}_{td,\boldsymbol{k}},\end{aligned} \tag{C.1}$$

where **Cov** denotes convolution. The Fourier-transformed tidal field can also be written as

$$K_{ij,\boldsymbol{k}} = \left(\frac{k_ik_j}{k^2} - \frac{1}{3}\delta^{ij}\right)\delta_{\boldsymbol{k}} \equiv s_{ij}(\boldsymbol{k})\delta_{\boldsymbol{k}}. \tag{C.2}$$

Then, the third-order tidal operator (see equation 3.106) can be written in Fourier space,

$$O^{(3)}_{td,\boldsymbol{k}} = \frac{8}{21}\int_{\boldsymbol{q}_1}\int_{\boldsymbol{q}_2} s^{ij}(\boldsymbol{k}-\boldsymbol{q}_1)s_{ij}(\boldsymbol{q}_1)\left[1 - \frac{3}{2}s^{mn}(\boldsymbol{k}-\boldsymbol{q}_1-\boldsymbol{q}_2)s_{mn}(\boldsymbol{q}_2)\right]\delta_{\boldsymbol{k}-\boldsymbol{q}_1-\boldsymbol{q}_2}\delta_{\boldsymbol{q}_1}\delta_{\boldsymbol{q}_2}. \tag{C.3}$$

We then substitute this bias expansion with the SPT solutions order by order into equation 5.13. The resulting kernels are the following,

Symmetrized First-order Kernel

$$S^{(1)}_{(s)}(\boldsymbol{k}) = b_1 + f\left(\mu^2 - i\frac{4\pi\alpha}{k^3}\mu\right). \tag{C.4}$$

Symmetrized Second-order Kernel

$$\begin{aligned} S^{(2)}_{(s)}(\boldsymbol{k}_1,\boldsymbol{k}_2) &= b_1 F_2^{(s)}(\boldsymbol{k}_1,\boldsymbol{k}_2) + b_2 + b_{K^2}\left[\frac{(\boldsymbol{k}_1\cdot\boldsymbol{k}_2)^2}{k_1^2k_2^2} + \frac{1}{3}\right] \\ &+ f\left(\mu_{12}^2 - i\frac{4\pi\alpha}{k_{12}^3}\mu_{12}\right)G_2^{(s)}(\boldsymbol{k}_1,\boldsymbol{k}_2) - \frac{f}{2}\left\{b_1\left[\mu_1^2+\mu_2^2+\mu_1\mu_2\left(\frac{k_1}{k_2}+\frac{k_2}{k_1}\right)\right]\right\} \\ &+ f\left[2\mu_1^2\mu_2^2 + \mu_1\mu_2\left(\mu_2^2\frac{k_2}{k_1} + \mu_1^2\frac{k_1}{k_2}\right) - i4\pi\alpha\mu_1\mu_2\left(\frac{1}{k_1^2}+\frac{1}{k_2^2}\right)\left(\frac{\mu_1}{k_2}+\frac{\mu_2}{k_1}\right)\right]. \end{aligned} \tag{C.5}$$

Unsymmetrized Third-order Kernel

$$\begin{aligned} S^{(3)}(\boldsymbol{k}_1;\boldsymbol{k}_2,\boldsymbol{k}_3) &= b_1F_3(\boldsymbol{k}_1,\boldsymbol{k}_2,\boldsymbol{k}_3) + 2b_2\left[F_2(\boldsymbol{k}_2,\boldsymbol{k}_3) + F_2^{(s)}(\boldsymbol{k}_1,\boldsymbol{k}_3)\right] + b_3 \\ &+ 2b_{K^2}s^{ij}(\boldsymbol{k}_1)s_{ij}(\boldsymbol{k}_2+\boldsymbol{k}_3) + b_{K^3}s^i_j(\boldsymbol{k}_1)s^j_l(\boldsymbol{k}_2)s^l_i(\boldsymbol{k}_3) \\ &+ s^{ij}(\boldsymbol{k}_1)s_{ij}(\boldsymbol{k}_2+\boldsymbol{k}_3)\left[1 - \frac{3}{2}s^{mn}(\boldsymbol{k}_2)s_{mn}(\boldsymbol{k}_3)\right] + f\left(\mu_{123}^2 - i\frac{4\pi\alpha}{k^3}\mu_{123}\right)G_3(\boldsymbol{k}_1,\boldsymbol{k}_2,\boldsymbol{k}_3) \\ &+ fk_{123}\mu_{123}\left(\frac{\mu_{23}}{k_{23}}\right)G_2(\boldsymbol{k}_2,\boldsymbol{k}_3)\left[b_1 + f\,(b_1+f)\left(\mu_1^2 - i\frac{4\pi\alpha}{k_1^3}\mu_1\right)\right] \\ &+ fk_{123}\mu_{123}\left(\frac{\mu_2}{k_2}\right)\left[b_1F_2(\boldsymbol{k}_1,\boldsymbol{k}_3) + b_2 + b_{K^2}s^{ij}(\boldsymbol{k}_1)s_{ij}(\boldsymbol{k}_3) + f\left(\mu_{13}^2 - i\frac{4\pi\alpha}{k_{13}^3}\mu_{13}\right)G_2^{(s)}(\boldsymbol{k}_1,\boldsymbol{k}_3)\right] \\ &+ f^2\frac{(k_{123}\mu_{123})^2}{2}\left(\frac{\mu_2}{k_2}\right)\left(\frac{\mu_3}{k_3}\right)\left[b_1 + f\,(b_1+f)\left(\mu_1^2 - i\frac{4\pi\alpha}{k_1^3}\mu_1\right)\right]. \end{aligned} \tag{C.6}$$

Note that all SPT kernels in the expression above are the symmetrized version. The subscripted variables are

$$\begin{aligned} \boldsymbol{k_{ij}} = \boldsymbol{k_i} + \boldsymbol{k_j} \quad \text{and} \quad \mu_{ij} = \hat{\boldsymbol{k}}_{\boldsymbol{ij}}\cdot\hat{\boldsymbol{s}}, \\ \boldsymbol{k_{123}} = \boldsymbol{k_1} + \boldsymbol{k_2} + \boldsymbol{k_3} \quad \text{and} \quad \mu_{123} = \hat{\boldsymbol{k}}_{\boldsymbol{123}}\cdot\hat{\boldsymbol{s}}. \end{aligned} \tag{C.7}$$

D

Integrals of Spherical Harmonics

D.1 Integral over N spherical Harmonics

This appendix aims to show the constraint on spherical harmonics indices given by the integral over N spherical Harmonics,

$$\int d\Omega_s \prod_{n=1}^{N} Y_{j_n,m_{j_n}}(\hat{\boldsymbol{s}}). \tag{D.1}$$

Let us write the spherical harmonic function as

$$Y_{j,m_j}(\theta,\varphi) = \sqrt{\frac{2j+1}{4\pi}\frac{(l-m_j)!}{(l+m_j)!}}\mathcal{P}_j^{m_j}(\cos\theta)e^{im_j\varphi}, \tag{D.2}$$

where $\mathcal{P}_j^{m_j}$ is the *associated Legendre polynomial*. Then, the integral is proportional to

$$\int d\Omega_s \prod_{n=1}^{N} Y_{j_n,m_{j_n}}(\hat{\mathbf{s}}) \propto \int_0^{2\pi} d\varphi \mathbf{exp}\left[i\sum_{n=1}^{N} m_{j_n}\varphi\right] \int_{-1}^{1} d\cos\theta \prod_{n=1}^{N} \mathcal{P}_{j_n}^{m_{j_n}}(\cos\theta). \tag{D.3}$$

From this proportionality, let us discuss the conditions in which the integral is non-vanishing. First of all, the integral over φ puts a constraint

$$\sum_{n=1}^{N} m_{j_n} = 0. \tag{D.4}$$

The second integral is determined by assessing if the product is odd or even. Recall that $\mathcal{P}_j^{m_j}$ have the parity property,

$$\mathcal{P}_j^{m_j}(-x) = (-1)^{j-m_j}\mathcal{P}_j^{m_j}(x). \tag{D.5}$$

Hence, the integral is non-zero only if

$$\sum_{n=1}^{N} (j_n - m_{j_n}) = \text{even}. \tag{D.6}$$

Combining with the first constraint D.4, we have the constraint on the angular momentum indices,

$$\sum_{n=1}^{N} j_n = \text{even}. \tag{D.7}$$

Therefore, the integral over a product of N spherical Harmonics is non-vanishing only if equations D.4 and D.7 are satisfied simultaneously.

Notice that the constraint D.7 is the same even if some of the spherical harmonic functions are complex conjugated. The conjugation only changes the sign of the projection indices $Y^*_{j_n,m_{j_n}} = Y_{j_n,-m_{j_n}}$ and therefore alters the signs in constraint D.4 only.

References

[1] J. Hou, Z. Slepian, and R. N. Cahn, "Measurement of parity-odd modes in the large-scale 4-point correlation function of Sloan Digital Sky Survey Baryon Oscillation Spectroscopic Survey twelfth data release CMASS and LOWZ galaxies," *Mon. Not. Roy. Astron. Soc.*, vol. 522, no. 4, pp. 5701–5739, 2023.

[2] O. H. E. Philcox, "Probing parity violation with the four-point correlation function of BOSS galaxies," *Phys. Rev. D*, vol. 106, p. 063501, 2022.

[3] P. Paul, C. Clarkson, and R. Maartens, "Apparent parity violation in the observed galaxy trispectrum," 2 2024.

[4] A. Friedman, "On the Curvature of space," *Z. Phys.*, vol. 10, pp. 377–386, 1922.

[5] G. Lemaitre, "A Homogeneous Universe of Constant Mass and Growing Radius Accounting for the Radial Velocity of Extragalactic Nebulae," *Annales Soc. Sci. Bruxelles A*, vol. 47, pp. 49–59, 1927.

[6] A. G. Riess *et al.*, "Observational evidence from supernovae for an accelerating universe and a cosmological constant," *Astron. J.*, vol. 116, pp. 1009–1038, 1998.

[7] P. J. E. Peebles, "Recombination of the Primeval Plasma," *Astrophys. J.*, vol. 153, p. 1, 1968.

[8] A. G. Riess *et al.*, "Type Ia supernova discoveries at z $>$ 1 from the Hubble Space Telescope: Evidence for past deceleration and constraints on dark energy evolution," *Astrophys. J.*, vol. 607, pp. 665–687, 2004.

[9] N. Aghanim *et al.*, "Planck 2018 results. VI. Cosmological parameters," *Astron. Astrophys.*, vol. 641, p. A6, 2020, [Erratum: Astron.Astrophys. 652, C4 (2021)].

[10] P. J. E. Peebles and J. T. Yu, "Primeval Adiabatic Perturbation in an Expanding Universe," , vol. 162, p. 815, Dec. 1970.

[11] D. Eisenstein, "Dark energy and cosmic sound," *New Astronomy Reviews*, vol. 49, no. 7, pp. 360–365, 2005, wide-Field Imaging from Space. [Online]. Available: https://www.sciencedirect.com/science/article/pii/S1387647305000850

[12] A. G. DESI Collaboration Adame *et al.*, "DESI 2024 VI: Cosmological Constraints from the Measurements of Baryon Acoustic Oscillations," *arXiv e-prints*, p. arXiv:2404.03002, Apr. 2024.

[13] A. Lue, L.-M. Wang, and M. Kamionkowski, "Cosmological signature of new parity violating interactions," *Phys. Rev. Lett.*, vol. 83, pp. 1506–1509, 1999.

[14] R. Jackiw and S. Y. Pi, "Chern-Simons modification of general relativity," *Phys. Rev. D*, vol. 68, p. 104012, 2003.

[15] N. Aghanim *et al.*, "Planck 2018 results. I. Overview and the cosmological legacy of Planck," *Astron. Astrophys.*, vol. 641, p. A1, 2020.

[16] V. Acquaviva, N. Bartolo, S. Matarrese, and A. Riotto, "Second order cosmological perturbations from inflation," *Nucl. Phys. B*, vol. 667, pp. 119–148, 2003.

[17] J. M. Maldacena, "Non-Gaussian features of primordial fluctuations in single field inflationary models," *JHEP*, vol. 05, p. 013, 2003.

[18] N. Bartolo, E. Komatsu, S. Matarrese, and A. Riotto, "Non-Gaussianity from inflation: Theory and observations," *Phys. Rept.*, vol. 402, pp. 103–266, 2004.

[19] E. Komatsu and D. N. Spergel, "Acoustic signatures in the primary microwave background bispectrum," *Phys. Rev. D*, vol. 63, p. 063002, 2001.

[20] R. Holman and A. J. Tolley, "Enhanced Non-Gaussianity from Excited Initial States," *JCAP*, vol. 05, p. 001, 2008.

[21] P. D. Meerburg, J. P. van der Schaar, and P. S. Corasaniti, "Signatures of Initial State Modifications on Bispectrum Statistics," *JCAP*, vol. 05, p. 018, 2009.

[22] L. Senatore, K. M. Smith, and M. Zaldarriaga, "Non-Gaussianities in Single Field Inflation and their Optimal Limits from the WMAP 5-year Data," *JCAP*, vol. 01, p. 028, 2010.

[23] Y. Akrami *et al.*, "Planck 2018 results. IX. Constraints on primordial non-Gaussianity," *Astron. Astrophys.*, vol. 641, p. A9, 2020.

[24] O. Doré *et al.*, "Cosmology with the SPHEREX All-Sky Spectral Survey," *arXiv e-prints*, p. arXiv:1412.4872, Dec. 2014.

[25] S. Camera, A. Raccanelli, P. Bull, D. Bertacca, X. Chen, P. Ferreira, M. Kunz, R. Maartens, Y. Mao, M. Santos, P. R. Shapiro, M. Viel, and Y. Xu, "Cosmology on the Largest Scales with the SKA," in *Advancing Astrophysics with the Square Kilometre Array (AASKA14)*, Apr. 2015, p. 25.

[26] A. Raccanelli, O. Doré, D. J. Bacon, R. Maartens, M. G. Santos, S. Camera, T. M. Davis, M. J. Drinkwater, M. Jarvis, R. Norris, and D. Parkinson, "Probing primordial non-Gaussianity via iSW measurements with SKA continuum surveys," , vol. 2015, no. 1, pp. 042–042, Jan. 2015.

[27] N. Kaiser, "On the Spatial correlations of Abell clusters," *Astrophys. J. Lett.*, vol. 284, pp. L9–L12, 1984.

[28] V. Desjacques, D. Jeong, and F. Schmidt, "Large-Scale Galaxy Bias," *Phys. Rept.*, vol. 733, pp. 1–193, 2018.

[29] S. Matarrese and L. Verde, "The effect of primordial non-Gaussianity on halo bias," *Astrophys. J. Lett.*, vol. 677, pp. L77–L80, 2008.

[30] L. Verde and S. Matarrese, "Detectability of the Effect of Inflationary Non-Gaussianity on Halo Bias," , vol. 706, no. 1, pp. L91–L95, Nov. 2009.

[31] N. Dalal, O. Dore, D. Huterer, and A. Shirokov, "The imprints of primordial non-gaussianities on large-scale structure: scale dependent bias and abundance of virialized objects," *Phys. Rev. D*, vol. 77, p. 123514, 2008.

[32] A. Taruya, K. Koyama, and T. Matsubara, "Signature of primordial non-Gaussianity on the matter power spectrum," , vol. 78, no. 12, p. 123534, Dec. 2008.

[33] J.-O. Gong and S. Yokoyama, "Scale dependent bias from primordial non-Gaussianity with trispectrum," *Mon. Not. Roy. Astron. Soc.*, vol. 417, p. 79, 2011.

[34] N. Kaiser, "Clustering in real space and in redshift space," *Mon. Not. Roy. Astron. Soc.*, vol. 227, pp. 1–27, 1987.

[35] J. C. Jackson, "Fingers of God: A critique of Rees' theory of primoridal gravitational radiation," *Mon. Not. Roy. Astron. Soc.*, vol. 156, pp. 1P–5P, 1972.

[36] R. Scoccimarro, H. M. P. Couchman, and J. A. Frieman, "The Bispectrum as a Signature of Gravitational Instability in Redshift-Space," *Astrophys. J.*, vol. 517, pp. 531–540, 1999.

[37] W. O. Leonard, Z. Slepian, and J. Hou, "A Model for the Redshift-Space Galaxy 4-Point Correlation Function," 2 2024.

[38] P. Papai and I. Szapudi, "Non-Perturbative Effects of Geometry in Wide-Angle Redshift Distortions," *Mon. Not. Roy. Astron. Soc.*, vol. 389, p. 292, 2008.

[39] P. H. F. Reimberg, F. Bernardeau, and C. Pitrou, "Redshift-space distortions with wide angular separations," *JCAP*, vol. 01, p. 048, 2016.

[40] A. Einstein, "The foundation of the general theory of relativity." *Annalen Phys.*, vol. 49, no. 7, pp. 769–822, 1916.

[41] A. G. Riess, S. Casertano, W. Yuan, J. B. Bowers, L. Macri, J. C. Zinn, and D. Scolnic, "Cosmic Distances Calibrated to 1% Precision with Gaia EDR3 Parallaxes and Hubble Space Telescope Photometry of 75 Milky Way Cepheids Confirm Tension with ΛCDM," , vol. 908, no. 1, p. L6, Feb. 2021.

[42] L. Verde, N. Schöneberg, and H. Gil-Marín, "A tale of many H_0," 11 2023.

[43] W. L. Freedman, "Measurements of the Hubble Constant: Tensions in Perspective," *Astrophys. J.*, vol. 919, no. 1, p. 16, 2021.

[44] G. 't Hooft, "Magnetic Monopoles in Unified Gauge Theories," *Nucl. Phys. B*, vol. 79, pp. 276–284, 1974.

[45] A. M. Polyakov, "Particle Spectrum in Quantum Field Theory," *JETP Lett.*, vol. 20, pp. 194–195, 1974.

[46] A. H. Guth, "The Inflationary Universe: A Possible Solution to the Horizon and Flatness Problems," *Phys. Rev. D*, vol. 23, pp. 347–356, 1981.

[47] A. D. Linde, "A New Inflationary Universe Scenario: A Possible Solution of the Horizon, Flatness, Homogeneity, Isotropy and Primordial Monopole Problems," *Phys. Lett. B*, vol. 108, pp. 389–393, 1982.

[48] A. Albrecht and P. J. Steinhardt, "Cosmology for Grand Unified Theories with Radiatively Induced Symmetry Breaking," *Phys. Rev. Lett.*, vol. 48, pp. 1220–1223, 1982.

[49] A. D. Linde, "Chaotic Inflation," *Phys. Lett. B*, vol. 129, pp. 177–181, 1983.

[50] F. Lucchin and S. Matarrese, "Power Law Inflation," *Phys. Rev. D*, vol. 32, p. 1316, 1985.

[51] A. D. Linde, "Hybrid inflation," *Phys. Rev. D*, vol. 49, pp. 748–754, 1994.

[52] K. Freese, J. A. Frieman, and A. V. Olinto, "Natural inflation with pseudo - Nambu-Goldstone bosons," *Phys. Rev. Lett.*, vol. 65, pp. 3233–3236, 1990.

[53] A. A. Starobinsky, "A New Type of Isotropic Cosmological Models Without Singularity," *Phys. Lett. B*, vol. 91, pp. 99–102, 1980.

[54] N. Aghanim *et al.*, "Planck 2018 results. V. CMB power spectra and likelihoods," *Astron. Astrophys.*, vol. 641, p. A5, 2020.

[55] J. M. Bardeen, "Gauge Invariant Cosmological Perturbations," *Phys. Rev. D*, vol. 22, pp. 1882–1905, 1980.

[56] M. Sasaki, "Large Scale Quantum Fluctuations in the Inflationary Universe," *Prog. Theor. Phys.*, vol. 76, p. 1036, 1986.

[57] V. F. Mukhanov, "Quantum Theory of Gauge Invariant Cosmological Perturbations," *Sov. Phys. JETP*, vol. 67, pp. 1297–1302, 1988.

[58] A. H. Guth and S. Y. Pi, "Fluctuations in the New Inflationary Universe," *Phys. Rev. Lett.*, vol. 49, pp. 1110–1113, 1982.

[59] S. W. Hawking, "The Development of Irregularities in a Single Bubble Inflationary Universe," *Phys. Lett. B*, vol. 115, p. 295, 1982.

[60] A. A. Starobinsky, "Dynamics of Phase Transition in the New Inflationary Universe Scenario and Generation of Perturbations," *Phys. Lett. B*, vol. 117, pp. 175–178, 1982.

[61] J. M. Bardeen, P. J. Steinhardt, and M. S. Turner, "Spontaneous Creation of Almost Scale - Free Density Perturbations in an Inflationary Universe," *Phys. Rev. D*, vol. 28, p. 679, 1983.

[62] T. S. Bunch and P. C. W. Davies, "Quantum Field Theory in de Sitter Space: Renormalization by Point Splitting," *Proc. Roy. Soc. Lond. A*, vol. 360, pp. 117–134, 1978.

[63] Y. Akrami *et al.*, "Planck 2018 results. X. Constraints on inflation," *Astron. Astrophys.*, vol. 641, p. A10, 2020.

[64] D. Zegeye *et al.*, "CMB-S4: Forecasting Constraints on $f_{\rm NL}$ Through μ-distortion Anisotropy," *Phys. Rev. D*, vol. 108, no. 10, p. 103536, 2023.

[65] P. Creminelli and M. Zaldarriaga, "Single field consistency relation for the 3-point function," *JCAP*, vol. 10, p. 006, 2004.

[66] J. Ganc and E. Komatsu, "A new method for calculating the primordial bispectrum in the squeezed limit," *JCAP*, vol. 12, p. 009, 2010.

[67] E. Komatsu, "Hunting for Primordial Non-Gaussianity in the Cosmic Microwave Background," *Class. Quant. Grav.*, vol. 27, p. 124010, 2010.

[68] E. Silverstein and D. Tong, "Scalar speed limits and cosmology: Acceleration from D-cceleration," *Phys. Rev. D*, vol. 70, p. 103505, 2004.

[69] M. Alishahiha, E. Silverstein, and D. Tong, "DBI in the sky," *Phys. Rev. D*, vol. 70, p. 123505, 2004.

[70] N. Arkani-Hamed, P. Creminelli, S. Mukohyama, and M. Zaldarriaga, "Ghost inflation," *JCAP*, vol. 04, p. 001, 2004.

[71] D. Babich, P. Creminelli, and M. Zaldarriaga, "The Shape of non-Gaussianities," *JCAP*, vol. 08, p. 009, 2004.

[72] P. Creminelli, A. Nicolis, L. Senatore, M. Tegmark, and M. Zaldarriaga, "Limits on non-gaussianities from wmap data," *JCAP*, vol. 05, p. 004, 2006.

[73] N. Bartolo and G. Orlando, "Parity breaking signatures from a Chern-Simons coupling during inflation: the case of non-Gaussian gravitational waves," *JCAP*, vol. 07, p. 034, 2017.

[74] P. Meszaros, "The behaviour of point masses in an expanding cosmological substratum," *Astron. Astrophys.*, vol. 37, pp. 225–228, 1974.

[75] H. Kodama and M. Sasaki, "Cosmological Perturbation Theory," *Prog. Theor. Phys. Suppl.*, vol. 78, pp. 1–166, 1984.

[76] E. V. Linder, "Cosmic growth history and expansion history," *Phys. Rev. D*, vol. 72, p. 043529, 2005.

[77] S. e. a. Alam, "The Eleventh and Twelfth Data Releases of the Sloan Digital Sky Survey: Final Data from SDSS-III," , vol. 219, no. 1, p. 12, Jul. 2015.

[78] A. G. Adame *et al.*, "DESI 2024 VI: Cosmological Constraints from the Measurements of Baryon Acoustic Oscillations," 4 2024.

[79] A. Babul and S. D. M. White, "Quasar-modulated galaxy clustering in a cold dark matter universe," , vol. 253, pp. 31P–34P, Dec. 1991.

[80] R. G. Bower, P. Coles, C. S. Frenk, and S. D. M. White, "Cooperative Galaxy Formation and Large-Scale Structure," , vol. 405, p. 403, Mar. 1993.

[81] F. Schmidt and F. Beutler, "Imprints of Reionization in Galaxy Clustering," *Phys. Rev. D*, vol. 96, no. 8, p. 083533, 2017.

[82] M. Davis, G. Efstathiou, C. S. Frenk, and S. D. M. White, "The evolution of large-scale structure in a universe dominated by cold dark matter," , vol. 292, pp. 371–394, May 1985.

[83] C. G. Lacey and S. Cole, "Merger rates in hierarchical models of galaxy formation. 2. Comparison with N body simulations," *Mon. Not. Roy. Astron. Soc.*, vol. 271, p. 676, 1994.

[84] N. A. Bahcall and R. M. Soneira, "The spatial correlation function of rich clusters of galaxies." , vol. 270, pp. 20–38, Jul. 1983.

[85] A. A. Klypin and A. I. Kopylov, "The spatial covariance function for rich clusters of galaxies," *Pisma v Astronomicheskii Zhurnal*, vol. 9, pp. 75–81, Feb. 1983.

[86] C. Wagner, F. Schmidt, C.-T. Chiang, and E. Komatsu, "The angle-averaged squeezed limit of nonlinear matter N-point functions," *JCAP*, vol. 08, p. 042, 2015.

[87] T. Matsubara, "Nonlinear perturbation theory integrated with nonlocal bias, redshift-space distortions, and primordial non-Gaussianity," , vol. 83, no. 8, p. 083518, Apr. 2011.

[88] D. Bertacca, N. Bartolo, M. Bruni, K. Koyama, R. Maartens, S. Matarrese, M. Sasaki, and D. Wands, "Galaxy bias and gauges at second order in General Relativity," *Class. Quant. Grav.*, vol. 32, no. 17, p. 175019, 2015.

[89] A. Elia, S. Kulkarni, C. Porciani, M. Pietroni, and S. Matarrese, "Modelling the clustering of dark matter haloes in resummed perturbation theories," , vol. 416, no. 3, pp. 1703–1716, Sep. 2011.

[90] A. Elia, S. Kulkarni, C. Porciani, M. Pietroni, and S. Matarrese, "Modeling the clustering of dark-matter haloes in resummed perturbation theories," *Mon. Not. Roy. Astron. Soc.*, vol. 416, pp. 1703–1716, 2011.

[91] M. Mirbabayi, F. Schmidt, and M. Zaldarriaga, "Biased Tracers and Time Evolution," *JCAP*, vol. 07, p. 030, 2015.

[92] P. McDonald and A. Roy, "Clustering of dark matter tracers: generalizing bias for the coming era of precision LSS," , vol. 2009, no. 8, p. 020, Aug. 2009.

[93] T. Fujita and Z. Vlah, "Perturbative description of biased tracers using consistency relations of LSS," *JCAP*, vol. 10, p. 059, 2020.

[94] P. McDonald and A. Roy, "Clustering of dark matter tracers: generalizing bias for the coming era of precision LSS," , vol. 2009, no. 8, p. 020, Aug. 2009.

[95] L. Senatore, "Bias in the Effective Field Theory of Large Scale Structures," *JCAP*, vol. 11, p. 007, 2015.

[96] R. Angulo, M. Fasiello, L. Senatore, and Z. Vlah, "On the Statistics of Biased Tracers in the Effective Field Theory of Large Scale Structures," *JCAP*, vol. 09, p. 029, 2015.

[97] G. Battaglia, A. Helmi, H. Morrison, P. Harding, E. W. Olszewski, M. Mateo, K. C. Freeman, J. Norris, and S. A. Shectman, "The Radial velocity dispersion profile of the Galactic Halo: Constraining the density profile of the dark halo of the Milky Way," *Mon. Not. Roy. Astron. Soc.*, vol. 364, pp. 433–442, 2005, [Erratum: Mon.Not.Roy.Astron.Soc. 370, 1055 (2006)].

[98] Q. Guo, S. White, C. Li, and M. Boylan-Kolchin, "How do galaxies populate dark matter haloes?" , vol. 404, no. 3, pp. 1111–1120, May 2010.

[99] Q. Guo, S. White, M. Boylan-Kolchin, G. De Lucia, G. Kauffmann, G. Lemson, C. Li, V. Springel, and S. Weinmann, "From dwarf spheroidals to cD galaxies: simulating the galaxy population in a ΛCDM cosmology," , vol. 413, no. 1, pp. 101–131, May 2011.

[100] X. Yang, H. J. Mo, and F. C. van den Bosch, "Galaxy Groups in the SDSS DR4. II. Halo Occupation Statistics," , vol. 676, no. 1, pp. 248–261, Mar. 2008.

[101] J. M. Bardeen, J. R. Bond, N. Kaiser, and A. S. Szalay, "The Statistics of Peaks of Gaussian Random Fields," *Astrophys. J.*, vol. 304, pp. 15–61, 1986.

[102] Y. B. Zeldovich, "Gravitational instability: An Approximate theory for large density perturbations," *Astron. Astrophys.*, vol. 5, pp. 84–89, 1970.

[103] R. K. Sheth, H. J. Mo, and G. Tormen, "Ellipsoidal collapse and an improved model for the number and spatial distribution of dark matter haloes," *Mon. Not. Roy. Astron. Soc.*, vol. 323, p. 1, 2001.

[104] W. H. Press and P. Schechter, "Formation of galaxies and clusters of galaxies by selfsimilar gravitational condensation," *Astrophys. J.*, vol. 187, pp. 425–438, 1974.

[105] J. R. Bond, S. Cole, G. Efstathiou, and N. Kaiser, "Excursion set mass functions for hierarchical Gaussian fluctuations," *Astrophys. J.*, vol. 379, p. 440, 1991.

[106] R. K. Sheth, H. J. Mo, and G. Tormen, "Ellipsoidal collapse and an improved model for the number and spatial distribution of dark matter haloes," *Mon. Not. Roy. Astron. Soc.*, vol. 323, p. 1, 2001.

[107] S. Matarrese, F. Lucchin, and S. A. Bonometto, "A Path-Integral Approach to Large-Scale Matter Distribution Originated by Non-Gaussian Fluctuations," , vol. 310, p. L21, Nov. 1986.

[108] H. D. Politzer and M. B. Wise, "Relations between spatial correlations of rich clusters of galaxies," , vol. 285, pp. L1–L3, Oct. 1984.

[109] L. G. Jensen and A. S. Szalay, "N-Point Correlations for Biased Galaxy Formation," , vol. 305, p. L5, Jun. 1986.

[110] P. McDonald, "Primordial non-Gaussianity: large-scale structure signature in the perturbative bias model," *Phys. Rev. D*, vol. 78, p. 123519, 2008.

[111] T. Giannantonio and C. Porciani, "Structure formation from non-Gaussian initial conditions: Multivariate biasing, statistics, and comparison with N-body simulations," , vol. 81, no. 6, p. 063530, Mar. 2010.

[112] V. Assassi, D. Baumann, D. Green, and M. Zaldarriaga, "Renormalized Halo Bias," *JCAP*, vol. 08, p. 056, 2014.

[113] A. Slosar, C. Hirata, U. Seljak, S. Ho, and N. Padmanabhan, "Constraints on local primordial non-Gaussianity from large scale structure," *JCAP*, vol. 08, p. 031, 2008.

[114] F. Schmidt and M. Kamionkowski, "Halo Clustering with Non-Local Non-Gaussianity," *Phys. Rev. D*, vol. 82, p. 103002, 2010.

[115] V. Acquaviva, N. Bartolo, S. Matarrese, and A. Riotto, "Gauge-invariant second-order perturbations and non-gaussianity from inflation," *Nuclear Physics B*, vol. 667, no. 1, pp. 119–148, 2003. [Online]. Available: https://www.sciencedirect.com/science/article/pii/S0550321303005509

[116] N. Bartolo, S. Matarrese, and A. Riotto, "Enhancement of non-gaussianity after inflation," *Journal of High Energy Physics*, vol. 2004, no. 04, p. 006, apr 2004. [Online]. Available: https://dx.doi.org/10.1088/1126-6708/2004/04/006

[117] ——, "Signatures of primordial non-gaussianity in the large-scale structure of the universe," *Journal of Cosmology and Astroparticle Physics*, vol. 2005, no. 10, p. 010, oct 2005. [Online]. Available: https://dx.doi.org/10.1088/1475-7516/2005/10/010

[118] E. Castorina, N. Hand, U. Seljak, F. Beutler, C.-H. Chuang, C. Zhao, H. Gil-Marín, W. J. Percival, A. J. Ross, P. D. Choi, K. Dawson, A. de la Macorra, G. Rossi, R. Ruggeri, D. Schneider, and G.-B. Zhao, "Redshift-weighted constraints on primordial non-gaussianity from the clustering of the eboss dr14 quasars in fourier space," *Journal of Cosmology and Astroparticle Physics*, vol. 2019, no. 09, p. 010, sep 2019. [Online]. Available: https://dx.doi.org/10.1088/1475-7516/2019/09/010

[119] E.-M. Mueller *et al.*, "The clustering of galaxies in the completed SDSS-IV extended Baryon Oscillation Spectroscopic Survey: Primordial non-Gaussianity in Fourier Space," 6 2021.

[120] G. D'Amico, M. Lewandowski, L. Senatore, and P. Zhang, "Limits on primordial non-Gaussianities from BOSS galaxy-clustering data," 1 2022.

[121] G. Cabass, M. M. Ivanov, O. H. E. Philcox, M. Simonović, and M. Zaldarriaga, "Constraints on multifield inflation from the BOSS galaxy survey," *Phys. Rev. D*, vol. 106, no. 4, p. 043506, 2022.

[122] A. Raccanelli, L. Samushia, and W. J. Percival, "Simulating redshift-space distortions for galaxy pairs with wide angular separation," , vol. 409, no. 4, pp. 1525–1533, Dec. 2010.

[123] A. J. S. Hamilton, "Linear redshift distortions: A Review," in *Ringberg Workshop on Large Scale Structure*, 8 1997.

[124] A. Raccanelli, D. Bertacca, D. Jeong, M. C. Neyrinck, and A. S. Szalay, "Doppler term in the galaxy two-point correlation function: wide-angle, velocity, Doppler lensing and cosmic acceleration effects," *Phys. Dark Univ.*, vol. 19, pp. 109–123, 2018.

[125] D. Bertacca, R. Maartens, A. Raccanelli, and C. Clarkson, "Beyond the plane-parallel and Newtonian approach: Wide-angle redshift distortions and convergence in general relativity," *JCAP*, vol. 10, p. 025, 2012.

[126] A. Raccanelli, D. Bertacca, O. Doré, and R. Maartens, "Large-scale 3D galaxy correlation function and non-Gaussianity," *JCAP*, vol. 08, p. 022, 2014.

[127] L. R. Abramo and D. Bertacca, "Disentangling the effects of Doppler velocity and primordial non-Gaussianity in galaxy power spectra," *Phys. Rev. D*, vol. 96, no. 12, p. 123535, 2017.

[128] R. N. Cahn and Z. Slepian, "Isotropic N-point basis functions and their properties," *J. Phys. A*, vol. 56, no. 32, p. 325204, 2023.

Acknowledgments

I would like to express my utmost gratitude to my supervisor Prof.Sabino Matarrese who has always been kind and supportive since my first attendance at his lecture to the whole preparation process of this thesis. His rich experience widened my perspective in the academic field and I have learned countless things thanks to him. Not to mention his punctuality makes my learning process smooth under his advice. Also, my great appreciation belongs to my fellow inspirational co-supervisors, both official and unofficial. The professionalism of Prof.Nicola Bartolo facilitates the production of this thesis, especially the parity violation in the 4PCF part. The recommended references and a discussion with Prof.Licia Verde and Prof.Alvise Raccanelli are foundational to the probing non-Gaussianity with scale-dependent bias part. In addition, Dr.Daniele Bertacca kindly provided references about the redshift space distortion effect, and our meetings were crucial for this project. Furthermore, I would like to thank the Padova Cosmology Group for a stimulating learning environment and friendly group of researchers and students. The Cosmo Student Meeting is a sandbox encouraging students like myself to practice academic activities and receive constructive criticism from professionals.

I acknowledge the Department of Physics and Astronomy of the University of Padova (DFA) for granting me the Departmental Scholarship, supporting my tuition fee and living expenses during my 2-year master's study in Italy. I am very thankful for my family who has always been there for me even if we are afar. Last but not least, I cannot convey enough appreciation for the invaluable friendship I received during my first time studying abroad, in no particular order, Ivan, Giovanni, Isabella, Julia, Lauren, JP, Sara, Blanca, Marisol, Luca, Isabel, Sergio, Augusto, Frank, Pichay, Roberto, Donut, Elif, and many more. Their company comforted my stay outside the country of origin, establishing a place that I could call my second home.